Black Earth Creek Watershed

Hydrologic Modeling Study

Impact of Green Infrastructure and other Land Use Practices on Flood Hydrographs

May 2022

US Army Corps of Engineers ®

Prepared by:

United States Army Corps of Engineers
St. Paul District
180 Fifth Street East, Suite 700
St. Paul, Minnesota 55101-1678

Table of Contents

Table of Tables

Table of Figures

Appendices

1 Motivation of Study

This study was performed as part of the Wisconsin Silver Jackets program in coordination with the Wisconsin Hazard Mitigation Team. Through the Silver Jackets program, the U.S. Army Corps of Engineers, the Federal Emergency Management Agency, additional federal, state, and sometimes local and tribal agencies provide a unified approach to addressing a state's flood risk priorities. The Silver Jackets team is a national coordination program activity funded by various authorities: Section 206 of the Flood Control Act of 1960; Section 22 of the Water Resources Development Act of 1974; and the Flood Control Act of 1955 (PL 84-99).

The Capital Area Regional Planning Commission (CARPC) sought assistance from the U.S. Army Corps of Engineers and the Wisconsin Silver Jackets Hazard Mitigation Team to complete a hydraulic and hydrologic study of the Black Earth Creek watershed in Dane County, WI. The purpose of the project is to estimate the effectiveness of various green infrastructure or land use management alternatives in reducing the flood vulnerability of communities in the basin. To estimate the effectiveness of watershed-scale land use changes and the implementation of agricultural best-management practices, a HEC-HMS model was developed. The creation of the HMS model as well as the results of various alternative simulations are presented in this report. Additional report content includes a description of the Black Earth Creek watershed, a compilation of available hydrological and meteorological data sources, and a literature review of various land management practices used to inform the development of alternatives. Supplementary materials developed for this study, including a qualitative climate change assessment, flow frequency analysis at Black Earth, WI, and an HEC-RAS hydraulic model, are described in appendices to this report.

2 Vertical and Horizontal Control

All elevation data in this report references the North American Vertical Datum of 1988 (NAVD 88), unless otherwise stated. The horizontal coordinate system used for processing information in ArcGIS is the Albers Conical Equal Area projection. Maps throughout this report use the Albers Conical Equal Area projection. Horizontal and vertical units are feet.

3 Watershed Description

The Black Earth Creek watershed lies in southern Wisconsin in the Wisconsin River basin and drains approximately 103 mi^2. The watershed is located west of Madison, WI. Black Earth Creek begins just outside of Middleton, WI, which is a suburb of Madison, and travels in a western direction to its confluence with the Wisconsin River. The creek flows through three villages, Cross Plains (population of 3,538), Black Earth (population of 1,338), and Mazomanie (population of 1,652). Brewery Creek flows into Black Earth Creek at the village of Cross Plains, Vermont Creek flows into Black Earth Creek at the village of Black Earth, and Halfway Prairie Creek and Wendt Creek flow into Black Earth Creek at the village of Mazomanie.

3.1 Topography

The Black Earth Creek watershed lies on the eastern edge of the Driftless Area, the unglaciated region of southwestern Wisconsin, southeastern Minnesota, Northeastern Iowa, and a small section of Northwestern Illinois. The Driftless Area is known for its karst topography with horizontal layers of

fractured sandstone, limestone, and impervious shale overlain by shallow soils (National Trout Center, 2020). Precipitation quickly percolates through fractures in the bedrock, forming well-oxygenated springs and streams at the base of the limestone bluffs (National Trout Center, 2020). The Black Earth Creek watershed shares some common features of the Driftless Area such as well-defined bluffs and well-drained, sandy and silty soils. The few natural lakes in the basin exist in the eastern half of the watershed, typically in the headwaters of small tributaries. Black Earth Creek itself is classified by the Wisconsin Department of Natural Resources (WI DNR) as a class 1 coldwater fishery characterized by a high gradient, coarse substrates, and many meandering riffle-pool sequences. A topographical map of the study area is shown in Figure 1. Figure 2 shows the slope of the watershed, and Figure 3 shows the drainage classification of the soils in the basin.

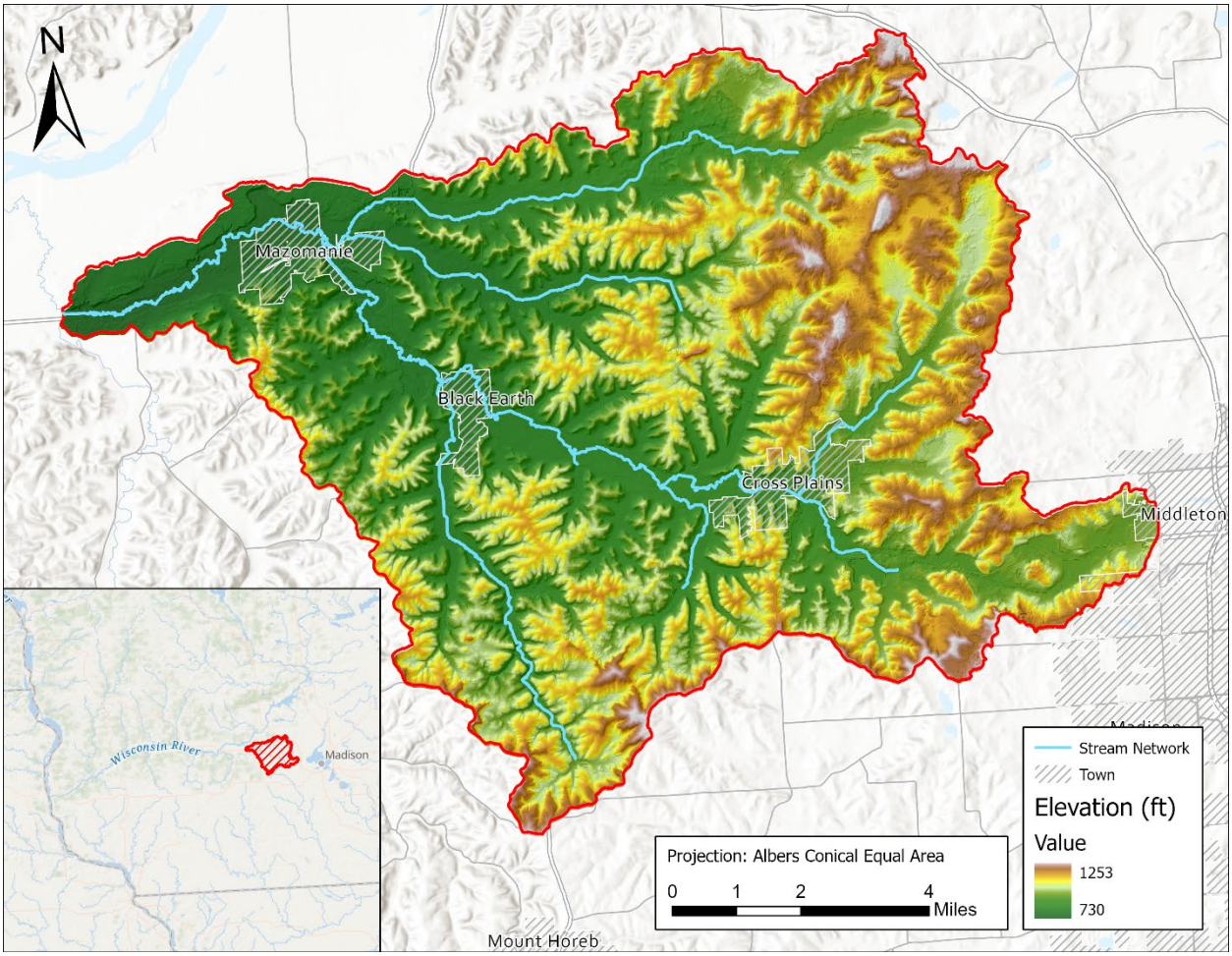

Figure 1. Topographic map of the Black Earth Creek watershed

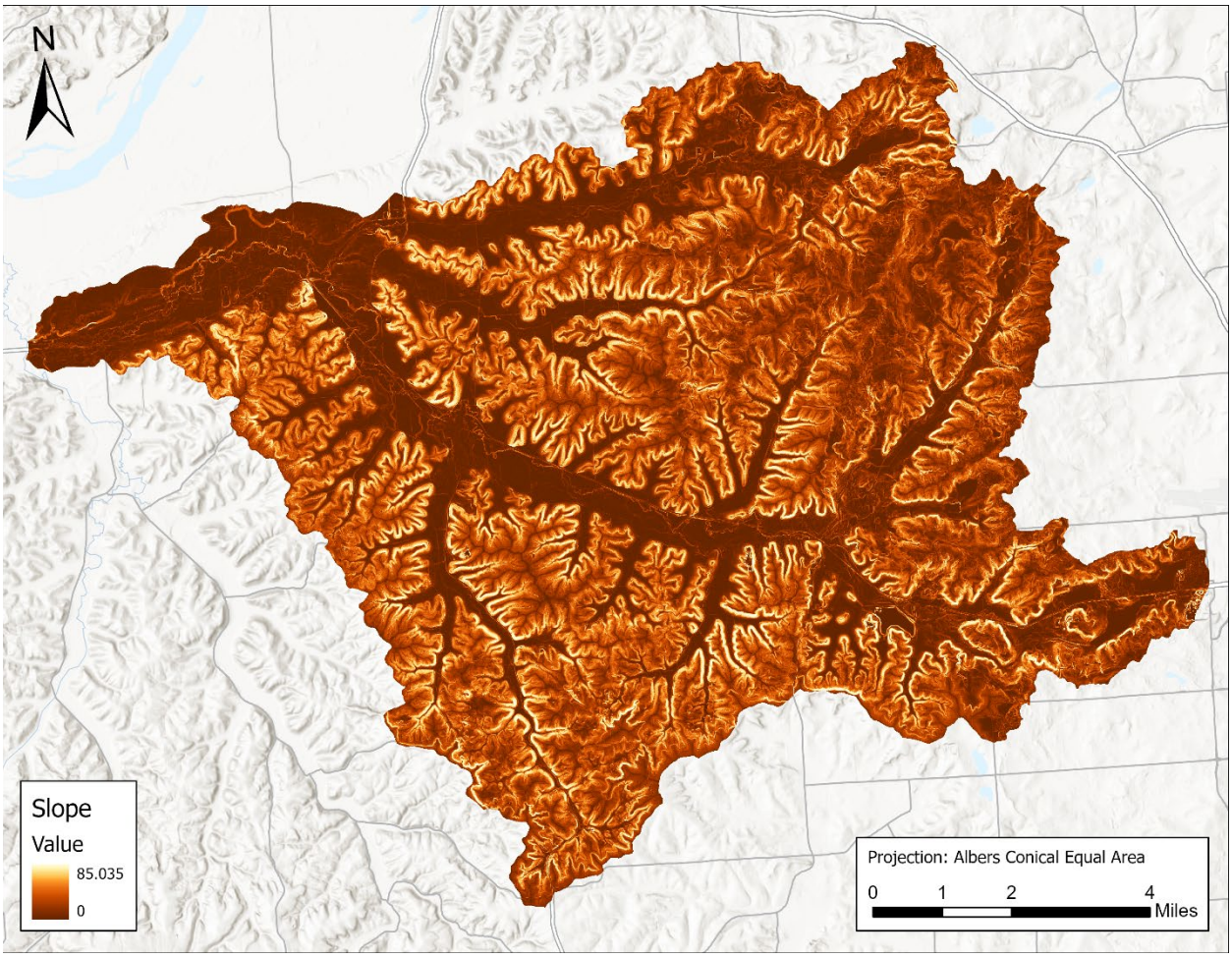

Figure 2. Slope - Black Earth Creek watershed

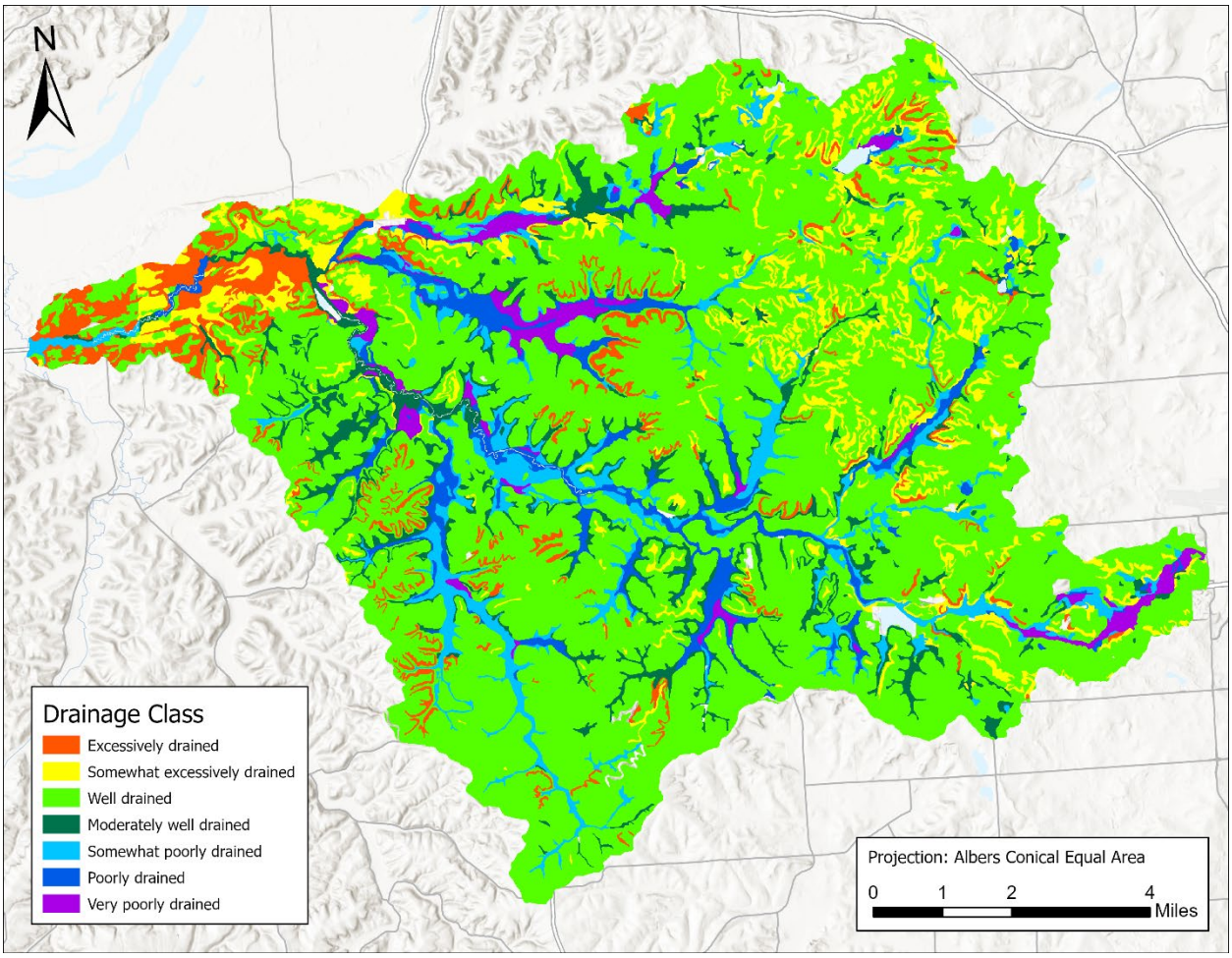

Figure 3. Drainage classification - Black Earth Creek watershed

3.2 Land Cover

As shown in Table 1, land cover in the basin is primarily cultivated cropland, deciduous forest, and hay/pasture. The majority of land within the Black Earth Creek floodplain is cultivated cropland. Deciduous forest dominates steep slopes, and ridge tops consist of a mixture of cropland and hay/pasture. The majority of the wetlands in the watershed are found along Wendt Creek and Vermont Creek. A map of land cover throughout the watershed is shown in Figure 4.

Table 1. Land cover statistics in the Black Earth Creek watershed (National Land Cover Dataset - 2016)

Land Cover Classification	Total Area (mi^2)	% of Total Area
Cultivated Crops	37.5	36%
Deciduous Forest	31.2	30%
Hay/Pasture	17.2	17%
Mixed Forest	6.1	6%
Developed, Open Space	3.8	4%
Developed, Low Intensity	2.8	3%
Other	4.6	4%

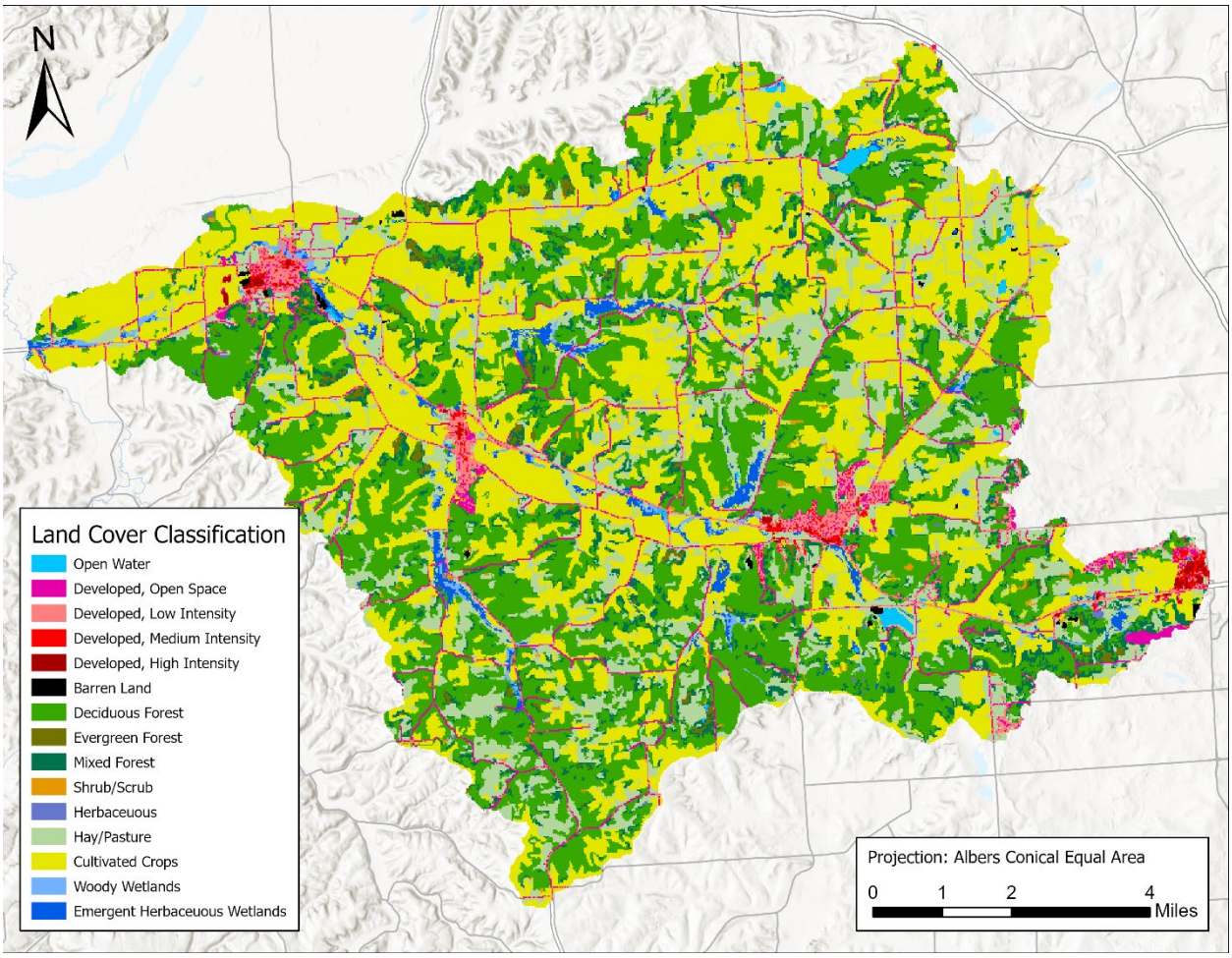

Figure 4. Land cover in the Black Earth Creek watershed (National Land Cover Dataset - 2016)

3.3 Agricultural Practices

According to the National Cropland Data Layer (NCDL) (USDA National Agricultural Statistics Service, 2019), the three most common crops planted in the Black Earth Creek basin are corn, alfalfa, and soybeans. These three crops make up 91% of all cultivated cropland and 35% of the total land area. Table 2 and Figure 5 show the distribution of agricultural land use by type as reported by the NCDL.

Table 2. Agricultural land use statistics - Black Earth Creek watershed (National Cropland Data Layer, 2019)

Crop Type	Total Area (mi^2)	% of Total Area	% of Agricultural Land
Corn	19.2	19%	49%
Alfalfa	9.4	9%	24%
Soybeans	6.9	7%	18%
Fallow	2.2	2%	6%
Winter Wheat	0.9	1%	2%
Oats	0.3	0%	1%
Other	0.4	0%	1%

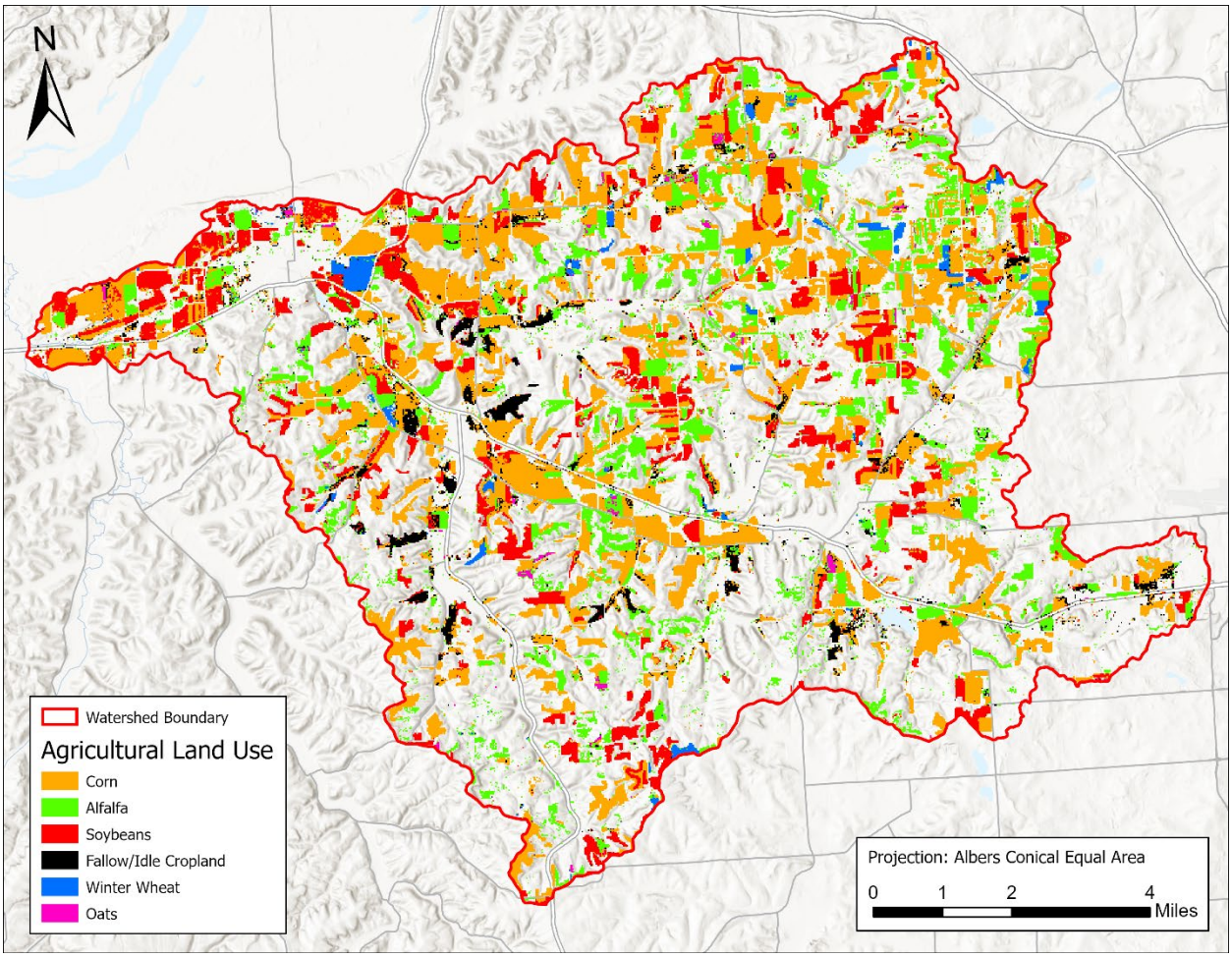

Figure 5. Agricultural land use - Black Earth Creek watershed (National Cropland Data Layer, 2019)

3.4 Green Infrastructure

Green infrastructure is defined by the 2019 Water Infrastructure Improvement Act as "the range of measures that use plant or soil systems, permeable pavement or other permeable surfaces or substrates, stormwater harvest and reuse, or landscaping to store, infiltrate, or evapotranspirate stormwater and reduce flows to sewer systems or to surface waters." While there are many different features that could be classified as green infrastructure, common practices include rain gardens, rainwater harvesting, green roofs, bioswales, and permeable pavement. According to the local sponsor, the presence of green infrastructure in urban areas of Black Earth Creek is currently limited.

4 Hydrological Data

4.1 Streamflow

There are a number of active and inactive streamflow gages in the Black Earth Creek basin. However, the period of record of each gage varies, and observed flows have not been recorded for many flood events downstream of the village of Black Earth. Near Cross Plains, several gages have consistently recorded flows on Brewery Creek and Black Earth Creek since 2015. The Black Earth Creek at Black Earth, WI gage (USGS 05406500) has the longest period of record in the basin, with a continuous, daily record of 1954-

present, and a 15-minute record of 1986-2012, 2014-present. The largest recorded flood event on Black Earth Creek occurred in August 2018 with a flow of 2,930 cfs at the Black Earth Creek at Black Earth, WI gage. Records of other large, historic flood events that occurred prior to 1954 could not be found. Table 3 lists all available streamflow data in the basin, and Figure 6 shows the location of each active and inactive gage in the watershed along with whether the gage's data is used for calibration or validation of the hydrologic model.

Table 3. Active and inactive streamflow gages in the Black Earth Creek watershed

Map Number	Name	Operator	Gage ID	Record	Streamflow Type
1	Black Earth Creek at Mazomanie, WI	USGS	05406540	2005	Daily
2	Halfway Prairie Creek at Hudson Rd at Mazomanie, WI	USGS	05406524	2005	15-minute
3	Vermont Creek at CT Highway KP at Black Earth, WI	USGS	054065145	2005	15-minute
				2005	Daily
4	Black Earth Creek at Black Earth, WI	USGS	05406500	1986-2012, 2013-present	15-minute
				1954-present	Daily
				1954-present	Annual Peak
5	Black Earth Creek at S. Valley Rd Nr Black Earth, WI	USGS	05406497	1990-1993	Daily
6	Black Earth Ck Nr Treatment Plnt at Cross Plains, WI	USGS	05406479	2014-present	5-minute
				2014-present	Daily
				2016-2018	Annual Peak
7	Black Earth Creek at Mills Street at Cross Plains, WI	USGS	05406476	1990-1995	Daily
				1990-1994	Annual Peak
8	Black Earth Creek at Cross Plains, WI	USGS	05406460	1985-1986, 1990-1993, 2005	Daily
				1985, 1990-1991, 1993	Annual Peak
9	Black Earth Creek nr Brewery Rd at Cross Plains, WI	USGS	05406457	2010, 2014-2015, 2018-2019	5-minute
				2016-2017	15-minute
				2010-present	Daily
				2010-2011, 2013-2017	Annual Peak
10	Black Earth Ck at Stagecoach Rd Nr Cross Plains, WI	USGS	054064509	2005	15-minute
				2005	Daily
11	Black Earth Creek Low Flow No 3 Nr Cross Plains, WI	USGS	05406450	2005	15-minute
				2005	Daily
12		USGS	05406470	1990-2002, 2005	15-minute

	Brewery Creek at Cross Plains, WI			1985-1986, 1990-2002, 2005	Daily
				1985, 1990-1993, 1994-1998, 2000-2002	Annual Peak
13	Brewery Creek-Upstream Site-at Cross Plains, WI	USGS	05406469	2015-2019	15-minute

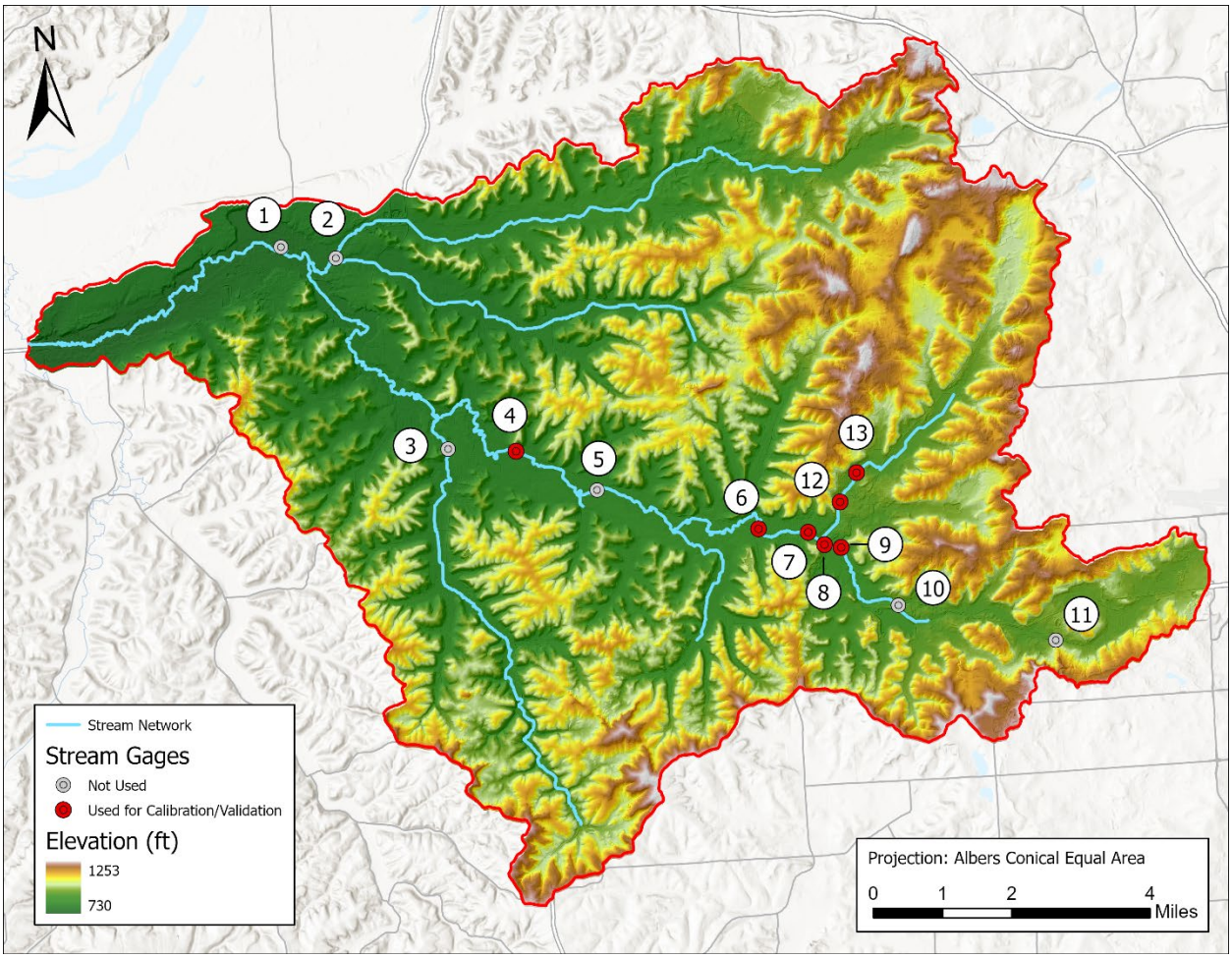

Figure 6. Locations of all active and inactive streamflow gages in the Black Earth Creek watershed

4.2 Dams/Reservoirs

Currently, there are no dams in the Black Earth Creek watershed listed in the National Inventory of Dams (NID) (U.S. Army Corps of Engineers, 2020a). In the past, there was a small dam on Black Earth Creek at the village of Mazomanie that diverted water into Lake Marion, a 17-acre recreational fishery with a maximum storage capacity of 100 ac-ft. However, the dam was decommissioned by the WI DNR in 2012, and the lake is now fed by a groundwater well. Since the dam was small and no longer exists, it is not included in the hydrologic model.

5 Meteorological Data

5.1 Precipitation

Hourly, gridded precipitation data covering the study area is available via the Next Generation Radar (NEXRAD) network (National Weather Service, 2020b). NEXRAD Multisensor Precipitation Estimator (MPE) data for this region is continuous from 2010 to the present. Precipitation is estimated by measuring the reflectivity of radar beams emitted from a central location. Error is introduced into precipitation estimates when the radar beams are either blocked (such as by mountains or structures) or encounter atmospheric phenomena other than raindrops (such as hail stones) (National Weather Service, 2020a). Error also increases further away from the radar source due to range degradation (National Weather Service, 2020a). Since the entire Black Earth Creek basin lies within 100 miles of two NEXRAD stations (La Crosse, WI and Milwaukee, WI), the gridded precipitation data is likely to be relatively high quality.

There are a number of hourly, point precipitation gages surrounding the Black Earth Creek watershed. However, their spatial and temporal distributions vary. Inside the watershed, only daily precipitation gages are available, and their period of record is limited. To evaluate the accuracy of the NEXRAD gridded data, develop gridded precipitation datasets for periods prior to 2010, and analyze antecedent conditions that may affect model calibration, data from nine precipitation gages within the Black Earth Creek watershed and 13 gages outside the watershed were used. These gages are listed in Table 4 and shown in Figure 7 and Figure 8. Hourly data was used to develop gridded precipitation datasets for periods prior to 2010. Daily data was used to evaluate the accuracy of the NEXRAD gridded data, adjust the magnitude of gridded precipitation datasets if necessary, and analyze antecedent conditions prior to calibration and validation events.

Table 4. Precipitation gages in and around the Black Earth Creek watershed used in this study

Map Number	Name	Network	Gage ID	Hourly Record	Daily Record
1	MAZOMANIE WWTP, WI US	GHCND	USC00475189	-	2002-present
2	GARFOOT CREEK RAIN GAGE #1 NEAR CROSS PLAINS, WI	USGS	430432089414100	-	1990-1998
3	GARFOOT CREEK RAIN GAGE #2 NEAR CROSS PLAINS, WI	USGS	430525089411500	-	1990-1998
4	BLACK EARTH CREEK TRIBUTARY AT CROSS PLAINS, WI	USGS	054064785	-	1999-2003
5	GARFOOT CREEK RAIN GAGE #3 NEAR CROSS PLAINS, WI	USGS	430543089393500	-	1990-1998
6	BREWERY CREEK AT CROSS PLAINS, WI	USGS	05406470	-	2000-2003
7	BREWERY CREEK RAIN GAGE #3 NEAR CROSS PLAINS, WI	USGS	430751089372000	-	1990-1998
8	BREWERY CREEK RAIN GAGE #2 NEAR CROSS PLAINS, WI	USGS	430900089355400	-	1990-1998
9	BREWERY CREEK RAIN GAGE #3 NEAR CROSS PLAINS, WI	USGS	431010089360000	-	1990-1998

10	STEUBEN 4 SE, WI US	COOP	478164	1980-1997	-
	LA FARGE, WI US	COOP	474404	1948-2013	-
12	LONE ROCK TRI CO AIRPORT, WI US	COOP	474821	1948-1982	-
	SAUK CITY WWTP, WI US	GHCND	USC00477576	-	2008-present
14	PRAIRIE DU SAC 2 N, WI US	GHCND	USC00476838	-	1908-2006
	WAUNAKEE 4.9 W, WI US	GHCND	US1WIDA0062	-	2018-present
16	ARLINGTON, WI US	COOP	470308	1975-2013	-
	MADISON DANE CO REGIONAL AIRPORT, WI US	COOP GHCND	474961 USW00014837	1948-2013	1939-present
18	MADISON WEATHER BUREAU CITY, WI US	COOP	474966	1950-1963	-
	CHARMANY FARM, WI US	COOP GHCND	471416 USC00471416	1963-2013	1959-present
20	VERONA 5.5 WNW, WI US	GHCND	US1WIDA0049	-	2017-2020
	MOUNT HOREB WWTP, WI US	GHCND	USC00475674	-	2007-present
22	BLANCHARDVILLE, WI US	COOP	470890	1948-2013	-

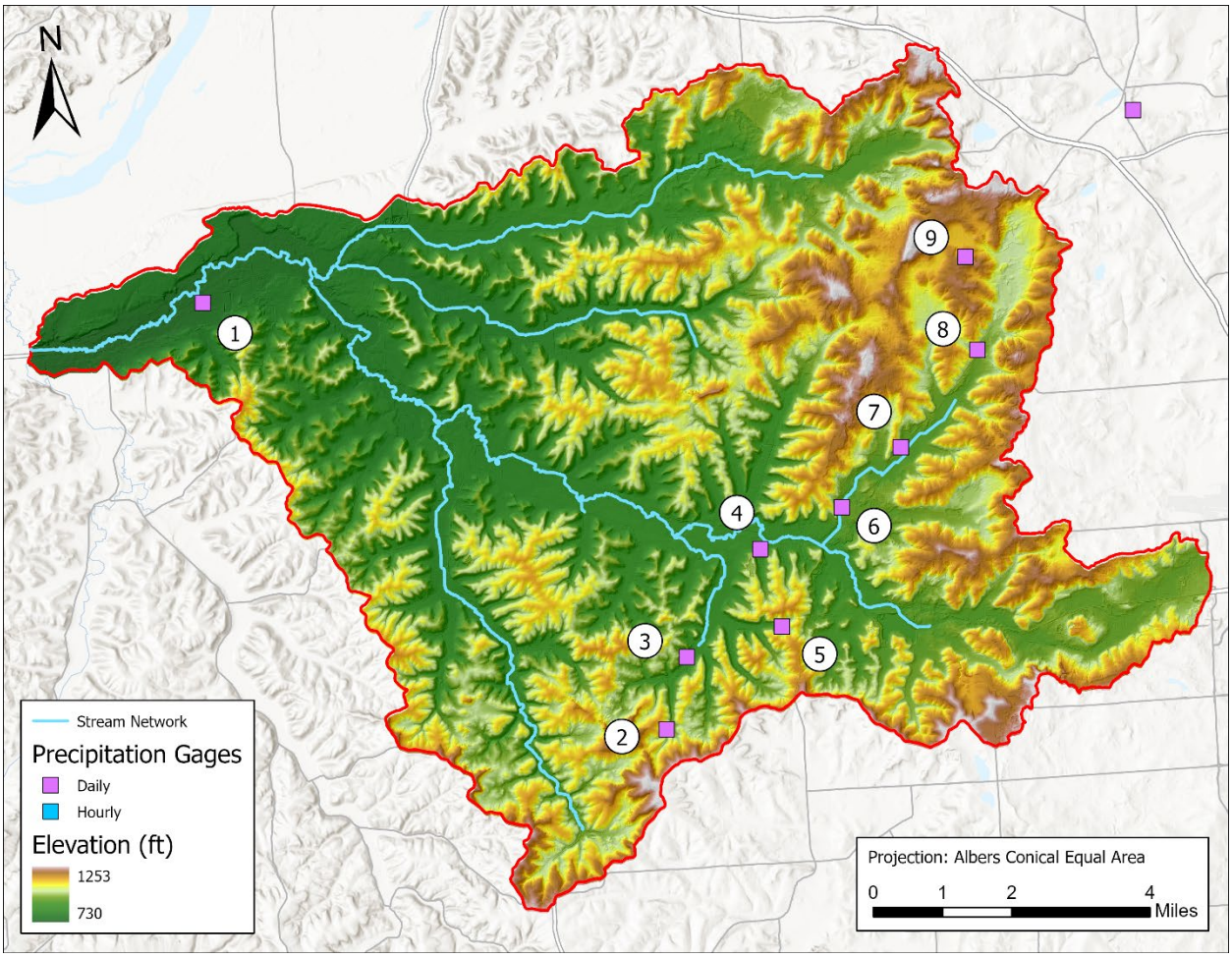

Figure 7. Precipitation gages within the Black Earth Creek watershed used for this study

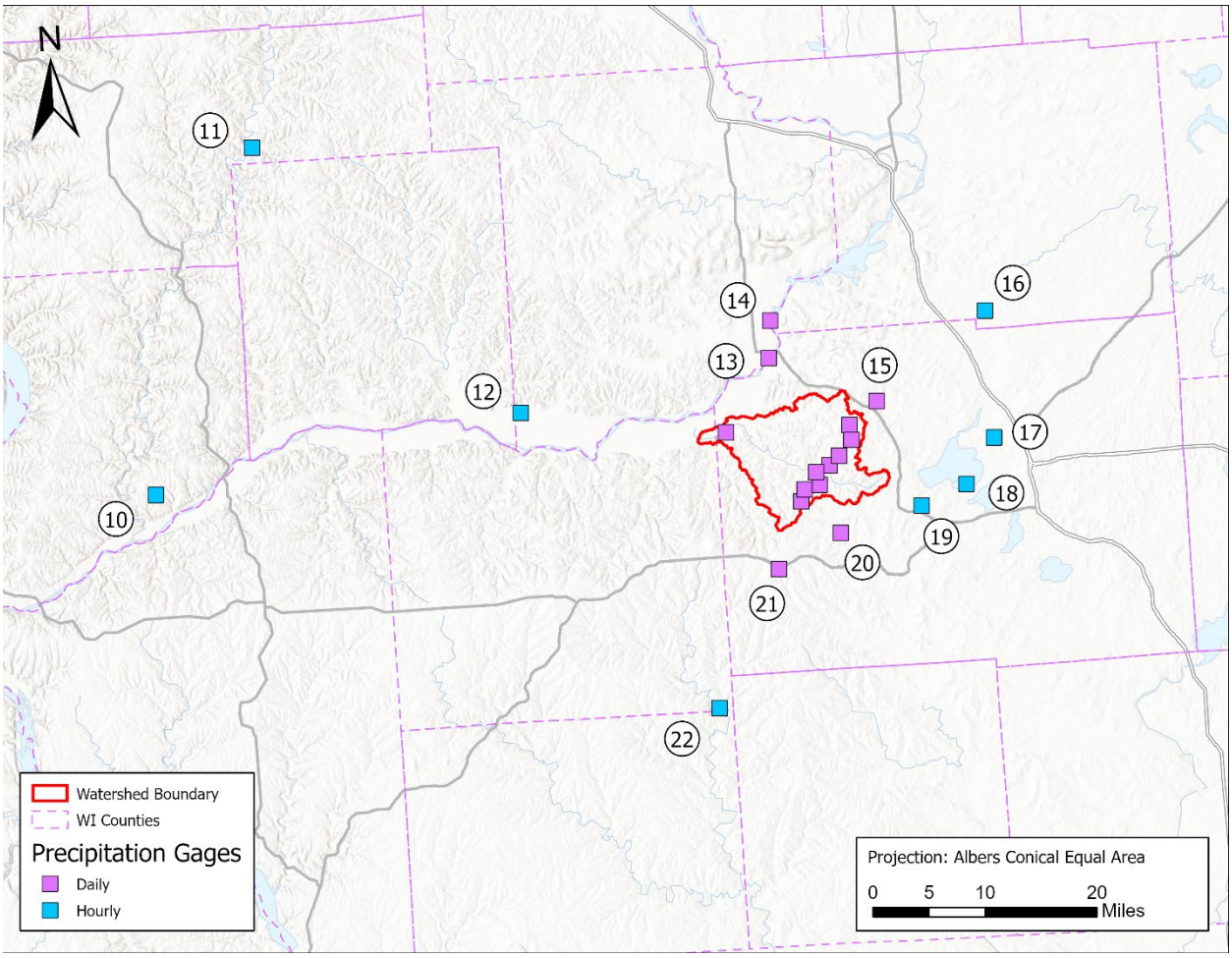

Figure 8. Precipitation gages outside the Black Earth Creek watershed used for this study

To confirm the accuracy of the NEXRAD gridded precipitation datasets, HEC-MetVue (U.S. Army Corps of Engineers Hydrologic Engineering Center, 2019) was used to compute rainfall totals using the NEXRAD data for the August 2018 and September-October 2019 storm events at six precipitation gage sites near the Black Earth Creek watershed. The NEXRAD totals were then compared to the observed totals at those sites. As shown in Table 5 and Table 6, average differences between the gaged and gridded data were small.

Table 5. Comparison of gaged vs. gridded precipitation data, 2018 simulation period (Aug 18-31, 2018)

Precipitation Gage	Map Number	Gage Total (in)	NEXRAD Total (in)	Difference	Average Difference
MADISON DANE CO REGIONAL AIRPORT, WI US	17	5.88	6.18	-5%	**-3%**
MAZOMANIE WWTP, WI US	1	6.66	6.17	7%	
MOUNT HOREB WWTP, WI US	21	8.75	8.32	5%	
SAUK CITY WWTP, WI US	13	6.8	6.84	-1%	
WAUNAKEE 4.9 W, WI US	15	5.62	6.47	-15%	
VERONA 5.5 WNW, WI US	20	12.34	13.26	-7%	

Table 6. Comparison of the gaged vs. gridded precipitation data, 2019 simulation period (Sep 29-Oct 10, 2019)

Precipitation Gage	Map Number	Gage Total (in)	NEXRAD Total (in)	Difference	Average Difference
MADISON DANE CO REGIONAL AIRPORT, WI US	17	4.9	5.41	-10%	**+3%**
MAZOMANIE WWTP, WI US	1	5.62	6.15	-9%	
MOUNT HOREB WWTP, WI US	21	4.34	4.17	4%	
SAUK CITY WWTP, WI US	13	6.41	5.7	11%	
WAUNAKEE 4.9 W, WI US	15	5.87	5.22	11%	
VERONA 5.5 WNW, WI US	20	5.19	4.63	11%	

To verify the gridded precipitation data adequately captures the temporal distribution of rainfall, HEC-MetVue was used to compute hourly rainfall hyetographs at the Verona 5.5 WNW, WI US gage for the 2018 and 2019 simulation periods. These hyetographs were then converted to daily totals and compared to observed data (Figure 9 and Figure 10). While the daily timestep of the observed data makes comparison difficult, the timing of both datasets appears to match reasonably well. This observation, along with small average differences in total precipitation between gaged and gridded data, indicates the NEXRAD data adequately captures the timing, distribution, and magnitude of rainfall in the Black Earth Creek basin.

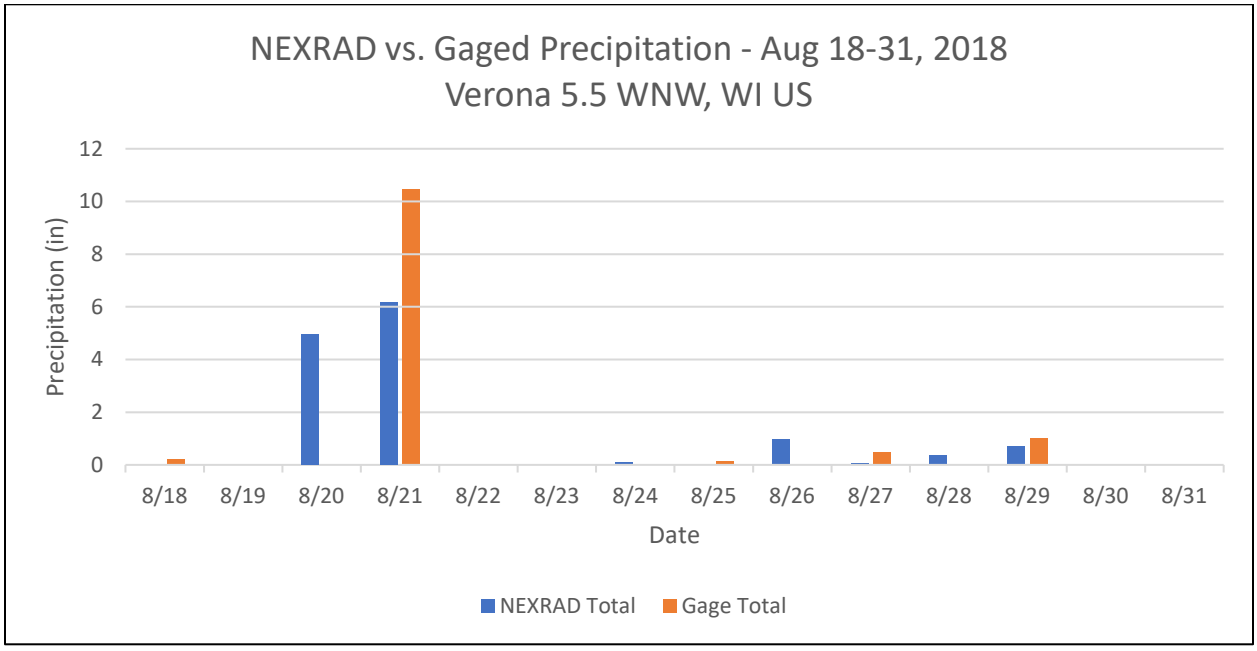

Figure 9. Comparison of gaged vs. gridded data at the Verona 5.5 WNW, WI US gage (2018 simulation period)

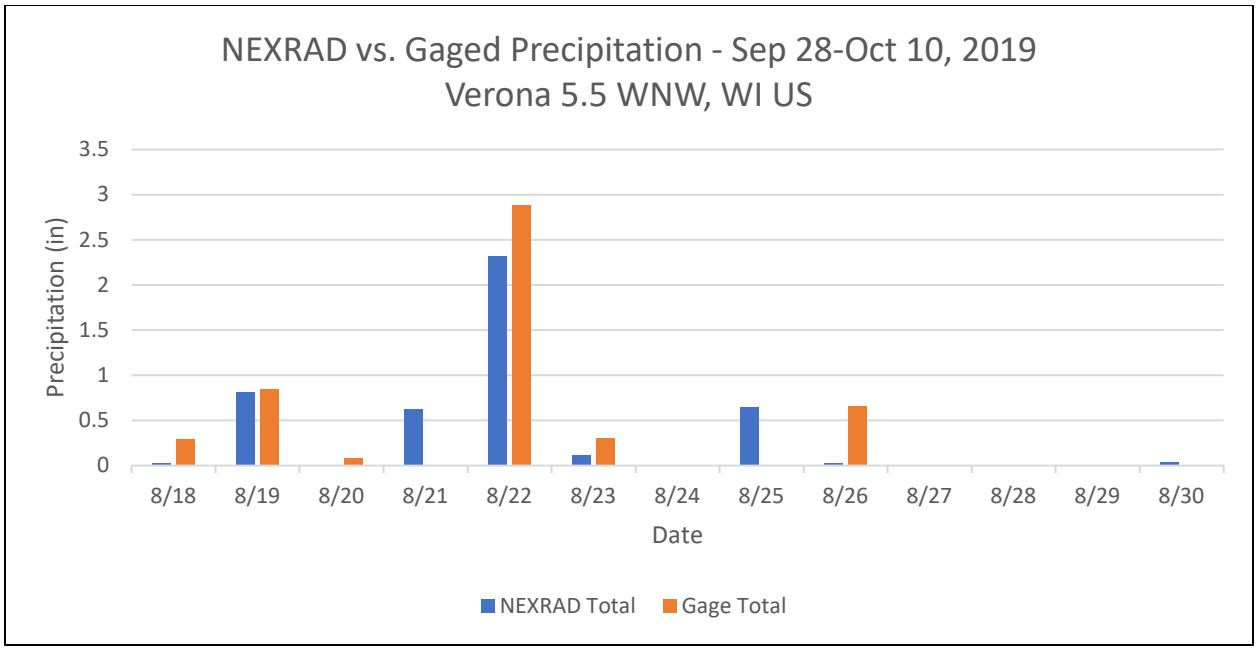

Figure 10. Comparison of gaged vs. gridded data at the Verona 5.5 WNW, WI US gage (2019 simulation period)

For calibration and validation events taking place between 2008 and 2020 (Jun 2016, Jul 2017, Aug 2018, and Sep-Oct 2019), the NEXRAD gridded precipitation data was used as the input to the HMS model. For calibration and validation events prior to 2008 (Jul 1993 and Jul-Aug 2001), precipitation grids were developed using the GageInterp tool (U.S. Army Corps of Engineers Hydrologic Engineering Center, 2016) and precipitation data collected at the gages shown in Table 4.

To develop a grid for the July 1993 event, first, an hourly grid was created utilizing all hourly gages that collected data during the event. These gages were all outside the Black Earth Creek watershed. Then, a daily grid was created utilizing all daily gages that collected data during the event, which included a number of gages within the watershed. Rainfall totals during the simulation period were compared for the hourly and daily grid for each subbasin in the HMS model. The rainfall totals for the daily grid were approximately 1.14 times higher across all subbasins than totals for the hourly grid. Although the daily grid was developed using gages inside the watershed, and therefore more accurately captured the total volume of precipitation, the hourly grid was assumed to better capture the timing of precipitation, since it used an hourly timestep. Therefore, the hourly grid was used in the HMS model, and a precipitation ratio of 1.14 was applied to all subbasins to more closely match the totals observed at gages inside the watershed.

To develop a grid for the July-August 2001 event, an hourly grid was created utilizing all hourly gages that collected data during the event. As in 1993, all hourly gages were outside the watershed. However, unlike the 1993 event, where multiple gages inside the watershed recorded daily data during the event, only one gage within the watershed recorded precipitation totals during the 2001 event (Brewery Creek at Cross Plains, WI, USGS 05406470). To improve the accuracy of the hourly grid, HEC-MetVue was used to compare the gridded total during the simulation period at the Brewery Creek gage to its recorded total. The gage record showed 1.4 times as much precipitation over the simulation period than the gridded data; therefore, the hourly grid was used in the HMS model, and a precipitation ratio of 1.4 was applied to all subbasins to more closely match the totals observed at the gage inside the watershed.

5.2 Temperature/Drought Index

Daily maximum and minimum temperature data is available at the Madison Dane County Regional Airport, Charmany Farm, and Lone Rock Tri County Airport weather stations for each station's period of record. For this study, daily maximum temperatures at Charmany Farm are considered representative of daily maximum temperatures throughout the Black Earth Creek basin. Drought conditions are evaluated in this study by using Keetch-Byram Index (KBI) values computed by the Midwest Regional Climate Center (MRCC) at the Lone Rock Tri County Airport and Madison Dane County Regional Airport weather stations. The average of the two stations' KBI values is assumed to be representative of the KBI in the Black Earth Creek basin. Temperature and KBI are used in this study as metrics when exploring how antecedent conditions may explain differences in calibrated initial loss values in the hydrologic model.

6 Climate Change

The potential for climate change to impact the hydrology of the Black Earth Creek basin was considered in accordance with USACE Engineering Construction Bulletin *(ECB) 2018-14, Guidance for Incorporating Climate Change Impacts to Inland Hydrology in Civil Works Studies, Designs and Projects* (U.S. Army Corps of Engineers, 2020b), as well as USACE Engineering Technical Letter *(ETL) 1110-2-3, Detection of Nonstationarities in Annual Maximum Discharges* (U.S. Army Corps of Engineers, 2017). The guidance requires a literature review, an evaluation of the stationarity assumption, first order statistical analysis of both observed and projected streamflow data, and a relative assessment of the vulnerability of a given watershed to the impacts of climate change for select USACE business lines including flood risk management. The full qualitative climate change assessment completed for this study is included in Appendix D. Important findings from the climate assessment are summarized in the following section.

6.1 Summary of Climate Assessment Findings

There is strong consensus within peer reviewed literature that temperature, precipitation, and streamflow have increased over the observed record in the Upper Mississippi River basin (UMR). Projections of future climate show strong consensus on increases in future temperature, moderate consensus on increases in precipitation, and less consensus amongst projections of future streamflow in the UMR. In the Black Earth Creek basin, a nonstationarity detection and trend analysis was conducted on the annual instantaneous peak streamflow record at the Black Earth Creek at Black Earth, WI USGS gage (05406500) over its period of record (1954-2020). The analysis found no strong nonstationarities in the annual peak streamflow record and no significant positive or negative trend. However, while there is no notable trend in peak streamflow, monthly average streamflow at the Black Earth, WI gage has been increasing over time. A trend analysis showed a significant, positive trend in monthly average streamflow for all individual months over the 1954-2020 period. The annual 25th percentile of daily flow recorded at the gage was also shown to be increasing throughout the period of record. These results indicate the "normal" flow, or "baseflow," in the creek is increasing, even though extreme flood events may not be becoming more frequent.

7 Literature Review

A literature review was conducted to determine how various agricultural best management practices (BMPs) and land use practices may impact soil infiltration, storage capacity, or runoff potential. Available literature indicates cover crops, no-till, and prairie, or contour, buffer strips all have potential to reduce flood risk. Wetland restoration has also been shown to affect a watershed's runoff response.

A review of the capacity of urban green infrastructure improvements to reduce flood risk was conducted by the consulting firm Emmons & Olivier Resources, Inc. (EOR) and is not included in this report.

7.1 Cover Crops

Cover crops are non-cash crops that are either planted between the harvest and planting phases of a typical cropping system, providing vegetative cover year-round, or planted along with a cash crop. It is widely accepted that cover crops increase soil organic matter and improve soil structure, but the ability for cover crops to promote water infiltration varies across the scientific literature. Inconsistencies are primarily due to the wide range of cover crops available, the length of time after the adoption of cover crops in each study, and varying soil and climatic conditions. For example, a study conducted in a silty clay loam soil in Nebraska found grass and legume cover crops did not affect soil water infiltration after 12 years (Blanco-Canqui & Jasa, 2019). However, a three-year study conducted in the sandy soils of the southeastern USA coastal plain region found saturated hydraulic conductivity (Ksat) generally increased in cropping systems incorporating sun hemp or crimson clover cover crops (Hubbard et al., 2013). A second study conducted in the coastal plain region of the United States found hairy vetch and crimson clover cover crops increased soil infiltration rates when compared to fallow in both gravelly clay loam and sandy clay loam soil after three years (McVay et al., 1989).

The U.S. Department of Agriculture (USDA) published a literature review in 2016 exploring the effects of various soil health management practices on infiltration, saturated hydraulic conductivity, and runoff (U.S. Department of Agriculture, 2016). The publication reviewed 12 different studies conducted in the United States which measured the effect of cover crops on soil properties. The executive summary states:

"Use of cover crops (CC) commonly results in greater water infiltration because of the direct effects of improved canopy cover, improvement in soil aggregation, and the formation of macropores by cover-crop roots (which are left intact after termination). It improves porosity, infiltration, and Ksat from 3 percent to over 50 percent. Sandy soils show less improvement in infiltration and Ksat because these are already rapid; however, other physical and chemical soil properties are benefited. Use of cover crops reduced runoff in most studies."

A recent meta-analysis published in PLoS ONE provides the most detailed, quantitative information regarding the effect of cover crops on infiltration rates (Basche & DeLonge, 2019). The authors identified 23 experiments and 81 paired comparisons across the world where a cover crop treatment was compared to a control without cover crops. The mean increase in infiltration rate due to the adoption of cover crops was 34.8% ± 7.7% with a 95% confidence interval of 19.8% to 50.0%. Infiltration rates were slightly greater when cover crops were in place for more than four years, and improvements in infiltration rates were higher in coarsely textured soils with higher sand contents and less clay. There were also greater improvements in infiltration when experiments combined cover crops with no-till, as opposed to experiments with no-till only. The mean increase in infiltration rate measured in those experiments was 44.6% with a 95% confidence interval of 11.6% to 77.5%.

7.2 No-Till

Conventional tillage is a method of stirring the soil to bury plant residue and control weeds and is typically performed after a field is harvested in preparation for the next planting cycle. In cold weather climates, this results in a bare field surface from late fall to early spring. No-till is simply the absence of

conventional tillage, where plant residue is left on the field surface between harvesting and planting. No-till is widely accepted to reduce soil erosion, improve soil structure, increase soil organic matter, and improve nutrient cycling.

Like cover crops, no-till has been reported to improve water infiltration, but experimental evidence is mixed. Long-term watershed studies in Ohio have shown "…when corn is planted in soil covered by the residue of the previous crop (i.e. no-tillage management), surface runoff from summer storms is greatly reduced." (Edwards et al., 1992). An 8-year study in silt loam soils in Oklahoma found water infiltration in no-till soil was higher than in plowed soil under similar water contents, and seasonal variability of field infiltration varied less under no-till compared to conventional tillage (Dao, 1993). Conversely, a study in a clay loam soil in Texas found hydraulic conductivity was greater under conventional tillage than no-till, indicating greater runoff would be expected under no-till management (Evett et al., 1999). Some differences in performance of no-till and conventional tillage systems may be related to reduced wheel traffic under no-till. A 20-year study on clay loam and silt loam soils showed infiltration was reduced approximately 6 to 50 times under loads ranging from 10 Mg to 20 Mg (Blanco-Canqui & Lal, 2008). Other differences in performance of no-till and conventional tillage systems may be related to the period of time necessary to see changes in soil physical properties after adoption of a no-till system.

The USDA's literature review discussing the effects of various soil health management practices on infiltration, saturated hydraulic conductivity, and runoff (U.S. Department of Agriculture, 2016) reviewed 17 studies measuring the effects of no-till on soil physical properties. The executive summary states:

"Switching from conventional tillage (CT) to no-till (NT) may increase infiltration and saturated hydraulic conductivity (Ksat) in the first few years, depending on site conditions, or several years (2–8) may be needed for these improvements. There are a few exceptions where infiltration is not higher under NT compared to CT. Leaving residue cover provides additional benefits, such as minimizing crusting, improving soil aggregation, and conserving soil moisture. Although infiltration is generally greater immediately after tillage under CT compared to NT, it typically decreases throughout the year and is ultimately less."

The same meta-analysis discussed in the Cover Crops section also analyzed studies of no-till practices (Basche & DeLonge, 2019). The authors collected data from 52 experiments across the world and 207 paired comparisons of no-till versus conventional or reduced tillage. Ultimately, the effect of no-till was non-significant, with a mean increase in infiltration rate of 5.7% ± 9.7% with a 95% confidence interval of -13.3% to +24.7%. However, improvements in infiltration rates were higher when no-till was combined with residue retention practices. Infiltration rates were also higher with no-till in regions with 600 to 1,000 mm of annual precipitation. Only two experiments directly captured the effect of no-till plus a cover crop by comparing to conventional tillage plus a cover crop. The results of those two experiments were inconclusive.

7.3 Prairie Buffer Strips

Prairie buffer strips, also referred to as grass contour strips, buffer strips, or conservation buffers, are regions of native prairie vegetation within a row-cropped agricultural field. Unlike grassed waterways, which are typically planted with weak-stemmed grasses that lie flat under heavy rainfall and are designed to convey water while preventing erosion, prairie buffer strips are meant to intercept and infiltrate runoff, thereby increasing retention of soil and other nutrients like phosphorus and nitrogen.

Because prairie buffer strips are designed to intercept runoff, they are typically placed on contours or at a field's edge.

A significant amount of research on the effects of prairie buffer strips has been conducted by Iowa State University's STRIPS team. STRIPS stands for "Science-based Trials of Rowcrops Integrated with Prairie Strips." Between 2007 and 2014, STRIPS researchers collected data from 12 agricultural catchments at the Neal Smith National Wildlife Refuge in central Iowa and published numerous papers with their findings (Iowa State University, 2021). When researchers analyzed differences in hydrologic variables for the years 2008, 2009, and 2010, they found watersheds with prairie strips generally produced less runoff than watersheds without prairie strips (Hernandez-Santana et. al, 2013). Total runoff volume from fields with 10% prairie strip coverage was lower than the control watersheds for both high (>10 mm runoff) and low (<10 mm runoff) rainfall events. This effect was observed during the dormant season (April-June) as well as the active growing season (June-September). Peak flow rate was also significantly lower for prairie strip watersheds in both the dormant and active growing seasons, but only for low rainfall events (Hernandez-Santana et al., 2013). In a related analysis of the STRIPS data, this time through 2014, researchers found 1.6 times less water runoff leaving catchments with prairie strips relative to catchments without prairie strips, although it is not clear how runoff varied between rain event or season (Schulte et al., 2017). The STRIPS website claims "strategically adding about 10 percent prairie to row-cropped watersheds managed on a soy-corn rotation using no-till soil management techniques resulted in…44 percent reduction in water runoff" (Iowa State University, 2021). However, reading the collection of STRIPS publications available, it is not clear how this value of 44% was derived. While experiments showed prairie strips reduced runoff (Hernandez-Santana et al., 2013, Schulte et al., 2017) the magnitude of reduction varied by year, season, and rainfall event. It is also not clear whether this "reduction in water runoff" corresponded to a volumetric total over time or a peak reduction that could be expected during any given rain event.

In Wisconsin, the Sand County Foundation has performed modeling studies on three farms evaluating water quality benefits of prairie strips (Sand County Foundation, 2021). The researchers found reductions in sediment and phosphorus loss of 0% to 60% depending on the farm's physical characteristics, cropping system, and prairie strip design, which is significantly less than the 90% reduction in phosphorus runoff reported by the STRIPS team (Iowa State University, 2021). While phosphorus loss does not directly correspond to water runoff, the two variables are correlated, as phosphorus attaches to soil particles, with are carried by water.

In general, it is difficult to state with certainty how prairie strips would affect runoff in the Black Earth Creek basin, particularly during the large rain events emphasized in this study. Evidence suggests annual runoff volume would likely be reduced with large-scale adoption of prairie strips, with more reduction during spring and early summer when prairie grasses are active, but row crops have not yet fully matured (Hernandez-Santana et al., 2013). However, when the ground has been fully saturated during a large rainfall event, the effect of prairie strips may be limited. While the STRIPS team reported a 44% reduction in water runoff due to prairie strips (Iowa State University, 2021), research in Wisconsin suggests prairie strips can have very different effects in different regions (Sand County Foundation, 2021).

7.4 Wetland Restoration

Wetlands play an important ecosystem function and influence the hydrology of a watershed. Bullock and Acreman (2003) compiled a database of 439 published statements from 169 studies worldwide on the water quantity functions of wetlands. They found most floodplain wetlands reduce or delay floods, while headwaters wetlands typically either increase or have no effect on flood peaks. Bullock and Acreman also found evidence that wetlands evaporate more water than other land types, reducing flow in downstream rivers during dry periods.

A study in Iowa (Antolini et al., 2019) used a Soil Water Assessment (SWAT) hydrologic model to evaluate the runoff response of various agricultural BMPs in the Middle Cedar River Watershed. The authors developed several model scenarios consisting of a combination of BMPs "designed to progress towards goals identified by the Iowa Nutrient Reduction Strategy" for reduction of Nitrogen and Phosphorus, to include cover crops, reduced tillage, and grassed waterways. The authors also developed a wetlands scenario, in which wetlands were constructed in headwater reaches of the watershed. The study found the wetlands scenario to be the most effective at reducing flood economic losses but did not include an estimate of the construction and maintenance costs of the new wetlands.

A study funded by the International Joint Commission in the Rat River watershed in Manitoba, Canada following the 1997 flood event in the Red River of the North Basin (Simonovic & Juliano, 2001) used an HEC-HMS model to simulate low-frequency flood events under various wetland restoration scenarios. The study found wetlands can play a role in the magnitude of low-frequency flood events, with a greater wetland area corresponding to a decrease in flood volume. However, the magnitude of low-frequency flood peaks was not reduced in model simulations with a higher percentage of wetland area, and the authors ultimately concluded "the reduction in water volume is minimal in comparison to the amount of land to be restored."

8 HEC-HMS Watershed Delineation

Hydroconditioning of the digital elevation model (DEM) of the Black Earth Creek watershed was completed using ArcGIS Pro 2.4, and the GIS tools built into HEC-HMS 4.7 were used to create the geospatially-linked stream network, subbasins, and grid cell file necessary to run the HEC-HMS model.

8.1 DEM Processing

HEC-HMS uses a DEM of the watershed to develop the model elements and files. The DEM for the Black Earth Creek watershed was created by combining and clipping DEM files for Dane and Iowa counties. DEMs for both counties had cell sizes of 5 m x 5 m. The DEM files for each county were obtained by contacting each county directly.

To hydrocondition the resulting DEM, the "DEM Preparation" suite of tools in the Agricultural Conservation and Planning Framework (ACPF) toolbox (acpf_V3_Pro) was used (Porter et al., 2015). First, holes in the DEM were filled using the "DEM: Pit Fill/Hole Punch" tool, which removes all 'one cell sinks' and only retains 'true' depressions in the DEM. Then, impeded flows were visually identified by developing a depth grid and a flow network ("D8 Terrain Processing," "Identify Impeded Flow," and "Visualize Flowpaths" tools). Channels and boundary walls were then burned into the DEM at culverts, bridges, and roads using the "Manual cutter and dam builder" tool to more accurately capture the flow network in the watershed. This tool sets the elevation of all cells along a 'cut' line to the minimum

elevation of the DEM along the line and the elevation of all cells along a 'dam' line to the maximum elevation of the DEM along the line.

After hydroconditioning the DEM, it was reprojected to the Albers Conical Equal Area projected coordinate system and added to the HEC-HMS project. Within HEC-HMS, the GIS tools were used to create flow direction and flow accumulation rasters, identify the stream network, and delineate subbasins.

8.2 Subbasin Delineation

There is a total of 11 subbasins in the Black Earth Creek HMS model. Subbasins were delineated to capture each developed area in the watershed (Mazomanie, Black Earth, and Cross Plains) as well as each major tributary to Black Earth Creek (Brewery Creek, Vermont Creek, Wendt Creek, and Halfway Prairie Creek). The final subbasin delineation differentiates these elements and provides model outputs at important gaged locations.

8.3 Naming

Each subbasin and reach in the Black Earth Creek model follows a consistent naming convention using abbreviated names of upstream and downstream elements. Table 7 lists all abbreviations used in the model.

Table 7. Abbreviations used in the naming of subbasins and reaches in the Black Earth Creek HMS model

Abbreviation	Description	Abbreviation	Description
CP	Cross Plains, WI	BC	Brewery Creek
BE	Black Earth, WI	BEC	Black Earth Creek
MZ	Mazomanie, WI	VC	Vermont Creek
Out	outlet	HPC	Halfway Prairie Creek
us	upstream	WC	Wendt Creek
ds	downstream		

Subbasin names consist of the identifier "S_" followed by one or two abbreviations. The subbasins that encompass the villages of Mazomanie, Cross Plains, and Black Earth are labeled S_MZ, S_BE, and S_CP, respectively. Other subbasins are named for the upstream-most element and the downstream-most element. For example, the subbasin encompassing the area between Cross Plains and Black Earth is called S_BEC_ds_CP_to_BEC_us_BE, which translates to "subbasin from Black Earth Creek downstream of Cross Plains to Black Earth Creek upstream of Black Earth." Junction names consist of the identifier "J_" followed by two abbreviations. The first is the major stream, and the second is either the location relative to a developed area or, in the case of a confluence, the adjoining tributary. Reach names consist of the identifier "R_" followed by the upstream-most element and the downstream-most element.

8.4 Subbasin Definition

The subbasins adopted for the Black Earth Creek model are listed in Table 8 along with their associated drainage area. Reaches used in the model are shown in Table 9. A map of each subbasin in the model along with each reach and junction is shown in Figure 11.

Table 8. Subbasins in the Black Earth Creek HMS model

Subbasin Name	Subbasin Area (mi²)
S_BC_us_CP	9.0
S_BEC_us_CP	12.3
S_CP	4.5
S_BEC_ds_CP_to_BEC_us_BE	19.4
S_VC_us_BE	13.8
S_BE	3.1
S_BEC-VC_to_BEC_us_MZ	7.5
S_HPC_us_MZ	16.3
S_WC_us_MZ	10.7
S_MZ	3.1
S_BEC_ds_MZ_to_Out	3.4

Table 9. Reaches in the Black Earth Creek HMS model

Reach Name	Map Number
R_BEC_ds_MZ_to_Out	1
R_BEC-HPC_to_BEC_ds_MZ	2
R_HPC-WC_to_BEC-HPC	3
R_BEC_us_MZ_to_BEC-HPC	4
R_BEC-VC_to_BEC_us_MZ	5
R_VC_us_BE_to_BEC-VC	6
R_BEC_us_BE_to_BEC-VC	7
R_BEC_ds_CP_to_BEC_us_BE	8
R_BC-BEC_to_BEC_ds_CP	9
R_BC_us_CP_to_BC-BEC	10

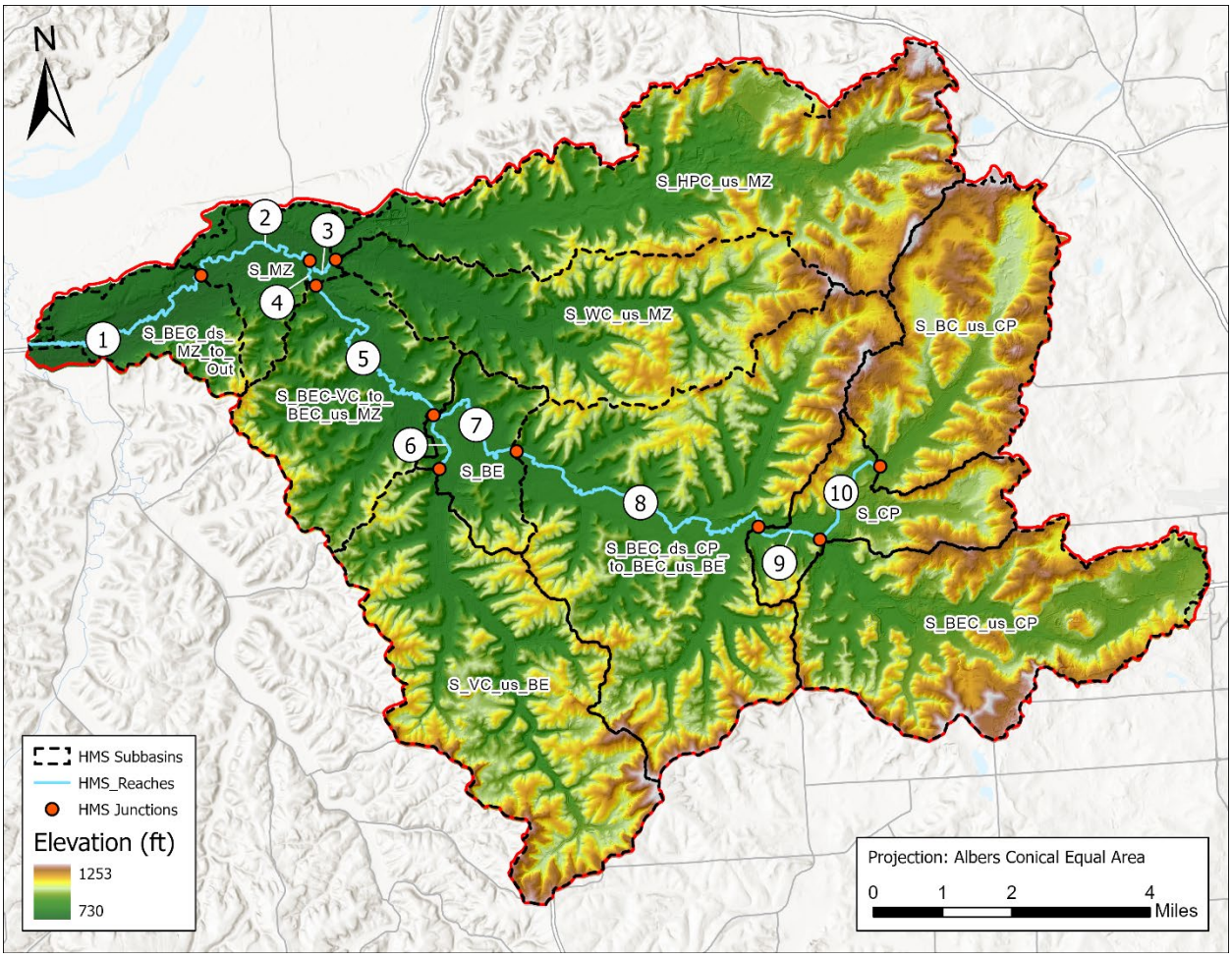

Figure 11. Subbasin delineation for Black Earth Creek HMS model

9 HEC-HMS Model Construction

The purpose of building the HEC-HMS model was to compare the current condition of the Black Earth Creek watershed to future conditions in which various green infrastructure or land use management practices are implemented. The model was constructed using HEC-HMS 4.7 (U.S. Army Corps of Engineers Hydrologic Engineering Center, 2020a). The HEC-HMS model utilized observed streamflow data from the United States Geological Survey (USGS). Basin travel time was originally determined from the Minnesota DNR's travel time tool (Minnesota Department of Natural Resources, 2020) and optimized to determine time of concentration (Tc) and shape/storage coefficient (R) unit hydrograph parameters for each subbasin.

9.1 Methods

Due to the comparative nature of this study and the understanding that an HEC-RAS hydraulic model with more detailed routing would be used later in the project, the Black Earth Creek HEC-HMS model utilizes fairly simple runoff and routing methods. The model uses Simple canopy method, the Initial and Constant loss method, the Mod Clark transform method, the Recession baseflow method, and the Muskingum routing method. No surface method was selected.

9.1.1 Canopy: Simple

This method is a simple representation of a plant canopy (U.S. Army Corps of Engineers Hydrologic Engineering Center, 2020b). All precipitation is intercepted until the canopy storage capacity is filled. Once the storage is filled, all further precipitation falls to the surface, or directly to the soil if no representation of the surface is included. All potential evapotranspiration is used to empty the canopy storage until the water in storage has been eliminated (U.S. Army Corps of Engineers Hydrologic Engineering Center, 2020b).

Typically, evapotranspiration is included in continuous HMS models that simulate multiple storm events to account for losses during dry periods (U.S. Army Corps of Engineers Hydrologic Engineering Center, 2020b). Since the Black Earth Creek HMS model is a comparative model that only simulates single storm events, and the land use changes investigated in this study are not expected to significantly alter the amount of evapotranspiration throughout the watershed, evaporation and evapotranspiration are not explicitly accounted for in the model. Therefore, all subbasins use the same values for the following canopy parameters: initial storage (%) = 0, max storage (in) = 0, crop coefficient = 1.0, and the simple uptake method. Evapotranspiration rates are not included in the meteorological model.

9.1.2 Rainfall-Runoff Transform: Mod Clark Parameterization

The Mod Clark method is a linear, quasi distributed transform method that is based on the Clark conceptual unit hydrograph (U.S. Army Corps of Engineers Hydrologic Engineering Center, 2020b). It fundamentally represents the subbasin as a collection of grid cells (U.S. Army Corps of Engineers Hydrologic Engineering Center, 2020b). The Clark method uses a time-area curve and the time of concentration (Tc) to develop a translation hydrograph (U.S. Army Corps of Engineers Hydrologic Engineering Center, 2020b). The time of concentration defines the maximum travel time in the subbasin. The Mod Clark method eliminates the time-area curve and instead uses a separate travel time index for each individual grid cell included in the model. (U.S. Army Corps of Engineers Hydrologic Engineering Center, 2020b). The travel time index for each cell is scaled by the overall time of concentration. Excess precipitation falling on each grid cell is lagged by the scaled time index and then routed through a linear

reservoir. The outputs from the routing are then combined to produce the final hydrograph (U.S. Army Corps of Engineers Hydrologic Engineering Center, 2020b).

A time of concentration grid was produced using the Minnesota DNR Travel Time Tool (Minnesota Department of Natural Resources, 2020), a GIS-based tool that uses the watershed DEM to produce an estimate of the time of concentration for each grid cell in the basin. The Travel Time Tool employs the National Land Cover Database (NLCD) and National Wetland Inventory (NWI) connectors as well as DEM and flow accumulation rasters to characterize the flow conditions for each grid cell in the model. The NLCD defines the land cover and Manning's roughness coefficient which affects travel time. The NWI connector helps define the type of surface (lake, river, wetland, crop land) that affects the travel speed. The flow accumulation grid helps to define the size of the channel as it travels through the sub-basin. The computed Tc values were used as initial Tc parameters for each sub-basin prior to calibration.

The relationship between Clarks' storage coefficient (R) and Tc varies geographically, and previous studies in the region can be used to inform the initial selection of the storage coefficient parameter. To estimate initial values of R, the calibrated HEC-HMS model for the *2017 CWMS HEC-HMS Model Development of the Upper Mississippi River between Anoka, MN and Lock and Dam 10* study (U.S. Army Corps of Engineers, St. Paul District, 2020) was used. In this model, the WI04_BlackEarthCK subbasin encompasses the Black Earth Creek watershed. The calibrated R/(Tc+R) relationship for the WI04_BlackEarthCK subbasin was approximately 0.8. This R/(Tc+R) relationship was used to compute initial estimates of R in the Black Earth Creek model using the computed Tc values from the Minnesota DNR Travel Time Tool.

During calibration, the Tc and R values were adjusted as needed for each subbasin. On average, subbasin Tc and R values were reduced by approximately 10%, and the R/(Tc+R) relationship of 0.8 was maintained. Initial Tc and R values for each subbasin are shown in Table 10.

Table 10. Initial Mod Clark parameters for the Black Earth Creek HMS model

Subbasin Name	Initial Tc	Initial R	Initial R/(Tc+R)
S_BC_us_CP	3.445	13.78	0.8
S_BEC_us_CP	3.564	14.256	0.8
S_CP	2.911	11.644	0.8
S_BEC_ds_CP_to_BEC_us_BE	5.348	21.392	0.8
S_VC_us_BE	5.596	22.384	0.8
S_BE	3.125	12.5	0.8
S_BEC-VC_to_BEC_us_MZ	3.900	15.6	0.8
S_HPC_us_MZ	9.327	37.308	0.8
S_WC_us_MZ	7.656	30.624	0.8
S_MZ	3.716	14.864	0.8
S_BEC_ds_MZ_to_Out	5.831	23.324	0.8

9.1.3 Loss: Initial and Constant

The Initial and Constant loss method is an appropriate loss method for this study, because the Black Earth Creek model is an event-based model that does not simulate the effects of evaporation or

evapotranspiration between storm events. The constant loss rate can also be modified to approximate changes in soil infiltration rates due to land use change, which accomplishes the goal of this study.

The Initial and Constant loss method is a simple representation of the soil layer. This method specifies the amount of incoming precipitation that will be infiltrated or stored in the watershed before surface runoff begins (U.S. Army Corps of Engineers Hydrologic Engineering Center, 2020b). Runoff begins once the initial deficit storage is used up and if the precipitation rate exceeds the infiltration rate. The constant loss rate determines the rate of infiltration that will occur after the initial loss is satisfied (U.S. Army Corps of Engineers Hydrologic Engineering Center, 2020b). If the constant loss rate exceeds the precipitation rate, no runoff occurs.

The percentage of each subbasin that is impervious area is also specified. In this method, no loss calculations are carried out on the impervious area; all precipitation on that portion of the subbasin is converted to direct runoff (U.S. Army Corps of Engineers Hydrologic Engineering Center, 2020b).

9.1.3.1 Initial Loss

During calibration, the initial loss was the most sensitive model parameter and varied considerably from event to event. In all calibration events, the initial loss varied by subbasin. Average initial loss across all calibrated subbasins ranged from 0.15 in to 7.18 in. Further discussion regarding the large variability in constant loss values selected for the model can be found in Section 9.4.2.

9.1.3.2 Constant Loss Rate

To estimate initial constant loss rates for each subbasin, the gridded SSURGO (GSSURGO) product produced by the Natural Resources Conservation Service (NRCS) was used. Through linkage of various GSSURGO soil tables, a grid of representative saturated hydraulic conductivity (Kat_R) was computed for the top horizon (H1) of the GSSURGO soil layer. The H1 horizon of the GSSURGO soils extends from the ground surface to approximately 30 cm below the surface. The mean value of Ksat_R was computed for each subbasin in the HMS model using the Zonal Statistics tool in ArcGIS using the subbasin polygons to define the zones.

In the Black Earth Creek model, because evapotranspiration rates are not explicitly defined, the constant loss rate accounts for all forms of loss from the soil. However, in this study it is assumed the majority of loss during a rainfall-driven, summer or fall flood event is due to infiltration. Therefore, initial values for the constant rate (in/hr) were set to the average Ksat_R for each subbasin. Table 11 shows the initial constant loss rates for each subbasin as well as the ratio of each loss rate to the summation of all loss rates in the watershed.

Table 11. Initial constant loss rates in the Black Earth Creek HMS model

Subbasin Name	Initial Constant Rate (in/hr)	Initial Ratio
S_BC_us_CP	2.677	0.08
S_BEC_us_CP	1.878	0.05
S_CP	2.219	0.06
S_BEC_ds_CP_to_BEC_us_BE	1.803	0.05
S_VC_us_BE	1.741	0.05
S_BE	1.839	0.05
S_BEC-VC_to_BEC_us_MZ	2.523	0.07
S_HPC_us_MZ	2.757	0.08
S_WC_us_MZ	2.767	0.08
S_MZ	6.961	0.20
S_BEC_ds_MZ_to_Out	7.904	0.23

During calibration, the initial constant loss rates corresponding to Ksat_R were too high. To match the magnitudes of observed flood peaks, constant rates were decreased substantially. However, the spatial distribution of loss rates across the watershed was maintained as much as possible during the calibration process. Subbasins that had the largest Ksat_R values generally have the largest calibrated constant loss rates, and subbasins that had the smallest Ksat_R values generally have the smallest calibrated constant loss rates. After calibration, loss rates were compared to typical values of saturated hydraulic conductivity published by Rawls, et. al. (1982) for the soils that make up the majority of the basin (silty to sandy loam) to ensure the values adopted during calibration were reasonable.

9.1.3.3 Impervious Percentage

The percent impervious value in HEC-HMS represents the percentage of the subbasin which is directly connected impervious area. No loss calculations are carried out on the impervious area. All precipitation on the impervious portion of a subbasin becomes excess precipitation and is subject to surface storage and direct runoff. Impervious area for each subbasin in the Black Earth Creek HMS model was computed using the NLCD 2016 Percent Developed Imperviousness dataset (U.S. Geological Survey, 2020). The NLCD 2016 Percent Developed Imperviousness dataset represents urban impervious surfaces as a percentage of developed surface over every 30-meter pixel in the United States. To compute impervious percentage for each subbasin, the Zonal Statistics tool within ArcGIS was utilized using subbasin polygons to define zones. The resulting total impervious areas for each subbasin shown in Table 12 were adopted for the model.

Table 12. Percentage of impervious area for each subbasin in the Black Earth Creek HMS model

Subbasin Name	Impervious Area (%)
S_BC_us_CP	6
S_BEC_us_CP	10
S_CP	21
S_BEC_ds_CP_to_BEC_us_BE	5
S_VC_us_BE	4
S_BE	18
S_BEC-VC_to_BEC_us_MZ	6
S_HPC_us_MZ	4
S_WC_us_MZ	5
S_MZ	24
S_BEC_ds_MZ_to_Out	7

9.1.4 Baseflow: Recession

The recession baseflow technique was used in this study. Recession baseflow is described using an initial discharge per square mile, a recession constant, and a ratio to peak. The initial discharge per square mile represents the amount of baseflow before the storm event occurs and the model begins producing runoff (U.S. Army Corps of Engineers Hydrologic Engineering Center, 2020b). This value was adjusted in calibration to match the observed hydrographs at the start of the simulation. The recession constant describes the rate at which baseflow recedes between storm events (U.S. Army Corps of Engineers Hydrologic Engineering Center, 2020b). An initial recession constant was estimated based on the modeling results for the *2017 CWMS HEC-HMS Model Development of the Upper Mississippi River between Anoka, MN and Lock and Dam 10* study (U.S. Army Corps of Engineers, St. Paul District, 2020). The ratio to peak describes how to reset the baseflow. When the ratio of the current flow value divided by the peak is below the specified ratio to peak value, the baseflow is reset (U.S. Army Corps of Engineers Hydrologic Engineering Center, 2016b). The initial values of the ratio to peak were adopted from the CWMS modeling efforts of the study area (U.S. Army Corps of Engineers, St. Paul District, 2020). Initial values for the recession constant and ratio to peak for each subbasin in the Black Earth Creek model are shown in Table 13.

Table 13. Initial baseflow parameters in the Black Earth Creek HMS model

Subbasin Name	Initial Recession Constant	Initial Ratio to Peak
S_BC_us_CP	0.95	0.2
S_BEC_us_CP	0.95	0.2
S_CP	0.95	0.2
S_BEC_ds_CP_to_BEC_us_BE	0.95	0.2
S_VC_us_BE	0.95	0.2
S_BE	0.95	0.2
S_BEC-VC_to_BEC_us_MZ	0.95	0.2
S_HPC_us_MZ	0.95	0.2
S_WC_us_MZ	0.95	0.2
S_MZ	0.95	0.2
S_BEC_ds_MZ_to_Out	0.95	0.2

It is important to note the recession baseflow method does not conserve mass during a simulation. After the ratio to peak is reached, the model adds volume to maintain the recession baseflow. However, this added volume did not impact the calibration of the Black Earth Creek HMS model, as model results indicated volume was not added to the hydrograph until after the flood peak had receded.

9.1.5 Routing: Muskingum

The HEC-HMS software offers multiple methods for simulating routing through a channel reach. Commonly employed methods include Mod Puls routing, Muskingum-Cunge routing, and Muskingum routing. The Muskingum routing method was used for this study, because it uses the fewest model parameters while still adequately modeling the travel time and attenuation of the flood wave. Any alternatives that require a more detailed routing model, such as re-meandering of Black Earth Creek, would be evaluated using an HEC-RAS model.

Inputs for the Muskingum routing method are the Muskingum K (hr), the Muskingum X, and the number of subreaches. The Muskingum K estimates the travel time through a particular reach. Muskingum X represents a weighting between inflow and outflow, and ranges from 0 to 0.5, where 0 represents maximum attenuation and 0.5 represents no attenuation. The number of subreaches affects the attenuation of the hydrograph, where a value of 1 represents maximum attenuation.

The Muskingum K parameter was initially estimated by computing the difference in time of concentration between the upstream-most and downstream-most junctions. The Muskingum X parameter was initially set to 0.25, and the number of subreaches was initially set to 1. Throughout the calibration process, the Muskingum K and X parameters were adjusted to match the shape of the observed hydrograph while the number of subreaches stayed constant. Initial routing parameters are shown in Table 14.

Table 14. Initial Muskingum routing parameters in the Black Earth Creek HMS model

Reach	Initial Parameters		
	K (hrs)	X	Subreaches
R_BEC_ds_MZ_to_Out	0.346	0.25	1
R_BEC-HPC_to_BEC_ds_MZ	0.324	0.25	1
R_HPC-WC_to_BEC-HPC	2.507	0.25	1
R_BEC_us_MZ_to_BEC-HPC	1.104	0.25	1
R_BEC-VC_to_BEC_us_MZ	0.271	0.25	1
R_VC_us_BE_to_BEC-VC	1.988	0.25	1
R_BEC_us_BE_to_BEC-VC	0.148	0.25	1
R_BEC_ds_CP_to_BEC_us_BE	0.289	0.25	1
R_BC-BEC_to_BEC_ds_CP	1.054	0.25	1
R_BC_us_CP_to_BC-BEC	1.943	0.25	1

9.2 Control Specifications

The control specifications specify the start and end dates of a simulation and the computational time interval used in the simulation (U.S. Army Corps of Engineers Hydrologic Engineering Center, 2020b). The control specifications for each calibration and verification event were set up to capture the precipitation causing the runoff response as well as the complete runoff hydrograph. Generally, model simulations began several days prior to the start of a rainfall event and continued past the hydrograph peak until the discharge appeared to reach baseflow conditions. A 15-minute computation step was used. This modeling effort only included rainfall runoff modeling and did not include events which were affected by snowmelt. Table 15 summarizes the control specifications used for the calibration and validation events.

Table 15. Control specifications for the Black Earth Creek HMS model

Purpose	Event	Simulation Start Date	Simulation End Date
Calibration	Sep-Oct 2019	28 Sep 2019	10 Oct 2019
Calibration	Aug 2018	18 Aug 2018	31 Aug 2018
Calibration	Jul 1993	03 Jul 1993	14 Jul 1993
Validation	Jul 2017	17 Jul 2017	27 Jul 2017
Validation	Jun 2016	12 Jun 2016	19 Jun 2016
Validation	Jul-Aug 2001	30 Jul 2001	06 Aug 2001

9.3 Calibration and Validation

Once the HEC-HMS model was constructed, it was calibrated to three large, rainfall-driven flood events to model the rainfall-runoff response of the basin. Events were selected to capture large, rainfall-driven flood events at the Black Earth Creek at Black Earth, WI gage (USGS 05406500) during the period in which 15-minute data is available at the site (1986-2019). The number of streamflow gages that recorded data during the event was also considered when selecting calibration events. Snowmelt-driven

events were not selected, because and alternatives selected for analysis are likely to primarily affect runoff from rainfall.

Table 16 lists each calibration event along with its peak flow and rank among all flood events taking place during the months of May through November between 1986 and 2019 at the Black Earth Creek at Black Earth, WI gage. The number of gage locations with 5-minute or 15-minute discharge data during the event is also listed. Annual exceedance probabilities for each event were determined from the flow frequency analysis conducted as part of this study, included in Appendix E.

Table 16. Events used to calibrate the Black Earth Creek HMS model

Calibration Event	Peak Flow at Black Earth (cfs)	Rank at Black Earth	Exceedance Probability	Number of Locations with Observed Data
Sep-Oct 2019	1,060	4	13%	4
Aug 2018	2,930	1	0.3%	4
Jul 1993	1,320	3	6%	2

To ensure the HEC-HMS model reliably models observed events, the model was validated with three rainfall-driven flood events. Table 17 shows each validation event along with its peak flow at Black Earth, rank among flood events taking place during the months of May through November between 1986 and 2019, and number of gage locations with 5-minute or 15-minute discharge data. Validation events were selected to capture large flood events in the observed record while making use of as much observed data as possible. Since NEXRAD precipitation data is only available after 2008, more recent events were given higher priority when determining which events to include for validation. Although the 2016 and 2017 events were smaller in magnitude than some other flood events in the basin, they had observed data for a large number of gage locations and could therefore be used to validate calibration of subbasins at and above Cross Plains.

Table 17. Events used to validate the Black Earth Creek HMS model

Validation Event	Peak Flow at Black Earth (cfs)	Rank at Black Earth	Exceedance Probability	Number of Locations with Observed Data
Jul 2017	546	10	40%	4
Jun 2016	663	9	32%	4
Jul-Aug 2001	1,720	2	3%	1

9.3.1 Calibration Parameters and Approach

The parameters used to calibrate the Black Earth Creek HMS model included subbasin parameters for the constant loss rate, the Mod Clark time of concentration (Tc) and storage coefficient (R), the baseflow recession constant, and the ratio to peak, as well as the Muskingum K and X routing parameters for each reach. The initial parameters shown in Section 9.1 were used as initial parameters in each calibration event model. The initial loss parameter was assumed to be zero prior to calibration for each event, and the initial baseflow was determined for each event based on observed streamflow at the beginning of the simulation period. Subbasin area and impervious percentage were not used as calibration parameters and remained constant for all events.

The Black Earth Creek HMS model was calibrated from upstream to downstream. The two subbasins upstream of Cross Plains (S_BC_us_CP and S_BEC_us_CP) were calibrated to observed discharges at their outlets. Then, the subbasin for the Village of Cross Plains (S_CP) was calibrated using observed discharges just downstream of Cross Plains. Finally, the subbasin between Cross Plains and Black Earth (S_BEC_ds_CP_to_BEC_us_BE) was calibrated to observed discharges at the Black Earth Creek at Black Earth, WI gage. As much as possible, spatial variation of physical properties was maintained across the subbasins, as shown previously in Table 10 and Table 11. A summary of each calibration parameter and the corresponding approach during calibration is shown in Table 18. A complete list of all initial and calibrated model parameters for each subbasin and routing reach in the Black Earth Creek HMS model is included in Appendix B.

Table 18. Summary of calibration approach for each parameter in the Black Earth Creek HMS model

Parameter	Calibration Approach
Constant Loss Rate	Basin-average saturated hydraulic conductivity (Ksat) values were estimated from GSSURGO soil data as an initial constant loss rate estimate. The goal was to obtain reasonable loss rates across the basin that reflected the given soil types and maintained the spatial distribution of the Ksat values present in the GSSURGO soil data.
Initial Loss Rate	Initial loss was adjusted independently for each calibration event and therefore is not consistent across all three calibration events. This parameter is highly dependent upon antecedent moisture conditions in the watershed and varies greatly from event to event.
Percent Impervious	Percent impervious was computed using the NLCD 2016 Percent Impervious land cover dataset. Initial estimated values were not changed during the calibration process.
Time of Concentration (Tc)	Time of concentration grids were produced utilizing the MN DNR travel time tool. The goal was to identify a consistent Tc value for each subbasin for all three calibration events.
Storage Coefficient (R)	Initial R/(Tc+R) values adopted from a previously calibrated HMS model of the Trempealeau River (U.S. Army Corps of Engineers, St. Paul District, 2020) were used to estimate the storage coefficient. The goal was to maintain consistent basin-averaged R/(Tc+R) values for each subbasin.
Initial Baseflow	Initial baseflow was estimated using observed streamflow data for each calibration event and therefore is not consistent across all three calibration events.
Recession Constant	Initial recession constants were adopted from a previously calibrated HMS model (U.S. Army Corps of Engineers, St. Paul District, 2020). The goal was to determine a consistent recession constant for each subbasin across all three calibration events.
Ratio to Peak	Initial ratio to peak values were adopted from a previously calibrated HMS model (U.S. Army Corps of Engineers, St. Paul District, 2020). The goal was to determine a consistent ratio to peak for each subbasin across all three calibration events.
Routing	Muskingum routing was utilized throughout the model. The goal was to obtain adequate timing of flows through each reach.

Since no streamflow data was available downstream of the Black Earth Creek at Black Earth, WI gage, and all subbasins downstream of the gage have similar physical characteristics, all subbasins downstream of the Black Earth gage were grouped together, and their calibration parameters were adjusted according to the average change from initial parameter values in the upstream, calibrated subbasins. An example of this process is shown in Table 19.

Table 19. Methodology for calibrating parameters of subbasins lacking observed data

Subbasin		Constant Loss Rate		
		Initial Estimate	Calibrated Value	% of Initial
Observed data available	S_BC_us_CP	2.677	0.669	25%
	S_BEC_us_CP	1.878	0.619	33%
	S_CP	2.219	0.466	21%
	S_BEC_ds_CP_to_BEC_us_BE	1.803	0.316	18%
Observed data is not available	S_VC_us_BE	1.741	0.420	24%
	S_BE	1.839	0.444	24%
	S_BEC-VC_to_BEC_us_MZ	2.523	0.609	24%
	S_HPC_us_MZ	2.757	0.665	24%
	S_WC_us_MZ	2.767	0.667	24%
	S_MZ	6.961	1.679	24%
	S_BEC_ds_MZ_to_Out	7.904	1.906	24%

A similar process was used to estimate initial loss for uncalibrated subbasins. However, representative values for available water storage within the soil column were used for each subbasin in place of the 'Initial Estimate' values shown in Table 19. To estimate available water storage within the soil for each subbasin, the GSSURGO product produced by the NRCS was used. Through linkage of various GSSURGO soil tables, a grid of representative available water storage was computed for the first 150 cm of soil depth (AWS0150). The mean value of AWS0150 was computed for each subbasin in the HMS model using the Zonal Statistics tool in ArcGIS using subbasin polygons to define the zones.

9.3.2 Calibration Targets

The goal for calibration was to match the timing of the observed flood peak, the shape of the observed hydrograph, the magnitude of the observed flood peak, and the volume of discharge during the simulation period for three calibration events and three validation events. Nash-Sutcliffe Efficiency Index Coefficients were computed for each calibration event to assess how well the simulated results replicate the observed data. Nash-Sutcliffe Coefficients can range from negative infinity to one. A coefficient of one indicates the model being applied is able to replicate observed data exactly. Typically, a Nash-Sutcliffe Coefficient of 0.7 or greater indicates the model adequately represents the observed data. In this report, calibration and validation results are shown at the Black Earth Creek at Black Earth, WI gage. To view calibration and validation results at all gage locations, see Appendix C.

Observed streamflow used for calibration was either recorded on a 5-minute or 15-minute timestep. Gridded precipitation data was measured hourly, and the HEC-HMS model is computed on a 15-minute timestep.

9.3.3 September-October 2019 Calibration Event

The September-October 2019 calibration event simulation began on 28 Sep 2019 and ended on 10 Oct 2019. 2019 was a wet year, with a significant, snowmelt-driven flood event in March followed by several rainfall-driven flood events with peak flows of at least 500 cfs at Black Earth throughout the summer and

early fall. In the 10 days leading up to the simulation period, the average rainfall recorded at the Mazomanie WWTP and Charmany Farm weather stations was 0.16 inches.

The Nash-Sutcliffe Coefficient for the September-October 2019 calibration event at the Black Earth Creek at Black Earth, WI gage (model element: J_BEC_us_BE) is 0.888. The model replicates the magnitude of the observed flood peak and the shape of the observed hydrograph well, although the timing of the flood peak is several hours earlier in the model.

Figure 12 shows how the modeled discharge compares to observed data at the Black Earth gage for the September-October 2019 event. The 'Sep 2019 Calibration' discharge is the model output using the final calibration parameters for the 2019 event. Observed data was recorded on a 15-minute timestep. Table 20 shows how the model results compare to observed data at Black Earth in terms of calibration metrics.

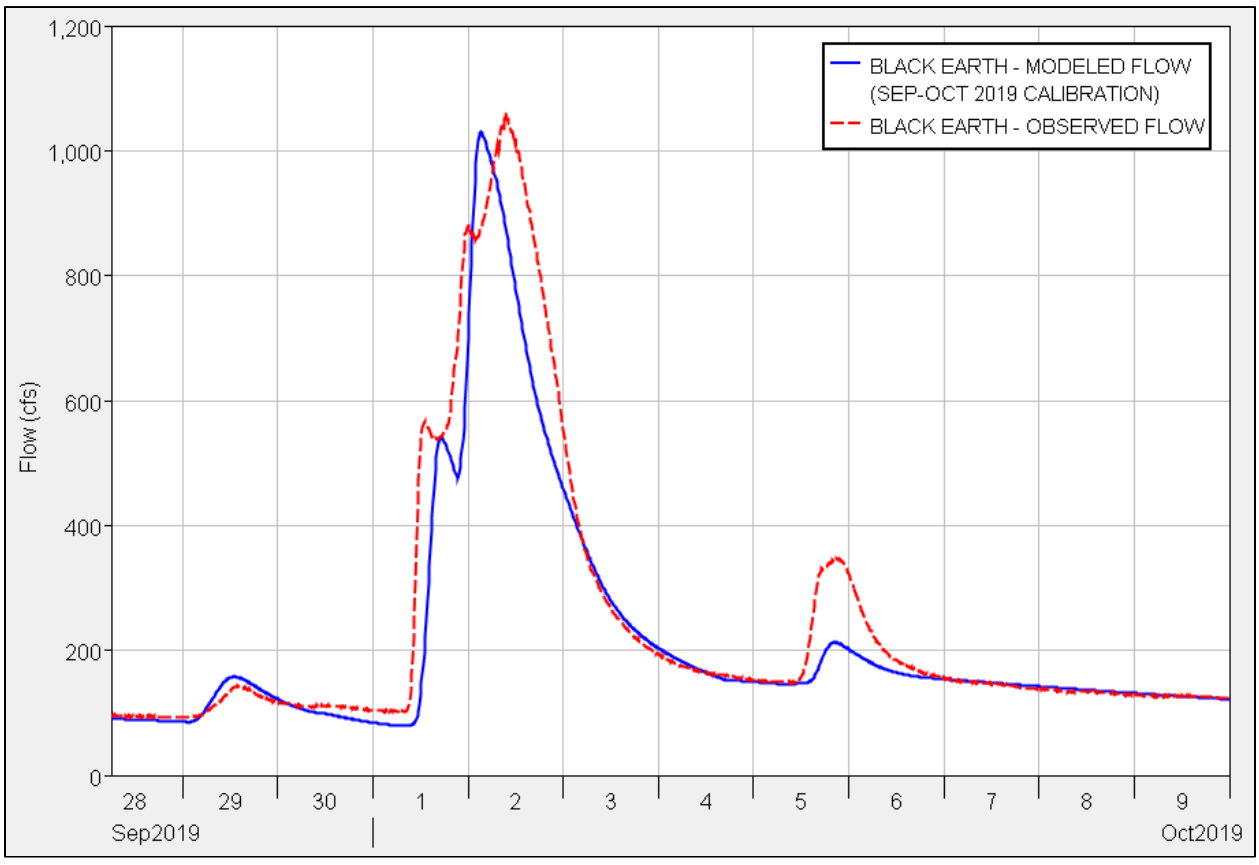

Figure 12. Calibration results for Sep-Oct 2019 event - Black Earth, WI

Table 20. Comparison of modeled and observed calibration metrics for Sep-Oct 2019 event - Black Earth, WI

J_BEC_us_BE	Calibrated Model	Observed Data	Difference
Peak Discharge (cfs)	1,031	1,060.0	-2.8%
Volume (in)	2.09	2.35	-11.1%
Timing of Peak (date, time)	02 Oct, 03:15	02 Oct, 09:30	-6.25 hrs
Nash-Sutcliffe Coefficient	0.888		

9.3.4 August 2018 Calibration Event

The August 2018 calibration event simulation began on 18 Aug 2018 and ended on 31 Aug 2018. 2018 began with the largest snowmelt-drive flood event ever recorded at the Black Earth gage (1,190 cfs) in late February. However, during the summer months, the basin was relatively dry, and flow at the Black Earth gage did not exceed 150 cfs during the months of July and August prior to the flood event. In the 10 days leading up to the simulation period, the average rainfall recorded at the Mazomanie WWTP and Charmany Farm weather stations was 0.12 inches. During the simulation period, record rainfall across the region translated to the largest flood event in recorded history on Black Earth Creek, with a peak flow of 2,930 cfs at Black Earth.

The Nash-Sutcliffe Coefficient for the August 2018 calibration event at the Black Earth Creek at Black Earth, WI gage (model element: J_BEC_us_BE) is 0.904. The model replicates the timing and magnitude of the observed flood peak and the shape of the observed hydrograph well.

Figure 13 shows how the modeled discharge compares to observed data at Black Earth for the August 2018 event. The 'Aug 2018 Calibration' discharge is the model output using the final calibration parameters for the 2018 event. Observed data was recorded on a 15-minute timestep. Table 21 shows how the model results compare to observed data at Black Earth in terms of calibration metrics.

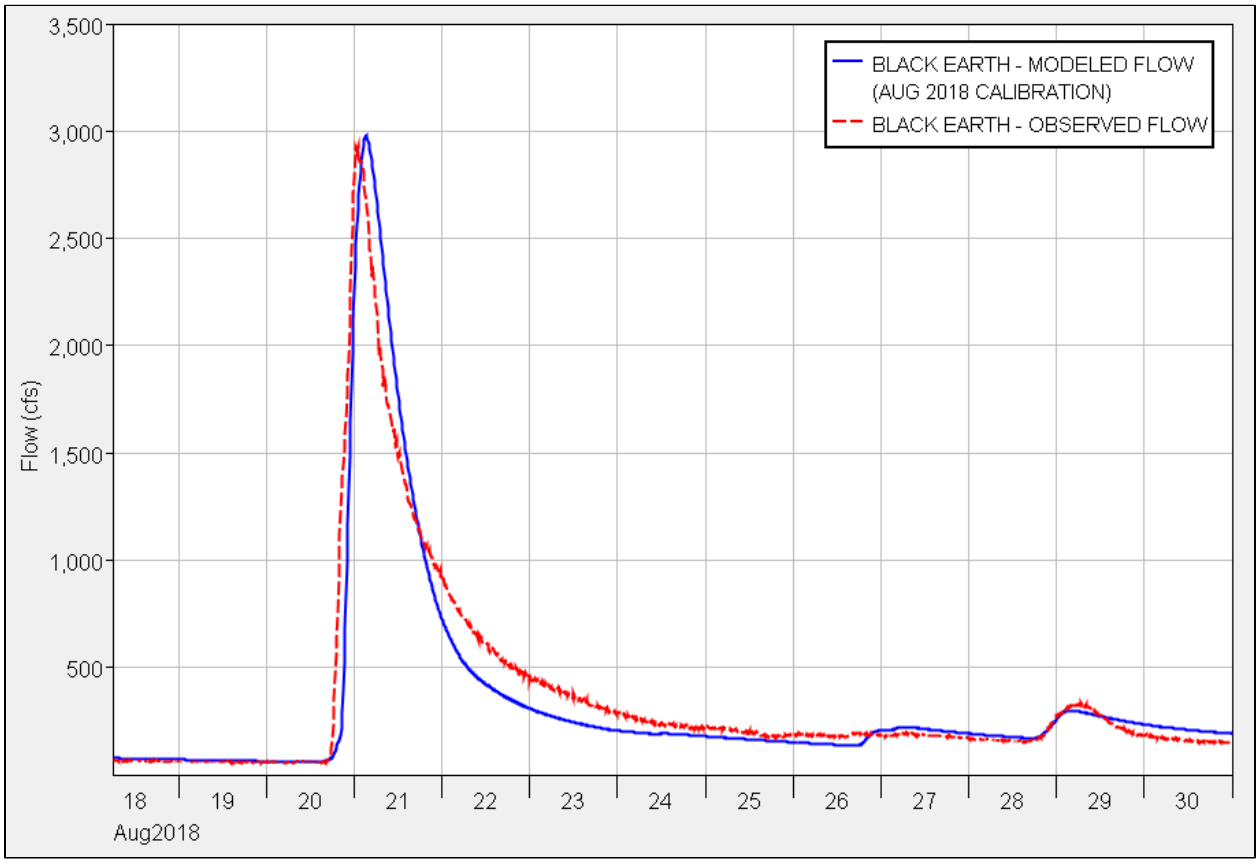

Figure 13. Calibration results for Aug 2018 event - Black Earth, WI

Table 21. Comparison of modeled and observed calibration metrics for Aug 2018 event - Black Earth, WI

J_BEC_us_BE	Calibrated Model	Observed Data	Difference
Peak Discharge (cfs)	2,978	2,930.0	+1.6%
Volume (in)	3.52	3.72	-5.4%
Timing of Peak (date, time)	21 Aug, 03:15	21 Aug, 01:00	+2.25 hrs
Nash-Sutcliffe Coefficient	0.904		

9.3.5 July 1993 Calibration Event

The July 1993 calibration event simulation began on 03 Jul 1993 and ended on 14 Jul 1993. 1993 began with a slow snowmelt that did not result in a flood event at Black Earth. A moderate rainfall event occurred in June, but flow at Black Earth remained below 300 cfs. In the 10 days leading up to the simulation period, the Charmany Farm weather station recorded 0.19 inches of rain.

The Nash-Sutcliffe Coefficient for the July 1993 calibration event at the Black Earth Creek at Black Earth, WI gage (model element: J_BEC_us_BE) is 0.864. The model replicates the timing and magnitude of the observed flood peak and the shape of the observed hydrograph well.

Figure 14 shows how the modeled discharge compares to observed data at Black Earth for the July 1993 event. The 'Jul 1993 Calibration' discharge is the model output using the final calibration parameters for the 1993 event. Observed data was recorded on a 15-minute timestep. Table 22 shows how the model results compare to observed data at Black Earth in terms of calibration metrics.

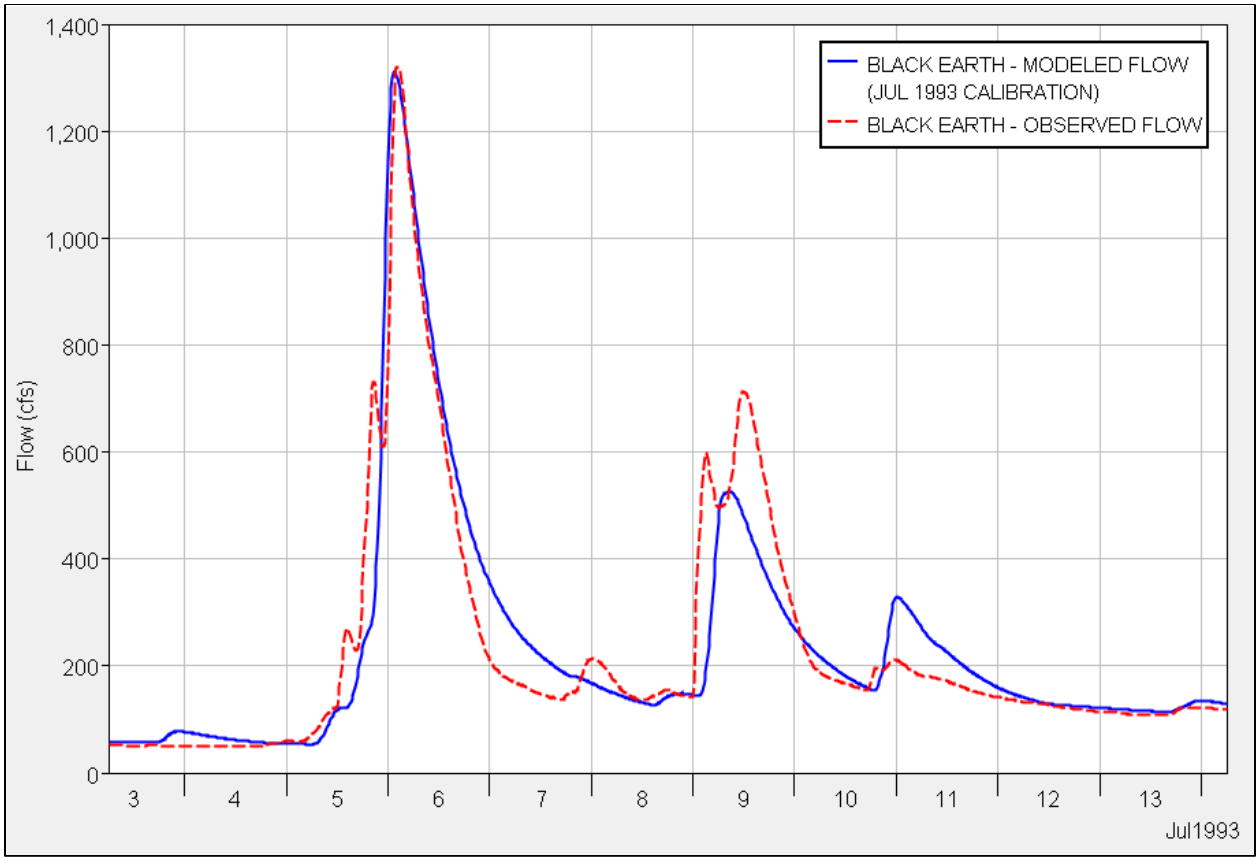

Figure 14. Calibration results for Jul 1993 event - Black Earth, WI

Table 22. Comparison of modeled and observed calibration metrics for Jul 1993 event - Black Earth, WI

J_BEC_us_BE	Calibrated Model	Observed Data	Difference
Peak Discharge (cfs)	1,311	1,320	-0.7%
Volume (in)	2.11	2.08	+1.4%
Timing of Peak (date, time)	06 Jul, 01:30	06 Jul, 02:00	-0.5 hrs
Nash-Sutcliffe Coefficient	0.864		

9.3.6 Model Refinement

Each calibration simulation event was calibrated independently, and then the parameters achieved in calibration for all three events were compared to each other. In general, the parameters determined for each event were similar; however, there were some differences in constant loss rates and significant differences in initial loss. Attempts were made to minimize differences in parameter values from event to event while still meeting the calibration targets as much as possible. Baseflow, transform, routing, and constant loss rate parameters were adjusted to be relatively consistent from event to event. Initial loss was adjusted as needed to match the magnitude of observed flood peaks, because differences in magnitudes between modeled and observed flows could not be resolved by adjusting the constant loss rate and maintaining a realistic range of constant loss rates between calibration events. The process of calibration and refinement was iterative. Ultimately, one set of final, refined calibration parameters was selected. These calibration parameters are referred to as the “generalized parameters” and are used for

model validation and alternative simulations. The final set of calibrated parameters included baseflow parameters (Recession Constant and Ratio to Peak), transform parameters (Tc and R), routing parameters (Muskingum K and X), and constant loss rate. Initial baseflow and initial loss were allowed to vary from event to event for each subbasin.

In general, the calibrated, generalized parameter model replicates the timing of the observed flood peaks well and replicates the shape of the observed hydrograph at each gage location to a reasonable degree for all three calibration events. The generalized parameter model also closely matches the magnitude of observed flood peaks. Figure 15 shows an example of a calibration event simulation before and after model refinement. The 'Sep-Oct 2019 Calibration' simulation is the independent event calibration (before model refinement), and the 'Generalized Parameters' simulation was run after the model refinement process.

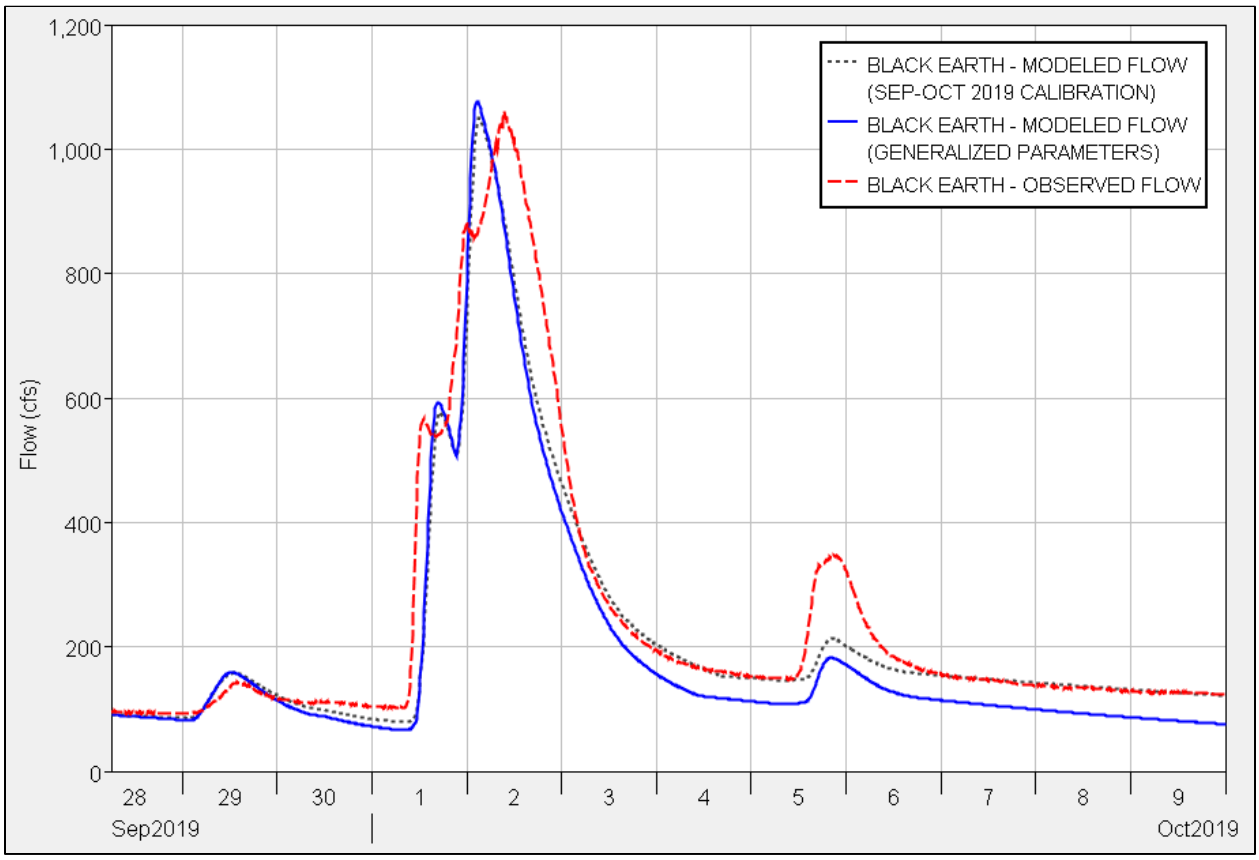

Figure 15. Comparison of independently calibrated event and generalized parameters, Sep-Oct 2019 calibration event - Black Earth Creek HMS model

The ability of the model to match observed flood peaks is due in large part to the fact that initial loss was allowed to vary from event to event. In the Black Earth Creek HMS model, the initial loss parameter is the most sensitive parameter that determines the magnitude of the flood peak. However, initial loss is known to vary between flood events and can be highly dependent on antecedent soil moisture conditions. Further exploration of the antecedent conditions that may drive the initial loss values for each calibration event is conducted in Section 9.4.2. The consistency in the other transform, routing, and constant loss rate parameters that were selected in the model refinement process across all three

calibration events is a good indicator that the selected model parameters adequately reflect the runoff response of the watershed.

9.3.7 Estimating Initial Baseflow for Validation Events

To estimate initial baseflow for each validation event, the initial baseflow identified for each subbasin was averaged between each calibration event. These average values were used in a preliminary simulation of each validation event. Then, subbasin initial baseflow values were adjusted to replicate observed data where observed streamflow data was available.

9.3.8 Estimating Initial Loss for Validation Events

Since the initial loss parameter was the most sensitive model parameter that determined how well the model replicated the magnitude of observed flood peaks, and initial loss varies from event to event, a means of estimating initial loss was required for each validation event. To estimate this parameter, the initial loss identified for each subbasin was averaged between each calibration event. These average values were used in a preliminary simulation of each validation event. Then, all initial loss values were uniformly multiplied by a factor such that the modeled peak flow at the Black Earth Creek at Black Earth, WI gage matched the observed peak. An example of this procedure is shown in Table 23 for the July 2017 validation event. Additional analysis discussed in Section 9.4.2 indicates the estimated initial loss values reasonably correspond to antecedent moisture conditions in the basin for each validation event.

Table 23. Procedure for estimating initial loss for validation events

Subbasin Name	Preliminary Initial Loss (avg. of calibration events)	Estimated Initial Loss for 2017 Validation Event	Multiplier
S_BC_us_CP	2.47	1.59	0.64
S_BEC_us_CP	4.72	3.03	0.64
S_CP	3.42	2.19	0.64
S_BEC_ds_CP_to_BEC_us_BE	3.88	2.50	0.64
S_VC_us_BE	2.88	1.86	0.64
S_BE	3.59	2.31	0.64
S_BEC-VC_to_BEC_us_MZ	3.37	2.17	0.64
S_HPC_us_MZ	3.53	2.26	0.64
S_WC_us_MZ	3.35	2.16	0.64
S_MZ	2.51	1.61	0.64
S_BEC_ds_MZ_to_Out	2.33	1.50	0.64

9.3.9 July 2017 Validation Event

The July 2017 validation event simulation began on 17 Jul 2017 and ended on 27 Jul 2017. 2017 was not a particularly dry or particularly wet year. The snowmelt-driven event that occurred in late January was small, and no significant flood events occurred leading up to the July rain event. The July rain event itself resulted in a moderate flood, with a peak flow of 546 cfs observed at the Black Earth gage. Observed, 15-minute streamflow data was available at all four calibration sites (S_BC_us_CP, S_BEC_us_CP, J_BEC_ds_CP, and J_BEC_us_BE).

The Nash-Sutcliffe Coefficient for the July 2017 validation event at the Black Earth Creek at Black Earth, WI gage (model element: J_BEC_us_BE) is 0.835. The model replicates the timing and magnitude of the observed flood peak and the shape of the observed hydrograph well. The model also replicates the timing and magnitude of the second, smaller flood peak to a reasonable degree, which significantly increases confidence in the model results. Figure 16 shows how the modeled discharge compares to observed data at Black Earth for the July 2017 event.

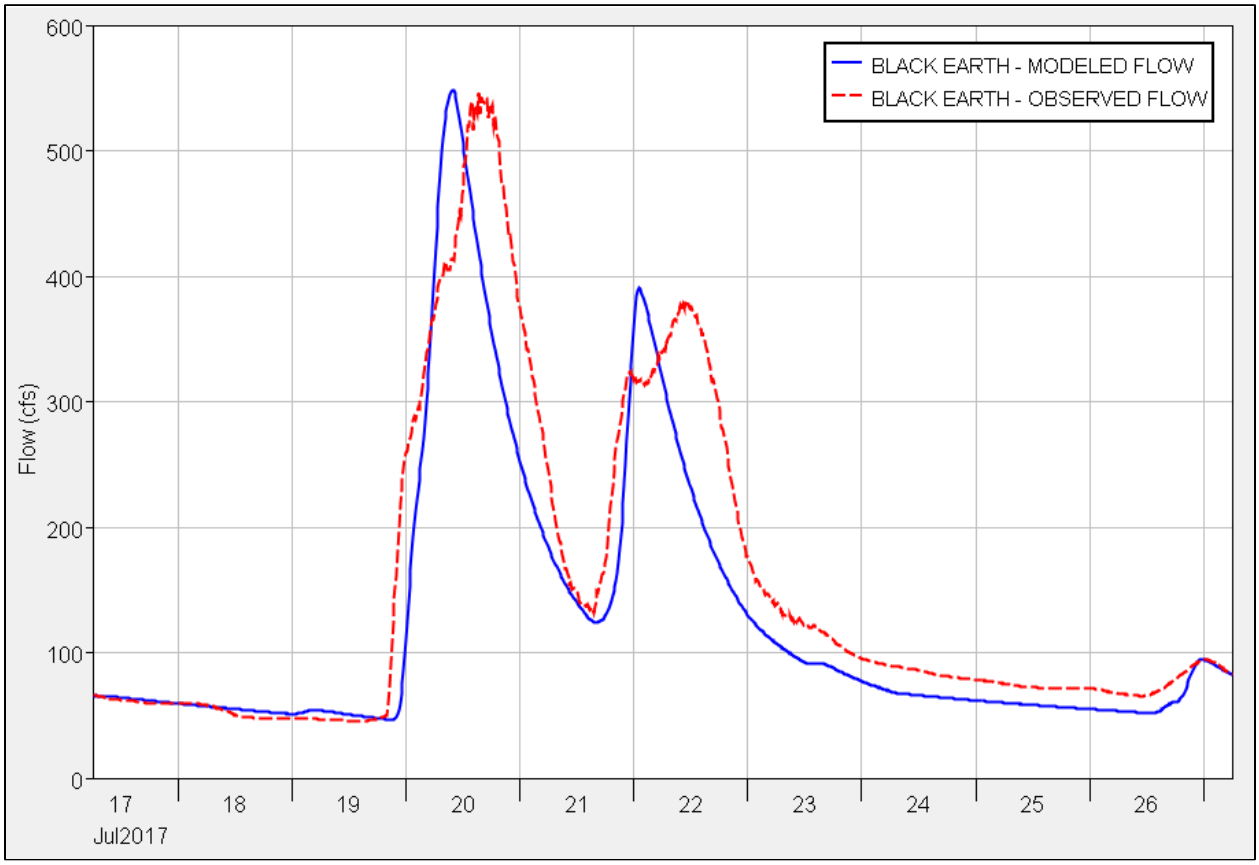

Figure 16. Validation results for July 2017 event - Black Earth, WI

9.3.10 June 2016 Validation Event

The June 2016 validation event simulation began on 12 Jun 2016 and ended on 19 Jun 2016. 2016 was a fairly dry year. There was no clear snowmelt-driven event, and flow at the Black Earth gage did not exceed 65 cfs through the months of May and June leading up to the June rain event. The June rain event itself resulted in a moderate flood, with a peak flow of 663 cfs observed at the Black Earth gage. Observed, 15-minute streamflow data was available at all four calibration sites (S_BC_us_CP, S_BEC_us_CP, J_BEC_ds_CP, and J_BEC_us_BE).

The Nash-Sutcliffe Coefficient for the June 2016 validation event at the Black Earth Creek at Black Earth, WI gage (model element: J_BEC_us_BE) is 0.882. The model replicates the timing and magnitude of the observed flood peak well. Figure 17 shows how the modeled discharge compares to observed data at Black Earth for the June 2016 event.

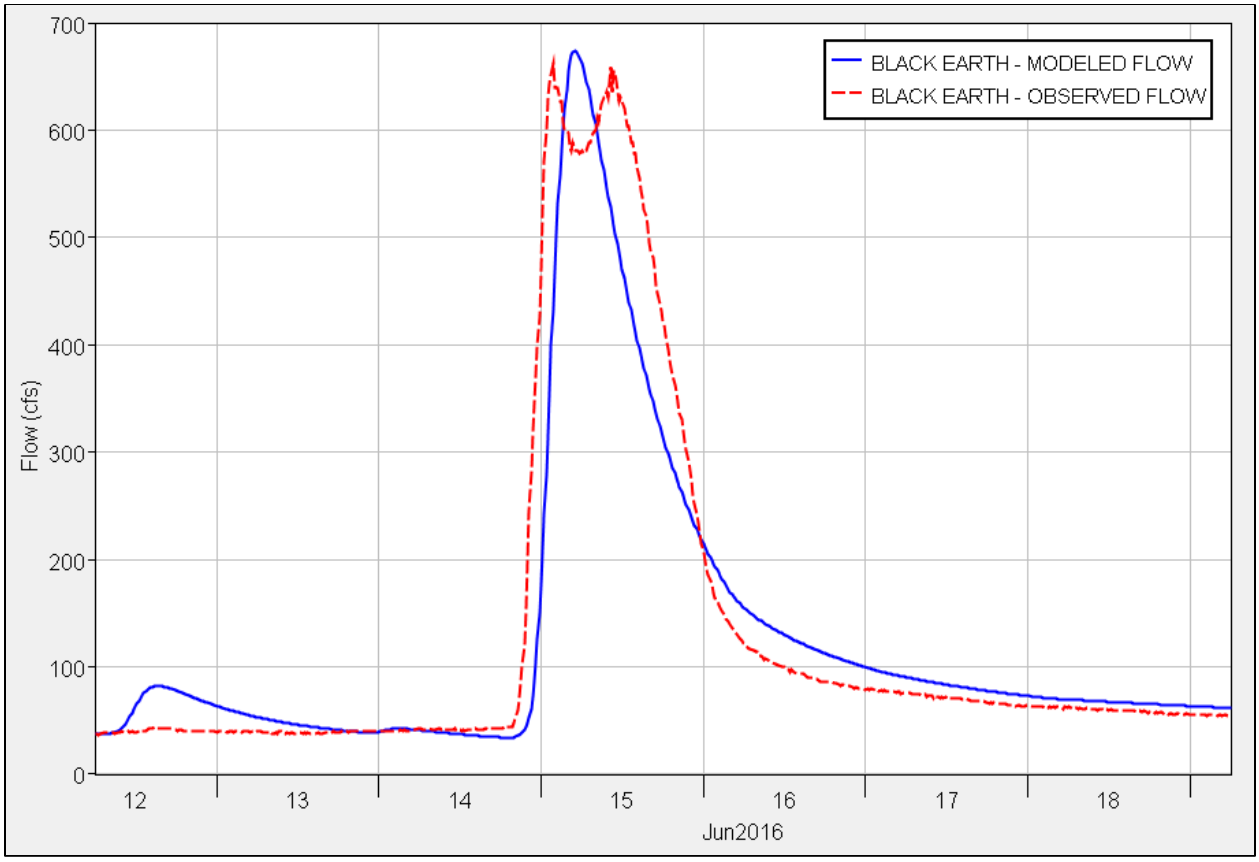

Figure 17. Validation results for June 2016 event - Black Earth, WI

9.3.11 July-August 2001 Validation Event

The July-August 2001 validation event simulation began on 30 Jul 2001 and ended on 06 Aug 2001. 2001 was a fairly dry year leading up to the July-August event. There was no clear snowmelt-driven event, and flow at the Black Earth was below 60 cfs approximately 40-50 days prior to the simulation period. However, a historic rainfall event at the end of July resulted in the second largest flood peak ever recorded at the Black Earth Creek at Black Earth, WI gage (1,720 cfs). Unlike the 2016 and 2017 validation events, observed, 15-minute streamflow data was only available at the Black Earth gage for the 2001 event.

The Nash-Sutcliffe Coefficient for the July-August 2001 validation event at the Black Earth Creek at Black Earth, WI gage (model element: J_BEC_us_BE) is 0.835. The model replicates the timing and magnitude of the observed flood peak well. Figure 18 shows how the modeled discharge compares to observed data at Black Earth for the July-August 2001 event.

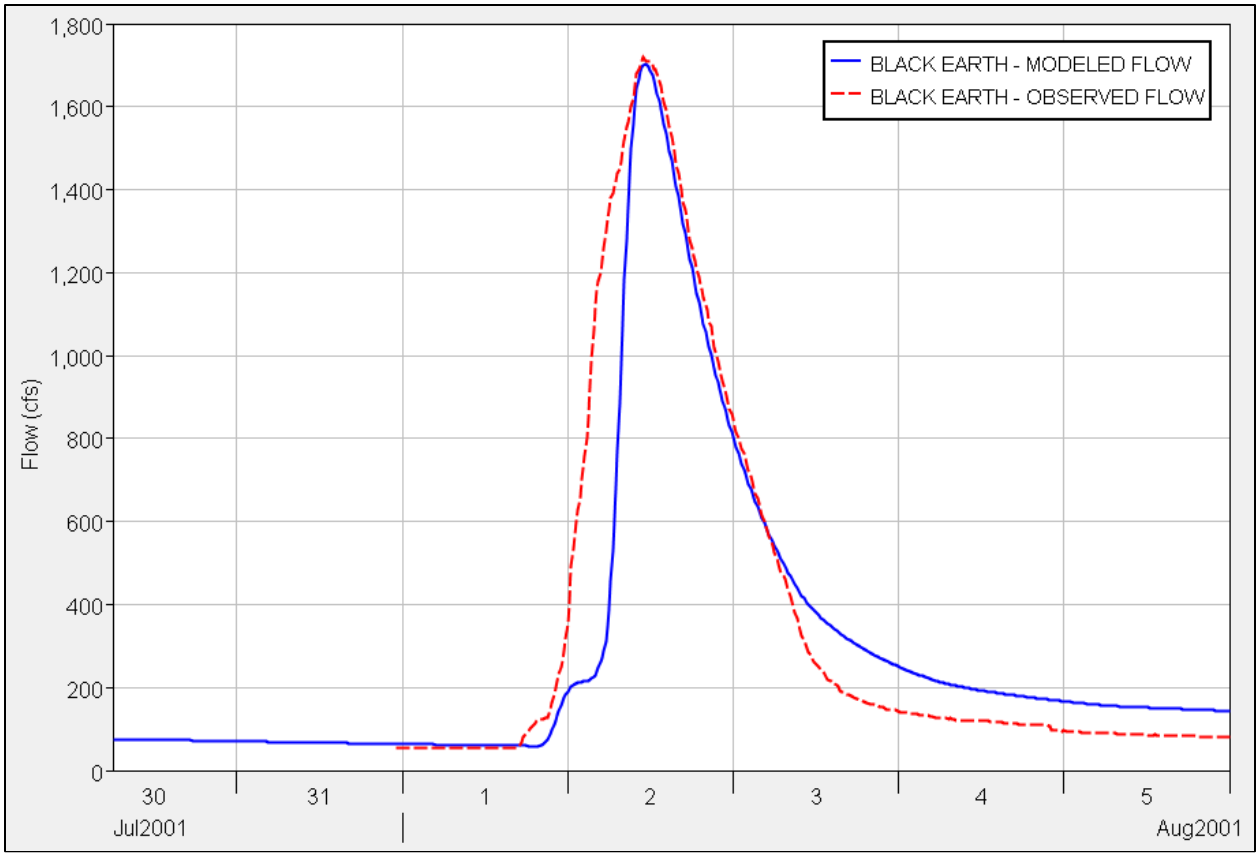

Figure 18. Validation results for Jul-Aug 2001 event - Black Earth, WI

9.4 Factors Influencing Calibration and Validation Success

In general, performance metrics for the three calibration events and the three validation events are good and indicate the HMS model adequately replicates the runoff response of the Black Earth Creek basin. However, the calibration could be improved with observed streamflow data downstream of Black Earth and greater availability of precipitation data within the watershed.

9.4.1 Spatial Distribution of Streamflow and Precipitation Gages

The downstream-most streamflow gage used for model calibration and validation was the Black Earth Creek at Black Earth, WI gage (USGS 05406500) just upstream of the Village of Black Earth. For all subbasins and reaches downstream of that gage, model parameters had to be estimated according to the calibrated parameters of elements upstream of Black Earth. If observed streamflow data was available for any of the calibration events on Black Earth Creek at Mazomanie or on Halfway Prairie Creek, Wendt Creek, or Vermont Creek, parameters could be adjusted to improve the model's performance at locations downstream of Black Earth.

In terms of precipitation data, the confidence in the model results could be improved with more spatially-distributed precipitation gages within the Black Earth Creek watershed itself. While the NEXRAD gridded data was validated via a comparison with gage totals outside the basin, gages inside the watershed would have provided a more robust comparison. Similarly, more gages across the watershed could have better informed the precipitation grids used for the 1993 and 2001 events. The

2001 grid in particular may not fully capture the magnitude and spatial distribution of rainfall during the event, since there was only one active precipitation gage in the basin.

9.4.2 Temporal Variation in the Initial Loss Parameter

In the Black Earth Creek HMS model, the value of the initial loss parameter significantly impacts the model's ability to replicate the magnitude of observed flood peaks. In general, initial loss represents storage capacity within the soil column as well as available depressional storage within the watershed. Since these physical characteristics change over time as a result of precipitation and temperature, the initial loss parameter was not held constant for all subbasins from event to event. Instead, initial loss was adjusted such that the model matched observed flood peaks.

To verify the initial loss values selected for each event are in accordance with known soil physical properties, initial loss values were compared to the available water storage in the first 150 cm of the soil column. While 150 cm is fairly deep, the majority of the soils in the Black Earth Creek watershed are well drained to excessively drained, and the level of discharge observed during the 2018 flood relative to the volume of precipitation that fell on the basin indicates a large amount of soil storage capacity. As discussed in Section 9.3.1, the average available water storage in the first 150 cm of the soil column for each subbasin was determined using the GSSURGO product produced by the NRCS. To develop a representative AWS0150 value for the entire watershed, the AWS0150 for each subbasin was averaged. This representative value was compared to the average initial loss across all subbasins for each event. As shown in Table 24, the calibrated initial loss values indicate the soil was almost fully saturated in September-October 2019 and almost fully dry in August 2018.

Table 24. Comparison of calibrated initial loss values and available water storage in the first 150 cm of soil

Representative AWS0150: 8.02 inches		
Calibration/Validation Event	**Average Initial Loss (in)**	**% of AWS0150**
Sep-Oct 2019	0.15	2%
Aug 2018	7.18	90%
Jul 2017	2.11	26%
Jun 2016	5.60	70%
Jul-Aug 2001	5.68	71%
Jul 1993	2.51	31%

To ensure the selected initial loss values were reasonable given observed antecedent conditions, the average initial loss values listed in Table 24 were plotted against precipitation, discharge, maximum temperature, and Keetch-Byram Drought Index (KBDI) values for the five days leading up to each simulation period. For this analysis, precipitation was taken as the average of the total precipitation measured at the Charmany Farm and Mazomanie WWTP weather stations. Discharge was measured at the Black Earth Creek at Black Earth, WI gage (USGS 05406500). Maximum temperature was recorded at the Charmany Farm weather station, and KBDI was taken as the average KBDI recorded at the Madison Airport and Lone Rock Airport weather stations. Linear regression was used to determine whether average initial loss correlates well with any of the observed parameters. As show in Figure 19, average initial loss has a negative relationship with precipitation and discharge and a positive relationship with maximum temperature and KBDI. The directionality of each relationship and the reasonably high

correlation coefficients (R^2) for only having six data points indicate the initial loss values selected for each calibration and validation event reasonably correspond to antecedent soil moisture conditions in the basin.

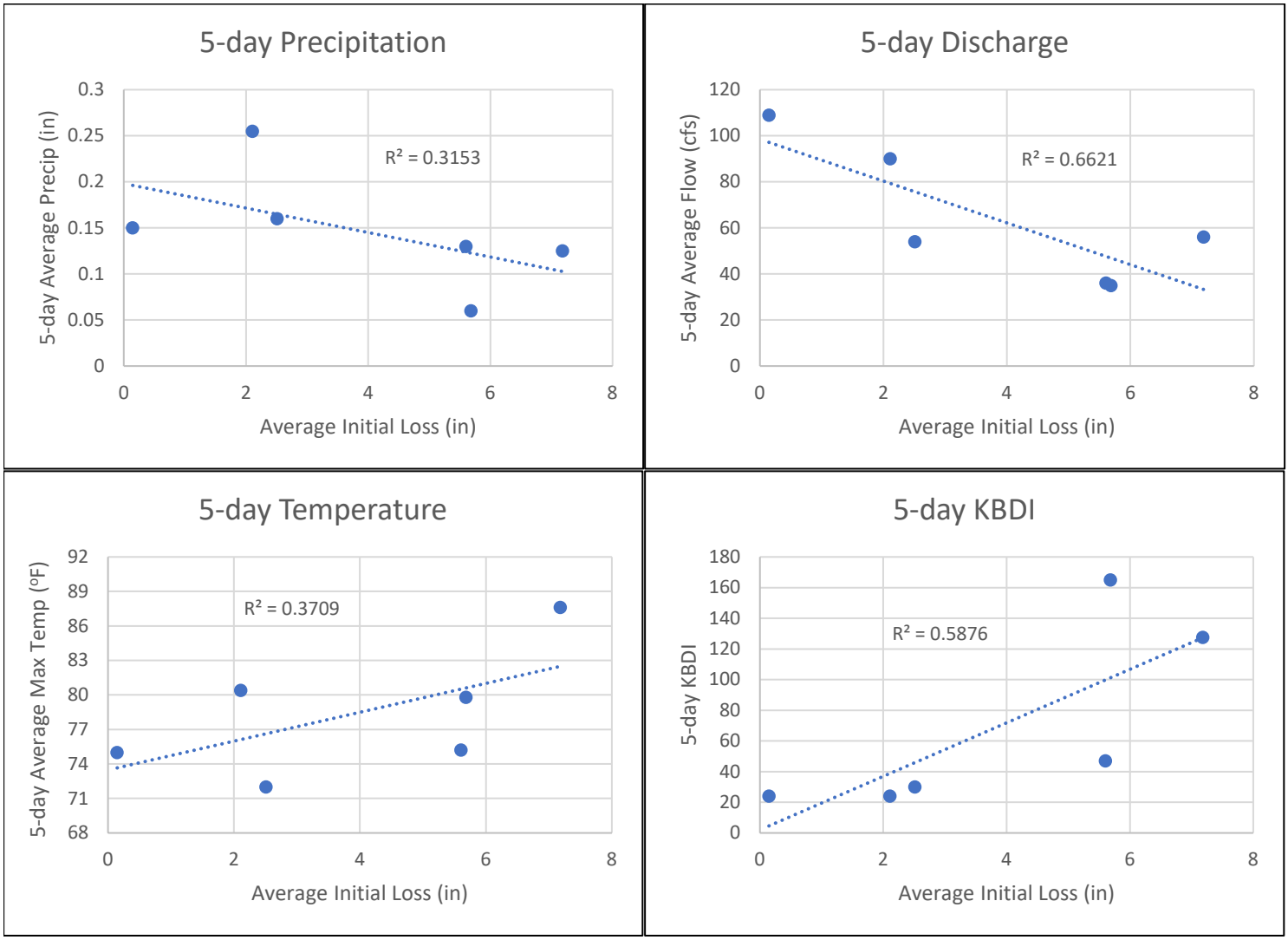

Figure 19. Relationship between average initial loss and observed, antecedent soil moisture indicators

10 Model Alternatives

To evaluate how land management changes impact the runoff response in the Black Earth Creek watershed, a number of alternative simulations were run using the HEC-HMS model. Meetings with the local sponsor's modeling subcommittee, made up of members of the USACE, EOR, and CARPC, informed the selection of alternatives. Alternative model parameterization in HEC-HMS was derived using results of the literature review conducted in Section 7 as well as data from EOR. All HEC-HMS model simulations were conducted by USACE.

In total, seven alternatives were modeled, *25% Ag Non-Contributing*, *100% Cover Crop*, *100% Cover Crop + No-Till*, *Prairie Strips*, *50% Impervious Area*, *Wetland Restoration*, and *Green Infrastructure*. The first

four alternatives simulated changes to row-cropped agricultural lands. No management changes were made to pasture lands because cover crops, no-till, and prairie strips are not as applicable to those fields. The *Wetland Restoration* alternative simulated additional storage in the basin. The last two alternatives simulated changes to impervious areas throughout the watershed. Alternative results were then compared to the baseline model results for each calibration event. The baseline model results are the calibration simulations using the generalized model parameters. HEC-HMS results are displayed in tabular form in the following sections. For hydrographs of model outputs, see Appendix A.

In addition to the HEC-HMS model, an HEC-RAS model of the mainstem of Black Earth Creek was also developed for this study. Documentation of the HEC-RAS model is included in Appendix F. After simulating each alternative in HEC-HMS, model output hydrographs were input into the HEC-RAS model. The HEC-RAS model results are shown in the following sections as inundated area for each alternative. Inundation maps are not included in this report.

10.1 25% Ag Non-Contributing

The first alternative, labeled "25% Ag Non-Contributing," simulated how the basin would respond if 25% of all row-cropped agricultural lands in the basin acted as non-contributing areas. That is, if all precipitation that fell on row-cropped fields either infiltrated into the ground or was stored, such that no runoff occurred. This alternative is not realistic, as some runoff from agricultural lands is bound to occur even with maximum human intervention, but it provides a reference frame for other alternatives.

To model this alternative, the baseline, generalized HEC-HMS model described in Section 9 was modified such that the area of each subbasin did not include 25% of row-cropped agricultural fields. Row-cropped fields were identified using the National Cropland Data Layer (USDA National Agricultural Statistics Service, 2019) and GIS software. Table 25 summarizes the distribution of agricultural land use within each subbasin, and Table 26 shows how each subbasin area was modified in the HMS model.

Table 25. Agricultural land use within each subbasin in the Black Earth Creek HMS model, National Cropland Data Layer (2019)

Subbasin	% Row Crops[1]	% Hay/Pasture	% Non-Ag
S_BC_us_CP	45%	23%	32%
S_BEC_us_CP	25%	19%	56%
S_CP	26%	20%	54%
S_BEC_ds_CP_to_BEC_us_BE	31%	19%	50%
S_VC_us_BE	21%	20%	59%
S_BE	48%	8%	45%
S_BEC-VC_to_BEC_us_MZ	41%	12%	47%
S_HPC_us_MZ	47%	14%	39%
S_WC_us_MZ	45%	15%	40%
S_MZ	36%	15%	49%
S_BEC_ds_MZ_to_Out	52%	7%	40%

[1] Row Crops NCDL fields include corn, sorghum, soybeans, sunflower, sweet corn, barley, spring wheat, winter wheat, double crop, rye, oats, millet, dry beans, potatoes, other crops, miscellaneous vegetables and fruits, peas, herbs, triticale, carrots, strawberries, double crop of winter wheat and corn, double crop of triticale and corn, and pumpkins.

Table 26. Area of each subbasin when 25 % of row-cropped agricultural lands are removed

Subbasin	Original Area (mi^2)	% Row Crops	25% of Row Cropped Area (mi^2)	Alternative Area (mi^2)
S_BC_us_CP	9.01	45%	1.02	7.99
S_BEC_us_CP	12.28	25%	0.78	11.50
S_CP	4.51	26%	0.29	4.22
S_BEC_ds_CP_to_BEC_us_BE	19.38	31%	1.50	17.88
S_VC_us_BE	13.84	21%	0.73	13.11
S_BE	3.05	48%	0.36	2.69
S_BEC-VC_to_BEC_us_MZ	7.47	41%	0.77	6.70
S_HPC_us_MZ	16.30	47%	1.92	14.37
S_WC_us_MZ	10.72	45%	1.20	9.53
S_MZ	3.14	36%	0.28	2.85
S_BEC_ds_MZ_to_Out	3.38	52%	0.44	2.94

Model simulations with the alternative subbasin areas listed above were run for the three calibration events. In all three events, the peak flow at Black Earth, Cross Plains, and Mazomanie decreased by approximately 8% (Table 27). Table 28 shows how the maximum inundation for the *25% Ag Non-Contributing* alternative compares to the maximum inundation for the baseline model. Note while this alternative does not simulate a specific intervention or land use practice, it's results may help put the peak flow reductions associated with other alternatives into perspective.

Table 27. Peak flow reductions under the 25% Ag Non-Contributing alternative

Flood Event	Peak Flow (cfs)		
	Baseline	25% Ag Non-Contributing	% Decrease
	Cross Plains, WI (model element: J_BEC_ds_CP)		
Jul 1993	891	817	-8%
Aug 2018	2,792	2,574	-8%
Sep-Oct 2019	596	550	-8%
	Black Earth, WI (model element: J_BEC_us_BE)		
Jul 1993	1,248	1,147	-8%
Aug 2018	2,979	2,748	-8%
Sep-Oct 2019	1,076	993	-8%
	Mazomanie, WI (model element: J_BEC_ds_MZ)		
Jul 1993	2,239	2,047	-9%
Aug 2018	3,540	3,245	-8%
Sep-Oct 2019	1,769	1,624	-8%

Table 28. Inundation area reduction under the 25% Ag Non-Contributing alternative

Flood Event	Maximum Inundation (acres)		
	Baseline	25% Ag Non-Contributing	% Decrease
Jul 1993	1,349	1,293	4%
Aug 2018	1,986	1,915	4%
Sep-Oct 2019	1,242	1,195	4%

10.2 100% Cover Crop

The second alternative, labeled "100% Cover Crop," simulated how the basin would respond if cover crops were adopted in all non-pasture, agricultural fields designated as row crops in the National Cropland Data Layer (USDA National Agricultural Statistics Service, 2019). This alternative assumed cover cropping is not currently practiced in any row-cropped field in the basin. In reality, some cover cropping is likely practiced in the basin, but there is no data quantifying its extent. Therefore, this alternative represents an estimate of the maximum effectiveness of widespread adoption of cover crops in reducing flood risk.

To model the adoption of cover crops, the constant loss rate for each subbasin in the HMS model was modified to simulate increased soil infiltration rates on agricultural fields. According to the literature review in Section 7, increasing soil infiltration is the primary mode by which cover crops can reduce runoff. The meta-analysis conducted by Basche and DeLonge provided the most complete and quantitative estimate of the effect of cover cropping on soil infiltration rates, reporting a mean increase in infiltration rate of 34.8% ± 7.7% and a 95% confidence interval of 19.8% to 50.0% (Basche & DeLonge, 2019). These values were adopted for the *100% Cover Crop* alternative. The maximum rate of increase selected for this alternative (50.0%) is in line with the upper range of Ksat rates of increase reported by the USDA in its 2016 literature review (U.S. Department of Agriculture, 2016).

Infiltration was assumed to account for all losses during large flood events. Under this assumption, the loss rate parameter in HEC-HMS directly corresponds to the soil infiltration rate. In reality, other factors such as evaporation, evapotranspiration, and depressional storage influence the loss rate. Compared to the infiltration rate, those factors likely play a relatively small role in the value of the constant loss rate during large, rainfall-driven events. However, because they are not accounted for in this analysis, the model results may overestimate reductions in peak flow due to the adoption of cover crops.

Since the constant loss rate for each subbasin is representative of the entire subbasin area, increases in loss rates were scaled relative to the percentage of the subbasin that consists of row-cropped agricultural lands. The percentage of row-cropped agricultural lands was computed for each subbasin using the National Cropland Data Layer and was shown previously in Table 25. Table 29 shows the scaled increase in loss rate for each subbasin using the mean increase in infiltration rate reported by Basche and DeLonge (34.8%) as well as the low (19.8%) and high (50.0%) confidence bounds. Table 30 shows the corresponding loss rate for each subbasin. "Mean" corresponds to rates of increase equivalent to the mean rate of increase reported by Basche and DeLonge, while "low" and "high" correspond to rates of increase equivalent to the lower and upper bounds of the 95% confidence interval.

Table 29. Mean, lower confidence bound (low) and upper confidence bound (high) increases in infiltration rates due to the adoption of cover crops reported by Basche and DeLonge for each subbasin in the Black Earth Creek HMS model

Subbasin	% Row Crop	Alternative Loss Rate Increase		
		Mean	Low	High
S_BC_us_CP	45%	15.7%	8.9%	22.5%
S_BEC_us_CP	25%	8.8%	5.0%	12.7%
S_CP	26%	9.0%	5.1%	13.0%
S_BEC_ds_CP_to_BEC_us_BE	31%	10.8%	6.1%	15.5%
S_VC_us_BE	21%	7.4%	4.2%	10.6%
S_BE	48%	16.6%	9.4%	23.8%
S_BEC-VC_to_BEC_us_MZ	41%	14.4%	8.2%	20.7%
S_HPC_us_MZ	47%	16.4%	9.4%	23.6%
S_WC_us_MZ	45%	15.5%	8.8%	22.3%
S_MZ	36%	12.6%	7.2%	18.2%
S_BEC_ds_MZ_to_Out	52%	18.2%	10.4%	26.1%

Table 30. Alternative constant loss rates adopted in the 100% Cover Crop alternative

Subbasin	Baseline Loss Rate (in/hr)	Alternative Loss Rate (in/hr)		
		Mean	Low	High
S_BC_us_CP	0.67	0.77	0.73	0.82
S_BEC_us_CP	0.66	0.72	0.70	0.75
S_CP	0.50	0.54	0.52	0.56
S_BEC_ds_CP_to_BEC_us_BE	0.34	0.37	0.36	0.39
S_VC_us_BE	0.44	0.47	0.46	0.49
S_BE	0.47	0.54	0.51	0.58
S_BEC-VC_to_BEC_us_MZ	0.64	0.73	0.69	0.77
S_HPC_us_MZ	0.70	0.82	0.77	0.87
S_WC_us_MZ	0.70	0.81	0.76	0.86
S_MZ	1.77	1.99	1.89	2.09
S_BEC_ds_MZ_to_Out	2.01	2.37	2.21	2.53

Model simulations with the alternative subbasin loss rates listed above were run for the three calibration events. Reductions in peak flow at Cross Plains, Black Earth, and Mazomanie ranged from 2% with the lowest increase in loss rates to 23% with the highest increase in loss rates. Table 31 shows the peak flow at Cross Plains, Black Earth, and Mazomanie for low, mean, and high simulations, with the change from baseline in parentheses. Table 32 shows how the maximum inundation for the *100% Cover Crop* alternative compares to the maximum inundation for the baseline model.

Table 31. Peak flow reductions under the 100% Cover Crop alternative

Flood Event	Peak Flow (cfs)			
	Baseline	Low	Mean	High
	Cross Plains, WI (model element: J_BEC_ds_CP)			
Jul 1993	891	865 (-3%)	845 (-5%)	826 (-7%)
Aug 2018	2,792	2,720 (-3%)	2,669 (-4%)	2,617 (-6%)
Sep-Oct 2019	596	541 (-9%)	501 (-16%)	459 (-23%)
	Black Earth, WI (model element: J_BEC_us_BE)			
Jul 1993	1,248	1,219 (-2%)	1,198 (-4%)	1,177 (-6%)
Aug 2018	2,979	2,909 (-2%)	2,859 (-4%)	2,809 (-6%)
Sep-Oct 2019	1,076	1,011 (-6%)	963 (-10%)	914 (-15%)
	Mazomanie, WI (model element: J_BEC_ds_MZ)			
Jul 1993	2,239	2,155 (-4%)	2,095 (-6%)	2,034 (-9%)
Aug 2018	3,540	3,457 (-2%)	3,396 (-4%)	3,337 (-6%)
Sep-Oct 2019	1,769	1,635 (-8%)	1,541 (-13%)	1,452 (-18%)

Table 32. Inundation area reduction under the 100% Cover Crop alternative

Flood Event	Maximum Inundation (acres)			
	Baseline	Low	Mean	High
Jul 1993	1,349	1,330 (-1%)	1,314 (-3%)	1,299 (-4%)
Aug 2018	1,986	1,965 (-1%)	1,950 (-2%)	1,933 (-3%)
Sep-Oct 2019	1,242	1,201 (-3%)	1,172 (-6%)	1,139 (-8%)

10.3 100% Cover Crop + No-Till

The third alternative, labeled "100% Cover Crop + No-Till," simulated how the basin would respond if cover crops and no-till were adopted in all non-pasture, agricultural fields designated as row crops in the National Cropland Data Layer (USDA, 2019). This alternative assumed both cover cropping and no-till is not currently practiced in any row-cropped field in the basin. In reality, it is likely both practices are employed in some capacity, but there is no data quantifying the extent of current best management practices. Therefore, this alternative represents an estimate of the maximum effectiveness of widespread adoption of cover crops and no-till in reducing flood risk. If data regarding the extent of current management practices were obtained, the analysis presented in this report could be refined to improve its overall accuracy.

To model the adoption of cover crops alongside no-till, the constant loss rate for each subbasin in the HMS model was modified to simulate increased soil infiltration rates on agricultural fields. According to the literature reviewed in Section 7, increasing soil infiltration is the primary mode by which both cover crops and no-till can reduce runoff. As was the case with the *100% Cover Crop* alternative, increases in infiltration rates reported in the meta-analysis conducted by Basche and DeLonge were adopted for the *100% Cover Crop + No-Till* alternative (Basche, 2019). The meta-analysis reported only two experiments that directly studied the effects of cover cropping and no-till by comparing to conventional tillage

without cover crops. However, there were 34 paired comparisons of no-till with cover crops vs. no-till without cover crops. In those 34 paired comparisons, the mean increase in infiltration rate was 44.6%, and the 95% confidence interval was 11.6% to 77.5%. Since Basche and DeLonge reported an insignificant change in infiltration rates due to no-till alone (5.7% ± 9.7%), it is assumed for the purpose of this study that implementing both cover crops and no-till when neither practice had previously been used would result in an increase in infiltration rate of between 11.6% and 77.5%.

As was the case with the *100% Cover Crop* alternative, infiltration was assumed to account for all losses during large flood events such that the loss rate parameter in HEC-HMS directly corresponds to the soil infiltration rate. Because of this, the model results may overestimate reductions in peak flow due to the adoption of cover crops and no-till.

Loss rates were scaled relative to the percentage of the subbasin that consists of row-cropped agricultural lands. **Error! Reference source not found.** shows the scaled increase in loss rate for each subbasin using the mean increase in infiltration rate reported by Basche and DeLonge (44.6%) as well as the low (11.6%) and high (77.5%) confidence bounds. **Error! Reference source not found.** shows the corresponding loss rate for each subbasin. "Mean" corresponds to rates of increase equivalent to the mean rate of increase reported by Basche and DeLonge, while "low" and "high" correspond to rates of increase equivalent to the lower and upper bounds of the 95% confidence interval.

Table 33. Mean, lower confidence bound (low) and upper confidence bound (high) increases in infiltration rates due to the adoption of cover crops in no-till fields reported by Basche and DeLonge for each subbasin in the Black Earth Creek HMS model

Subbasin	% Row Crop	Alternative Loss Rate Increase		
		Mean	Low	High
S_BC_us_CP	45%	20.1%	5.2%	34.9%
S_BEC_us_CP	25%	11.3%	2.9%	19.7%
S_CP	26%	11.6%	3.0%	20.1%
S_BEC_ds_CP_to_BEC_us_BE	31%	13.8%	3.6%	24.0%
S_VC_us_BE	21%	9.5%	2.5%	16.4%
S_BE	48%	21.2%	5.5%	36.9%
S_BEC-VC_to_BEC_us_MZ	41%	18.5%	4.8%	32.1%
S_HPC_us_MZ	47%	21.1%	5.5%	36.6%
S_WC_us_MZ	45%	19.9%	5.2%	34.6%
S_MZ	36%	16.2%	4.2%	28.1%
S_BEC_ds_MZ_to_Out	52%	23.3%	6.1%	40.5%

Table 34. Alternative constant loss rates adopted in the 100% Cover Crop + No-Till alternative

Subbasin	Baseline Loss Rate (in/hr)	Alternative Loss Rate (in/hr)		
		Mean	Low	High
S_BC_us_CP	0.67	0.80	0.70	0.90
S_BEC_us_CP	0.66	0.74	0.68	0.79
S_CP	0.50	0.56	0.51	0.60
S_BEC_ds_CP_to_BEC_us_BE	0.34	0.38	0.35	0.42
S_VC_us_BE	0.44	0.48	0.45	0.51
S_BE	0.47	0.57	0.49	0.64
S_BEC-VC_to_BEC_us_MZ	0.64	0.76	0.67	0.85
S_HPC_us_MZ	0.70	0.85	0.74	0.96
S_WC_us_MZ	0.70	0.84	0.74	0.94
S_MZ	1.77	2.05	1.84	2.26
S_BEC_ds_MZ_to_Out	2.01	2.47	2.13	2.82

Model simulations with the alternative subbasin loss rates listed above were run for the three calibration events. Reductions in peak flow at Cross Plains, Black Earth, and Mazomanie ranged from 1% with the lowest increase in loss rates to 34% with the highest increase in loss rates. Table 35 shows the peak flow at Cross Plains, Black Earth, and Mazomanie for low, mean, and high simulations, with the change from baseline in parentheses. Table 36 shows how the maximum inundation for the *100% Cover Crop + No-Till* alternative compares to the maximum inundation for the baseline model.

Table 35. Peak flow reductions under the 100% Cover Crop + No-Till alternative

Flood Event	Peak Flow (cfs)			
	Baseline	Low	Mean	High
	Cross Plains, WI (model element: J_BEC_ds_CP)			
Jul 1993	891	876 (-2%)	832 (-7%)	790 (-11%)
Aug 2018	2,792	2,750 (-1%)	2,635 (-6%)	2,533 (-9%)
Sep-Oct 2019	596	564 (-5%)	473 (-21%)	394 (-34%)
	Black Earth, WI (model element: J_BEC_us_BE)			
Jul 1993	1,248	1,231 (-1%)	1,184 (-5%)	1,138 (-9%)
Aug 2018	2,979	2,939 (-1%)	2,826 (-5%)	2,728 (-8%)
Sep-Oct 2019	1,076	1,038 (-3%)	931 (-13%)	836 (-22%)
	Mazomanie, WI (model element: J_BEC_ds_MZ)			
Jul 1993	2,239	2,189 (-2%)	2,055 (-8%)	1,923 (-14%)
Aug 2018	3,540	3,492 (-1%)	3,357 (-5%)	3,242 (-8%)
Sep-Oct 2019	1,769	1,689 (-5%)	1,482 (-16%)	1,327 (-25%)

Table 36. Inundation area reduction under the 100% Cover Crop + No-Till alternative

Flood Event	Maximum Inundation (acres)			
	Baseline	Low	Mean	High
Jul 1993	1,349	1,337 (-1%)	1,304 (-3%)	1,271 (-6%)
Aug 2018	1,986	1,974 (-1%)	1,939 (-2%)	1,910 (-4%)
Sep-Oct 2019	1,242	1,216 (-2%)	1,151 (-7%)	1,084 (-13%)

10.4 Prairie Strips

The fourth alternative, labeled "Prairie Strips," simulated how the basin would respond if prairie buffer strips were added to agricultural fields throughout the watershed. Since topography differs between fields, the Contour Buffer Strips tool in the ACPF toolbox was used to identify locations suitable for buffer strips (Porter et al., 2015). The Contour Buffer Strips tool identifies locations for buffer strips in non-pasture, agricultural fields along the contour and in areas of high slope. This alternative assumed all agricultural fields identified as being suitable for at least one buffer strip would effectively transition at least 10% of their area to buffer strips. This alternative also assumed prairie stripping is not currently practiced in any field in the watershed. In reality, the practice is likely employed in some capacity, but there is no data quantifying the extent of current best management practices. Therefore, this alternative represents an estimate of the maximum effectiveness of widespread prairie stripping in reducing flood risk.

To model the adoption of prairie strips, the area of each subbasin in the HMS model was modified to simulate reduced runoff from agricultural fields affected by prairie strips. According to the literature review in Section 7, strategically converting approximately 10% of a field's area to prairie strips can reduce runoff by 44% (Iowa State University, 2021). As discussed in Section 7.3, it is not clear if this value represents a reduction in the total volume of runoff, or if prairie strips are meant to reduce the runoff rate from any event by 44%. Also, research conducted in Wisconsin suggested runoff reductions from prairie strips can vary substantially across fields and across regions (Sand County Foundation, 2021). Therefore, two simulations were run for this alternative, one using a constant runoff reduction of 44% from each prairie stripped field, and one using a constant runoff reduction of 10% from each prairie stripped field. It is assumed the 10% reduction is closer to the reduction in runoff that would occur in reality, given the magnitude of each rainfall event.

Subbasin areas were scaled relative to the percentage of the subbasin that was made up of agricultural fields suitable for prairie strips, as identified by the ACPF tool. The area parameter of each subbasin was selected because a reduction in area leads to a 1:1 reduction in runoff in the HMS model. It is important to note the ACPF tool was only run on the Upper Black Earth Creek HUC-12 (070700050501) and Middle Black Earth Creek HUC-12 (0707000505020). The Upper Black Earth Creek HUC-12 covers the S_BC_us_CP, S_BEC_us_CP, and S_CP subbasins, and the Middle Black Earth Creek HUC-12 covers the S_BEC_ds_CP_to_BEC_us_BE, S_VC_us_BE, and S_BE subbasins. Since the topography of the Halfway Prairie Creek (S_HPC_us_MZ) and Wendt Creek (S_WC_us_MZ) subbasins is similar to Upper Black Earth Creek (both glaciated headwaters), the average area reduction computed in the Upper Black Earth Creek subbasins was applied to the Halfway Prairie Creek and Wendt Creek subbasins. Similarly, the topography of the remaining subbasins downstream of Black Earth is similar to the topography of Middle Black Earth Creek. Therefore, the average area reduction computed in the Middle Black Earth

Creek subbasins was applied to the remaining subbasins downstream of Black Earth. Table 37 shows the scaled decrease in area for each subbasin using the 44% reduction in runoff identified by the Iowa State University researchers (high) as well as a more conservative 10% reduction in runoff (low). Table 38 shows the final, adopted subbasin area for the high (44%) and low (10%) simulations.

Table 37. High and low reduction in subbasin area corresponding to comparable reductions in runoff due to the addition of prairie strips in suitable fields in the Black Earth Creek HMS model

HUC-12	Subbasin	Total Area (mi^2)	Area Fields w/ Prairie Strips (mi^2)	Alternative Area Reduction	
				High	Low
Upper Black Earth Creek	**S_BC_us_CP**	9.01	2.25	11%	3%
	S_BEC_us_CP	12.28	2.03	7%	2%
	S_CP	4.51	0.73	7%	2%
Middle Black Earth Creek	**S_BEC_ds_CP_to_BEC_us_BE**	19.38	3.01	7%	2%
	S_VC_us_BE	13.84	1.83	6%	1%
	S_BE	3.05	0.63	9%	2%
Lower Black Earth Creek	**S_BEC-VC_to_BEC_us_MZ**	7.47	-	7%	2%
Halfway Prairie Creek	**S_HPC_us_MZ**	16.30	-	8%	2%
	S_WC_us_MZ	10.72	-	8%	2%
Lower Black Earth Creek	**S_MZ**	3.14	-	7%	2%
	S_BEC_ds_MZ_to_Out	3.38	-	7%	2%

Table 38. Alternative subbasin areas adopted in the Prairie Strip alternative

Subbasin	Baseline Area (mi^2)	Alternative Area (mi^2)	
		High	Low
S_BC_us_CP	9.01	8.02	8.78
S_BEC_us_CP	12.28	11.39	12.08
S_CP	4.51	4.19	4.44
S_BEC_ds_CP_to_BEC_us_BE	19.38	18.06	19.08
S_VC_us_BE	13.84	13.04	13.66
S_BE	3.05	2.78	2.99
S_BEC-VC_to_BEC_us_MZ	7.47	6.93	6.81
S_HPC_us_MZ	16.30	14.92	14.60
S_WC_us_MZ	10.72	9.82	9.61
S_MZ	3.14	2.91	2.86
S_BEC_ds_MZ_to_Out	3.38	3.13	3.08

Model simulations with the alternative subbasin areas listed above were run for the three calibration events. Reductions in peak flow at Cross Plains, Black Earth, and Mazomanie were approximately 8% with the high decrease in runoff and 2% with the lower, more conservative runoff reduction estimate. Table 39 shows the peak flow at Cross Plains, Black Earth, and Mazomanie for high and low simulations,

with the change from baseline in parentheses. Table 40 shows how the maximum inundation for the *Prairie Strip* alternative compares to the maximum inundation for the baseline model.

Table 39. Peak flow reductions under the Prairie Strips alternative

Flood Event	Peak Flow (cfs)		
	Baseline	High	Low
	Cross Plains, WI (model element: J_BEC_ds_CP)		
Jul 1993	891	815 (-9%)	874 (-2%)
Aug 2018	2,792	2562 (-8%)	2,740 (-2%)
Sep-Oct 2019	596	547 (-8%)	585 (-2%)
	Black Earth, WI (model element: J_BEC_us_BE)		
Jul 1993	1,248	1,150 (-8%)	1,226 (-2%)
Aug 2018	2,979	2,742 (-8%)	2,926 (-2%)
Sep-Oct 2019	1,076	996 (-7%)	1,058 (-2%)
	Mazomanie, WI (model element: J_BEC_ds_MZ)		
Jul 1993	2,239	2,068 (-8%)	2,153 (-4%)
Aug 2018	3,540	3,258 (-8%)	3,429 (-3%)
Sep-Oct 2019	1,769	1,638 (-7%)	1,711 (-3%)

Table 40. Inundation area reduction under the Prairie Strips alternative

Flood Event	Maximum Inundation (acres)		
	Baseline	High	Low
Jul 1993	1,349	1,296 (-4%)	1,332 (-1%)
Aug 2018	1,986	1,916 (-4%)	1,964 (-1%)
Sep-Oct 2019	1,242	1,197 (-4%)	1,227 (-1%)

10.5 Wetland Restoration

The fifth alternative, labeled “Wetland Restoration,” simulated how construction of off-channel wetlands across the watershed would affect discharge in Black Earth Creek during a flood event. A total of nine priority wetland areas were identified by CARPC using the Wetlands by Design GIS tool (Freshwater Network, 2020). Three cohorts of students at the University of Wisconsin-Madison (UWM), in coordination with CARPC, developed conceptual designs for seven of the nine sites. EOR obtained the results of the UWM analysis and provided USACE with a summary that included the location of each site, the storage volume provided by the site, and the depth of the storage area. EOR estimated the storage characteristics for the two sites the students did not develop a conceptual design for. This information is shown in Table 41.

Table 41. Location and storage characteristics of the nine priority wetland restoration sites identified by CARPC

Site/Location	HMS Subbasin	Storage Volume (ac-ft)	Storage Depth (ft)
Brewery Creek #1	S_BC_us_CP	13	1
Brewery Creek #2	S_BC_us_CP	6	1
Black Earth Creek #1	S_BEC_us_CP	58.5	1
Garfoot Creek	S_BEC_ds_CP_to_BEC_us_BE	29.4	2
Vermont Creek	S_VC_us_BE[1]	40	1
Black Earth Creek #2	S_BEC-VC_to_BEC_us_MZ	54	1
Black Earth Creek #3	S_BEC-VC_to_BEC_us_MZ	17.4	1.7
Wendt Creek #1	S_WC_us_MZ	8.7	1.7
Wendt Creek #2	S_WC_us_MZ	8.7	1.7

[1]This storage area falls within the S_VC_us_BE and S_BE subbasins. For this analysis, the storage area is assumed to be located entirely within the S_VC_us_BE subbasin.

Each storage area is assumed to be constructed as an off-channel wetland with an inlet structure designed to accept flows from the main river channel above an approximate baseflow discharge. To simulate the effect of each wetland storage area in HMS, a reservoir element was placed at the subbasin outlet of the six unique subbasins shown in Table 41. While the proposed storage areas are not necessarily located at subbasin outlets and therefore will not capture runoff from the entire subbasin, it is assumed modeling the storage areas at the subbasin outlets will result in a similar hydrologic effect at downstream locations. For example, a subbasin could have been created specifically for Garfoot Creek, which lies between Cross Plains and Black Earth, and a reservoir could be added just downstream of the new subbasin. In this case, runoff from Garfoot Creek would be reduced, but a significant portion of runoff from the original subbasin would bypass the reservoir. This method would likely result in a similar effect on peak flow at Black Earth as the method adopted for this study. In the future, if more detailed modeling at each specific wetland site is required, the subbasins in the HMS model can be modified accordingly.

Storage characteristics of each reservoir added to the HMS model were derived from the information provided by EOR in Table 41. For the subbasins where two storage areas were identified, the storage characteristics of each wetland were combined, such that the storage of the reservoir was equal to the total storage volume of the two sites, and the storage depth was equal to the average depth of the two sites. The inflow into each reservoir element was set equal to the total runoff from its associated subbasin. For the reservoir element associated with the S_BEC-VS_to_BEC_us_MZ subbasin, the outflow from the R_BEC-VS_to_BEC_us_MZ reach was also added as inflow to the reservoir. This ensured flow from the mainstem of Black Earth Creek also traveled through the reservoir, not just local runoff between Black Earth and Mazomanie. Pertinent information for each reservoir added to the model, including total storage, storage depth, inflow node, and outflow node, is shown in Table 42. The location of each reservoir is shown on the map in Figure 20.

Table 42. Pertinent data for reservoir elements added to the HMS model

Map Number	Reservoir Element	Storage Volume (ac-ft)	Storage Depth (ft)	Inflow	Outflow
1	Res_S_BC_us_CP	19	1	S_BEC_us_CP	J_BC_us_CP
2	Res_S_BEC_us_CP	58.5	1	S_BC_us_CP	J_BC-BEC
3	Res_S_BEC_ds_CP_ to_BEC_us_BE	29.4	2	S_BEC_ds_CP_ to_BEC_us_BE	J_BEC_us_BE
4	Res_S_VC_us_BE	40	1	S_VC_us_BE	J_VC_us_BE
5	Res_S_BEC-VC_ to_BEC_us_MZ	71.4	1.4	S_BEC-VC_ to_BEC_us_MZ + All upstream elements	J_BEC_us_MZ
6	Res_S_WC_us_MZ	17.4	1.7	S_WC_us_MZ	J_HPC-WC

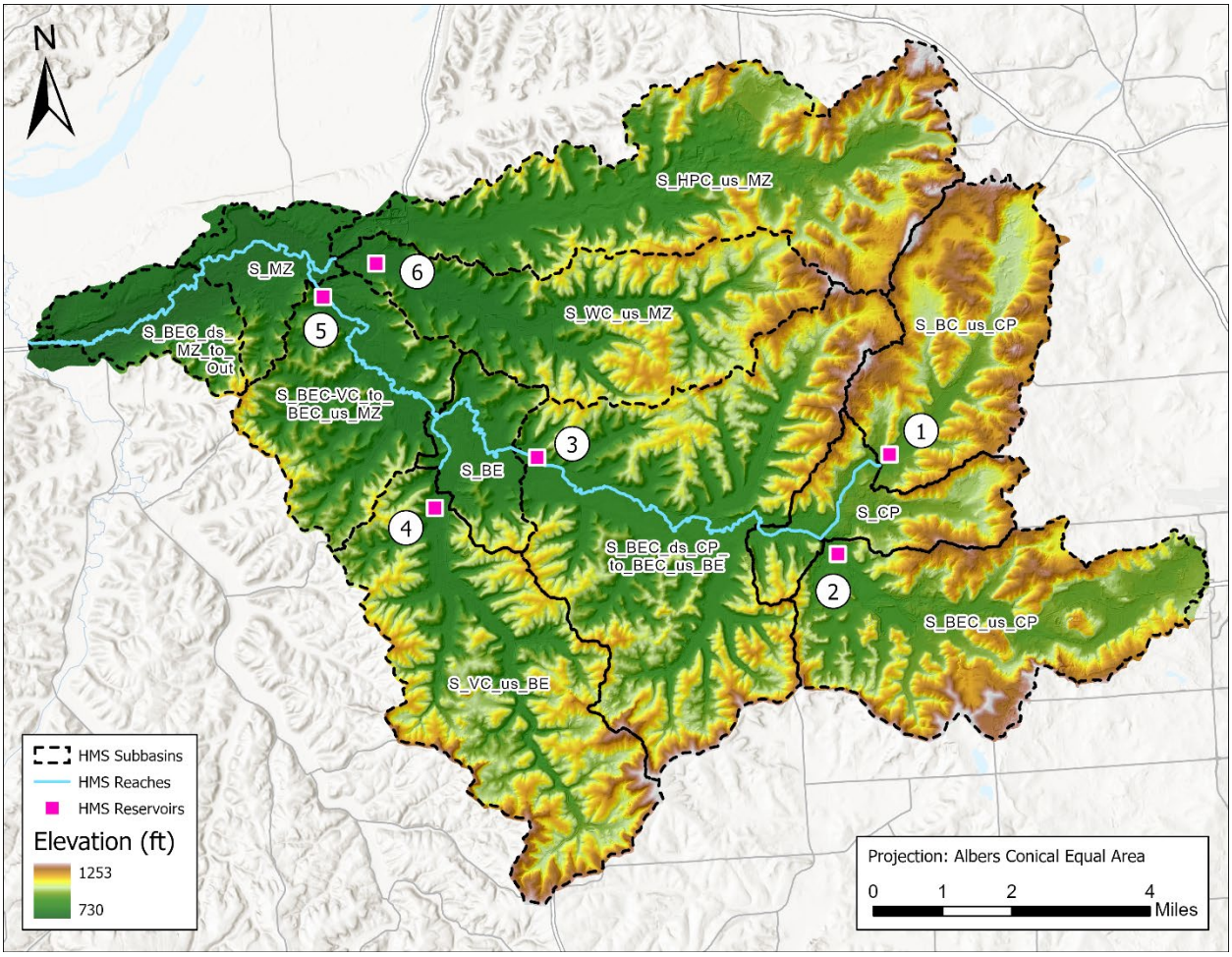

Figure 20. Map of reservoir elements added to the HMS model

Flows were routed through each reservoir using the Outflow Curve method and an elevation-storage-discharge relationship. The elevation-storage relationship for each reservoir was developed assuming

the maximum storage of the wetland corresponded to the storage depth, and minimal additional storage was available above the storage depth elevation. The storage-discharge relationship was developed assuming the reservoir could discharge the baseflow of its upstream element(s) until the maximum storage capacity was reached. At that point, the reservoir would release inflow. This is approximately how the proposed off-channel storage areas would operate. Example elevation-storage and storage-discharge relationships are shown in Table 43 and Table 44 for the Brewery Creek reservoir (Res_S_BC_us_CP).

Table 43. Elevation-storage relationship, Res_S_BC_us_CP

Elevation (ft)	Storage (ac-ft)
0	0
1	19
1.1	20.1

Table 44. Storage-discharge relationship, Res_S_BC_us_CP

Storage (ac-ft)	Discharge (cfs)
0	0
0.1	19
19	20
20	100
20.1	10,000

The exact discharge values used to create the storage-discharge relationship for each reservoir were selected such that all of the storage in the reservoir was available at beginning of the flood wave. To accomplish this, the discharge corresponding to the maximum storage capacity of the reservoir (20 cfs in Table 44), was set approximately equal to the baseflow prior to the flood wave. This ensured the baseflow of the stream passed through the reservoir, and storage was not used until discharge began to exceed baseflow. The behavior of each reservoir during the simulation is similar to the example shown in Figure 21.

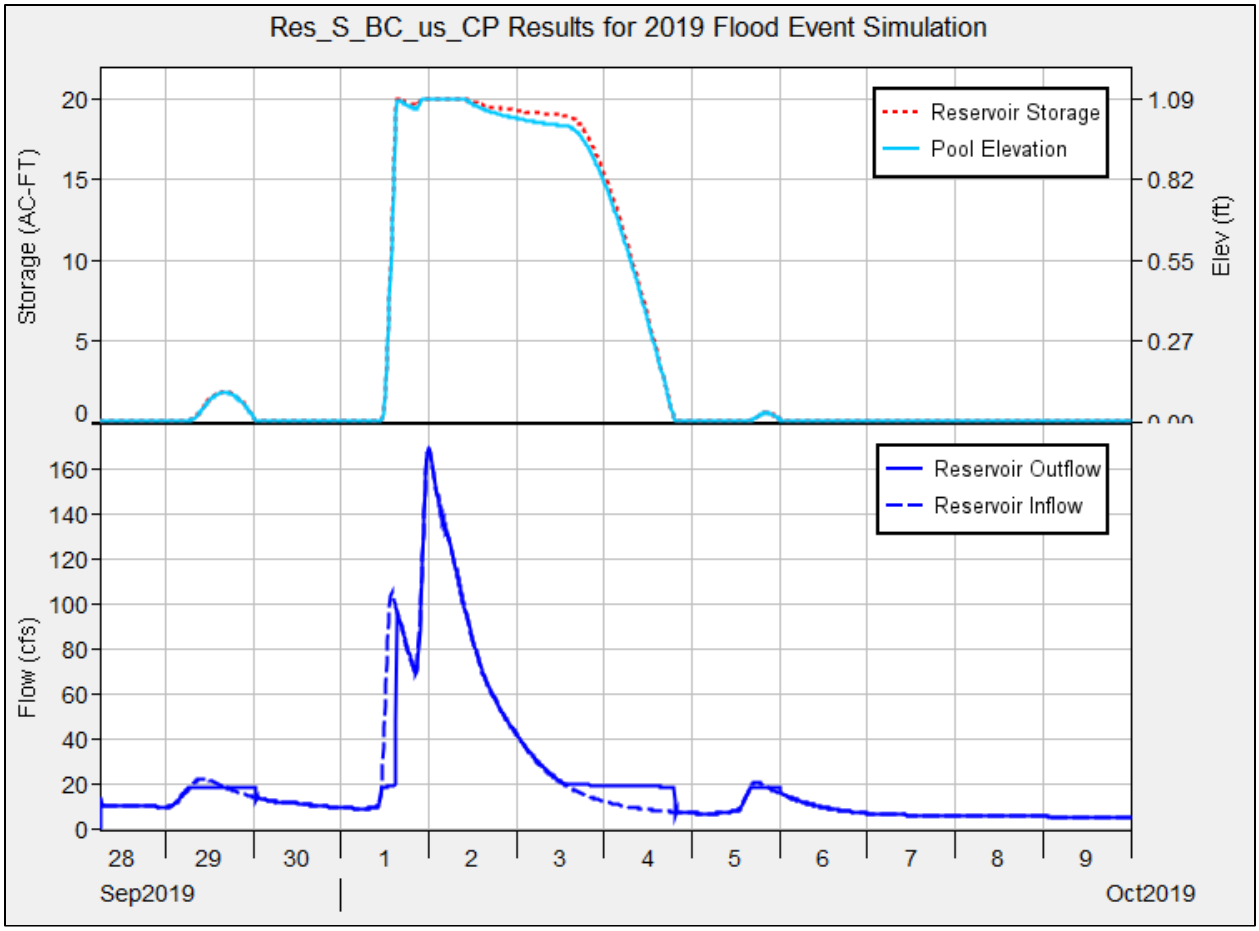

Figure 21. Brewery Creek reservoir (Res_S_BC_us_CP) during the 2019 flood event simulation (WR1)

Since the specific outlet capacity of each proposed storage area is not known, and baseflow leading up to the flood event differs between the three calibration events, only the 2019 event was simulated for this alternative. The 2019 event was selected because it is the smallest of the three events and would therefore show the maximum flood reducing effect for the alternative. In order to simulate other flood events, the storage-discharge relationship for each reservoir would need to be modified to ensure the reservoir did not fill prior to the onset of the flood wave, since the discharge threshold for entry into each reservoir is not known. If more detailed design of the proposed storage areas is conducted in the future, the storage-discharge relationship for each reservoir can be modified to more accurately simulate this alternative under multiple flood events.

Two simulations were run for the Wetland Restoration alternative. The first simulated the nine priority wetland sites as they are described above. This simulation was labeled "WR1." Reductions in peak flow at Cross Plains, Black Earth, and Mazomanie ranged from 1% to 4% in the WR1 simulation. In the second simulation, labeled "WR2," the storage capacity for each reservoir was doubled. Reductions in peak flow at Cross Plains, Black Earth, and Mazomanie ranged from 9% to 17% in the WR2 simulation. These results are shown in Table 45. Table 46 shows how the maximum inundation for each *Wetland Restoration* simulation compares to the maximum inundation for the baseline model.

Table 45. Peak flow reductions under the Wetland Restoration alternative

Flood Event	Peak Flow (cfs)		
	Baseline	WR1	WR2
	Cross Plains, WI (model element: J_BEC_ds_CP)		
Sep-Oct 2019	596	588 (-1%)	494 (-17%)
	Black Earth, WI (model element: J_BEC_us_BE)		
Sep-Oct 2019	1,076	1,033 (-4%)	921 (-14%)
	Mazomanie, WI (model element: J_BEC_ds_MZ)		
Sep-Oct 2019	1,769	1,727 (-2%)	1,610 (-9%)

Table 46. Inundation area reduction under the Wetland Restoration alternative

Flood Event	Maximum Inundation (acres)		
	Baseline	WR1	WR2
Sep-Oct 2019	1,242	1,221 (-2%)	1,180 (-5%)

10.6 50% Impervious Area

The sixth alternative, labeled "50% Impervious Area," simulated how the basin would respond if 50% of the impervious area in each subbasin was converted to non-impervious area. Similar to the *25% Ag Non-Contributing* alternative, the *50% Impervious Area* alternative does not simulate a particular intervention or land use practice. However, it provides a reference for other alternatives. To model the *50% Impervious Area* alternative in HMS, the impervious percentage was simply reduced by 50% for each subbasin, as shown in Table 47. Note these impervious percentages include roads.

Table 47. Impervious percentage for each subbasin adopted for the 50% Impervious Area alternative

Subbasin	Baseline Impervious %	Alternative Impervious %
S_BC_us_CP	6	3.0
S_BEC_us_CP	10	5.0
S_CP	21	10.5
S_BEC_ds_CP_to_BEC_us_BE	5	2.5
S_VC_us_BE	4	2.0
S_BE	18	9.0
S_BEC-VC_to_BEC_us_MZ	6	3.0
S_HPC_us_MZ	4	2.0
S_WC_us_MZ	5	2.5
S_MZ	24	12.0
S_BEC_ds_MZ_to_Out	7	3.5

Model simulations with the alternative subbasin impervious percentages listed above were run for the three calibration events. Reductions in peak flow at Cross Plains, Black Earth, and Mazomanie ranged

from 9% to 21% (Table 48). Table 49 shows how the maximum inundation for the *50% Impervious Area* alternative compares to the maximum inundation for the baseline model.

Table 48. Peak flow reductions under the 50% Impervious Area alternative

Flood Event	Peak Flow (cfs)		
	Baseline	50% Impervious Area	% Decrease
	Cross Plains, WI (model element: J_BEC_ds_CP)		
Jul 1993	891	703	-21%
Aug 2018	2,792	2,334	-16%
Sep-Oct 2019	596	505	-15%
	Black Earth, WI (model element: J_BEC_us_BE)		
Jul 1993	1,248	1,042	-17%
Aug 2018	2,979	2462	-17%
Sep-Oct 2019	1,076	978	-9%
	Mazomanie, WI (model element: J_BEC_ds_MZ)		
Jul 1993	2,239	1,921	-14%
Aug 2018	3,540	2,832	-20%
Sep-Oct 2019	1,769	1,569	-11%

Table 49. Inundation area reduction under the 50% Impervious Area alternative

Flood Event	Maximum Inundation (acres)		
	Baseline	50% Impervious Area	% Decrease
Jul 1993	1,349	1,239	8%
Aug 2018	1,986	1,802	9%
Sep-Oct 2019	1,242	1,175	5%

10.7 Green Infrastructure

The seventh alternative, labeled "Green Infrastructure," simulated how the implementation of a suite of green infrastructure practices in urban areas would affect the basin's runoff response. Since the HMS model simulates runoff at a basin-wide scale, individual green infrastructure practices could not be modeled explicitly. However, the aggregate effect of a suite of green infrastructure practices on HMS model parameters could be estimated by running several small-scale models in various urban areas and extrapolating the results across the basin.

For this study, EOR performed several small-scale model simulations of green infrastructure practices in Cross Plains, Black Earth, and Mazomanie using the Environmental Protection Agency (EPA) National Stormwater Calculator (EPA, 2019). The National Stormwater Calculator estimates annual runoff from a specific site (less than 12 acres) using green infrastructure, or low impact development, controls. The user enters the percentage of impervious cover currently present at the site. The tool estimates rainfall depth for a user-defined recurrence interval (100-year, 50-year, etc.) using rainfall recorded at a nearby rain gage (EPA, 2017). The calculator then computes the runoff depth from the given storm event with green infrastructure in place. The user can select a variety of green infrastructure practices, including

downspout disconnection, rainwater harvesting, rain gardens, green roofs, street planters, infiltration basins, and porous pavements.

EOR ran the National Stormwater Calculator at two sites in each village, one site in a residential area with approximately 40% impervious cover, and one site in a downtown or commercial area with approximately 70% impervious cover. For residential sites, a total of 35% of the impervious surfaces were treated with a green infrastructure practice. For downtown/commercial sites, a total of 50% of impervious surfaces were treated with a green infrastructure practice. The suite of green infrastructure practices applied for each type of site, as well as the percentage of the modeled area treated by each practice, is shown in Table 50. The type and percentage of each practice applied to each site were selected by the EOR using literature and engineering judgement, with input from the local sponsor's steering committee. While many combinations of green infrastructure practices are possible, the suites selected for modeling are targeted for runoff reduction and represent a reasonable investment in green infrastructure in each village.

Table 50. Type and scale of green infrastructure practices used at each type of site in the National Stormwater Calculator

	Site Type	
	Residential	Downtown/Commercial
Green Infrastructure Practices	Roof downspout connection (20%) Permeable pavement (10%) Rain gardens (5%)	Infiltration basins (20%) Permeable pavement (20%) Rainwater harvesting (10%) Green roofs (10%)
Total Area Treated	35%	50%

After running the National Stormwater Calculator for each site type in each village with green infrastructure in place (six simulations in all), the model was run again. This time, all green infrastructure was removed, and the impervious percentage was reduced such that the model produced similar runoff to the runoff that was computed with green infrastructure in place. The modified impervious percentage was then compared to the original impervious percentage for each simulation. In this way, each suite of green infrastructure practices could be effectively reduced to an equivalent reduction in impervious cover. Table 51 shows the original impervious percentage in each National Stormwater Calculator simulation as well as the "functional" impervious percentage. The "functional" impervious percentage is the impervious percentage that produced the same runoff depth with no green infrastructure controls in place as the simulation with the original impervious area and green infrastructure controls in place. Note the six simulations shown are for the 1% Annual Exceedance Probability (AEP), or 100-year rainfall event. EOR also ran simulations using the 2% AEP (50-year) and 20% AEP (5-year) events, but the functional impervious percentage was similar across all events. The equivalent reduction in impervious area also did not vary considerably across simulations, with an average equivalent reduction of 26%.

Table 51. Results of National Stormwater Calculator model – 0.01% AEP (100-year) event

Simulation	Original Impervious %	Functional Impervious %	Equivalent Reduction in Impervious Area
Residential 1	38	28	26%
Residential 2	41	30	27%
Residential 3	47	34	28%
Commercial 1	68	53	22%
Commercial 2	69	51	26%
Commercial 3	70	52	26%

To simulate widespread implementation of the green infrastructure improvements analyzed with the National Stormwater Calculator, the impervious percentage for each subbasin in the HMS model was reduced relative to the amount of impervious area within the subbasin that could be treated with green infrastructure. Impervious areas considered treatable by green infrastructure were all impervious surfaces within the Cross Plains, Black Earth, and Mazomanie village limits (including roads) and all non-road impervious surfaces outside the village limits. Since the equivalent reduction in impervious area expected from implementing green infrastructure was approximately 26% in each National Stormwater Calculator simulation, 26% of the treatable impervious surfaces were removed, and a new impervious percentage for each subbasin was computed. Table 52 shows the original impervious percentage for each subbasin, the impervious percentage that can be treated with green infrastructure, and the final, computed impervious percentage adopted for the alternative. Note all percentages presented in the table are a percentage of the total land area of the subbasin.

Table 52. Impervious percentage for each subbasin adopted for the Green Infrastructure alternative

Subbasin	Original Impervious %	Treatable Impervious %	Alternative Impervious %
S_BC_us_CP	6.2	0.5	6.1
S_BEC_us_CP	9.7	4.2	8.6
S_CP	21.5	17.6	17.0
S_BEC_ds_CP_to_BEC_us_BE	4.6	0.3	4.5
S_VC_us_BE	4.0	0.0	4.0
S_BE	18.3	14.9	14.4
S_BEC-VC_to_BEC_us_MZ	5.8	0.3	5.7
S_HPC_us_MZ	3.6	0.0	3.6
S_WC_us_MZ	4.5	0.1	4.5
S_MZ	23.5	18.9	18.6
S_BEC_ds_MZ_to_Out	6.8	1.3	6.4

Model simulations with the alternative subbasin impervious percentages listed above were run for the three calibration events. Reductions in peak flow at Cross Plains, Black Earth, and Mazomanie ranged from 0% to 4% (Table 53). Table 54 shows how the maximum inundation for the *Green Infrastructure* alternative compares to the maximum inundation for the baseline model.

Table 53. Peak flow reductions under the Green Infrastructure alternative

Flood Event	Peak Flow (cfs)		
	Baseline	Green Infrastructure	% Decrease
	Cross Plains, WI (model element: J_BEC_ds_CP)		
Jul 1993	891	891	0%
Aug 2018	2,792	2,688	-4%
Sep-Oct 2019	596	576	-3%
	Black Earth, WI (model element: J_BEC_us_BE)		
Jul 1993	1,248	1,248	0%
Aug 2018	2,979	2,881	-3%
Sep-Oct 2019	1,076	1,058	-2%
	Mazomanie, WI (model element: J_BEC_ds_MZ)		
Jul 1993	2,239	2,239	0%
Aug 2018	3,540	3,397	-4%
Sep-Oct 2019	1,769	1,725	-2%

Table 54. Inundation area reduction under the Green Infrastructure alternative

Flood Event	Maximum Inundation (acres)		
	Baseline	Green Infrastructure	% Decrease
Jul 1993	1,349	1,349	0%
Aug 2018	1,986	1,954	2%
Sep-Oct 2019	1,242	1,229	1%

11 Discussion

A summary of the mean peak flow reduction over the three calibration events at the three output locations (Cross Plains, Black Earth, and Mazomanie) for each alternative is shown in Figure 22. Figure 23 shows the average inundation reduction on the mainstem of Black Earth Creek over the three calibration events. Note only the 2019 flood event was simulated for the wetland restoration alternative. Alternatives are grouped by color, and the two reference alternatives (*50% Impervious Area* and *25% Ag Non-Contributing*) are shown as hashed, grey bars.

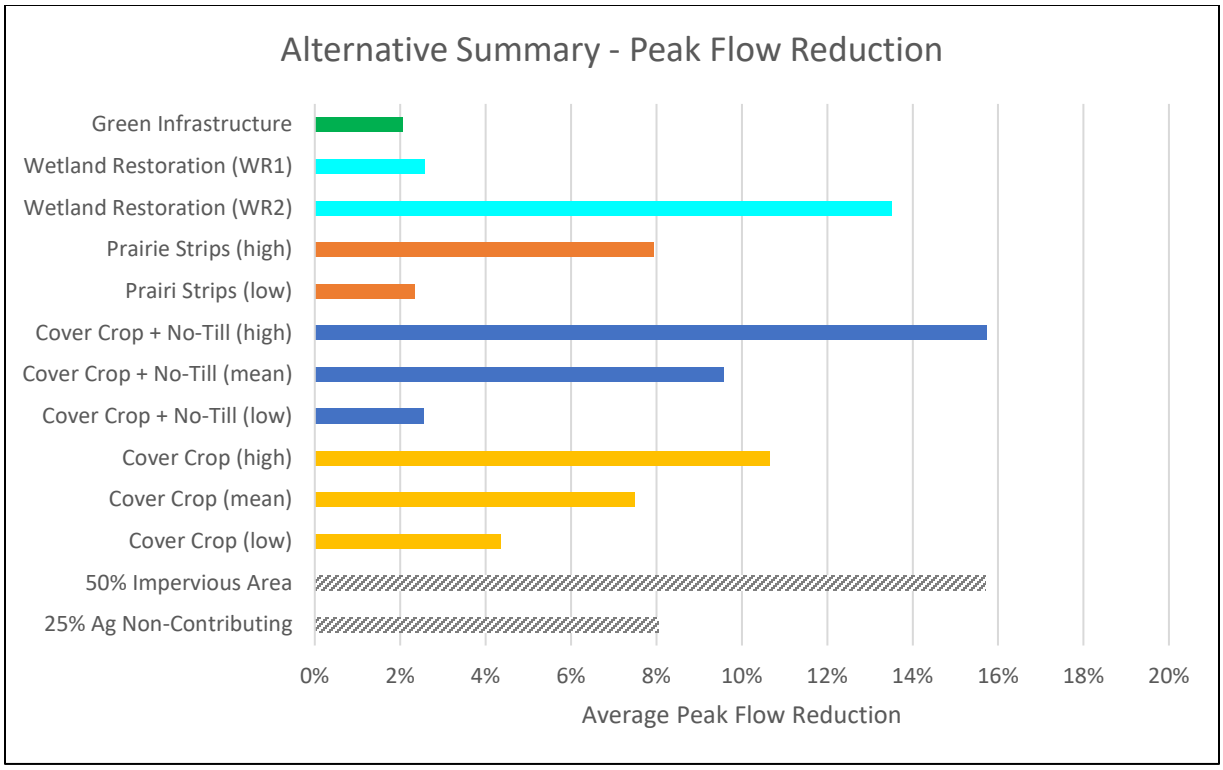

Figure 22. Average peak flow reduction for each alternative studied

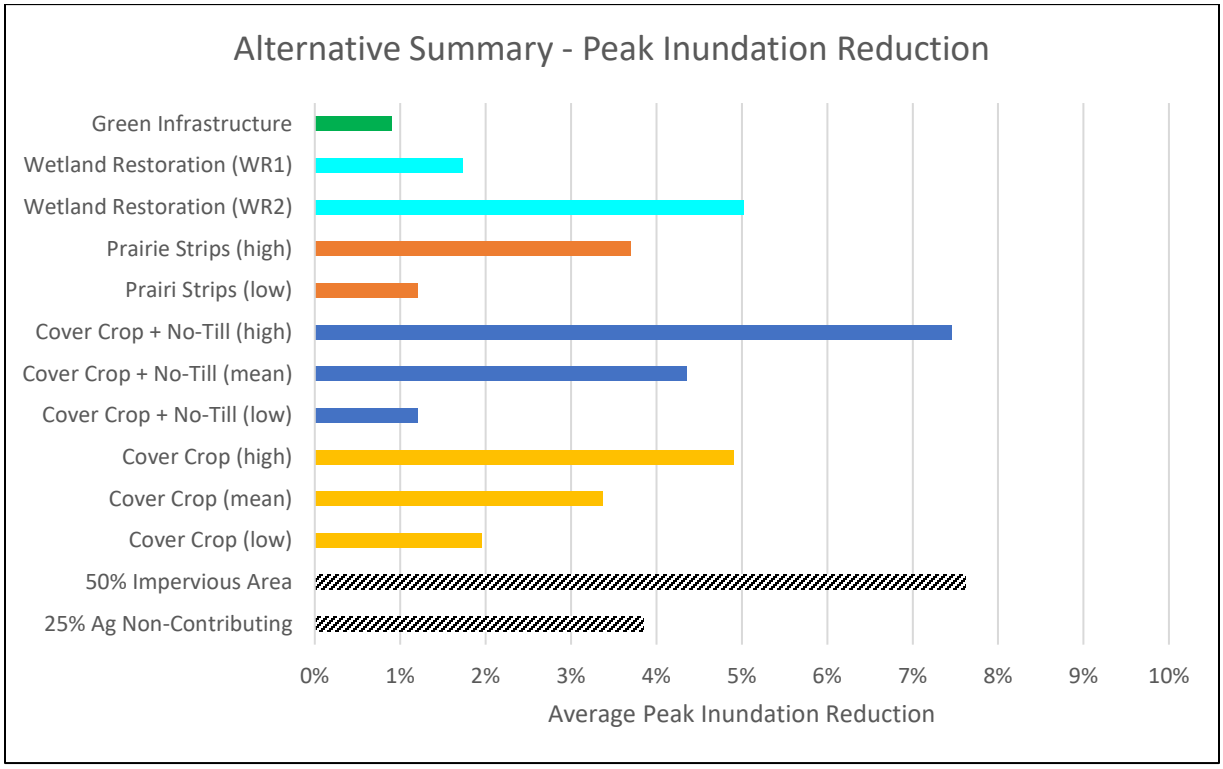

Figure 23. Average peak inundation reduction for each alternative studied

11.1 Cover Crops

The model results for the *100% Cover Crop* and *100% Cover Crop + No-Till* alternatives show the widespread implementation of cover crops throughout the Black Earth Creek basin may decrease peak flows observed at Cross Plains, Black Earth, and Mazomanie, and the addition of no-till farming practices would likely increase the effectiveness of cover crops in reducing flood peaks. Alternative simulations showed the magnitude of peak flow reduction ranged from 4% to 18% and could possibly be increased to 34% during some flood events with the addition of no-till. On average, the adoption of cover crops decreased the magnitude of peak flows by approximately 7% and decreased the peak inundation on Black Earth Creek by 3%.

Because there is probably already some use of cover crops and no-till in the basin, the actual, maximum decrease in peak flow expected throughout the basin is somewhat less than the model suggests. Both alternatives also assumed infiltration accounts for 100% of losses during a large flood event. While this is a reasonable assumption, it likely leads to an overestimation of the benefits of cover crops. The impact these two factors have on the results is not clear. However, it is assumed a realistic estimate of the potential peak flow reduction associated with widespread adoption of cover crops is somewhat lower than the model suggests, especially considering it is unlikely 100% of landowners would implement cover crops, even with a large public policy incentive.

11.2 No-Till

No alternative specifically studying the effects of no-till was developed, because no-till likely increases the rate of infiltration to a lesser degree than cover crops. According to Basche and DeLonge, the highest estimated increase in infiltration rates due to the adoption of no-till is approximately 24%, and the lowest estimated increase in infiltration rates due to the adoption of cover crops is approximately 36%. Therefore, it can be assumed if no-till were adopted in every row-cropped field in the basin, flood peaks would be reduced on average by less than 4%, since this is the lowest value computed in the *100% Cover Crop* alternative. However, as described in the previous section, the combination of no-till and cover crops may increase the rate of soil infiltration more than cover crops alone. Also, no-till seems to have a greater impact on infiltration rates when combined with residue retention practices (Basche & DeLonge, 2019). Both residue retention and cover crops increase soil organic matter, which increases plant available water. Therefore, if cover crops are not adopted, residue retention is another conservation practice that, combined with no-till, can increase water infiltration and retention within the soil.

11.3 Prairie Strips

The model results for the *Prairie Strips* alternative show the widespread implementation of prairie buffer strips throughout the basin may decrease peak flow on Black Earth Creek by 2% to 8%, which corresponds to a decrease in peak inundation on Black Earth Creek of 1% to 4%. However, a 2% reduction in peak flow is more likely, considering peak flow was only reduced by 8% when prairie strips were assumed to reduce runoff from all flood events by 44%. While this value is mentioned by the STRIPS researchers at Iowa State University, this magnitude of runoff reduction is more likely a measure of total volume reduction on an annual basis, not peak flow reduction during a single, large storm event. During the kind of intense rainfall event that leads to overland flooding of Black Earth Creek, the soil in agricultural fields is likely to become fully saturated, limiting the capacity of prairie buffer strips to infiltrate runoff. Buffer strips may still slow the velocity of flow on the field surface and trap sediment,

thereby reducing soil and phosphorus loss, but they should not be expected to significantly decrease water runoff during these events. Prairie buffer strips do offer other benefits though, such as improved biodiversity, and there is good evidence they reduce runoff from small rain events, which can significantly reduce nutrient loss over time (Schulte, 2017).

11.4 Wetland Restoration

Model results for the *Wetland Restoration* alternative show construction of off-channel wetland storage areas has the potential to decrease peak flow on Black Earth Creek during flood events similar in magnitude to the 2019 event (13% annual exceedance probability). However, the storage provided by the nine priority wetland sites alone only reduced peak flows by approximately 3% and peak inundation by approximately 2%. When storage at each site was doubled, peak flows were reduced by about 13%, which corresponded to a 5% reduction in inundation on Black Earth Creek. However, it is not clear whether increasing the amount of storage at each site, or increasing the number of constructed storage areas, is economically and politically feasible in the basin. It can also be assumed peak flows would be reduced less during larger flood events, as the storage areas are more likely to completely fill prior to the flood peak. Conversely, it is likely the storage areas would more effectively reduce flood peaks during smaller events. The storage areas may also have a more significant local flood risk impact, particularly on small tributaries such as Garfoot Creek.

11.5 Green Infrastructure

Model results for the *Green Infrastructure* alternative show a significant number of urban green infrastructure improvements throughout the basin would result in minimal peak flow reduction on Black Earth Creek (2%) and minimal change in inundation (1%). This result is expected, since there is very little impervious area in the watershed, and even less that can be treated with green infrastructure projects (i.e. not a major road). A higher percentage of impervious area treated with green infrastructure could be modeled, but it is not likely to result in significantly greater runoff reduction. There is just too much land producing runoff across the basin relative to the amount of land that can be treated with green infrastructure. However, this is not to say building green infrastructure improvements throughout the basin is a poor investment. There are a number of infrastructure, water quality, and quality of life improvements that can be gained from green infrastructure at a community or neighborhood scale. For example, the addition of green roofs and permeable pavement to a city block may reduce the likelihood of localized storm sewer flooding and reduce city maintenance costs and insurance claims in the long term.

11.6 Water and Sediment Control Basins (WASCOBs)

A water and sediment control basin (WASCOB) is a small embankment built across (perpendicular to) a small watercourse or drainageway in an agricultural field (Porter, 2015). The objective of WASCOB construction is to trap sediment and store runoff, reducing soil and nutrient loss. Depending on the size and number of WASCOBs in a field, runoff could be significantly reduced. To evaluate the storage potential of widespread construction of WASCOBs across the Black Earth Creek basin, EOR identified all sites in the Upper Black Earth Creek and Lower Black Earth Creek HUC-12 watersheds suitable for a WASCOB using the WASCOB tool in the ACPF toolbox. EOR then computed the combined storage of all WASCOBs identified by the tool. In total, this storage added up to only 18 ac-ft in the Upper Black Earth Creek basin and 11 ac-ft in the Middle Black Earth Creek basin. Considering the runoff volume from the

Brewery Creek subbasin alone during the 2019 flood event was 337 ac-ft, widespread construction of WASCOBs throughout the watershed cannot be expected to reduce flooding on Black Earth Creek.

12 Opportunities for Further Study

The analysis presented in this report summarizes how peak flows and maximum inundation for several historical, rainfall-driven flood events may be reduced due to widespread adoption of agricultural BMPs and urban green infrastructure projects. In the future, the Black Earth Creek HEC-HMS model could also be used to determine how such land use changes may impact hypothetical storm events, such as the 1% annual exceedance probability flood event at Cross Plains, Black Earth, or Mazomanie, if such information is valuable to the study sponsor. The HEC-RAS model produced for this study could be used to predict water surface profiles and flood extents for various events, although more detailed channel bathymetry data should be collected before using the model to produce detailed inundation maps.

While outside the scope of this study, future analysis is warranted regarding the cost of implementing agricultural BMP, wetland restoration, and urban green infrastructure projects across the watershed, as well as their expected non-hydrologic benefits. Many agricultural BMPs significantly impact water quality, which may lead to better aquatic species habitat and recreation opportunities, and green infrastructure improvements can benefit the community outside of major flood events. Wetlands provide habitat for migratory waterfowl and other native species. Landowners and local communities as a whole must also desire these projects and be incentivized to implement them if the benefits described in this report are to be realized.

13 References

1. Acreman, M. and Bullock, A. (2003). *The role of wetlands in the hydrological cycle*. Hydrology and Earth System Sciences, 7(3), 358-389.
2. Antolini, F., Dalzell, B., Hawthorne, P., Johnson, K., Tate, E., and Young, N. (2019). *Flood risk reduction from agricultural best management practices*. Journal of the American Water Resources Association, 56(1). https://onlinelibrary.wiley.com/doi/full/10.1111/1752-1688.12812
3. Basche, A. and DeLonge, M. (2019, September 19). *Comparing infiltration rates in soils managed with conventional and alternative farming methods: A meta-analysis*. PLoS ONE, 14(9). E0215702.
4. Blanco-Canqui, H. and Jasa, P. (2019, July 18). *Do Grass and Legume Cover Crops Improve Soil Properties in the Long Term?* Soil Science Society of America Journal, 83(4), 1181-1187.
5. Blanco-Canqui, H. and Lal, R. (2008, November 1). *Axle-load impacts on hydraulic properties and corn yield in no-till clay and silt loam*. Agronomy Journal, 100(6).
6. Dao, T. (1993). *Tillage and winter wheat residue management effects on water infiltration and storage*. Soil Science Society of America Journal, 57(6), 1586-1595.
7. Edwards, W., Shipitalo, M., Traina, S., Edwards, C., and Owens, L. (1992, December). *Role of lumbricus terrestris (L.) burrows on quality of infiltrating water*. Soil Biology and Biochemistry, 24(12), 155-1561.
8. Environmental Protection Agency (EPA) (2017). *National Stormwater Calculator (SWC)*. Retrieved from https://www.epa.gov/sites/default/files/2017-09/documents/swc_technical_factsheet_update_final_9-28-17.pdf
9. Environmental Protection Agency (EPA) (2019). National Stormwater Calculator Version 2.0.0.1. Retrieved from https://www.epa.gov/water-research/national-stormwater-calculator
10. Evett, S., Peters, F., Jones, O., Unger, P. (1999). *Soil hydraulic conductivity and retention curves from tension infiltrometer and laboratory data*. In M. T. van Genuchten, F. J. Leij, and L. Wu (eds.). Proc. Int. workshop characterization and measurement of the hydraulic properties of unsaturated porous media, 541-551.
11. Federal Emergency Management Agency (2009). *Flood Insurance Study: Dane County, Wisconsin and Incorporated Areas*. Volume 1 of 2. Washington, D.C.
12. Freshwater Network (2020). *Wetlands by Design*. Retrieved from https://freshwaternetwork.org/projects/wetlands-by-design/
13. Hernandez-Santana, V., Zhou, X., Helmers, M.J., Asbjornsen, H., Kolka, R., Tomer, M. (2013). *Native prairie filter strips reduce runoff from hillslopes under annual row-crop systems in Iowa, USA*. Journal of Hydrology, 477, 94-103.
14. Hubbard, R., Phatak, S., and Strickland, T. (2013, January). *Effects of cover crop systems on soil physical properties and carbon/nitrogen relationships in the coastal plain of the southeastern USA*. Soil and Tillage Research, 126, 276-283.
15. Iowa State University (2021). *FAQ: Why would I plant prairie strips on my farm?* Accessed December 13, 2021 from https://www.nrem.iastate.edu/research/STRIPS/content/faq-why-would-i-plant-prairie-strips-my-farm
16. McVay, K., Radcliffe, D., and Hargrove, W. (1989, November 1). *Winter Legume Effects on Soil Properties and Nitrogen Fertilizer Requirements*. Soil Science Society of America Journal, 53(6).

17. Minnesota Department of Natural Resources (2020). *MNDNR_Tools v10*. Retrieved from https://www.dnr.state.mn.us/mis/gis/tools/arcgis/index.html
18. National Trout Center (2020). *About the Driftless Area*. Retrieved from https://nationaltroutcenter.org/visit-ntc/driftless-area/
19. National Weather Service (2020a). *ABRFC Precipitation Processing Methodology*. Accessed December 15, 2020, from https://www.weather.gov/abrfc/pcpn_methods
20. National Weather Service (2020b). *Multisensor Precipitation Estimates (MPE)*. Retrieved December 15, 2020, from https://www.weather.gov/marfc/multisensor_precipitation
21. Porter, S., Tomer, M., Boomer, K., James, D. (2015). *Agricultural conservation planning framework (ACPF) toolbox.* U.S. Department of Agriculture – Agricultural Research Service. Retrieved from https://data.nal.usda.gov/dataset/agricultural-conservation-planning-framework-acpf-toolbox
22. "Public Law 115-436: Water Infrastructure Improvement Act" (2019). Accessed December 13, 2021 from https://www.congress.gov/115/plaws/publ436/PLAW-115publ436.pdf
23. Rawls, W. J., Brakensiek, D. L., Saxton, K. E. (1982). *Estimation of soil water properties*. Transactions of the ASAE, 25(5), 1316-1328.
24. Sand County Foundation (2021) *Estimating the water quality benefits of prairie strips using SnapPlus*. Accessed December 13, 2021 from https://sandcountyfoundation.org/uploads/SCF-Strips-SnapPlus-Handout-WEB-3.5.21.pdf
25. Schulte, L., Niemi, J., Helmers, M., Liebman, M., Arbuckle, G., James, D., Kolka, R., O'Neal, M., Tomer, M., Tyndall, J., Asbjornson, H., Drobney, P., Neal, J., Van Ryswyk, G., Witte, C. (2017). *Prairie strips improve biodiversity and the delivery of multiple ecosystem services from corn-soybean croplands*. PNAS, 114(42), 11247-11252.
26. Simonovic, S. and Juliano, K. (2001). *The role of wetlands during low frequency flooding events in the Red River Basin*. Canadian Water Resources Journal, 26(3), 377-397.
27. U.S. Army Corps of Engineers (2018). *Engineering and Construction Bulletin 2018-14: Guidance for Incorporating Climate Change Impacts to Inland Hydrology in Civil Works Studies, Designs, and Projects*. Washington, D.C.
28. U.S. Army Corps of Engineers (1994). *Engineer Manual (EM) 1110-2-1417 Flood-Runoff Analysis.* Washington, D.C.
29. U.S. Army Corps of Engineers (2017). *Engineering Technical Letter (ETL) 1100-2-3 Guidance for Detection of Nonstationarities in Annual Maximum Discharges*. Washington, D.C.
30. U.S. Army Corps of Engineers (2020a). *National Inventory of Dams*. Retrieved December 17, 2020, from https://nid.sec.usace.army.mil/ords/f?p=105:1
31. U.S. Army Corps of Engineers (2020b). *Engineering and Construction Bulletin 2018-14: Guidance for Incorporating Climate Change Impacts to Inland Hydrology in Civil Works Studies, Designs, and Projects*. Washington, D.C.
32. U.S. Army Corps of Engineers Hydrologic Engineering Center (2016). *GageInterp User's Manual, Version 1.6*. Davis, CA.
33. U.S. Army Corps of Engineers Hydrologic Engineering Center (2020a). *Hydrologic Modeling System HEC-HMS Software, Version 4.7.* Davis, CA.
34. U.S. Army Corps of Engineers Hydrologic Engineering Center (2020b). *Hydrologic Modeling System HEC-HMS User's Manual, Version 4.7.* Davis, CA.

35. U.S. Army Corps of Engineers Hydrologic Engineering Center (2017). *HEC-DSSVue HEC Data Storage System Visual Utility Engine, Version 3.0.* Davis, CA.
36. U.S. Army Corps of Engineers Hydrologic Engineering Center (2019). *HEC-MetVue Meteorological Visualization Engine, Version 3.0.* Davis, CA.
37. U.S. Army Corps of Engineers St. Paul District (2020). *CWMS HEC-HMS Model Development of the Upper Mississippi River between Anoka, MN and Lock and Dam 10.* St. Paul, MN.
38. USDA National Agricultural Statistics Service (2019). *National Cropland Data Layer*. Retrieved December 1, 2020 from https://www.nass.usda.gov/Research_and_Science/Cropland/Release/index.php
39. U.S. Department of Agriculture (2016). *Effects of implementation of soil health management practices on infiltration, saturated hydraulic conductivity (Ksat), and runoff*. Retrieved April 1, 2020 from https://www.nrcs.usda.gov/wps/portal/nrcs/detailfull/soils/health/mgnt/?cid=stelprdb1257753
40. U.S. Fish and Wildlife Service (2020). *National Wetland Inventory*. Retrieved from https://www.fws.gov/wetlands/data/Mapper.html
41. U.S. Geological Survey (2019). *NLCD 2016 Impervious Surface Conterminous United Sates*. Retrieved December 1, 2020 from https://www.mrlc.gov/data/nlcd-2016-percent-developed-imperviousness-conus

US Army Corps of Engineers®
St. Paul District

Appendix A:
Alternative HEC-HMS Results

Table of Tables

Table of Figures

25% Ag Non-Contributing

Table 1. Peak flow reductions under the 25% Ag Non-Contributing alternative

Flood Event	Peak Flow (cfs)		
	Baseline	25% Ag Non-Contributing	% Decrease
	Cross Plains, WI (model element: J_BEC_ds_CP)		
Jul 1993	891	817	-8%
Aug 2018	2,792	2,574	-8%
Sep-Oct 2019	596	550	-8%
	Black Earth, WI (model element: J_BEC_us_BE)		
Jul 1993	1,248	1,147	-8%
Aug 2018	2,979	2,748	-8%
Sep-Oct 2019	1,076	993	-8%
	Mazomanie, WI (model element: J_BEC_ds_MZ)		
Jul 1993	2,239	2,047	-9%
Aug 2018	3,540	3,245	-8%
Sep-Oct 2019	1,769	1,624	-8%

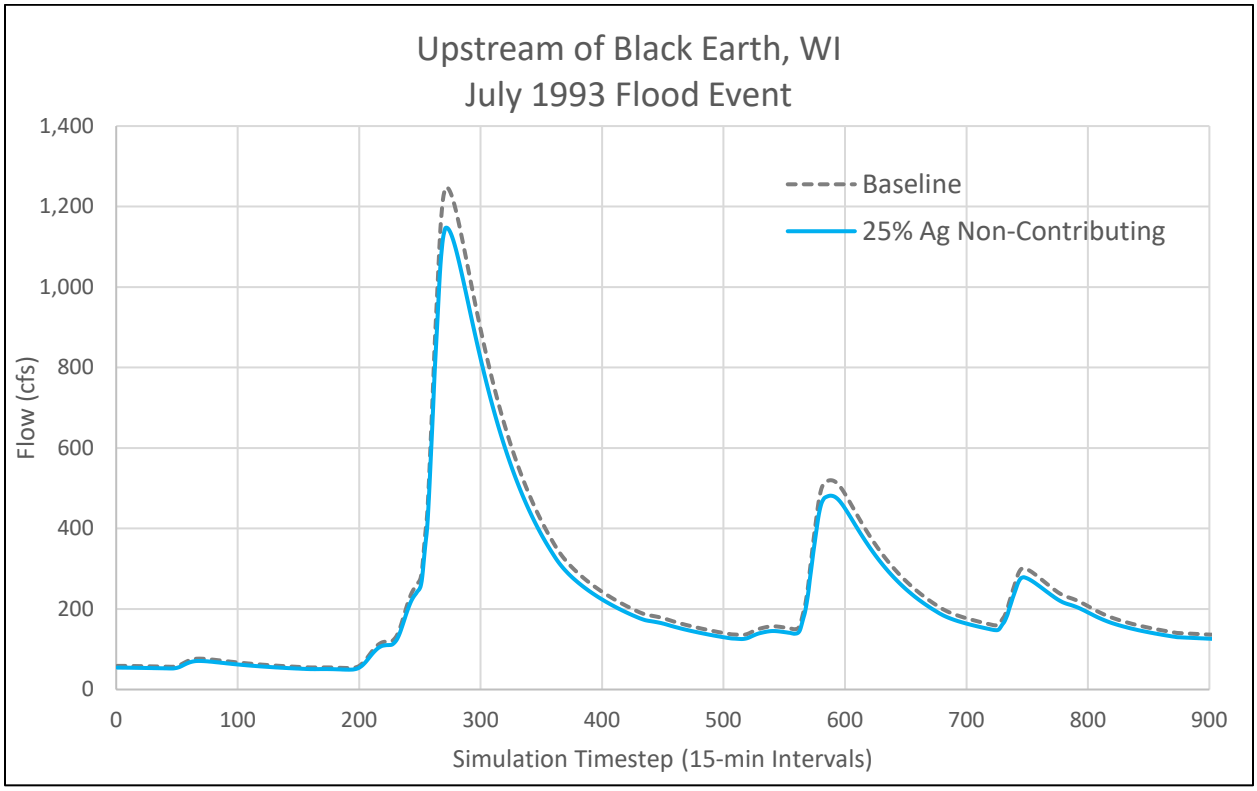

Figure 1. July 1993 simulation results at Black Earth, WI – 25% Ag Non-Contributing alternative

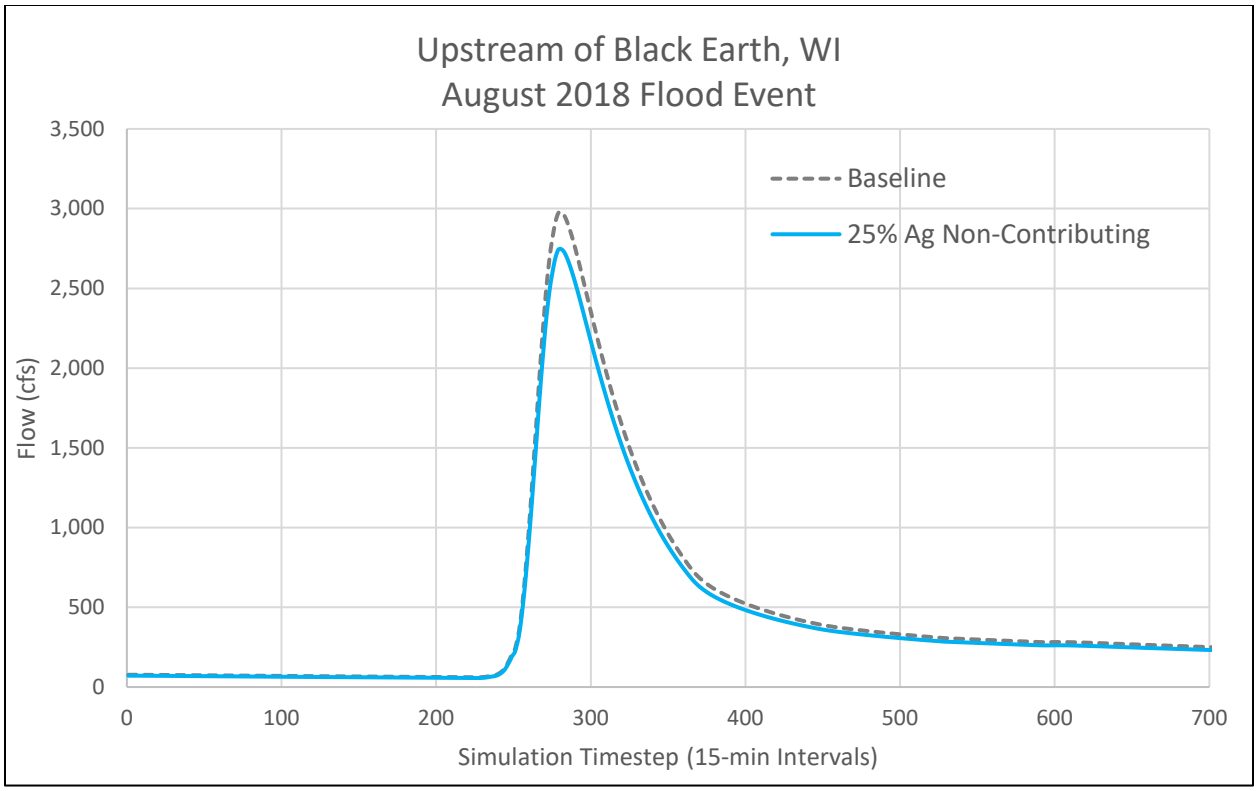

Figure 2. August 2018 simulation results at Black Earth, WI – 25% Ag Non-Contributing alternative

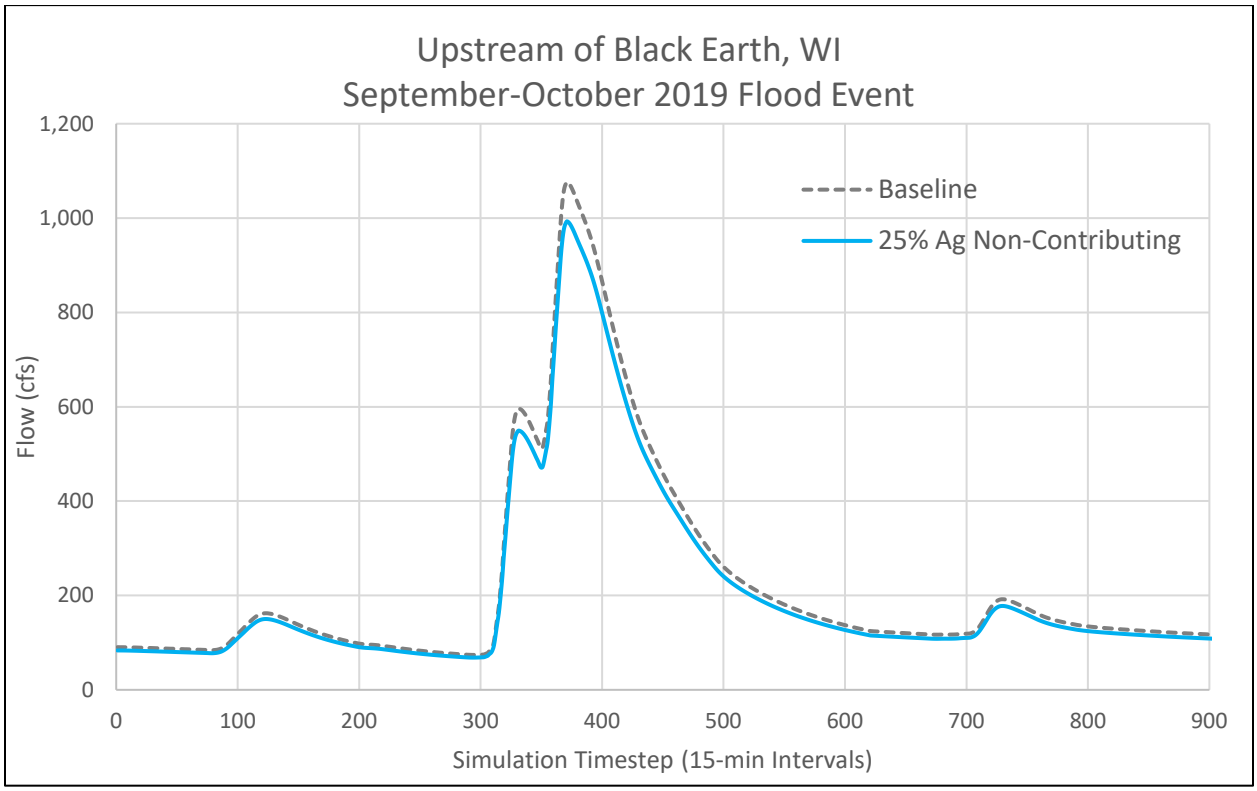

Figure 3. September-October 2019 simulation results at Black Earth, WI – 25% Ag Non-Contributing alternative

100% Cover Crop

Table 2. Peak flow reductions under the 100% Cover Crop alternative

Flood Event	Peak Flow (cfs)			
	Baseline	Low	Mean	High
	Cross Plains, WI (model element: J_BEC_ds_CP)			
Jul 1993	891	865 (-3%)	845 (-5%)	826 (-7%)
Aug 2018	2,792	2,720 (-3%)	2,669 (-4%)	2617 (-6%)
Sep-Oct 2019	596	541 (-9%)	501 (-16%)	459 (-23%)
	Black Earth, WI (model element: J_BEC_us_BE)			
Jul 1993	1,248	1,219 (-2%)	1,198 (-4%)	1,177 (-6%)
Aug 2018	2,979	2,909 (-2%)	2,859 (-4%)	2,809 (-6%)
Sep-Oct 2019	1,076	1,011 (-6%)	963 (-10%)	914 (-15%)
	Mazomanie, WI (model element: J_BEC_ds_MZ)			
Jul 1993	2,239	2,155 (-4%)	2,095 (-6%)	2,034 (-9%)
Aug 2018	3,540	3,457 (-2%)	3,396 (-4%)	3,337 (-6%)
Sep-Oct 2019	1,769	1,635 (-8%)	1,541 (-13%)	1,452 (-18%)

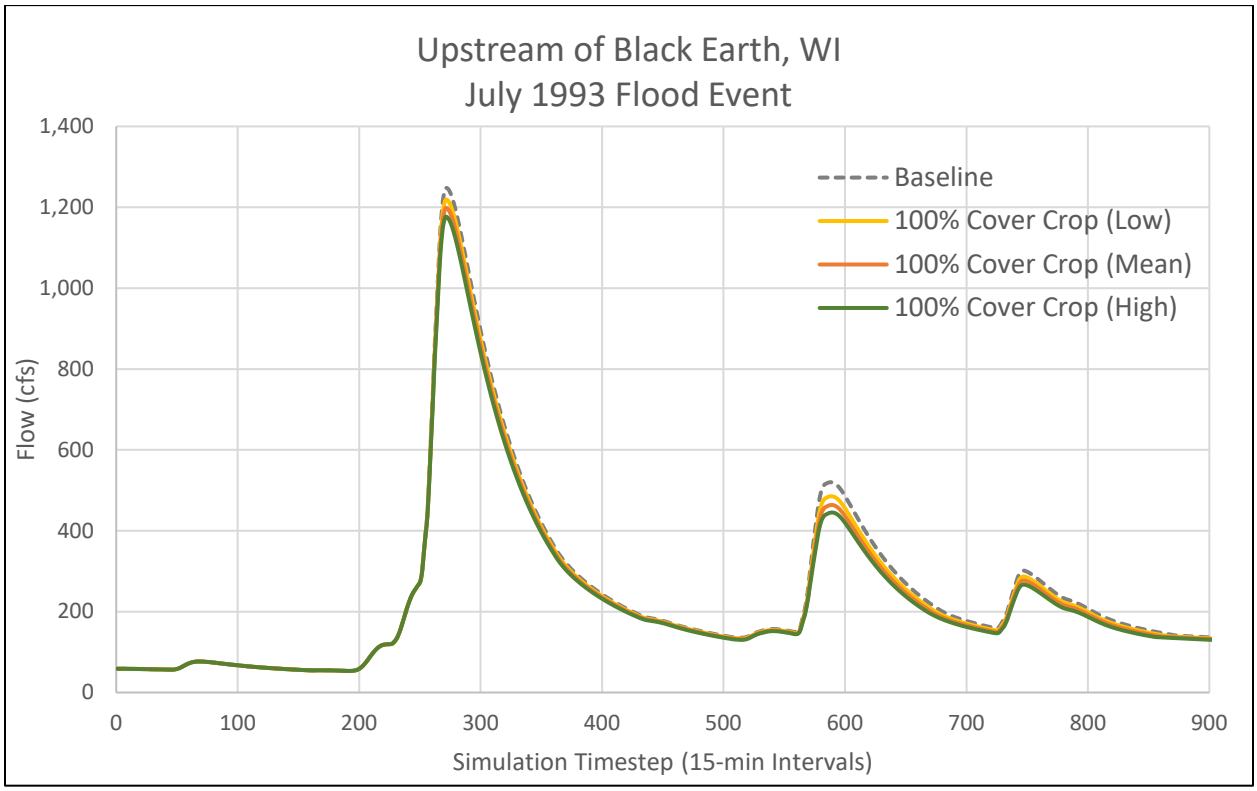

Figure 4. July 1993 simulation results at Black Earth, WI – 100% Cover Crop alternative

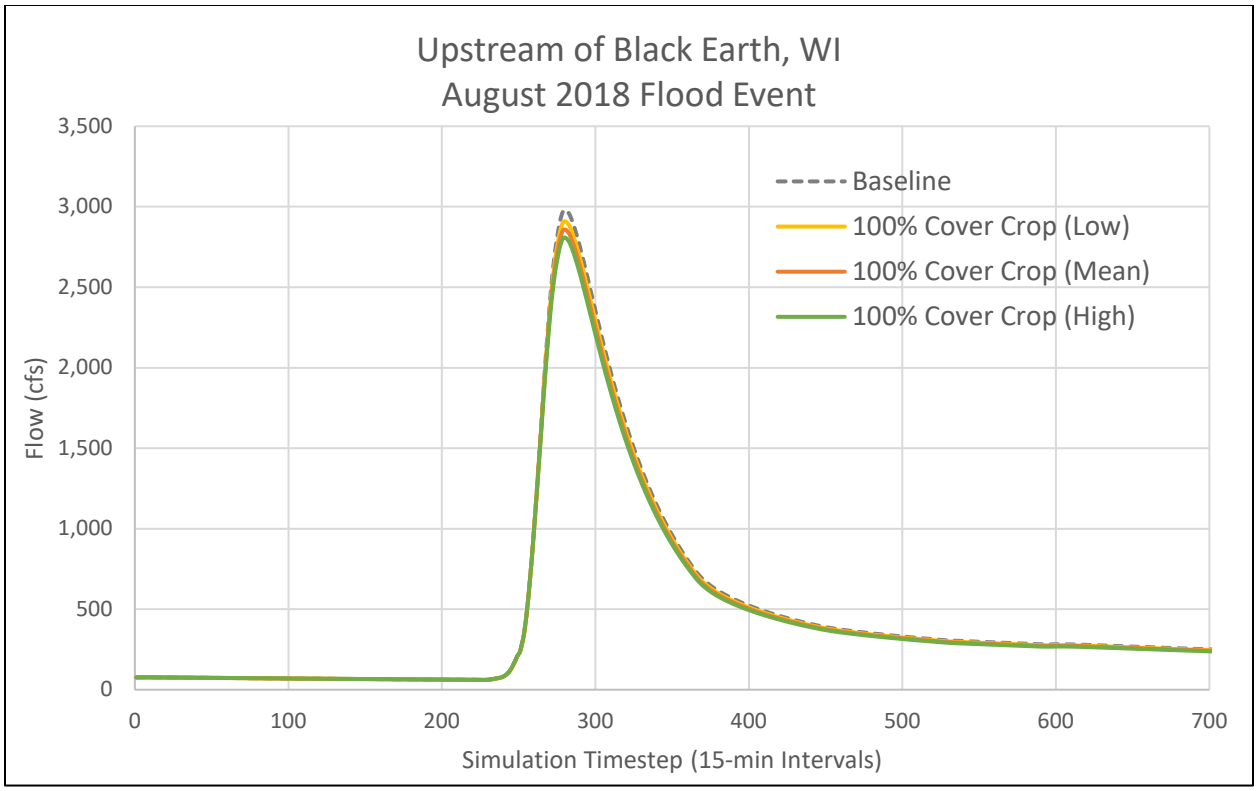

Figure 5. August 2018 simulation results at Black Earth, WI – 100% Cover Crop alternative

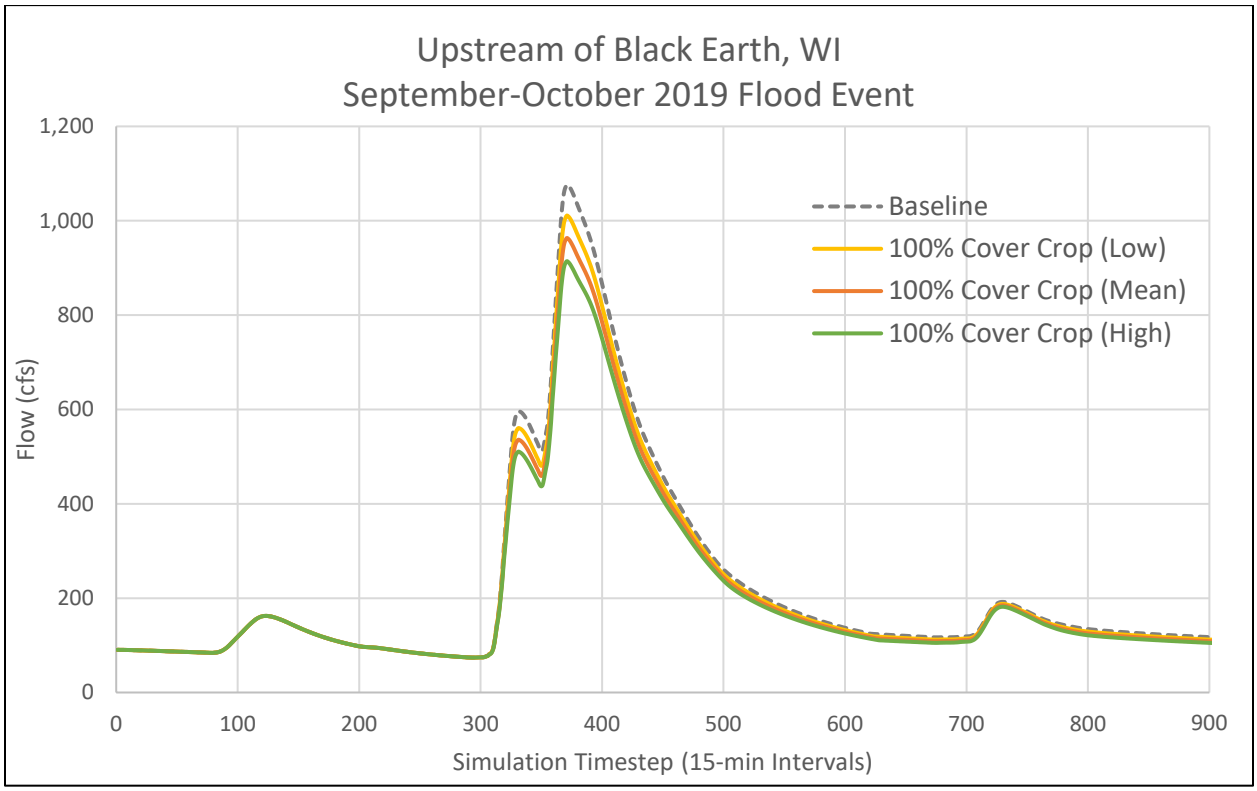

Figure 6. September-October 2019 simulation results at Black Earth, WI – 100% Cover Crop alternative

100% Cover Crop + No-Till

Table 3. Peak flow reductions under the 100% Cover Crop + No-Till alternative

Flood Event	Peak Flow (cfs)			
	Baseline	Low	Mean	High
	Cross Plains, WI (model element: J_BEC_ds_CP)			
Jul 1993	891	876 (-2%)	832 (-7%)	790 (-11%)
Aug 2018	2,792	2,750 (-1%)	2,635 (-6%)	2,533 (-9%)
Sep-Oct 2019	596	564 (-5%)	473 (-21%)	394 (-34%)
	Black Earth, WI (model element: J_BEC_us_BE)			
Jul 1993	1,248	1,231 (-1%)	1,184 (-5%)	1,138 (-9%)
Aug 2018	2,979	2,939 (-1%)	2,826 (-5%)	2,728 (-8%)
Sep-Oct 2019	1,076	1,038 (-3%)	931 (-13%)	836 (-22%)
	Mazomanie, WI (model element: J_BEC_ds_MZ)			
Jul 1993	2,239	2,189 (-2%)	2,055 (-8%)	1,923 (-14%)
Aug 2018	3,540	3,492 (-1%)	3,357 (-5%)	3,242 (-8%)
Sep-Oct 2019	1,769	1,689 (-5%)	1,482 (-16%)	1,327 (-25%)

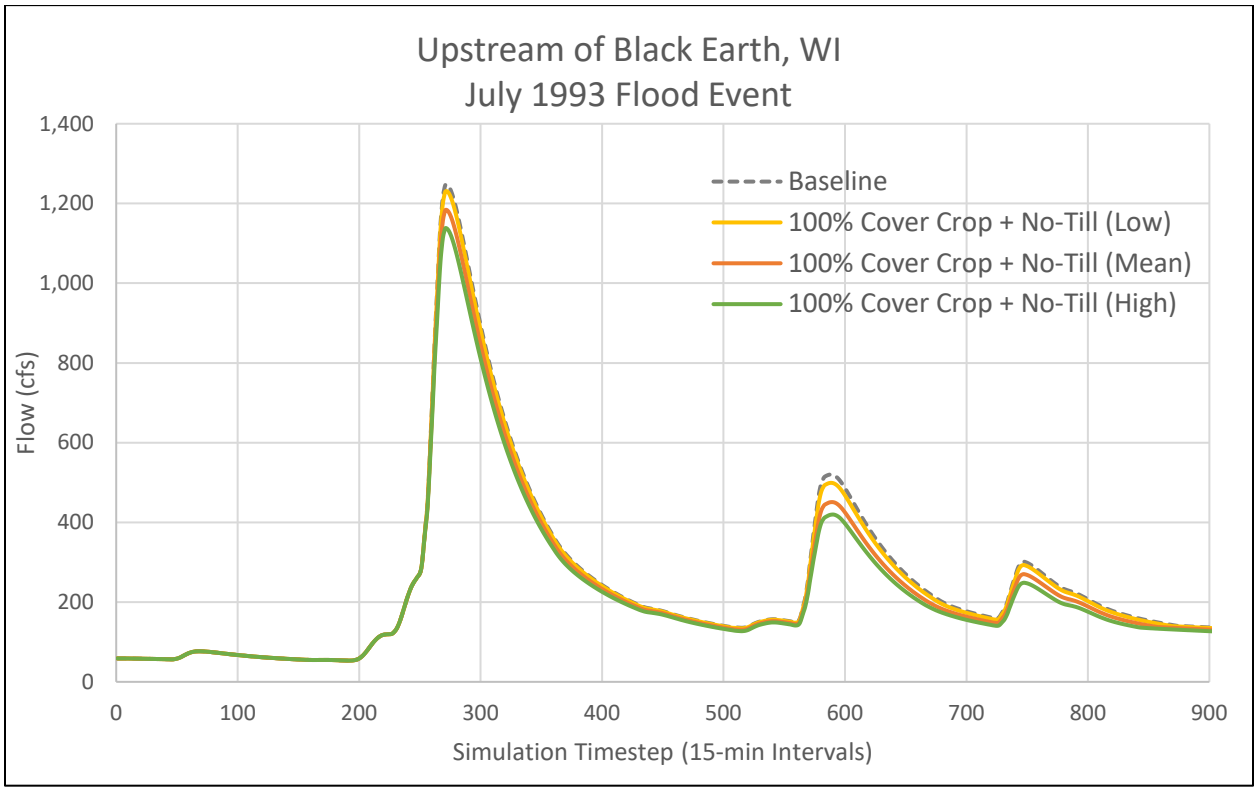

Figure 7. July 1993 simulation results at Black Earth, WI – 100% Cover Crop + No-Till alternative

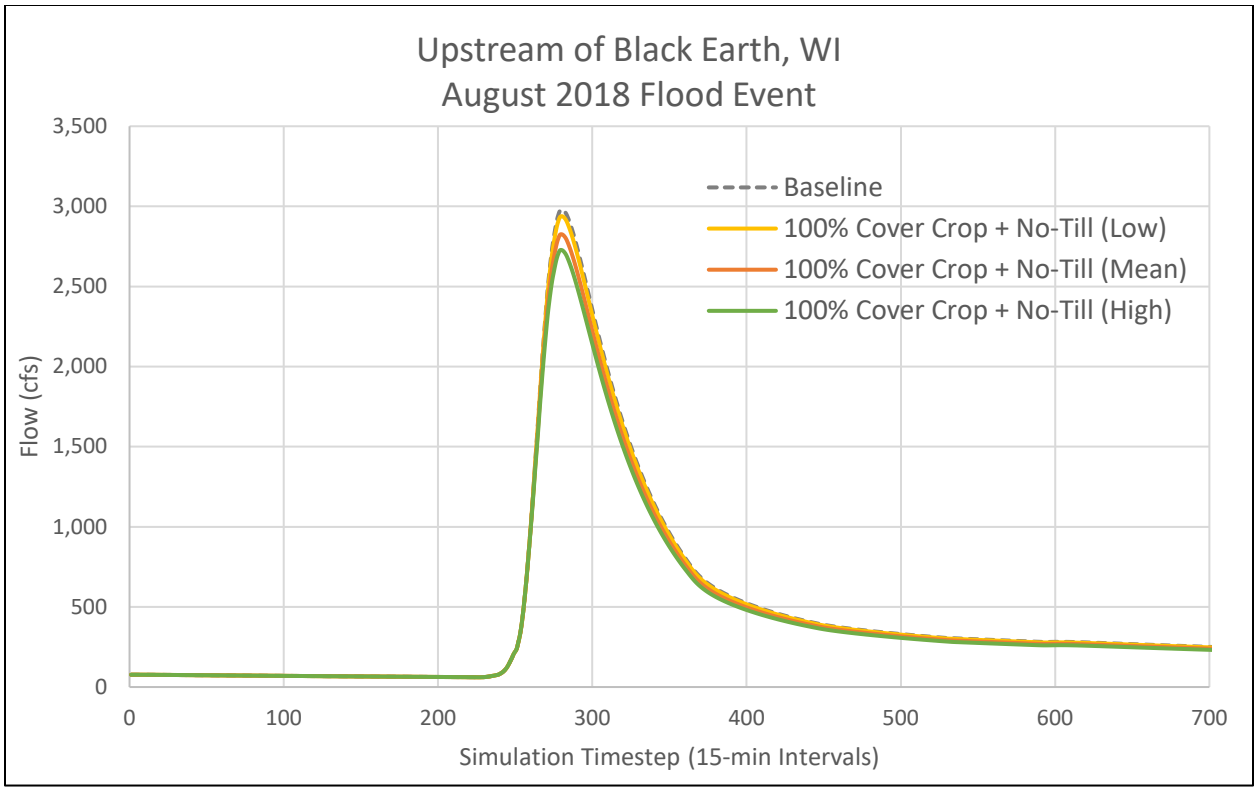

Figure 8. August 2018 simulation results at Black Earth, WI – 100% Cover Crop + No-Till alternative

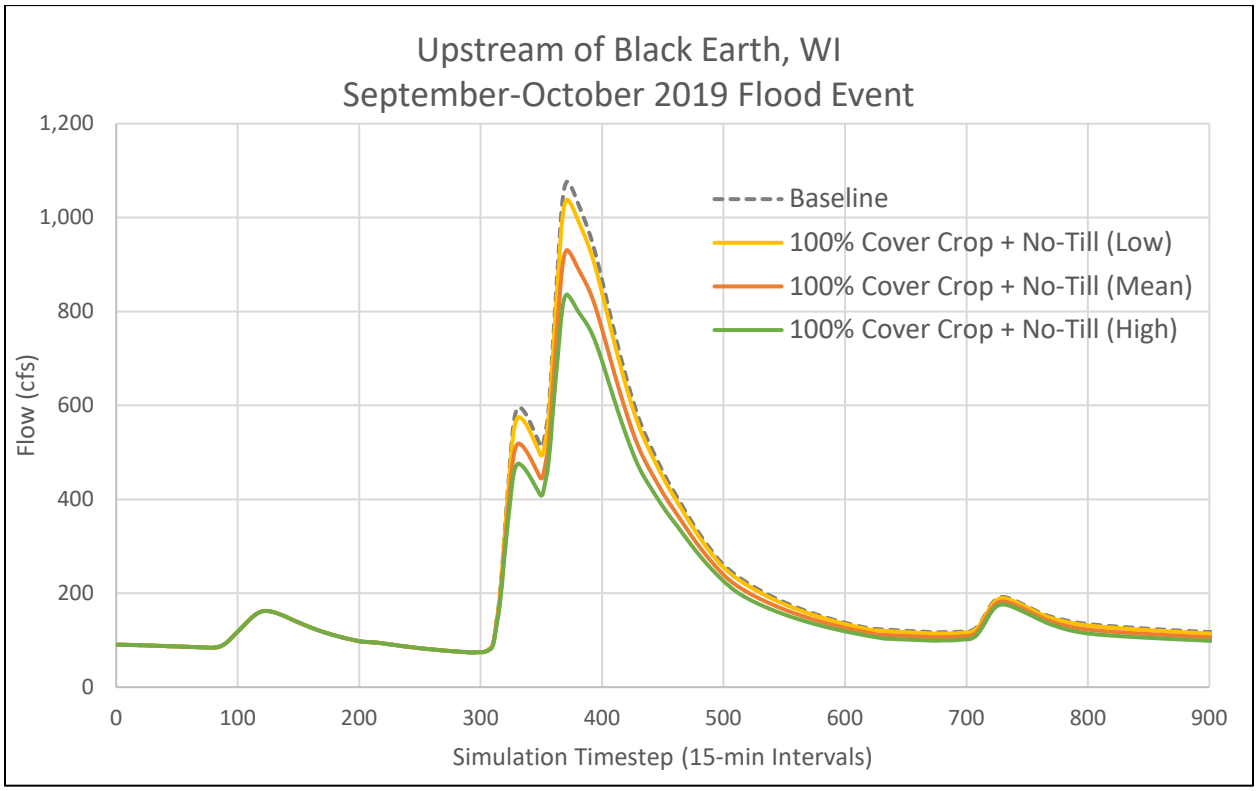

Figure 9. September-October 2019 simulation results at Black Earth, WI – 100% Cover Crop + No-Till alternative

Prairie Strips

Table 4. Peak flow reductions under the Prairie Strips alternative

Flood Event	Peak Flow (cfs)		
	Baseline	High	Low
	Cross Plains, WI (model element: J_BEC_ds_CP)		
Jul 1993	891	815 (-9%)	874 (-2%)
Aug 2018	2,792	2,562 (-8%)	2,740 (-2%)
Sep-Oct 2019	596	547 (-8%)	585 (-2%)
	Black Earth, WI (model element: J_BEC_us_BE)		
Jul 1993	1,248	1,150 (-8%)	1,226 (-2%)
Aug 2018	2,979	2,742 (-8%)	2,926 (-2%)
Sep-Oct 2019	1,076	996 (-7%)	1,058 (-2%)
	Mazomanie, WI (model element: J_BEC_ds_MZ)		
Jul 1993	2,239	2,068 (-8%)	2,153 (-4%)
Aug 2018	3,540	3,258 (-8%)	3,429 (-3%)
Sep-Oct 2019	1,769	1,638 (-7%)	1,711 (-3%)

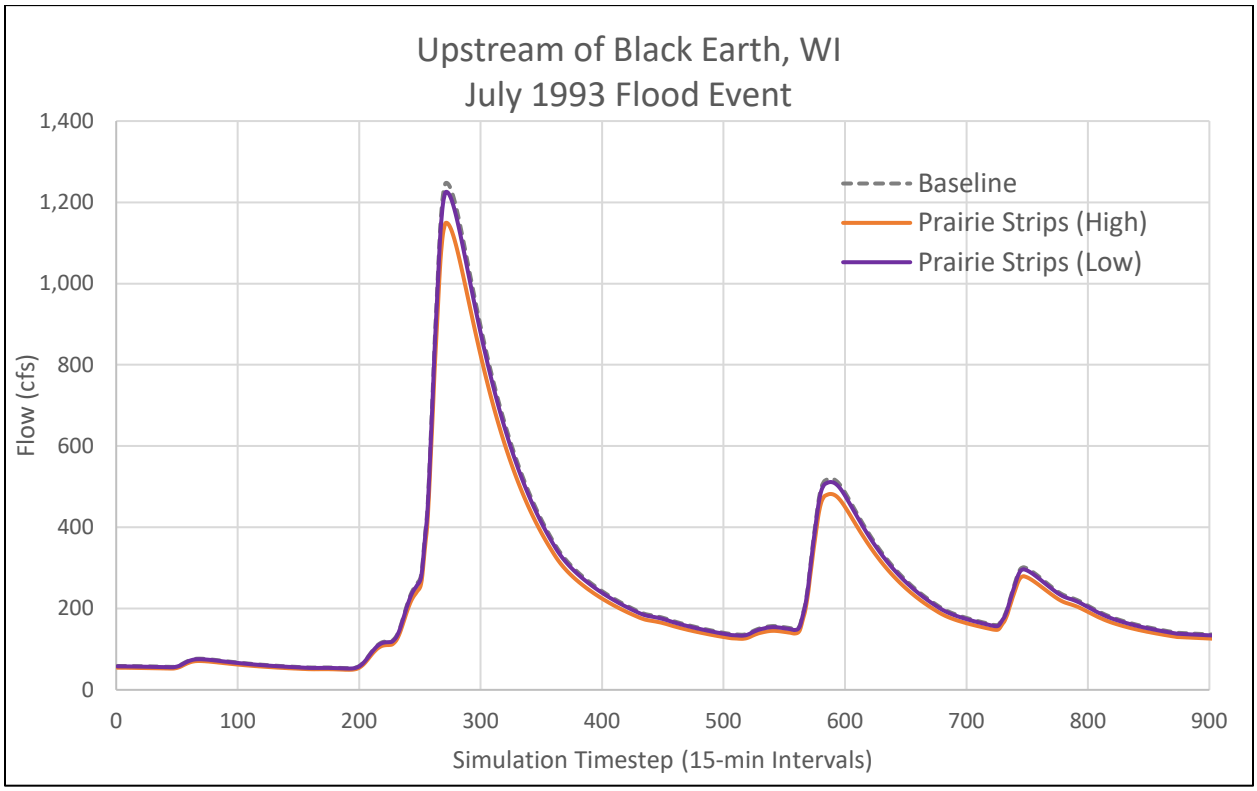

Figure 10. July 1993 simulation results at Black Earth, WI – Prairie Strips alternative

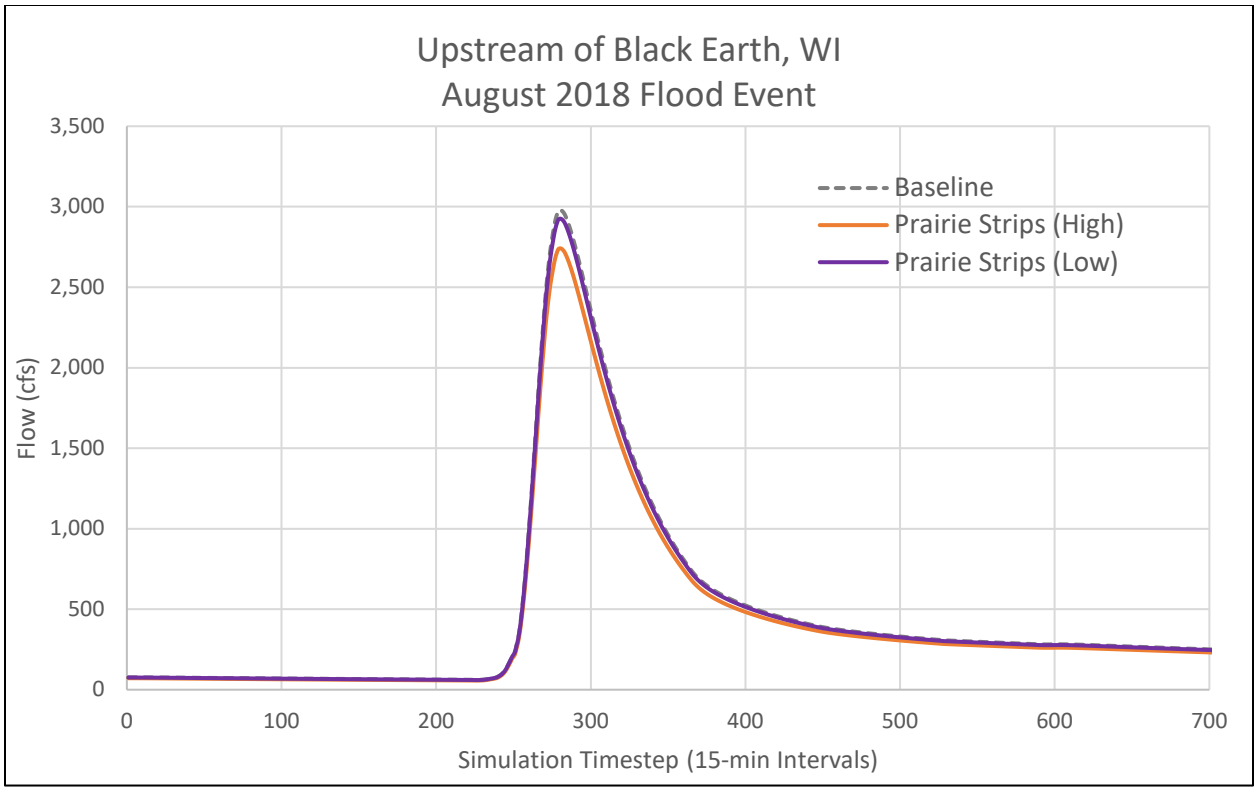

Figure 11. August 2018 simulation results at Black Earth, WI – Prairie Strips alternative

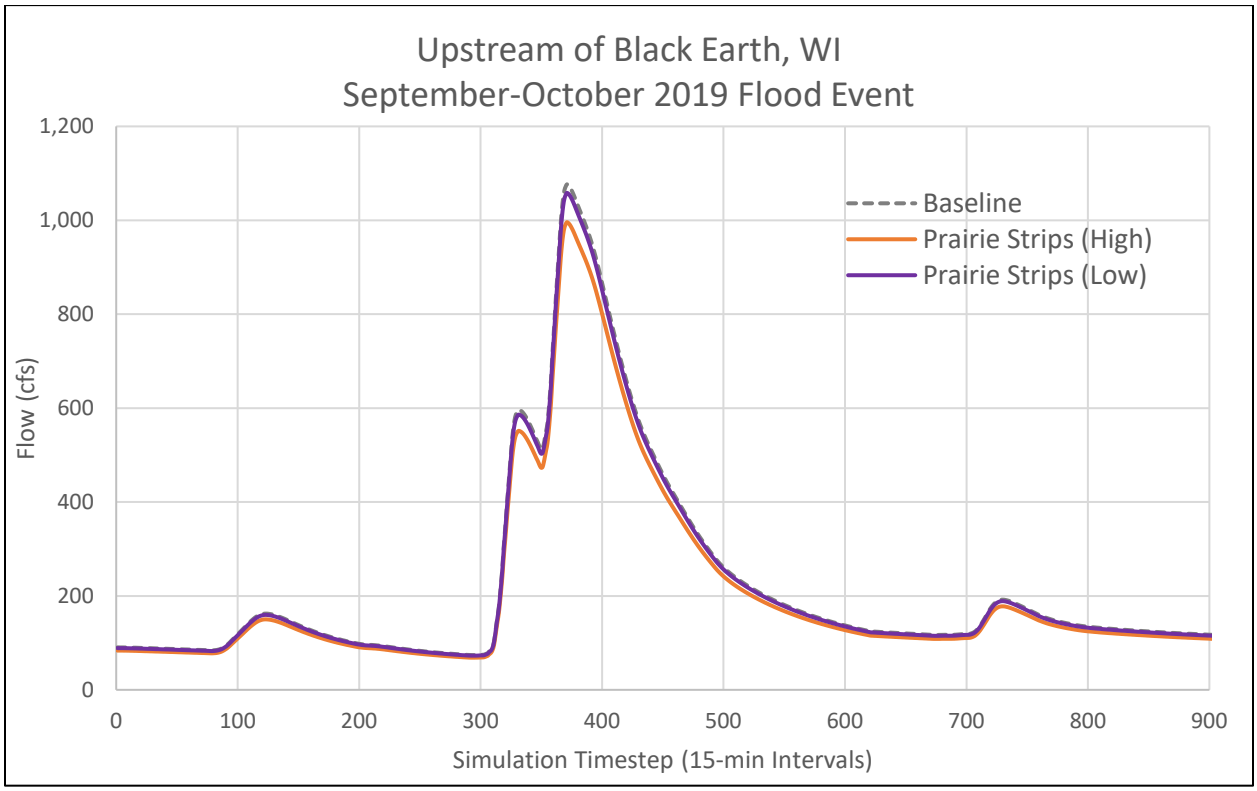

Figure 12. September-October 2019 simulation results at Black Earth, WI – Prairie Strips alternative

Wetland Restoration

Table 5. Peak flow reductions under the Wetland Restoration alternative

Flood Event	Peak Flow (cfs)		
	Baseline	WR1	WR2
	Cross Plains, WI (model element: J_BEC_ds_CP)		
Sep-Oct 2019	596	588 (-1%)	494 (-17%)
	Black Earth, WI (model element: J_BEC_us_BE)		
Sep-Oct 2019	1,076	1,033 (-4%)	921 (-14%)
	Mazomanie, WI (model element: J_BEC_ds_MZ)		
Sep-Oct 2019	1,769	1,727 (-2%)	1,610 (-9%)

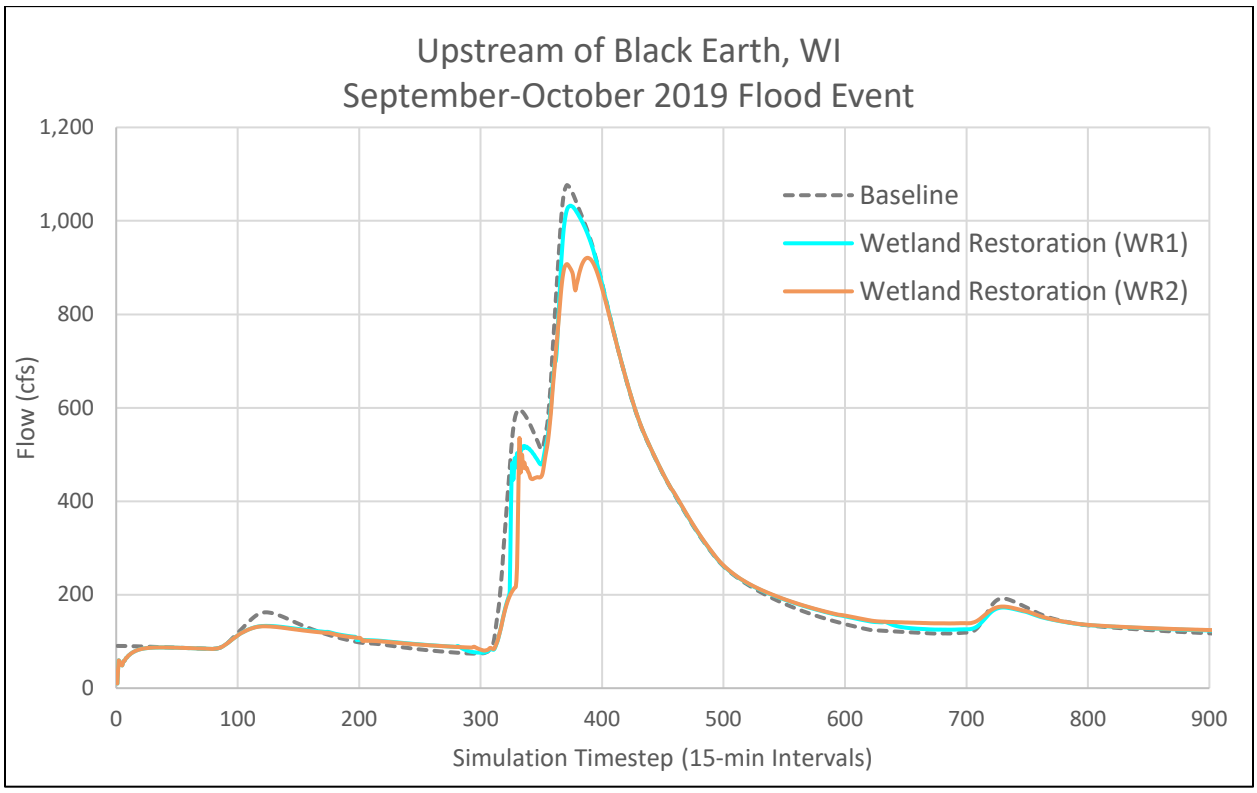

Figure 13. September-October 2019 simulation results at Black Earth, WI - Wetland Restoration alternative

50% Impervious Area

Table 6. Peak flow reductions under the 50% Impervious Area alternative

Flood Event	Peak Flow (cfs)		
	Baseline	50% Impervious Area	% Decrease
	Cross Plains, WI (model element: J_BEC_ds_CP)		
Jul 1993	891	703	-21%
Aug 2018	2,792	2,334	-16%
Sep-Oct 2019	596	505	-15%
	Black Earth, WI (model element: J_BEC_us_BE)		
Jul 1993	1,248	1,042	-17%
Aug 2018	2,979	2,462	-17%
Sep-Oct 2019	1,076	978	-9%
	Mazomanie, WI (model element: J_BEC_ds_MZ)		
Jul 1993	2,239	1,921	-14%
Aug 2018	3,540	2,832	-20%
Sep-Oct 2019	1,769	1,569	-11%

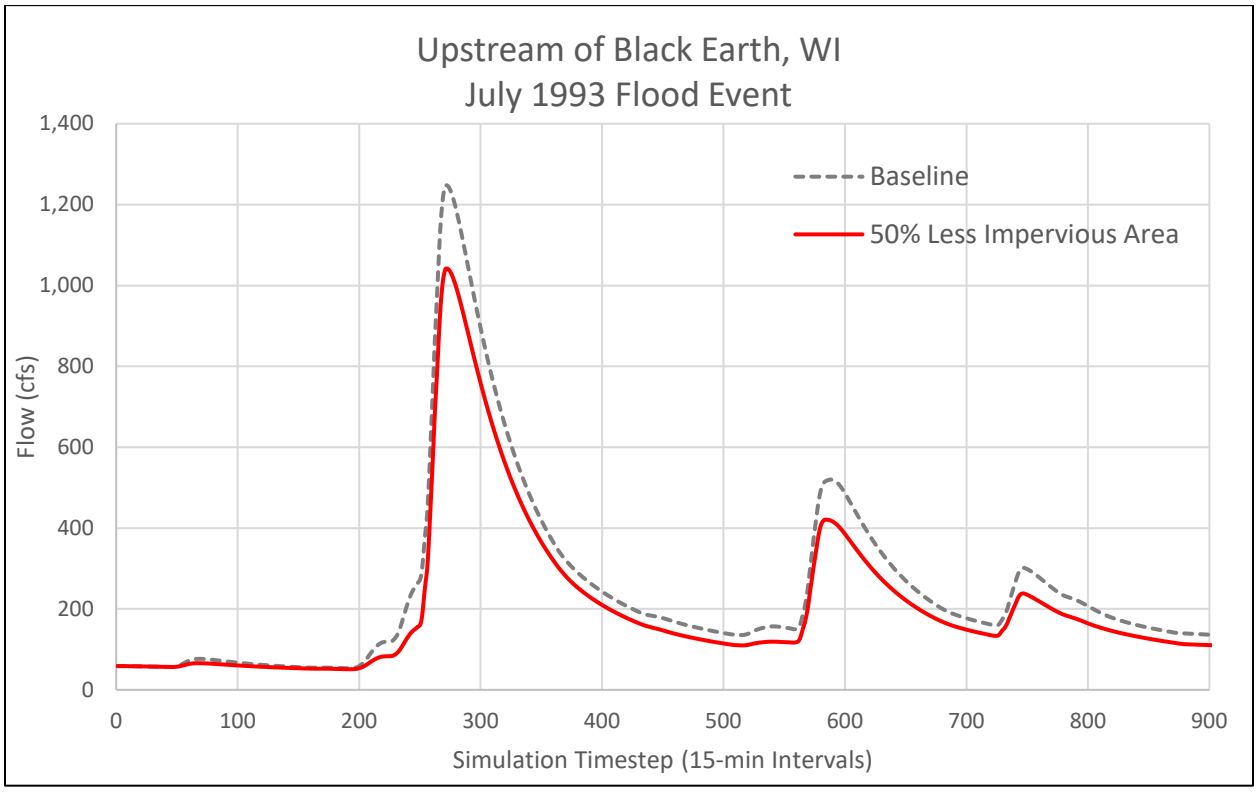

Figure 14. July 1993 simulation results at Black Earth, WI – 50% Impervious Area alternative

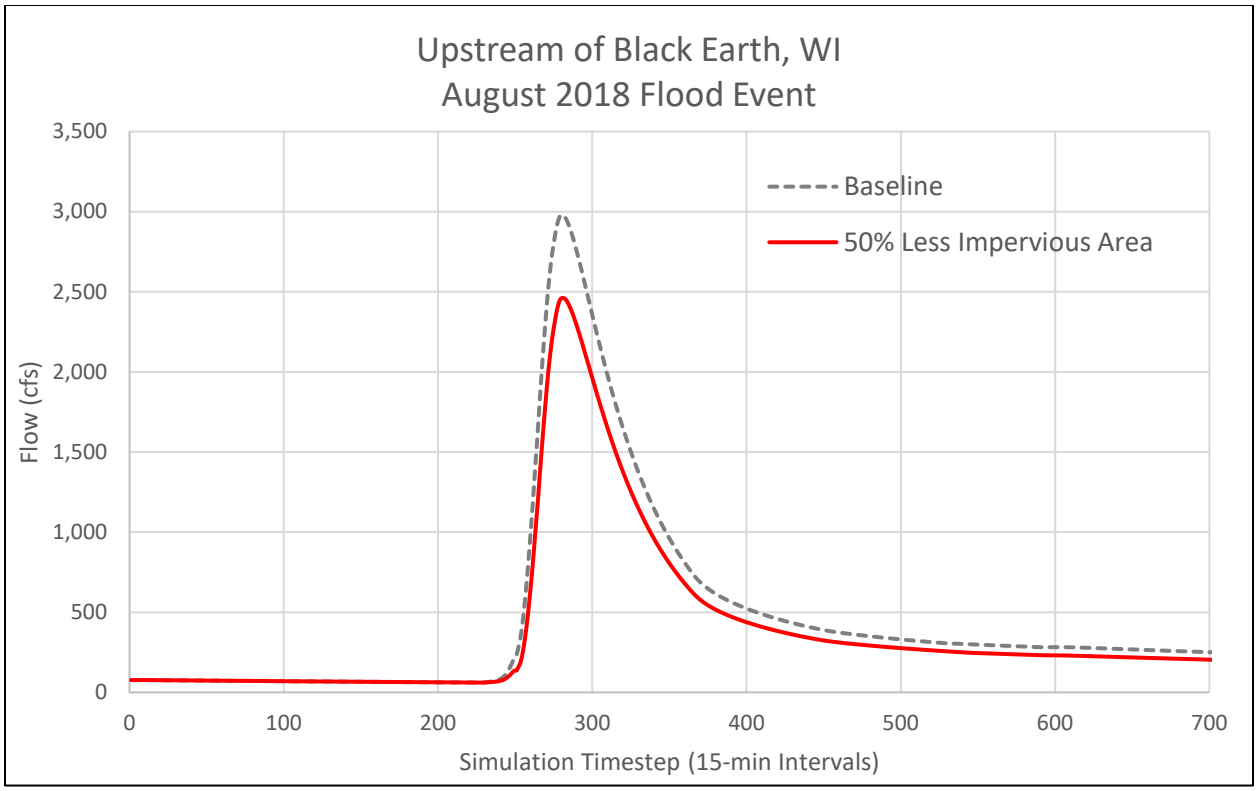

Figure 15. August 2018 simulation results at Black Earth, WI – 50% Impervious Area alternative

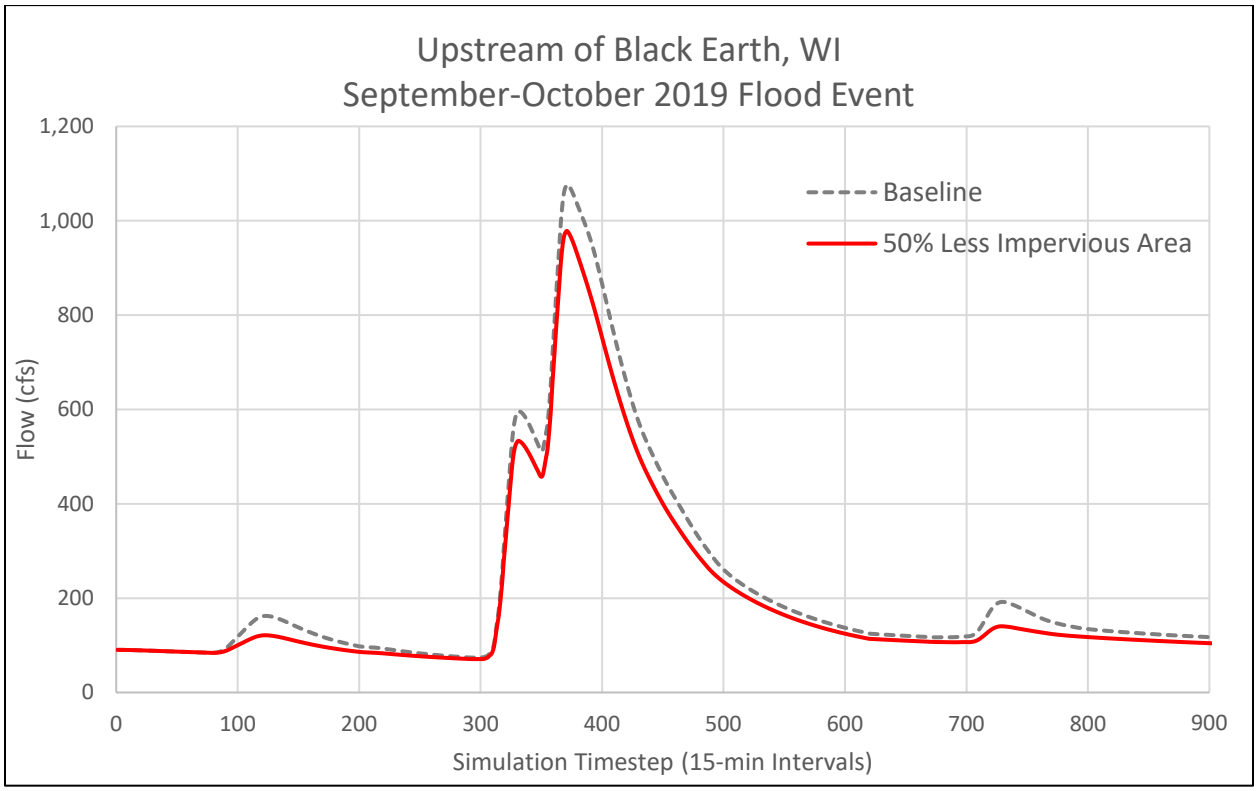

Figure 16. September-October 2019 simulation results at Black Earth, WI – 50% Impervious Area alternative

Green Infrastructure

Table 7. Peak flow reductions under the Green Infrastructure alternative

Flood Event	Peak Flow (cfs)		
	Baseline	Green Infrastructure	% Decrease
	Cross Plains, WI (model element: J_BEC_ds_CP)		
Jul 1993	891	891	0%
Aug 2018	2,792	2,688	-4%
Sep-Oct 2019	596	576	-3%
	Black Earth, WI (model element: J_BEC_us_BE)		
Jul 1993	1,248	1,248	0%
Aug 2018	2,979	2,881	-3%
Sep-Oct 2019	1,076	1,058	-2%
	Mazomanie, WI (model element: J_BEC_ds_MZ)		
Jul 1993	2,239	2,239	0%
Aug 2018	3,540	3,397	-4%
Sep-Oct 2019	1,769	1,725	-2%

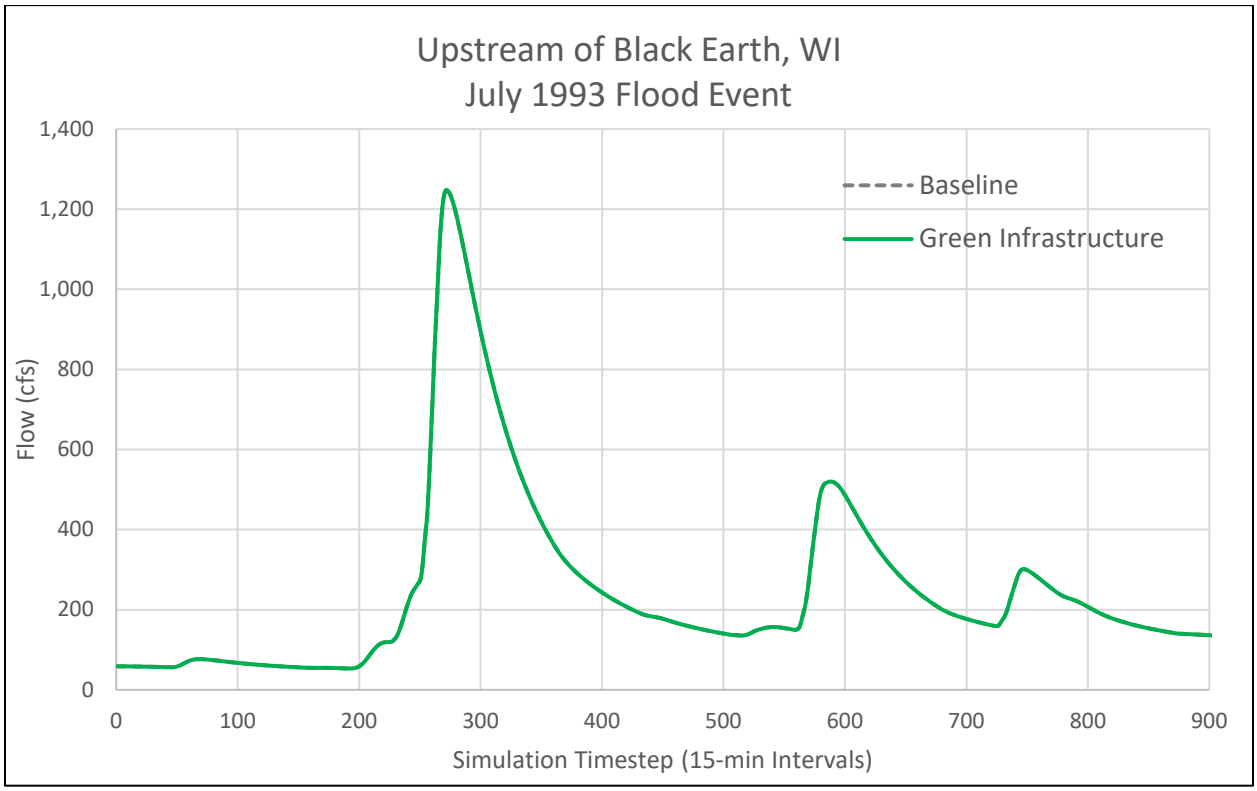

Figure 17. July 1993 simulation results at Black Earth, WI – Green Infrastructure alternative

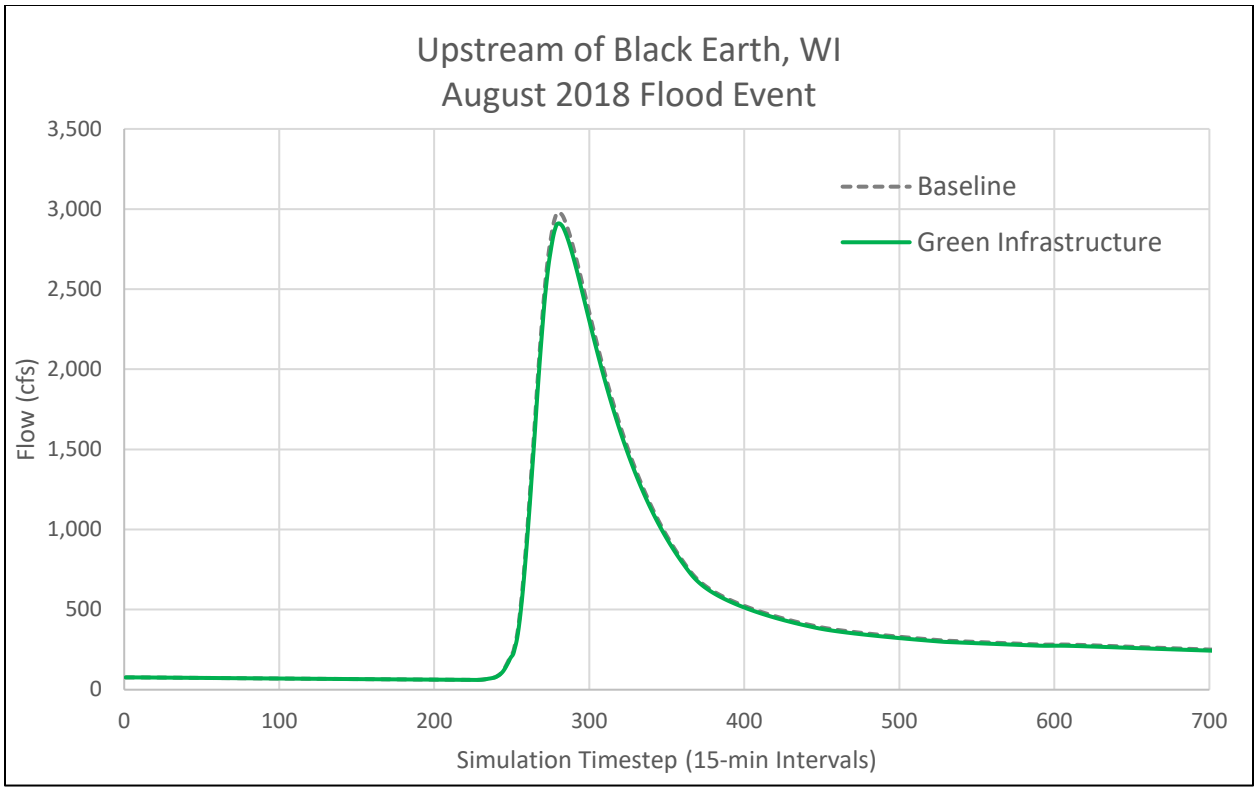

Figure 18. August 2018 simulation results at Black Earth, WI – Green Infrastructure alternative

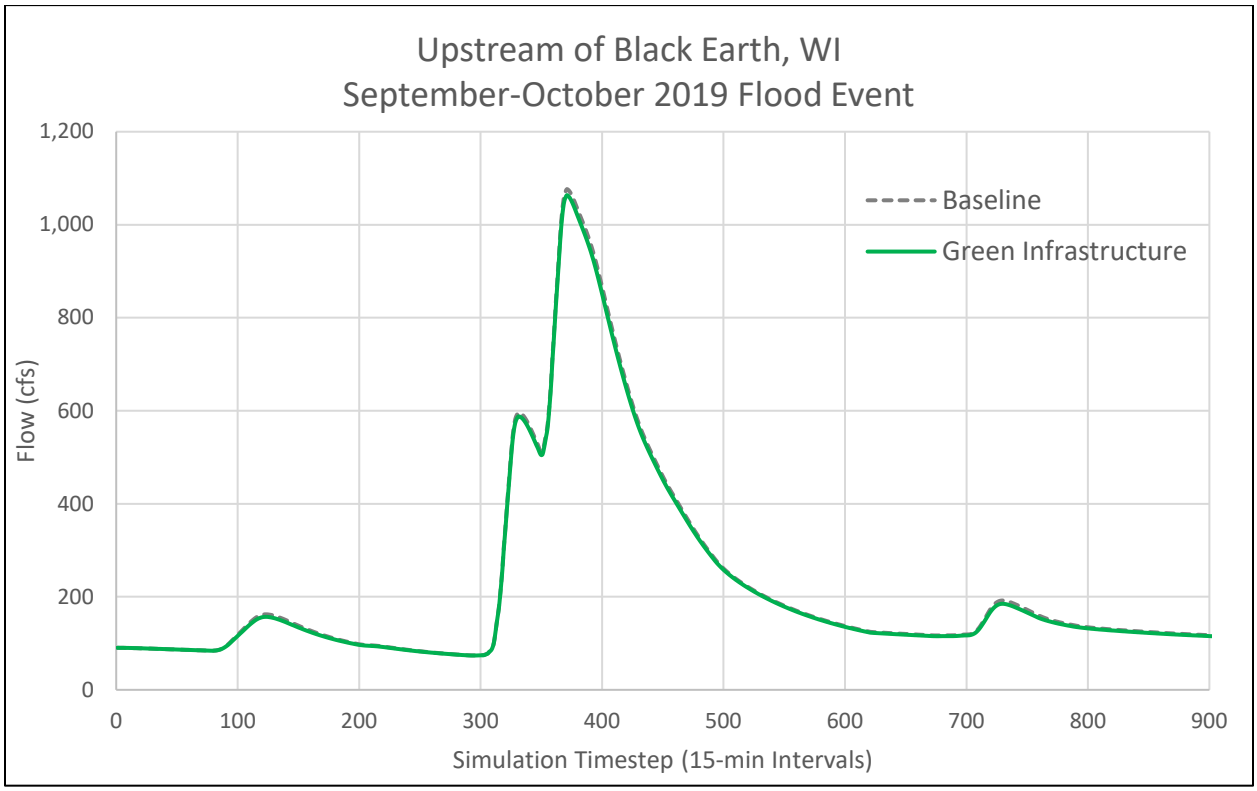

Figure 19. September-October 2019 simulation results at Black Earth, WI – Green Infrastructure alternative

US Army Corps
of Engineers®
St. Paul District

Appendix B:
HEC-HMS Parameters

Table of Tables

Subbasins

Table 1. AWS0150 and calibrated initial loss in the Black Earth Creek HMS model

Subbasin	Loss: Initial Loss (in)			
	AWS0150	Jul 1993	Aug 2018	Sep-Oct 2019
S_BC_us_CP	9.37	0	7.40	0
S_BEC_us_CP	8.46	4.25	8.30	1.6
S_CP	9.22	3.25	7.00	0
S_BEC_ds_CP_to_BEC_us_BE	7.91	3.25	8.40	0
S_VC_us_BE	7.11	2.25	6.39	0
S_BE	8.88	2.81	7.97	0
S_BEC-VC_to_BEC_us_MZ	8.33	2.64	7.48	0
S_HPC_us_MZ	8.73	2.76	7.84	0
S_WC_us_MZ	8.27	2.62	7.42	0
S_MZ	6.21	1.97	5.58	0
S_BEC_ds_MZ_to_Out	5.76	1.82	5.17	0

Table 2. Initial and calibrated constant loss rates in the Black Earth Creek HMS model

Subbasin	Loss: Constant Loss Rate (in/hr)				
	Initial Parameters	Jul 1993	Aug 2018	Sep-Oct 2019	Generalized Parameters
S_BC_us_CP	2.677	0.669	0.669	0.669	0.669
S_BEC_us_CP	1.878	0.619	0.749	0.619	0.662
S_CP	2.219	0.466	0.564	0.466	0.499
S_BEC_ds_CP_to_BEC_us_BE	1.803	0.316	0.383	0.316	0.338
S_VC_us_BE	1.741	0.420	0.485	0.420	0.442
S_BE	1.839	0.444	0.513	0.444	0.467
S_BEC-VC_to_BEC_us_MZ	2.523	0.609	0.703	0.609	0.640
S_HPC_us_MZ	2.757	0.665	0.769	0.665	0.700
S_WC_us_MZ	2.767	0.667	0.772	0.667	0.702
S_MZ	6.961	1.679	1.941	1.679	1.766
S_BEC_ds_MZ_to_Out	7.904	1.906	2.204	1.906	2.006

Table 3. Initial and calibrated time of concentration (Tc) parameters in the Black Earth Creek HMS model

Subbasin	Transform: Time of Concentration (Tc) (hrs)				
	Initial Parameters	Jul 1993	Aug 2018	Sep-Oct 2019	Generalized Parameters
S_BC_us_CP	3.445	2.841	3.445	3.445	3.24
S_BEC_us_CP	3.564	2.851	2.851	3.564	3.09
S_CP	2.911	2.911	1.863	2.911	2.56
S_BEC_ds_CP_to_BEC_us_BE	5.348	5.348	5.294	6.417	5.69
S_VC_us_BE	5.596	5.071	4.798	5.876	5.25
S_BE	3.125	2.832	2.680	3.281	2.93
S_BEC-VC_to_BEC_us_MZ	3.900	3.534	3.344	4.095	3.66
S_HPC_us_MZ	9.327	8.452	7.998	9.793	8.75
S_WC_us_MZ	7.656	6.938	6.565	8.039	7.18
S_MZ	3.716	3.367	3.186	3.902	3.49
S_BEC_ds_MZ_to_Out	5.831	5.284	5.000	6.122	5.47

Table 4. Initial and calibrated Clark's storage coefficient (R) in the Black Earth Creek HMS model

Subbasin	Transform: Clark's Storage Coefficient (R)				
	Initial Parameters	Jul 1993	Aug 2018	Sep-Oct 2019	Generalized Parameters
S_BC_us_CP	13.780	11.360	13.780	13.780	12.97
S_BEC_us_CP	14.256	11.405	11.405	14.256	12.36
S_CP	11.644	11.644	7.452	11.644	10.25
S_BEC_ds_CP_to_BEC_us_BE	21.392	21.392	21.178	25.668	22.75
S_VC_us_BE	22.384	20.282	19.194	23.503	20.99
S_BE	12.500	11.326	10.719	13.125	11.72
S_BEC-VC_to_BEC_us_MZ	15.600	14.135	13.377	16.380	14.63
S_HPC_us_MZ	37.308	33.805	31.992	39.172	34.99
S_WC_us_MZ	30.624	27.748	26.260	32.154	28.72
S_MZ	14.864	13.468	12.746	15.607	13.94
S_BEC_ds_MZ_to_Out	23.324	21.134	20.000	24.490	21.87

Table 5. Initial and calibrated initial baseflow in the Black Earth Creek HMS model

Subbasin	Baseflow: Initial Baseflow (cfs/mi^2)			
	Initial Parameters	Jul 1993	Aug 2018	Sep-Oct 2019
S_BC_us_CP	0	0.5	0.5	1.2
S_BEC_us_CP	0	1.5	2.0	2.2
S_CP	0	1.5	2.0	2.2
S_BEC_ds_CP_to_BEC_us_BE	0	1.5	2.0	2.2
S_VC_us_BE	0	1.3	1.6	2.0
S_BE	0	1.3	1.6	2.0
S_BEC-VC_to_BEC_us_MZ	0	1.3	1.6	2.0
S_HPC_us_MZ	0	1.3	1.6	2.0
S_WC_us_MZ	0	1.3	1.6	2.0
S_MZ	0	1.3	1.6	2.0
S_BEC_ds_MZ_to_Out	0	1.3	1.6	2.0

Table 6. Initial and calibrated recession constants in the Black Earth Creek HMS model

Subbasin	Baseflow: Recession Constant				
	Initial Parameters	Jul 1993	Aug 2018	Sep-Oct 2019	Generalized Parameters
S_BC_us_CP	0.95	0.95	0.95	0.9	0.93
S_BEC_us_CP	0.95	0.8	0.8	0.9	0.83
S_CP	0.95	0.95	0.8	0.9	0.88
S_BEC_ds_CP_to_BEC_us_BE	0.95	0.95	0.95	0.95	0.95
S_VC_us_BE	0.95	0.91	0.88	0.91	0.90
S_BE	0.95	0.91	0.88	0.91	0.90
S_BEC-VC_to_BEC_us_MZ	0.95	0.91	0.88	0.91	0.90
S_HPC_us_MZ	0.95	0.91	0.88	0.91	0.90
S_WC_us_MZ	0.95	0.91	0.88	0.91	0.90
S_MZ	0.95	0.91	0.88	0.91	0.90
S_BEC_ds_MZ_to_Out	0.95	0.91	0.88	0.91	0.90

Table 7. Initial and calibrated ratio to peak in the Black Earth Creek HMS model

Subbasin	Baseflow: Ratio to Peak				
	Initial Parameters	Jul 1993	Aug 2018	Sep-Oct 2019	Generalized Parameters
S_BC_us_CP	0.2	0.95	0.01	0.1	0.93
S_BEC_us_CP	0.2	0.8	0.1	0.2	0.83
S_CP	0.2	0.95	0.1	0.1	0.88
S_BEC_ds_CP_to_BEC_us_BE	0.2	0.95	0.1	0.15	0.95
S_VC_us_BE	0.2	0.91	0.08	0.14	0.90
S_BE	0.2	0.91	0.08	0.14	0.90
S_BEC-VC_to_BEC_us_MZ	0.2	0.91	0.08	0.14	0.90
S_HPC_us_MZ	0.2	0.91	0.08	0.14	0.90
S_WC_us_MZ	0.2	0.91	0.08	0.14	0.90
S_MZ	0.2	0.91	0.08	0.14	0.90
S_BEC_ds_MZ_to_Out	0.2	0.91	0.08	0.14	0.90

Table 8. Initial and calibrated initial storage parameters in the Black Earth Creek HMS model (canopy method)

Subbasin	Canopy: Initial Storage (%)				
	Initial Parameters	Jul 1993	Aug 2018	Sep-Oct 2019	Generalized Parameters
S_BC_us_CP	0	0	0	0	0
S_BEC_us_CP	0	0	0	0	0
S_CP	0	0	0	0	0
S_BEC_ds_CP_to_BEC_us_BE	0	0	0	0	0
S_VC_us_BE	0	0	0	0	0
S_BE	0	0	0	0	0
S_BEC-VC_to_BEC_us_MZ	0	0	0	0	0
S_HPC_us_MZ	0	0	0	0	0
S_WC_us_MZ	0	0	0	0	0
S_MZ	0	0	0	0	0
S_BEC_ds_MZ_to_Out	0	0	0	0	0

Table 9. Initial and calibrated maximum storage parameters in the Black Earth Creek HMS model (canopy method)

Subbasin	Canopy: Maximum Storage (in)				
	Initial Parameters	Jul 1993	Aug 2018	Sep-Oct 2019	Generalized Parameters
S_BC_us_CP	0	0	0	0	0
S_BEC_us_CP	0	0	0	0	0
S_CP	0	0	0	0	0
S_BEC_ds_CP_to_BEC_us_BE	0	0	0	0	0
S_VC_us_BE	0	0	0	0	0
S_BE	0	0	0	0	0
S_BEC-VC_to_BEC_us_MZ	0	0	0	0	0
S_HPC_us_MZ	0	0	0	0	0
S_WC_us_MZ	0	0	0	0	0
S_MZ	0	0	0	0	0
S_BEC_ds_MZ_to_Out	0	0	0	0	0

Table 10. Initial and calibrated crop coefficient parameters in the Black Earth Creek HMS model (canopy method)

Subbasin	Canopy: Crop Coefficient				
	Initial Parameters	Jul 1993	Aug 2018	Sep-Oct 2019	Generalized Parameters
S_BC_us_CP	1	1	1	1	1
S_BEC_us_CP	1	1	1	1	1
S_CP	1	1	1	1	1
S_BEC_ds_CP_to_BEC_us_BE	1	1	1	1	1
S_VC_us_BE	1	1	1	1	1
S_BE	1	1	1	1	1
S_BEC-VC_to_BEC_us_MZ	1	1	1	1	1
S_HPC_us_MZ	1	1	1	1	1
S_WC_us_MZ	1	1	1	1	1
S_MZ	1	1	1	1	1
S_BEC_ds_MZ_to_Out	1	1	1	1	1

Routing Reaches

Table 11. Initial and calibrated Muskingum K parameters in the Black Earth Creek HMS model

Reach	Routing: Muskingum K (hrs)				
	Initial Parameters	2019_09	2017_07	2017_05	Generalized Parameters
TR-OUT_to_TR-DG	4.89	9.17	3.44	7.34	6.65
TR-DG_to_TR-AR	17.74	33.26	12.47	26.61	24.11
TR-AR_to_EC	11.9	8.93	5.02	8.93	7.63
EC_to_PC	7.6	5.7	3.21	5.7	4.87
TR-PC_to_PC-PF	7.26	5.45	3.06	5.45	4.65
TR-PC_to_TR-BL	7.86	5.9	3.32	5.9	5.04

Table 12. Initial and calibrated Muskingum X parameters in the Black Earth Creek HMS model

Reach	Routing: Muskingum X				
	Initial Parameters	2019_09	2017_07	2017_05	Generalized Parameters
TR-OUT_to_TR-DG	0.25	0.05	0.05	0.1	0.1
TR-DG_to_TR-AR	0.25	0.05	0.05	0.1	0.1
TR-AR_to_EC	0.25	0.1	0.1	0.1	0.1
EC_to_PC	0.25	0.1	0.1	0.1	0.1
TR-PC_to_PC-PF	0.25	0.1	0.1	0.1	0.1
TR-PC_to_TR-BL	0.25	0.1	0.1	0.1	0.1

Table 13. Initial and calibrated number of subreaches in the Black Earth Creek HMS model

Reach	Routing: Number of Subreaches				
	Initial Parameters	2019_09	2017_07	2017_05	Generalized Parameters
TR-OUT_to_TR-DG	1	1	1	1	1
TR-DG_to_TR-AR	1	1	1	1	1
TR-AR_to_EC	1	1	1	1	1
EC_to_PC	1	1	1	1	1
TR-PC_to_PC-PF	1	1	1	1	1
TR-PC_to_TR-BL	1	1	1	1	1

US Army Corps of Engineers®
St. Paul District

Appendix C:
HEC-HMS Calibration & Validation Results

Table of Figures

Calibration: July 1993 event

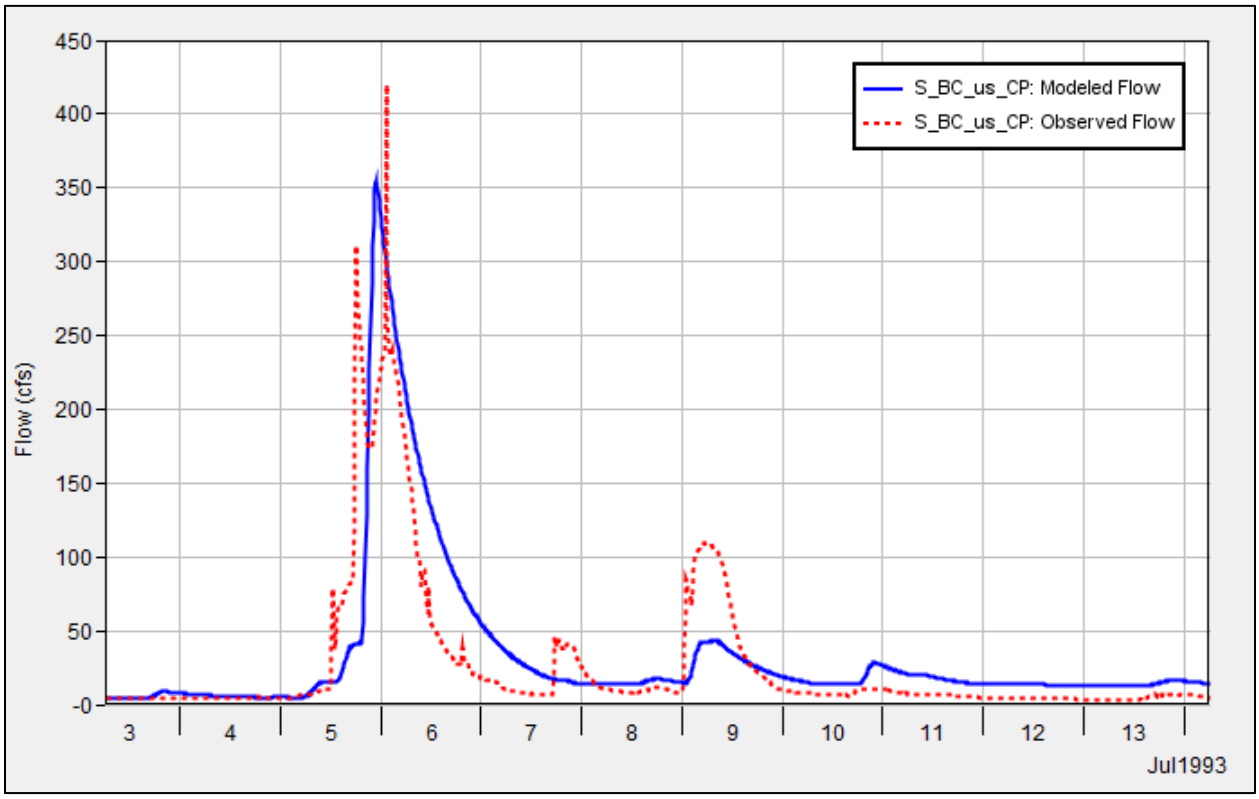

Figure 1. July 1993 calibration results, Brewery Creek at Cross Plains, WI

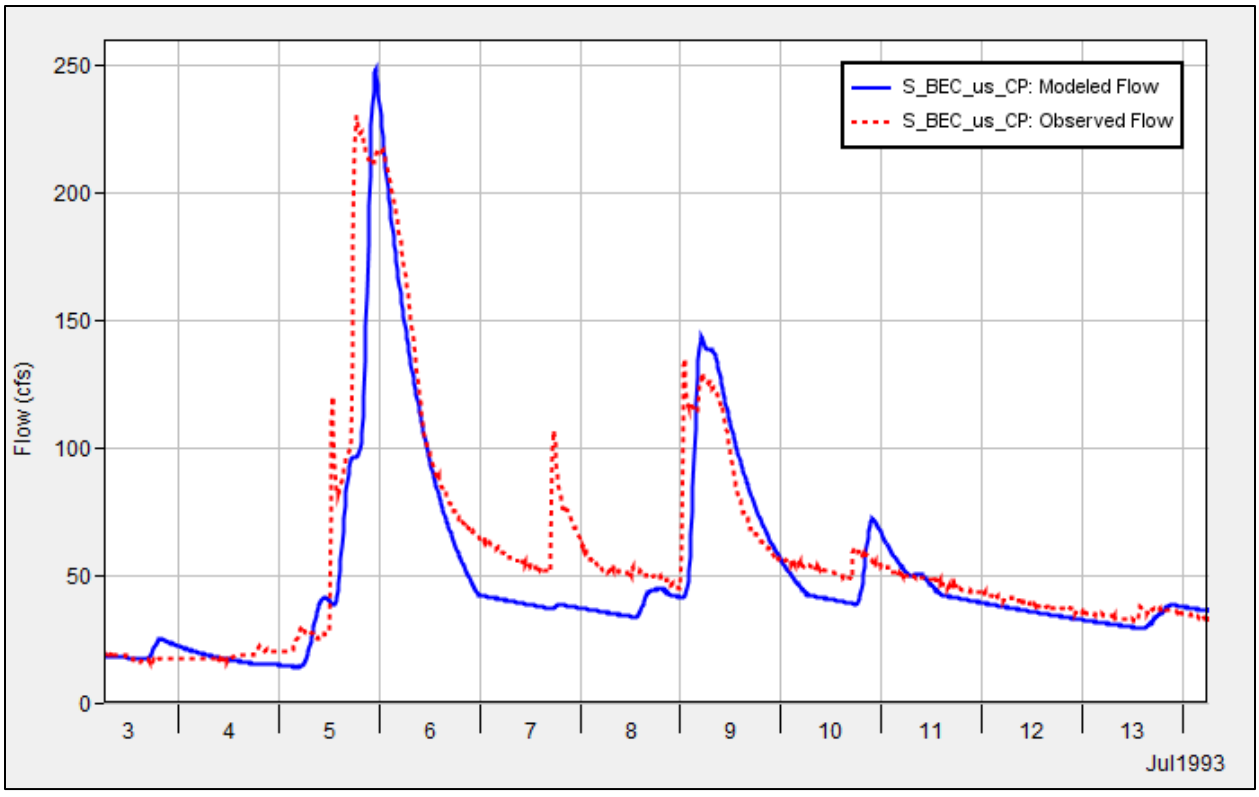

Figure 2. July 1993 calibration results, Black Earth Creek just upstream of Brewery Creek confluence

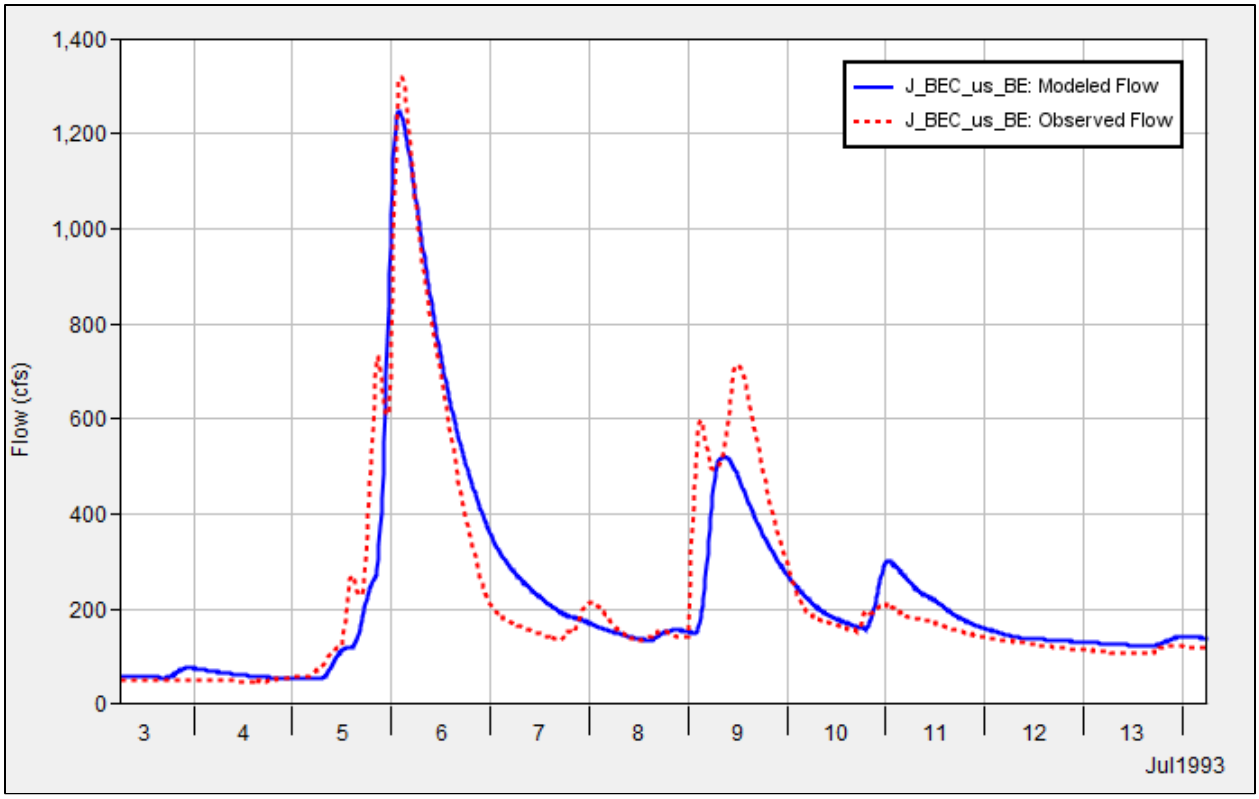

Figure 3. July 1993 calibration results, Black Earth Creek upstream of Black Earth, WI

Calibration: August 2018 event

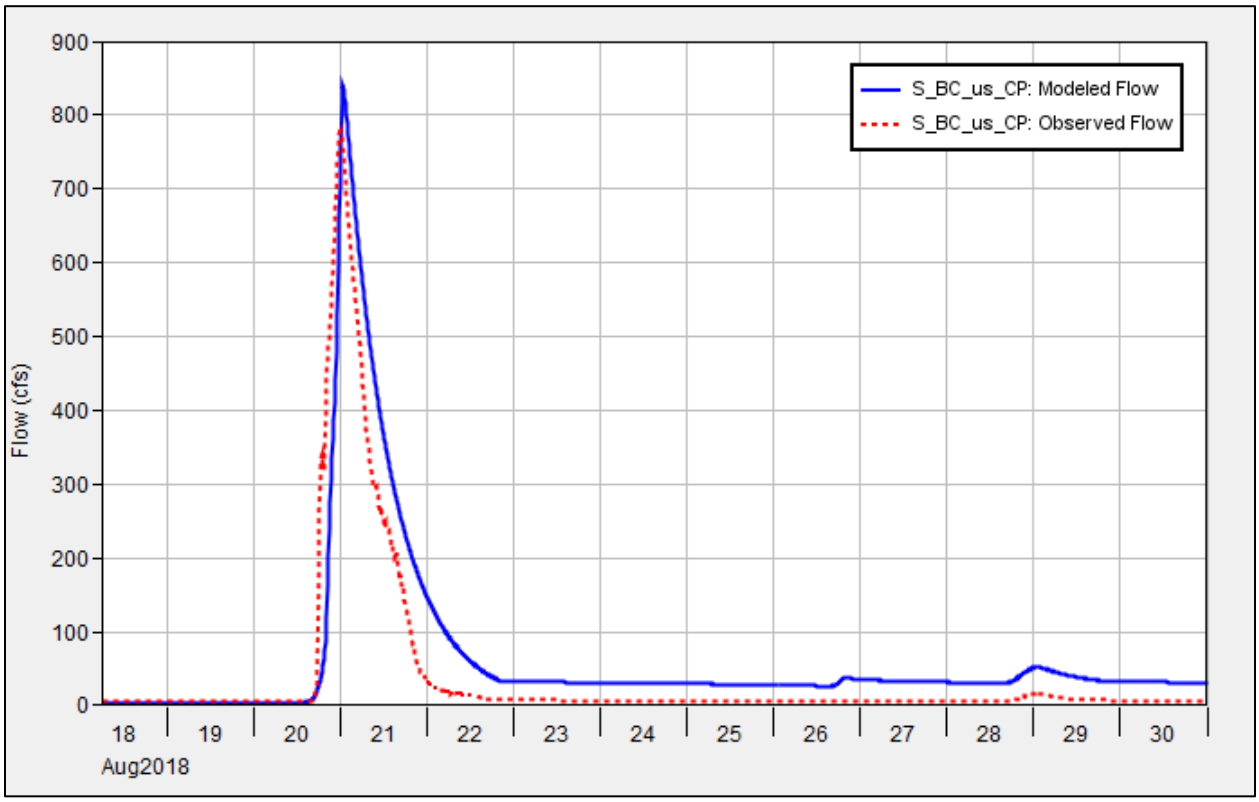

Figure 4. August 2018 calibration results, Brewery Creek at Cross Plains, WI

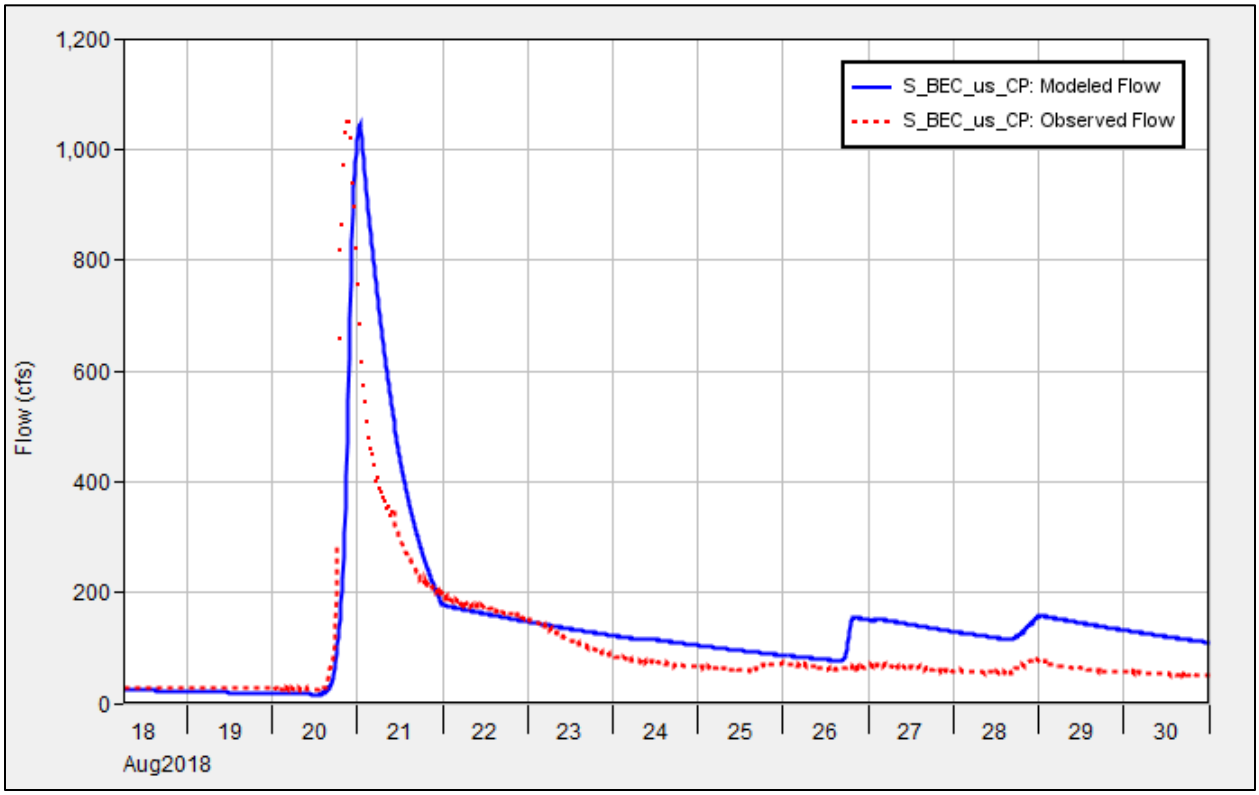

Figure 5. August 2018 calibration results, Black Earth Creek just upstream of Brewery Creek confluence

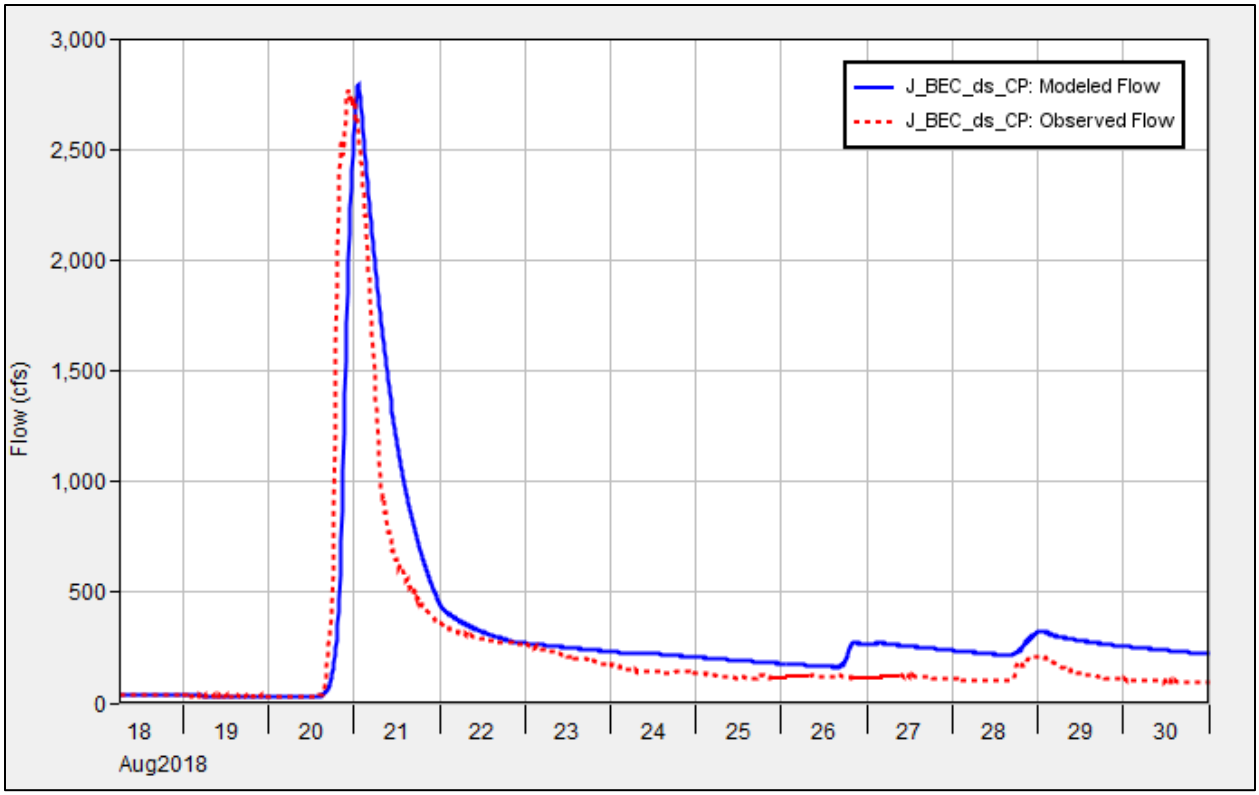

Figure 6. August 2018 calibration results, Black Earth Creek downstream of Cross Plains, WI

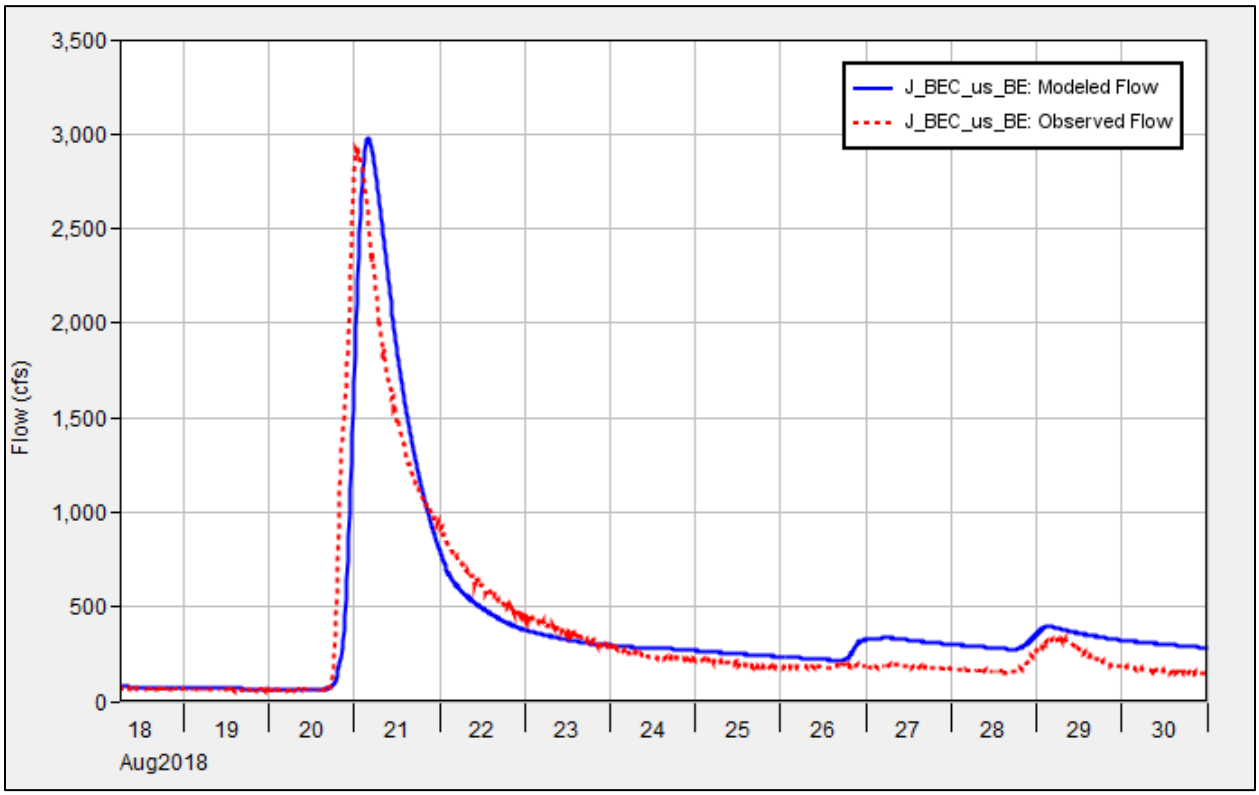

Figure 7. August 2018 calibration results, Black Earth Creek upstream of Black Earth, WI

Calibration: September-October 2019 event

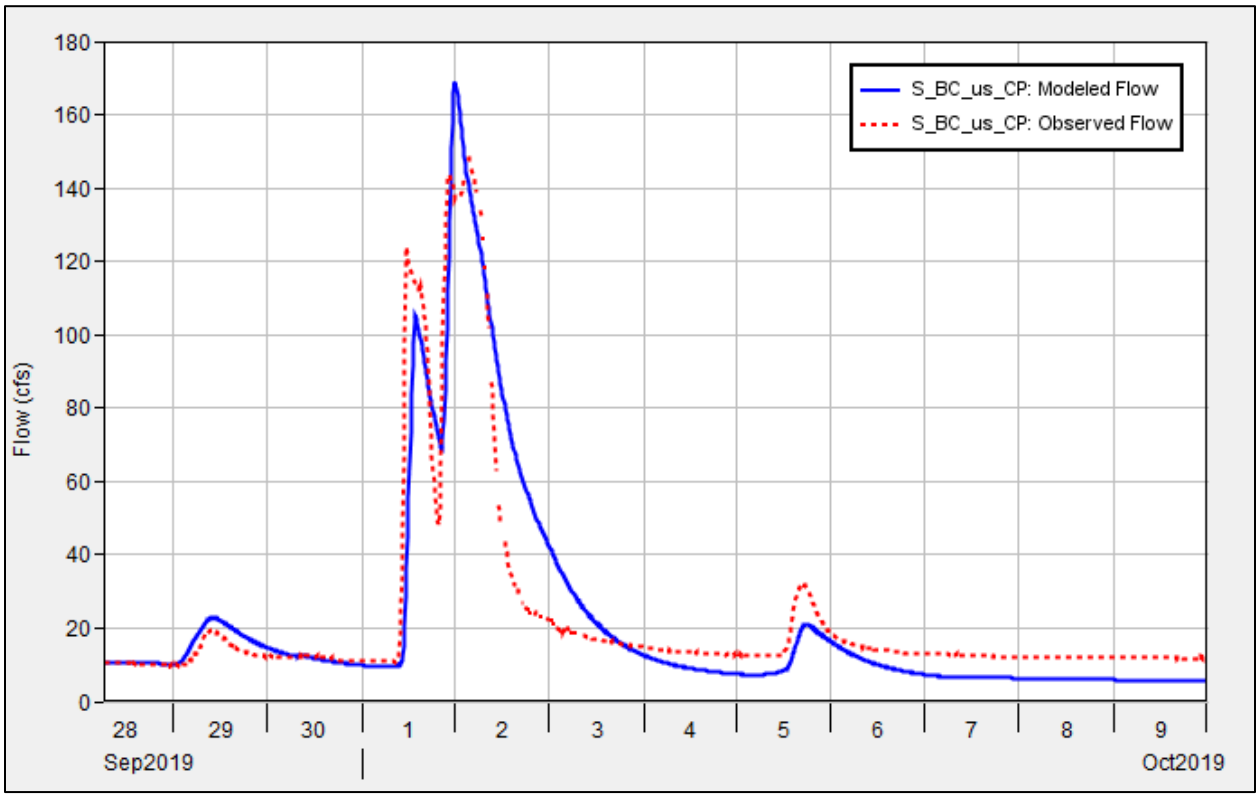

Figure 8. September-October 2019 calibration results, Brewery Creek at Cross Plains, WI

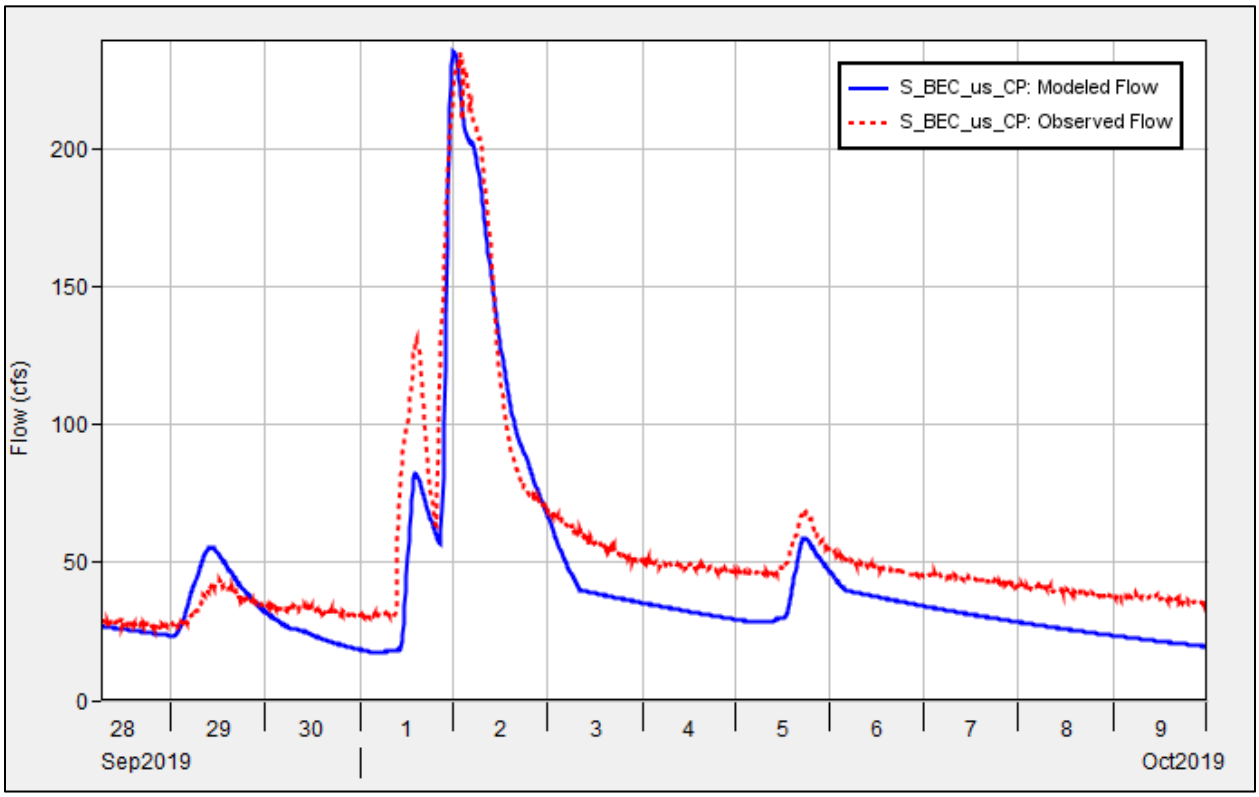

Figure 9. September-October 2019 calibration results, Black Earth Creek just upstream of Brewery Creek confluence

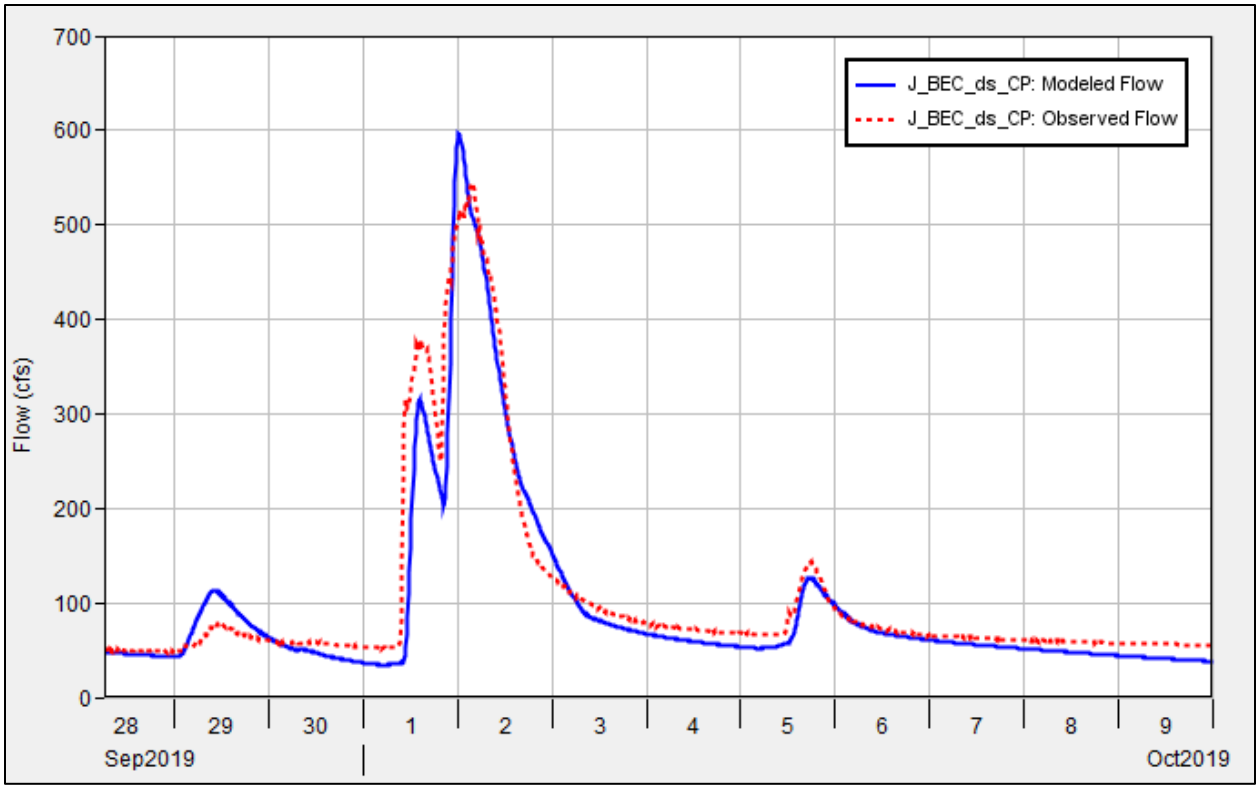

Figure 10. September-October 2019 calibration results, Black Earth Creek downstream of Cross Plains, WI

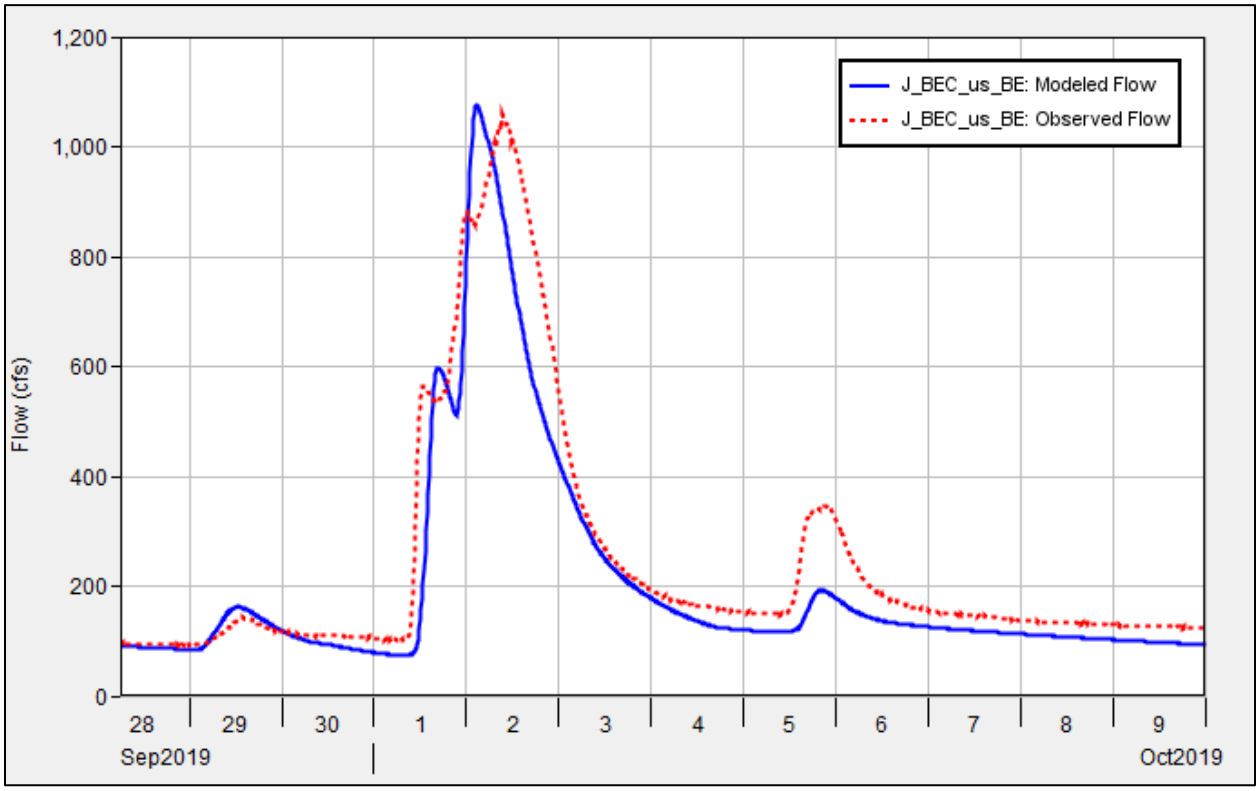

Figure 11. September-October 2019 calibration results, Black Earth Creek upstream of Black Earth, WI

Validation: June 2017 event

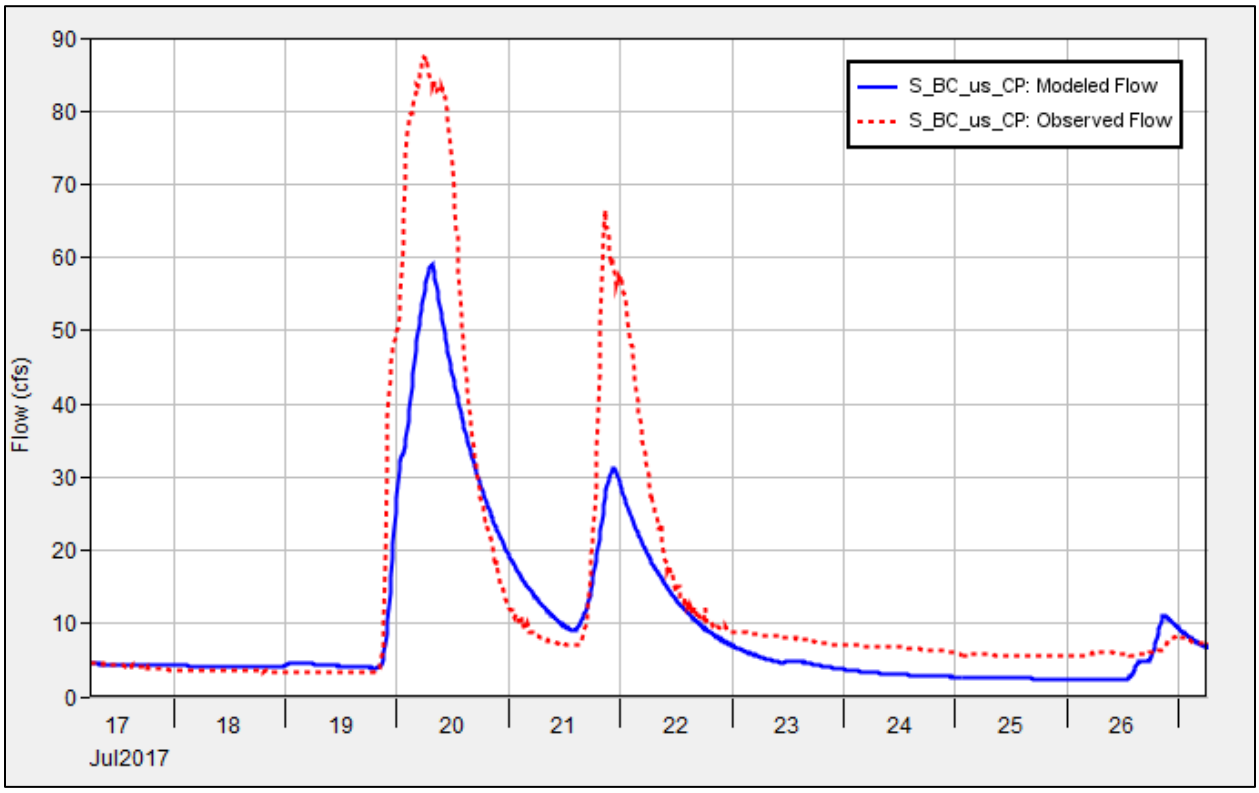

Figure 12. June 2017 calibration results, Brewery Creek at Cross Plains, WI

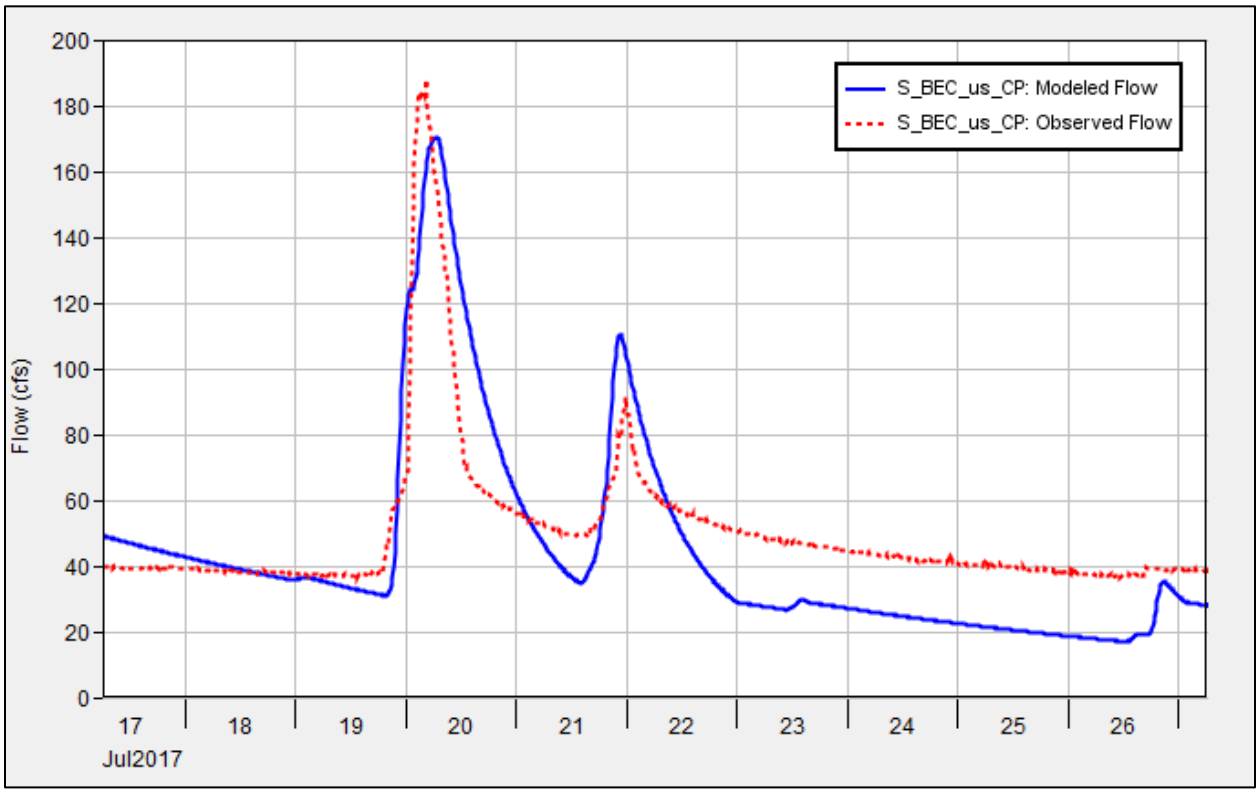

Figure 13. June 2017 calibration results, Black Earth Creek just upstream of Brewery Creek confluence

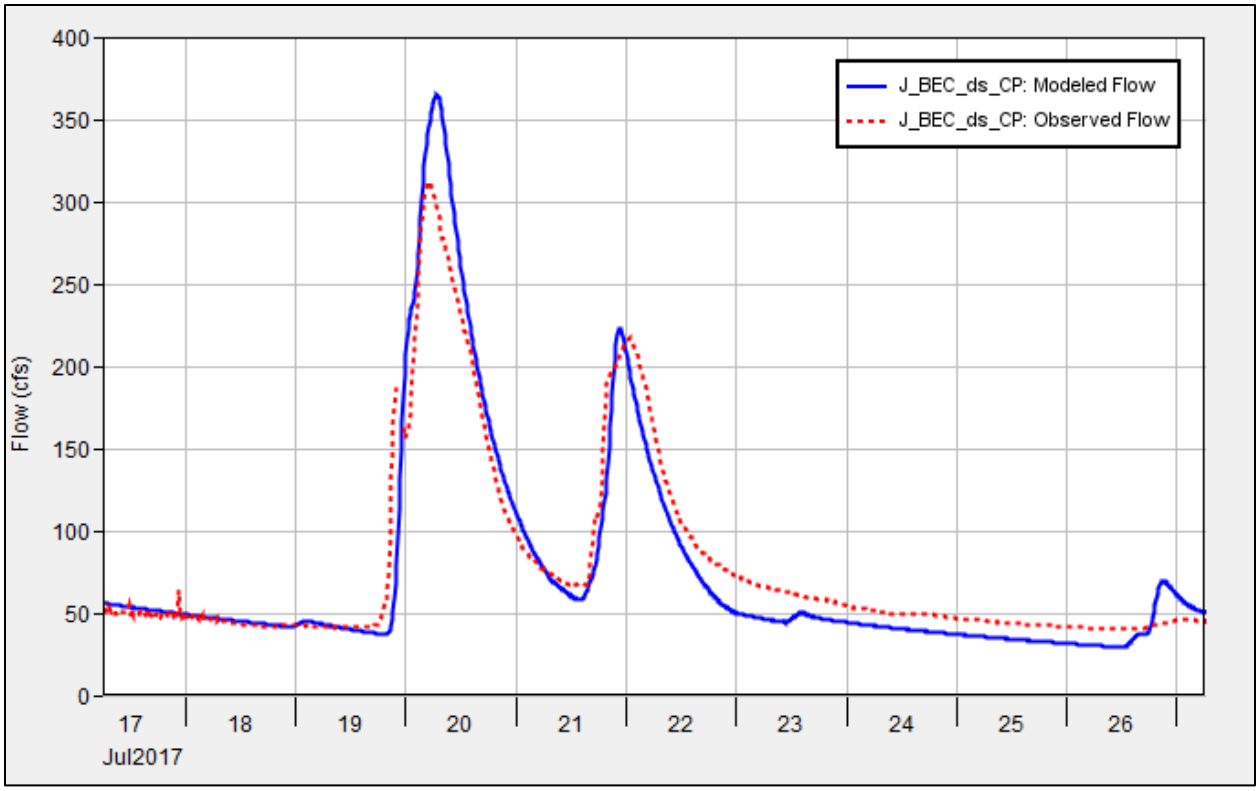

Figure 14. June 2017 calibration results, Black Earth Creek downstream of Cross Plains, WI

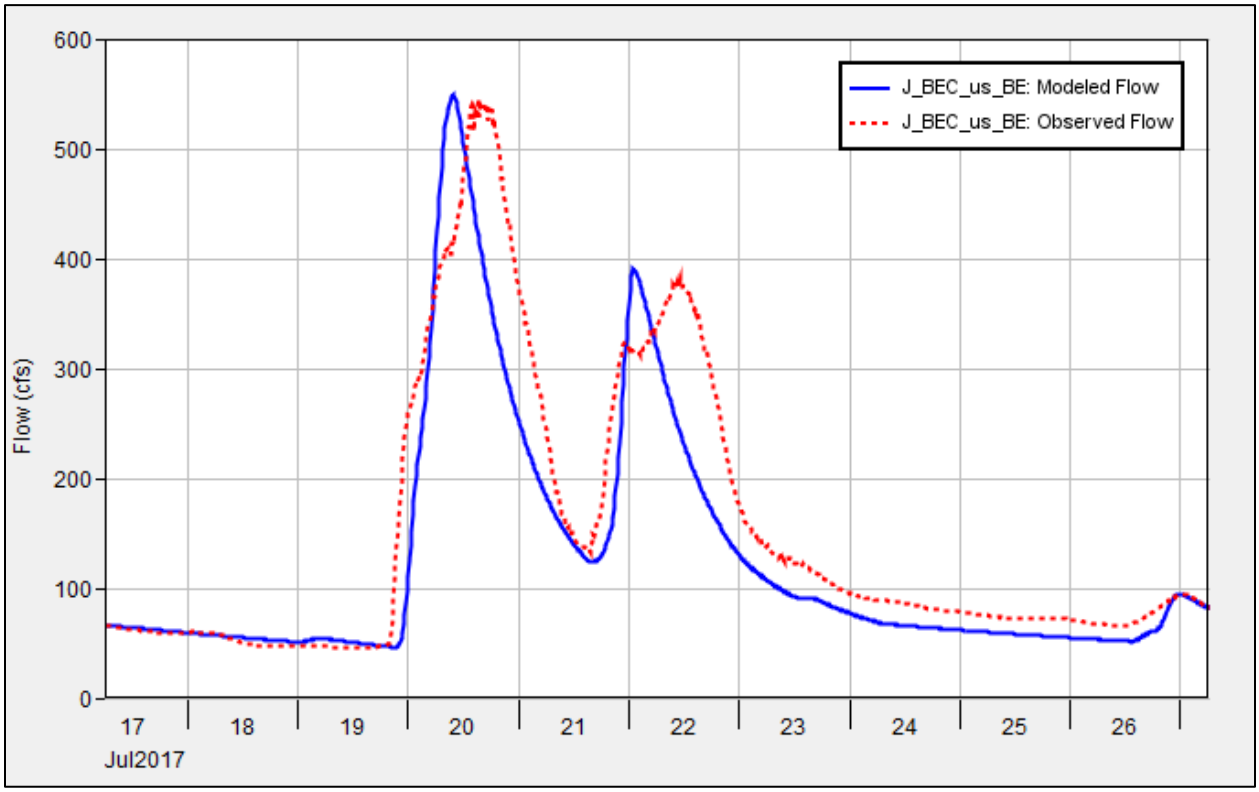

Figure 15. June 2017 calibration results, Black Earth Creek upstream of Black Earth, WI

Validation: June 2016 event

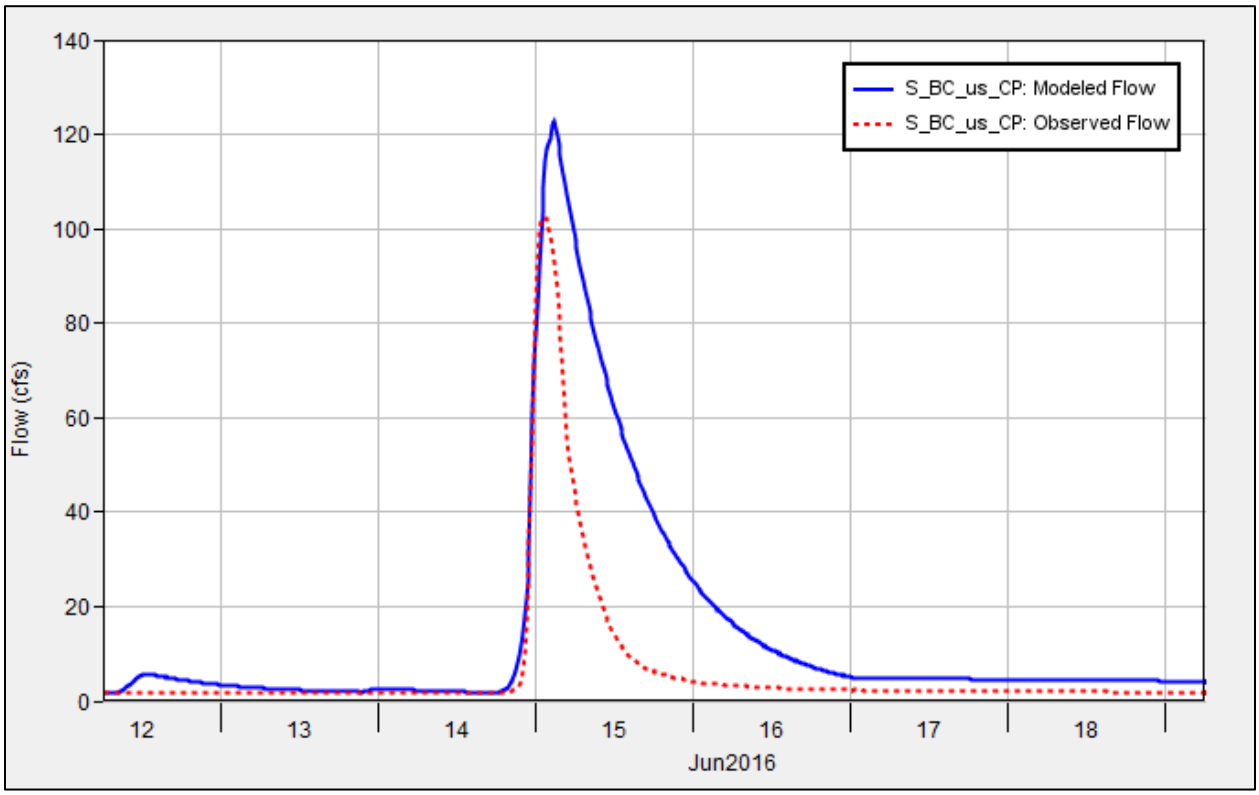

Figure 16. June 2016 calibration results, Brewery Creek at Cross Plains, WI

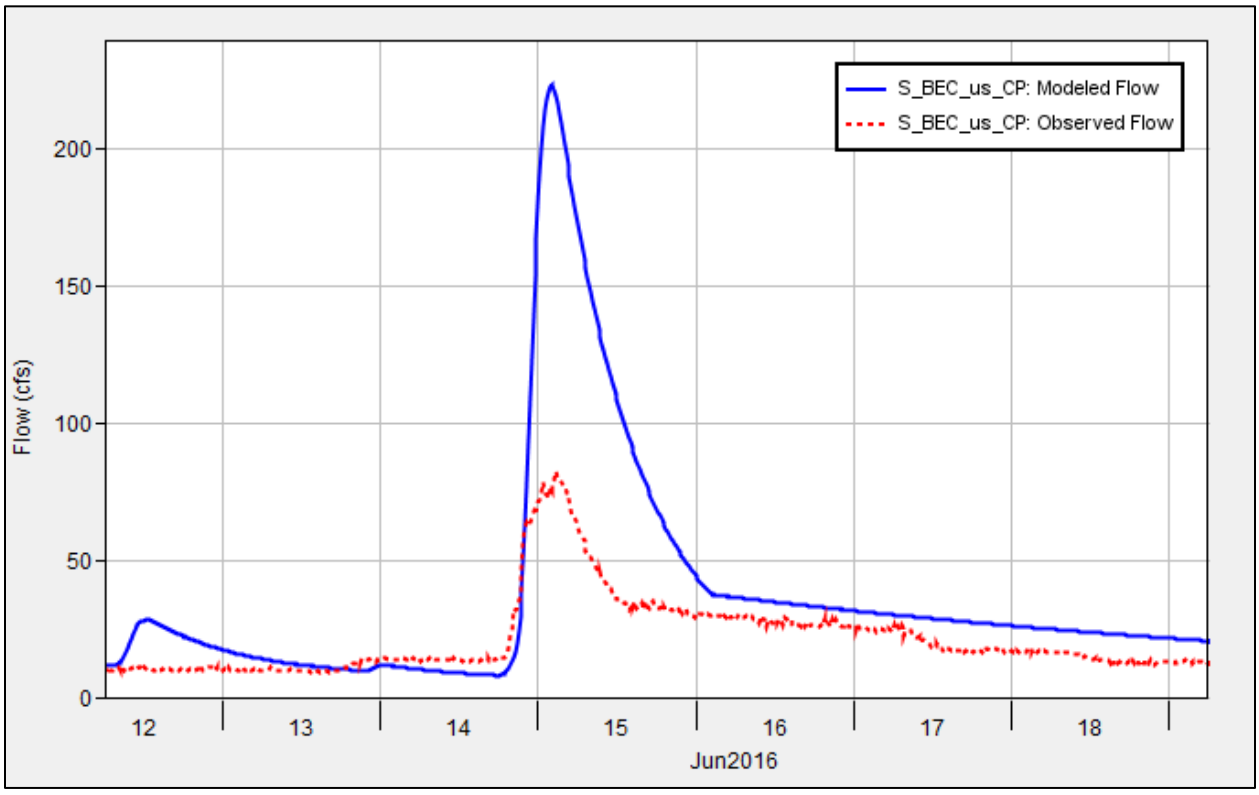

Figure 17. June 2016 calibration results, Black Earth Creek just upstream of Brewery Creek confluence

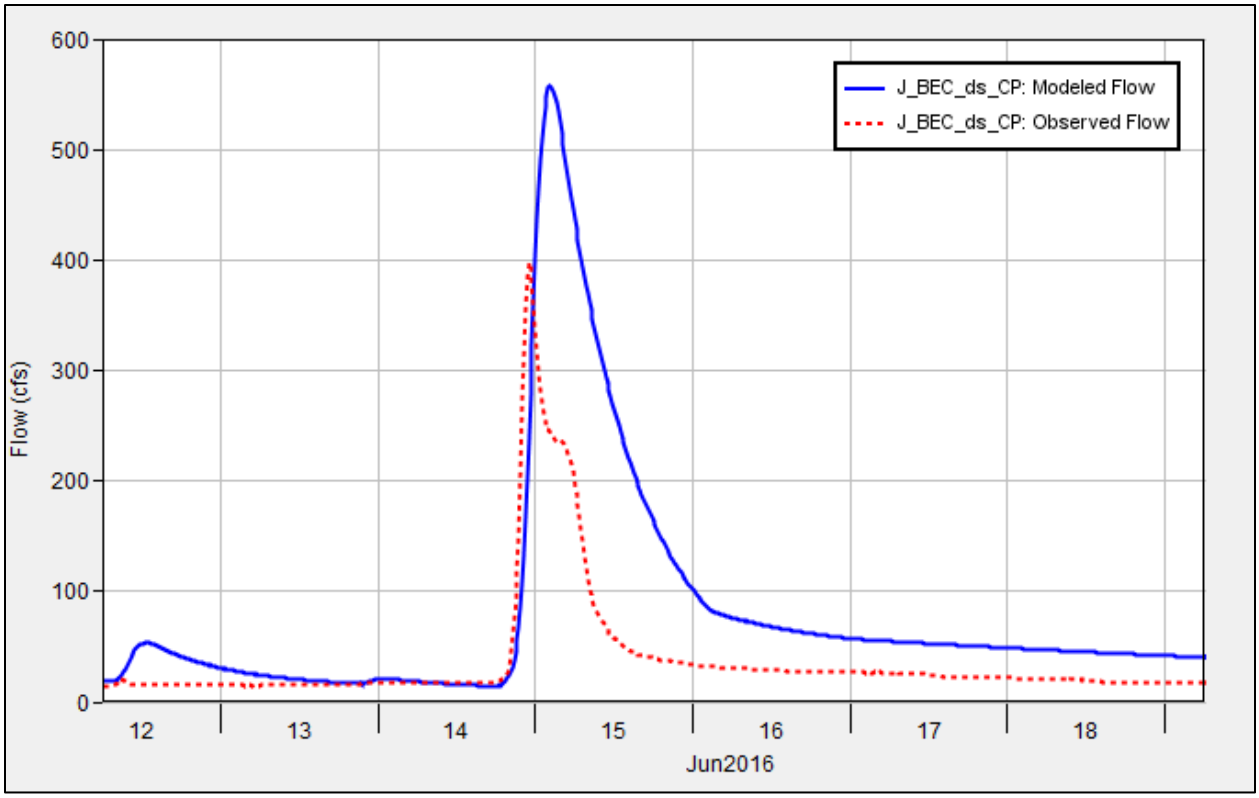

Figure 18. June 2016 calibration results, Black Earth Creek downstream of Cross Plains, WI

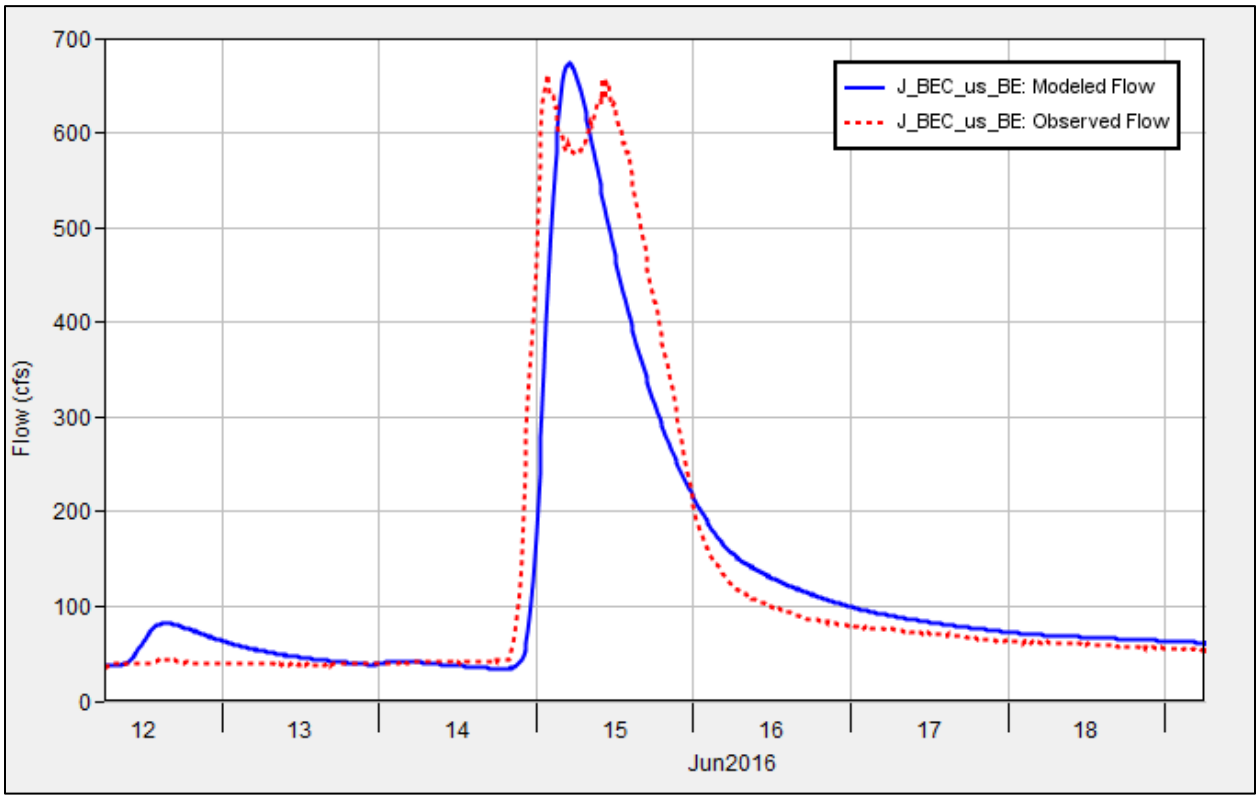

Figure 19. June 2016 calibration results, Black Earth Creek upstream of Black Earth, WI

Validation: July-August 2001 event

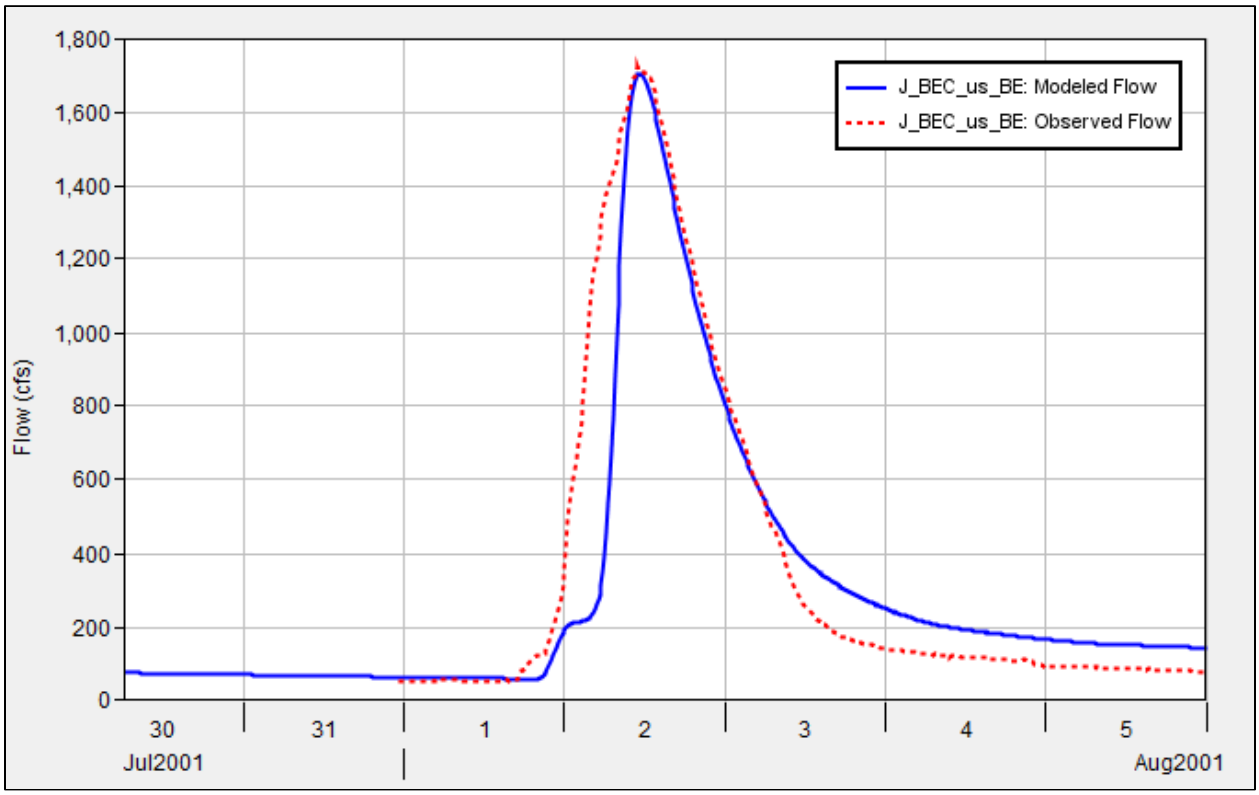

Figure 20. July-August 2001 calibration results, Black Earth Creek upstream of Black Earth, WI

US Army Corps of Engineers®
St. Paul District

Appendix D:
Climate Change Assessment

Table of Contents

Table of Tables

Table of Figures

1 Purpose

The purpose of this analysis is to provide past (observed) and potential future (projected) climate threats, vulnerabilities, and impacts to the Black Earth Creek watershed. Long-term, natural fluctuations in climate or anthropogenic driven climate change can alter regional precipitation, temperature, hydrology patterns, and ecosystem functions. While the analyses presented in this report are qualitative, they ensure changes in climate are identified and the potential benefits and/or negative impacts of any proposed land use changes or green infrastructure projects in the basin are discussed.

2 Motivation

United States Army Corps of Engineers (USACE) projects, programs, missions, and operations can accommodate the range of natural climate variability over their operating life spans. Recent scientific evidence shows that in some locations relevant to USACE operations, climate change has shifted the climatological baseline about which natural climate variability occurs and may also be changing the range of that variability. Therefore, assumptions of climatic baselines and a fixed range of natural variability, as captured in the observed hydrologic record, may no longer be appropriate for long-term projections of risk for USACE business lines such as flood risk reduction or ecosystem restoration.

Climate change impacts on the hydrology of the Black Earth Creek watershed are investigated in accordance with the USACE Engineering Construction Bulletin (ECB) 2018-14, *Guidance for Incorporating Climate Change Impacts to Inland Hydrology in Civil Works Studies, Designs and Projects* (USACE, 2018), as well as USACE Engineering Technical Letter (ETL) 1100-2-3 *Guidance for Detection of Nonstationarities in Annual Maximum Discharges* (USACE, 2017). This analysis uses a weight of evidence-based approach to make an assessment of climate change impacts to flood risk reduction projects in the Wisconsin Basin (Hydrologic Unit Code 'HUC' 0707) which contains the Black Earth Creek watershed.

3 Project Background

The Capital Area Regional Planning Commission (CARPC) sought assistance from the U.S. Army Corps of Engineers (USACE) and the Wisconsin Silver Jackets Hazard Mitigation Team to complete a hydraulic and hydrologic study of the Black Earth Creek watershed in Dane County, Wisconsin. The purpose of the project is to estimate the effectiveness of various green infrastructure or land use management alternatives in reducing the flood vulnerability of communities in the basin using a Hydrologic Engineering Center-Hydrologic Modeling System (HEC-HMS) model. The alternatives selected for modeling are widespread implementation of cover crops, no-till, and prairie strips on agricultural lands, restoring wetlands at key locations, and implementing a suite of green infrastructure improvements in urban areas, including downspout connections, permeable pavement, infiltration basins, green roofs, and rain gardens. The methodology and results of the alternative analysis are presented in the main report. Figure 1 shows the location of the Black Earth Creek watershed and relevant 2-digit and 4-digit HUC watersheds.

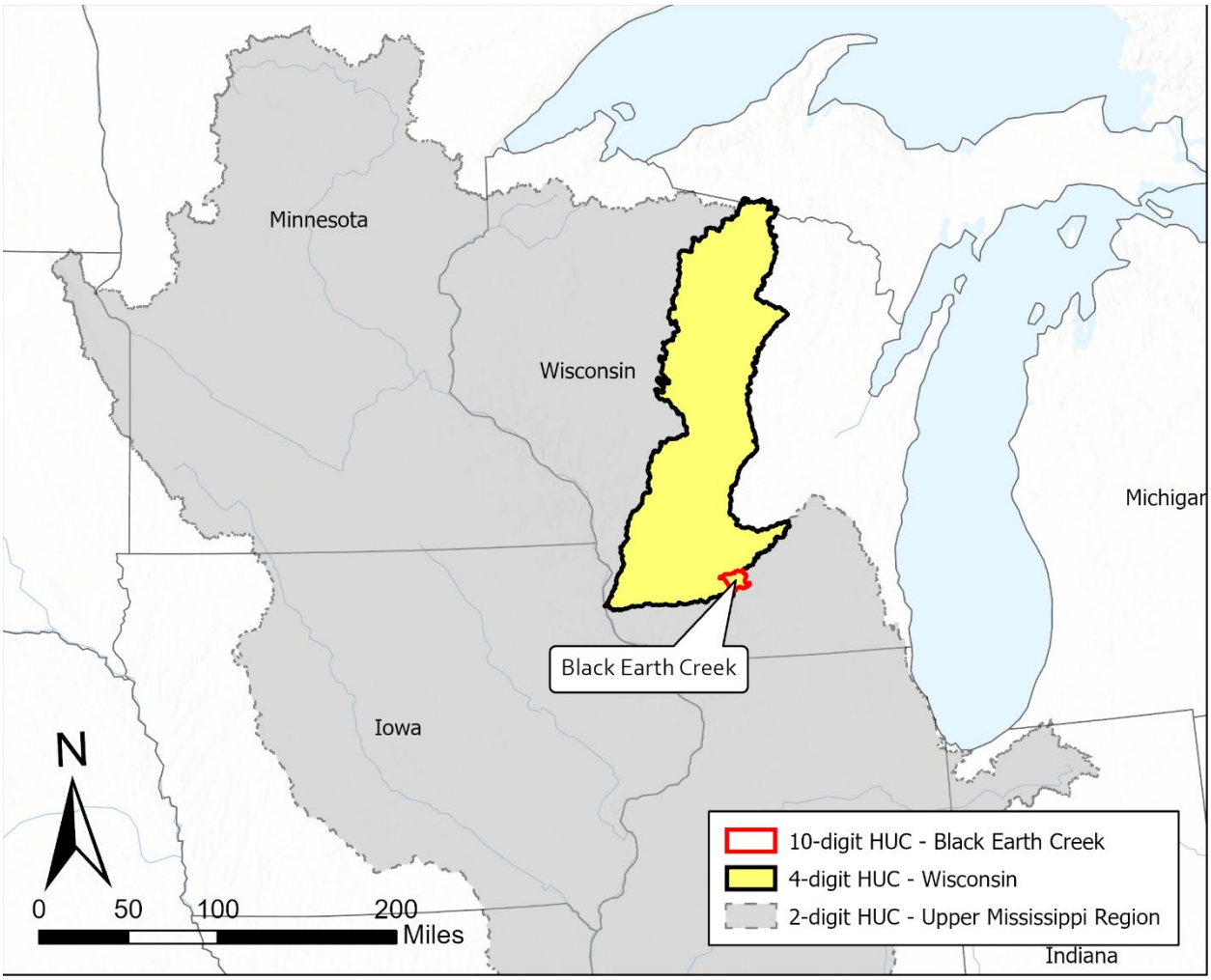

Figure 1. Location of the Black Earth Creek watershed within the Wisconsin basin

4 Literature Review

The Fourth National Climate Assessment (NCA4; (USGCRP, 2018) and Civil Works Technical Report CWTS-2015-13 (USACE, 2015) are the basis for this literature review. The NCA4 considers climate change research and impacts of climate change within the Continental United States (CONUS) and at a regional scale (USGCRP, 2018). The Civil Works Technical Report CWTS-2015-13 was published by USACE in 2015 and is a series of regional summary reports of peer reviewed climate literature that includes the Upper Mississippi Region (UMR), also referred to as Water Resources Region 07 (HUC 07), which encompasses the project area. The focus of these references is on summarizing trends identified within historic, observed temperature, precipitation, and streamflow records, as well as providing an indication of future, projections of hydrometeorology based on the outputs from global climate models (GCMs). In this assessment, background on observed and projected temperature and precipitation are provided as context for the impact that they have on observed and projected streamflow.

Temperature and precipitation have been measured since the late 1800s and provide insight into how the climate has changed over the past century. General circulation models (GCMs), also called global climate models, are used in combination with different greenhouse gas emission scenarios to project

future greenhouse gas concentrations in the atmosphere. Those projected greenhouse gas concentrations can be transformed to regional and local scales (a process called downscaling) for use as inputs in temperature and precipitation models, which can then be used as inputs to hydrologic models (Graham, Andreasson, and Carlsson, 2007). Long-term, continuous streamflow gages have been collecting daily measurements since the late 1800s and can be used to determine trends over time. Global and national scale studies attempt to project future changes in hydrology through a combination of GCMs, various downscaling techniques (e.g., statistical downscaling, dynamic downscaling using regional climate models (RCMs)), and macro-scale hydrologic models.

Uncertainty is inherent to modeling future climate due to the large spatial scale of the GCMs and the many variables needed to create projections of temperature and precipitation (USGCRP, 2017). Plus, hydrologic models introduce an additional layer of uncertainty. However, these methods represent the best available science to project hydroclimatic variables.

4.1 Air Temperature

In the UMR region, annual average temperatures between 1986-2016 for the Midwest have increased 1.26°F from the 1901-1960 annual average temperatures. In Wisconsin and Iowa, warming has been concentrated in the winter and spring, while summers have not warmed substantially in the state (Frankson, Kunkel, and Champion 2017; Frankson et al., 2017). Several additional studies have found similar shifts in winter and spring conditions across the Midwest as a whole, where observed records show early spring onsets, longer frost-free seasons, and less severe winters (Schwartz, Ault, and Betancourt, 2013; USGCRP, 2018; Westby, Lee, and Black, 2013; Wolter et al., 2015).

Although conditions vary from year to year, increases in both projected annual average temperature and the number of extreme heat days over the next century are expected in the Midwest (Pryor et al., 2014; Kunkel, Liang, and Zhu, 2010). Seasonally, climate model projections with moderate and high emission scenarios indicate steadily increasing air temperatures throughout the 21st century for both summer and winter seasons (Liu, Goodrick, and Stanturf, 2013; Scherer and Diffenbaugh, 2014). In general, a warmer and wetter winter is expected with the overall impact being significantly reduced snowpack, earlier melting, and a dramatically shortened snow season (Notaro et al., 2014; 2011). In Wisconsin specifically, Veloz et al. (2012) found that under high emission scenarios the future climate will resemble the current climate of states to the southwest such as Iowa and Missouri (Veloz et al., 2012).

4.2 Precipitation

In the Midwest region, average annual precipitation has increased by 5% to 15% from the first half of the last century (1901–1960) compared to present day (1986–2015). The annual amount of rain falling in extreme rain events, which is defined as observed precipitation above the 99th percentile, has increased by 42% from 1958 to 2016 (USGCRP, 2018, vol. 2, chap. 2). Furthermore, in a statistical analysis of the 1895-2002 period, the number of precipitation days per year and intensity of the precipitation showed a statistically significant, positive trend in the Midwest (Pryor, Howe, and Kunkel, 2009). More specifically, the Northeast climatic zone of Iowa and the Southwest climatic zone of Wisconsin, where the project is located, has shown a 10% to 15% increase in annual precipitation from 1895 to 2009 (McRoberts and Nielsen-Gammon, 2011).

Generally speaking, across the United States both annual precipitation and extreme precipitation totals and frequency are projected to increase (Johnson et al., 2012; Hagemann et al., 2013; Vavrus and Behnke, 2014). Important to flood risk planning, precipitation increases of 10-15% are projected in winter and spring for the HUC 07 encompassing the Black Earth Creek watershed from 2070–2099 relative to 1986–2015. However, in the summer and fall projected precipitation amounts are not expected to significantly change. A northward shift in the rain–snow transition zone in the central and eastern United States is projected by the end of the 21st century causing large areas that are currently snow dominated in the cold season to be rainfall dominated (USGCRP, 2017; Ning and Bradley, 2015; Notaro et al., 2014).

4.3 Hydrology

Observed hydrologic trends are strongly influenced by precipitation, temperature, and other factors such as land use and land cover in a region, groundwater dynamics, drainage patterns, channel geomorphology, and regulation. In the Midwest, annual average streamflow for both high and low flow has increased over time (Mauget, 2004; Xu et al., 2013; Small, Islam, and Vogel, 2006; Steffens and Franz, 2011). In the Driftless region of southwestern Wisconsin, which borders the project area, Juckem et al. (2008) concluded that land management changes that had started in the 1930s have been increasing baseflow while reducing stormflows through increased infiltration. The researchers further noted climatic change appears to control the timing and direction of the change, but land management magnified the hydrologic response (Juckem et al., 2008).

A number of global and national scale studies have attempted to project future changes in hydrology, relying primarily on a combination of GCMs and macro-scale hydrologic models. The complex interaction between precipitation, temperature, and hydrology makes it difficult to state with certainty how climate change will affect streamflow hydrology in the future. Increases in precipitation have the potential to increase streamflow; however, corresponding increases in temperature and evapotranspiration could outweigh effects of increased precipitation (Jha and Gassman, 2014). As the studies above indicate, no definitive statement can be made to describe how climate change will impact hydrology and streamflow in the region; however, it can be stated with relative certainty that climate change has the ability to alter basin hydrology.

4.4 Summary

Figure 2 shows a summary of the trends in discussed hydroclimatic variables, as well as an indication of the level of consensus within the peer reviewed literature considered for each variable in the UMR region. There is strong evidence through consensus in the literature that temperature, precipitation, and streamflow have increased over the observed record within the UMR. Projections of future climate show strong consensus on increases in future temperature, moderate consensus on increases in precipitation, and less consensus amongst projections of future streamflow.

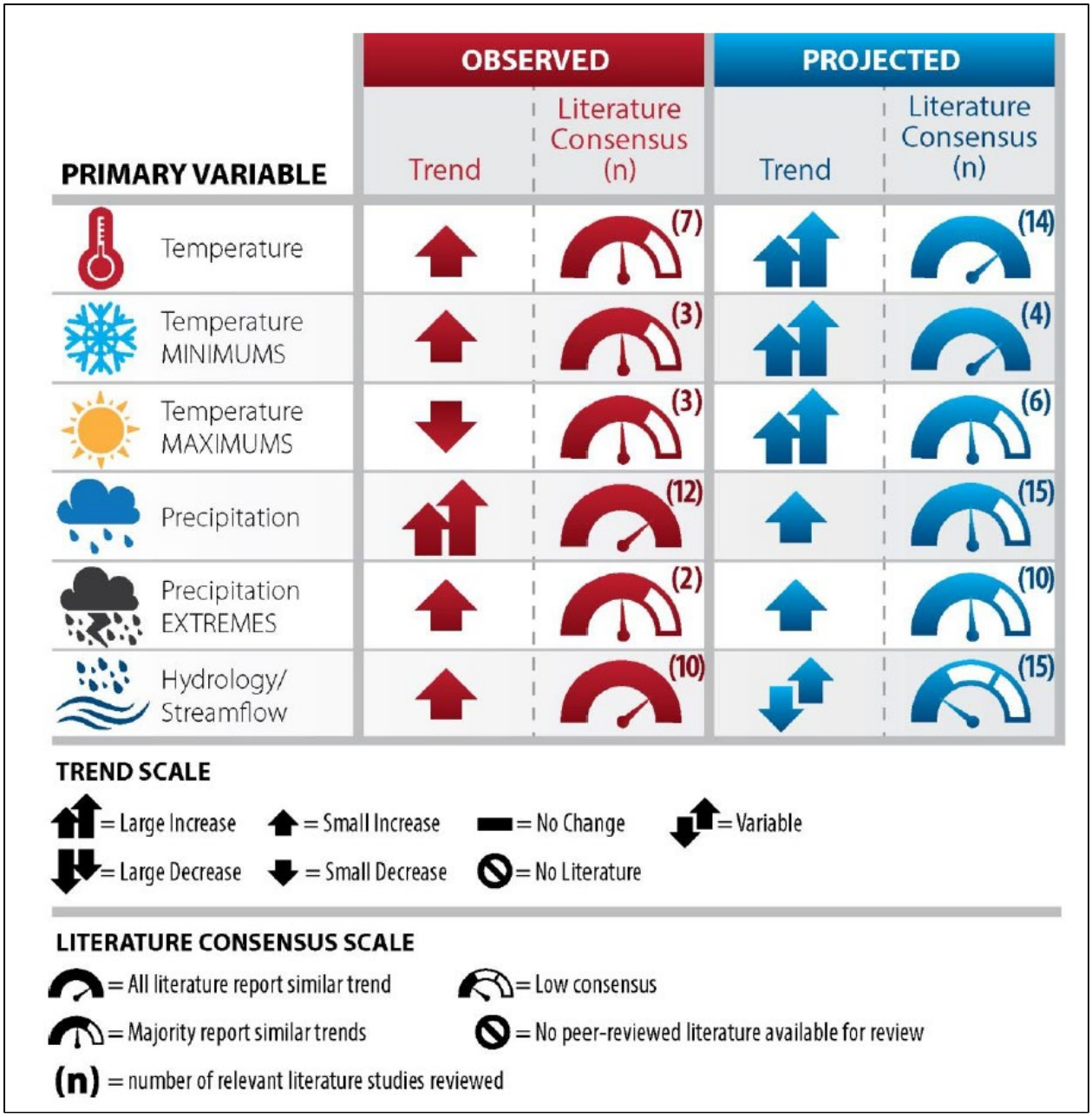

Figure 2. Summary matrix for the UMR region (HUC 07)

5 Nonstationarity Detection and Trend Analysis

The assumption that hydrologic time series data are stationary (statistical characteristics are unchanging) in time underlies traditional flow frequency analysis. Statistical tests can be used to test this assumption, using techniques outlined in Engineering Technical Letter (ETL) 1100-2-3. The Time Series Toolbox (TST) is a web-based tool to perform these tests on user inputted time series data. All nonstationarities identified by the TST are statistically significant; however, the relative strength of each nonstationarity is determined to understand its practical relevance. For a nonstationarity to be

considered strong it must have consensus across tests, robustness across statistical properties, and must represent an appreciable change in the magnitude of the mean and/or standard deviation/variance.

The important streamflow variables investigated for this project are annual instantaneous peak streamflow, monthly average streamflow, and the annual 25th percentile of daily streamflow. All streamflow data used in this analysis was recorded at the Black Earth Creek at Black Earth, WI USGS gage (05406500). This gage, shown in Figure 3, is centrally located in the Black Earth Creek watershed and has the longest period of record (1954-2020) of all streamflow gages in the basin. The gage captures flow from a drainage area of 45.6 square miles, of which 2.8 square miles is probably noncontributing. The gage is not affected by regulation.

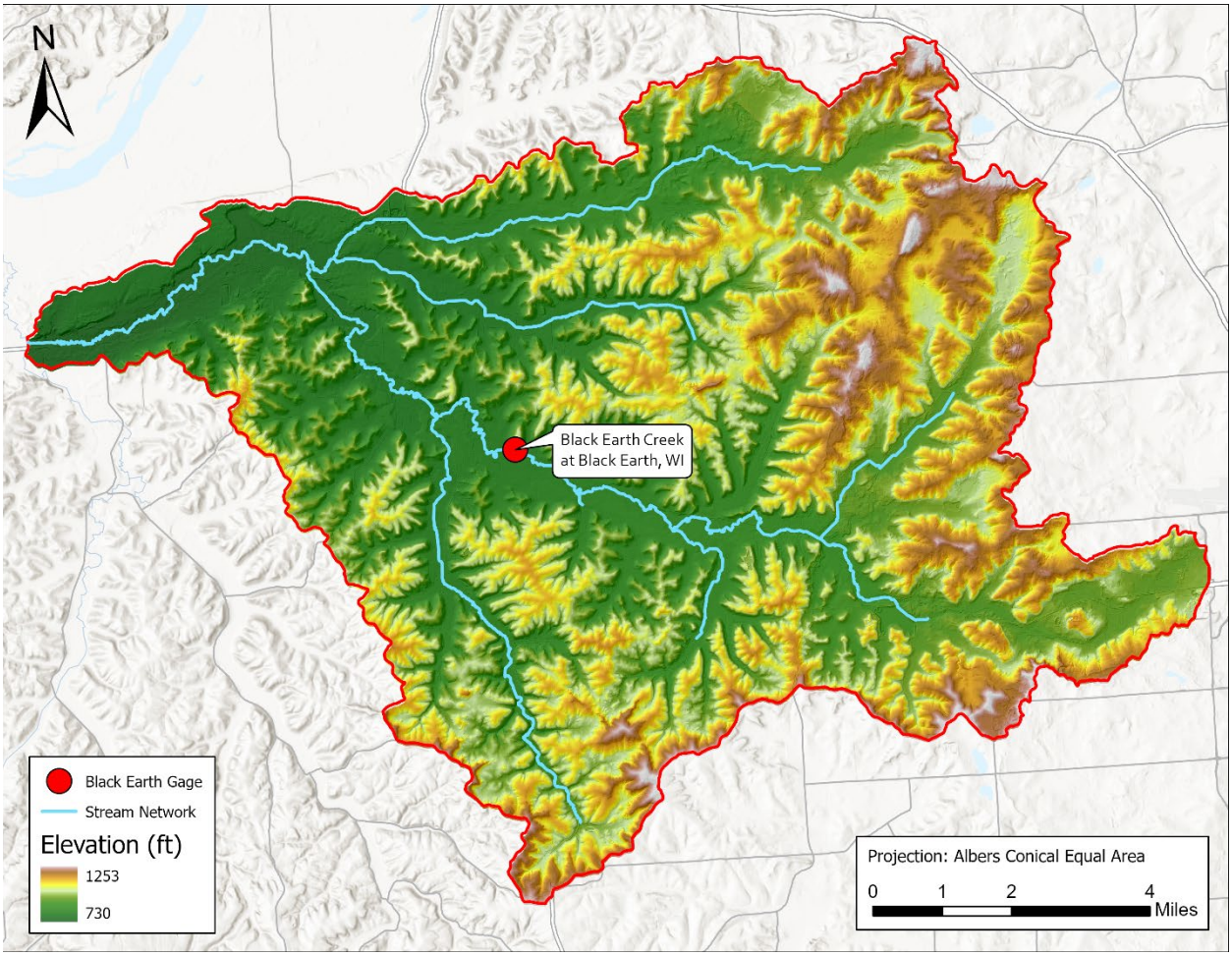

Figure 3. Location of Black Earth Creek at Black Earth, WI USGS gage (05406500)

5.1 Annual Peak Streamflow

Instantaneous annual peak flows are important for flood risk management and hydraulic structure design. These peaks represent the most severe loadings and are often the result of intense precipitation and/or snowmelt events. Figure 4 displays the observed annual instantaneous peak flow record at the Black Earth, WI USGS gage. The TST was used to complete a monotonic trend analysis. The analysis found no statistically significant trend in the observed annual peak flow for the period 1954-2020, with

t-Test, Mann-Kendall, and Spearman Rank Order applied using a 0.05 level of significance (p-values of 0.400, 0.940, and 0.816, respectively).

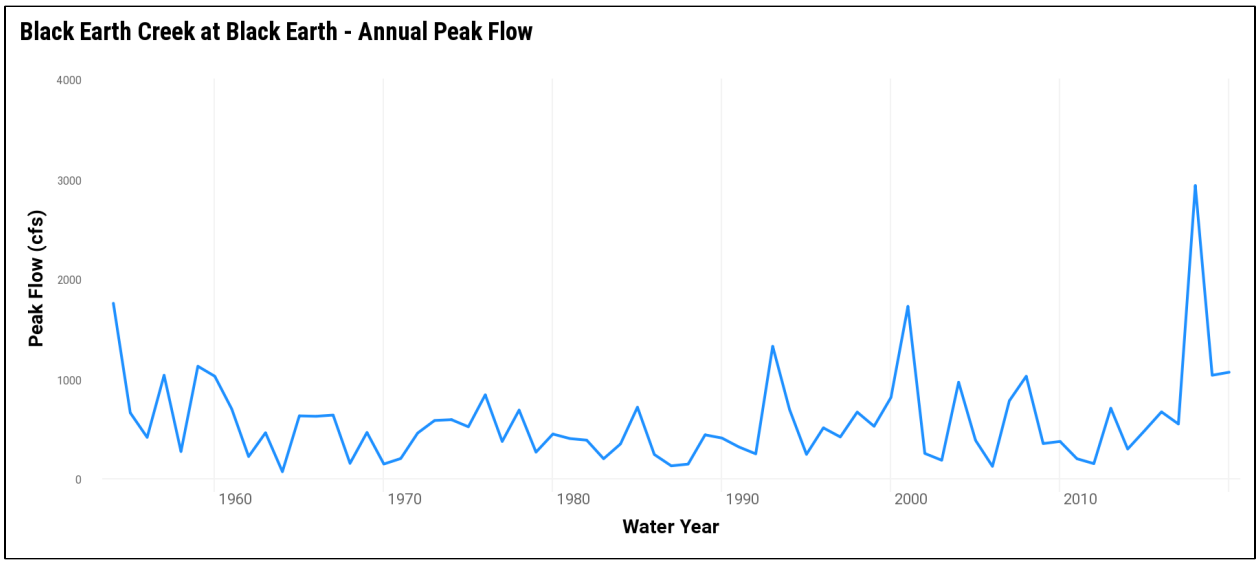

Figure 4. Annual peak flow at the Black Earth, WI USGS gage

For the Black Earth Creek peak flow record, a gradual change in mean was detected by the smooth Lombard-Wilcoxon test over the period 2014-2017. However, since no other statistical tests detected change points in the data, there are not considered to be any strong nonstationarities in the annual peak flow data.

5.2 Monthly Average Streamflow

Trends in average monthly streamflow can indicate whether the volume of water traveling through Black Earth Creek has tended to increase or decrease over time. Monthly average streamflow at the Black Earth USGS gage was computed during the period 1954-2020 using HEC-DSSVue (USACE, 2017). As shown in Figure 5, monthly average discharge has been increasing over the period of record and has been exceptionally high since approximately 2018.

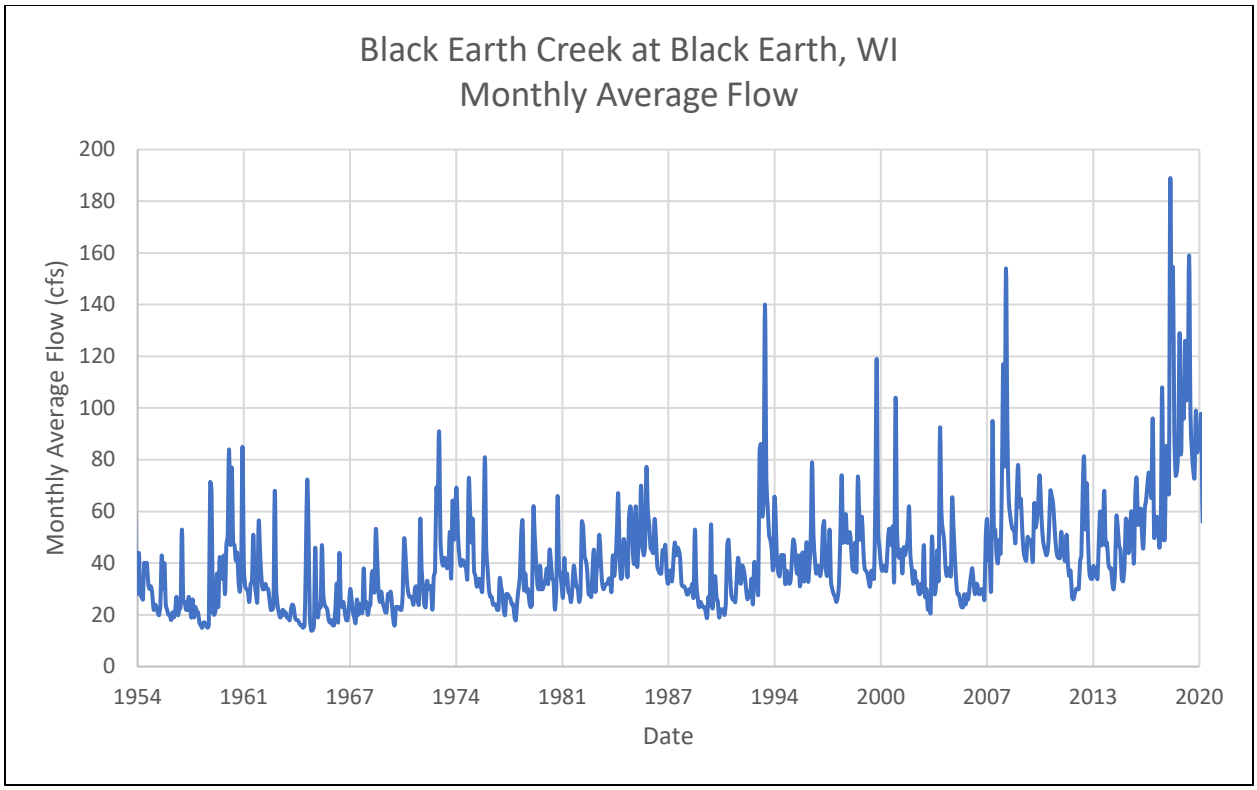

Figure 5. Monthly average flow at the Black Earth, WI USGS gage

After computing monthly average flow for the period of record, HEC-DSSVue was used to extract a monthly average timeseries for each month for the period 1954-2020. Then, the TST was used to identify trends in the average streamflow record for each month. For this analysis, monthly average flow values were assumed to be independent of one another from year to year. An example trend analysis of average flow during the month of April is shown in Figure 6. For all months of the calendar, a statistically significant, increasing trend was identified for the period 1954-2020. T-Test, Mann-Kendall, and Spearman Rank Order p-values for each monthly timeseries were much lower than the commonly accepted threshold for significance of 0.05.

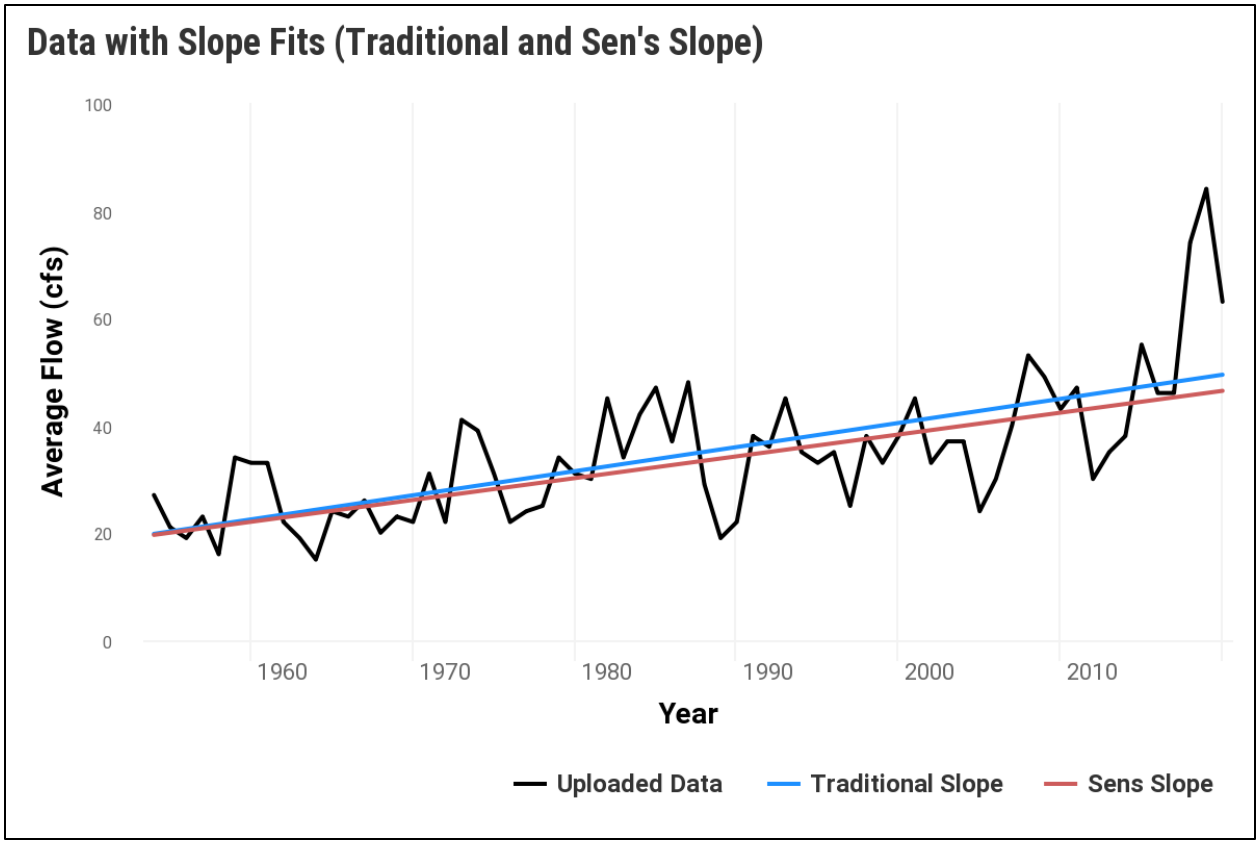

Figure 6. Trend analysis of average flow for the month of April at the Black Earth, WI USGS gage

5.3 Annual 25th Percentile of Daily Flows

The fact that no significant trend exists in the annual peak flow record suggests the frequency of extreme flood events is not increasing at Black Earth Creek. However, significant, positive trends in monthly average streamflow suggest baseflow has been increasing overtime. To further analyze this assertion and isolate periods in which the creek could be considered to be at "baseflow," the 25th percentile of daily flow values was computed for each year over the period 1954-2020. Visual inspection of the observed flow record on Black Earth Creek suggests the 25th percentile of daily flow is a good estimate of baseflow conditions. As shown in Figure 7, the 25th percentile daily flow value has generally increased overtime.

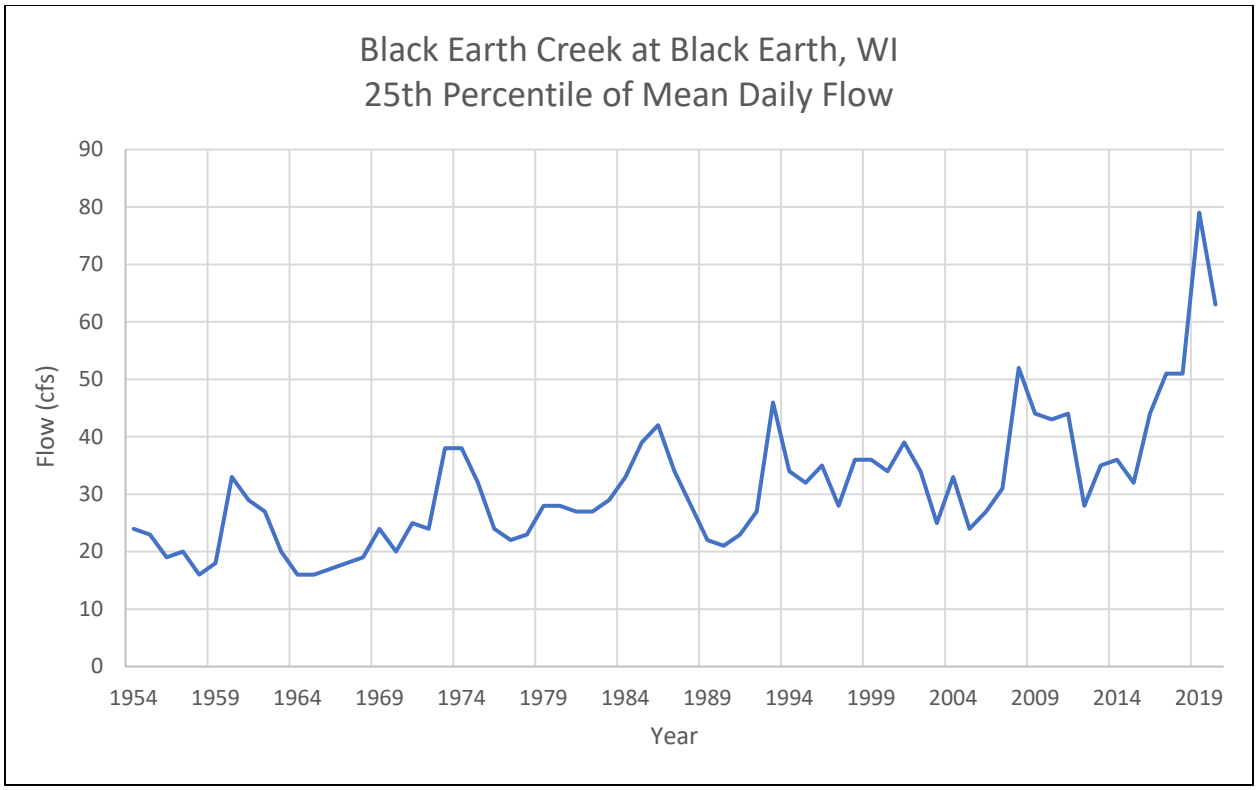

Figure 7. Annual 25th percentile of daily flow at the Black Earth, WI USGS gage

5.4 Summary

The USGS gage at Black Earth shows no significant trend in annual instantaneous peak flows during the period 1954-2020. No strong nonstationarities in the peak flow record could be identified. Monthly average discharge has been increasing with a significant, positive trend being identified for each month of the year over the period 1954-2020. The annual 25th percentile of daily flow recorded at the Black Earth gage has also increased throughout the period of record. Increasing trends in monthly average discharge and the annual 25th percentile of daily flow values indicate baseflow in Black Earth Creek has been increasing over time. However, the lack of any significant trends in the annual peak flow record suggests extreme flood events may not be increasing in magnitude.

6 Projected Hydrology and Vulnerability

In order to understand future without project conditions, the USACE developed several tools to project future streamflow and assess vulnerability to climate change at a regional scale. These tools were used to investigate projected changes to basin hydrology in response to climate change. HUC 0707, the Wisconsin basin shown in Figure 1, encompasses the project area and was used for this analysis.

6.1 USACE Climate Hydrology Assessment

The USACE Climate Hydrology Assessment Tool (CHAT) was used to investigate potential future trends in streamflow for the Lower Wisconsin watershed (HUC 07070005), which includes the Black Earth Creek basin, through water year 2099. Hydrologic model outputs were generated using meteorological inputs derived based on 64 different combinations of greenhouse gas emission scenarios and GCMs. Model outputs were compared to a historical model simulation of the period 1950-2005. Meteorological

conditions for the historic simulation were also derived from GCMs, but greenhouse gas emissions were assumed to be equivalent to reconstructed, historic levels. As expected, there was considerable variability in the projected annual maximum monthly flows for each basin across the 64 projections. This is shown by the yellow shading in Figure 8. This spread is indicative of the high degree of uncertainty associated with projected, climate-changed hydrology.

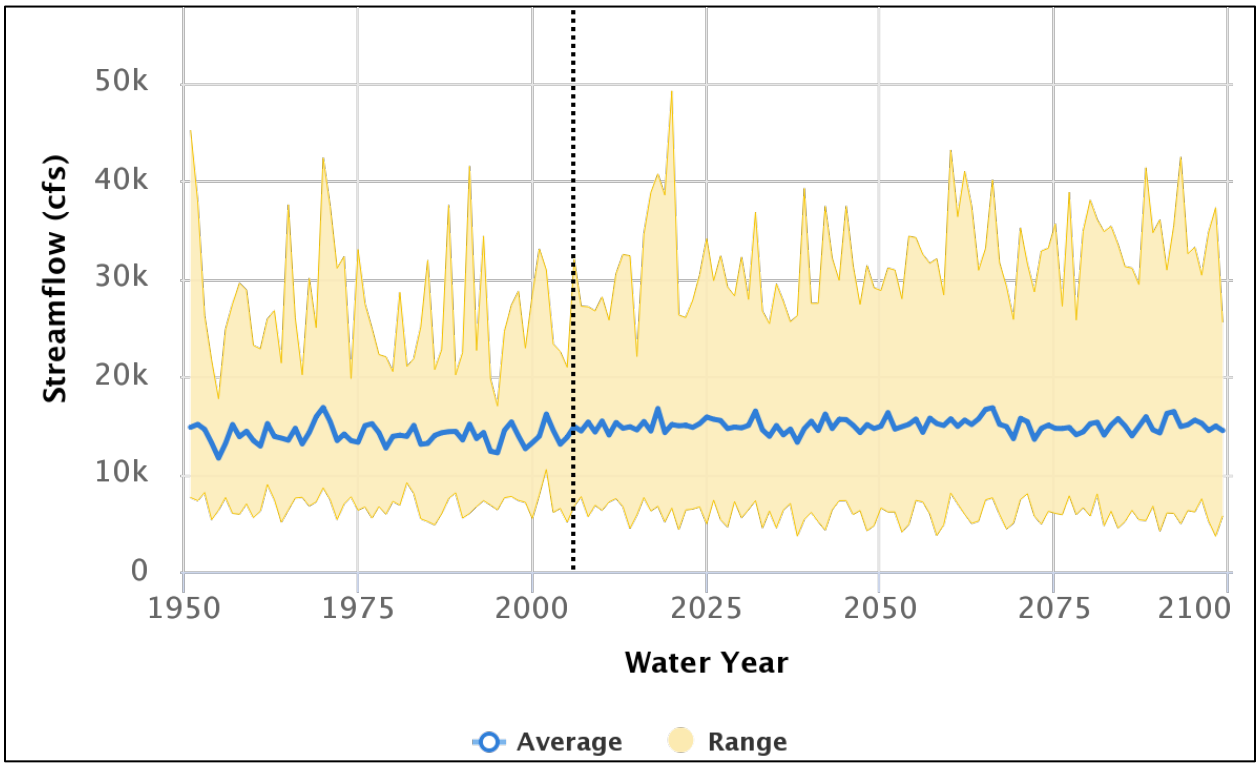

Figure 8. Range of 64 projected annual, maximum monthly streamflow for HUC 07070005

The computed trends in mean annual maximum monthly streamflow for the historical and future simulations for HUC 07070005 are shown below in Figure 9. Neither the historical nor projected trends are considered significant, with t-Test, Mann-Kendall, and Spearman Rank-Order p-values greater than the accepted level of significance of 0.05.

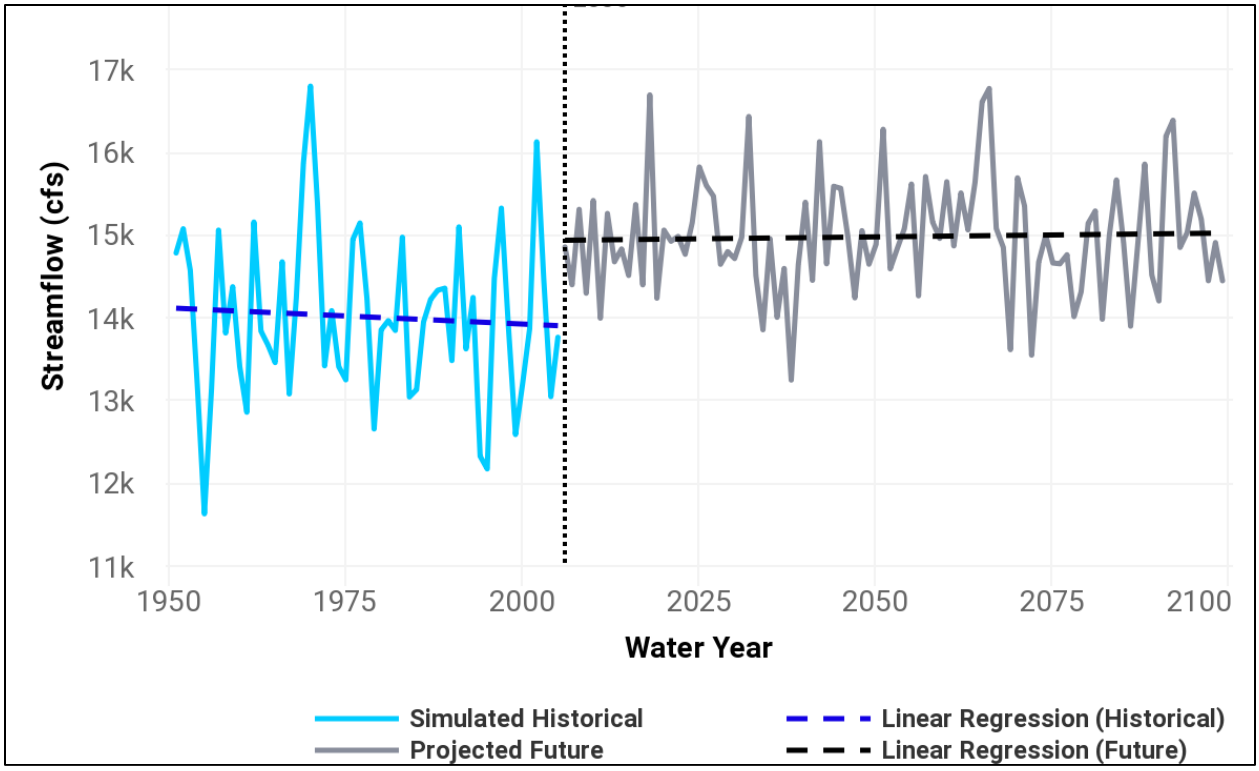

Figure 9. Trend in mean projected annual maximum monthly streamflow for HUC 0707

6.2 USACE Watershed Climate Vulnerability Assessment

The USACE Watershed Climate Vulnerability Assessment (VA) Tool completes a screening level, climate change assessment of vulnerability by comparing a selected watershed to all 4-digit HUC watersheds in the continental United States (CONUS). This tool is used to assess the relative vulnerability of a specific USACE business line within a watershed to projected climate change impacts. Vulnerability is measured using the Weighted Order Weighted Average (WOWA) method to compute a composite vulnerability score for each business line, 30-year time period (centered on 2050 or 2085), and scenario (wet – top 50% of cumulative runoff projections and dry – bottom 50% of cumulative runoff projections). Each WOWA score is based on a set of standardized indicators which reflect stressors related to climate, demographic changes, ecological changes, and other factors (USACE, 2016).

Because flood risk reduction is one of the primary goals of the Black Earth Creek Hydrologic Modeling Study, the Flood Risk Reduction business line was analyzed with the tool's default, National Standard settings. Indicators included within the WOWA score for Flood Risk Reduction are: long-term variability in hydrology, runoff elasticity (ratio of streamflow runoff to precipitation), local and cumulative flood magnification (indicator of how much high flows are projected to change over time within the HUC and in upstream HUC watersheds), and urban area within the 500-year floodplain. Figure 10 shows the results of the VA tool, and Table 1 shows the vulnerability scores for the two 30-year epochs.

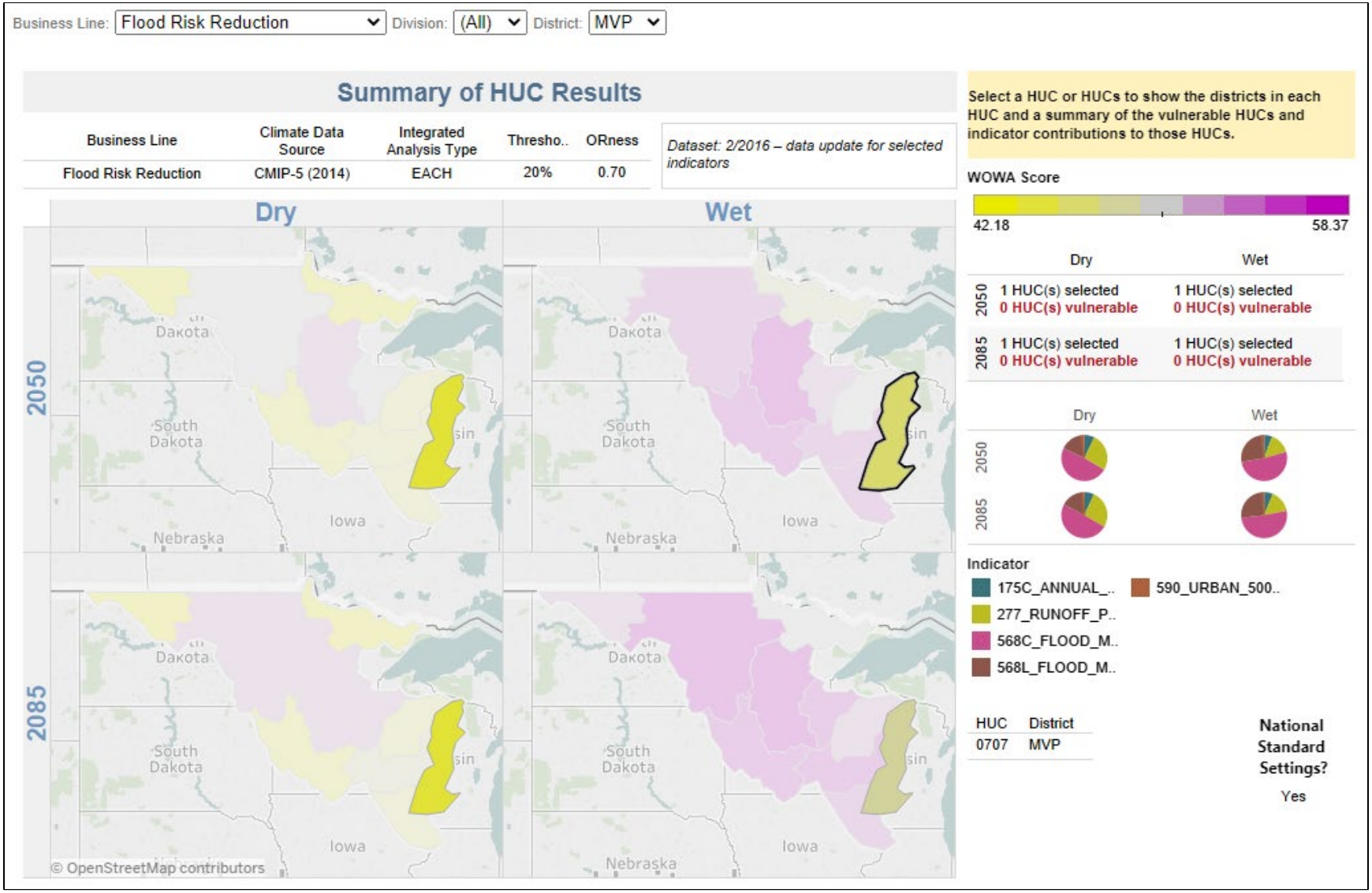

Figure 10. Projected vulnerability for Flood Risk Reduction in HUC 0707

Table 1. Comparison of projected vulnerability for Flood Risk Reduction

	2050		2085	
	WET	DRY	WET	DRY
Wisconsin (0707)	47.13	44.35	48.07	44.09

The Wisconsin (HUC 0707) watershed is not considered vulnerable to the impacts of climate change in comparison to the other 4-digit HUCs in CONUS. The major drivers of the computed vulnerability score are Flood Magnification and Runoff Elasticity. While the HUC 0707 watershed is not vulnerable in a relative sense, these indicators suggest the Wisconsin watershed is susceptible to increasing magnitudes of floods (measured as the monthly flow exceeded 10% of the time) and an increasing share of precipitation being converted into runoff (USACE, 2016).

7 Conclusion

The purpose of the Black Earth Creek Hydrologic Modeling Project is to evaluate various infrastructure projects, land use changes, or best management practices to reduce flood risk within the Black Earth Creek watershed. The alternatives selected for the study are widespread implementation of cover crops, no-till, and prairie strips on agricultural lands, wetland restoration, and a suite of green infrastructure improvements in urban areas. Both historic, observed hydrometeorological data, as well as projected, climate-changed hydrometeorological data was reviewed to support qualitative statements about how the alternatives studied may increase or decrease the basin's resilience to the effects of climate change.

Available climate change literature suggests a warmer and wetter climate in the future. There is consensus in the scientific literature that temperatures will increase. In Wisconsin, observed increases in temperature have been concentrated during winter and spring. Winter and spring precipitation is expected to increase, with more precipitation falling as rain instead of snow. The literature review also suggests a shift in seasonality, with snowpack declining in the project area and spring melt occurring earlier. Positive trends in observed, monthly streamflow as well as the 25th percentile of daily streamflow on Black Earth Creek support the consensus of increased precipitation in general. While increased frequency of intense precipitation events is also projected in the future, there is not a consensus on whether more frequent intense rainfall events will translate to more frequent extreme flood events in the scientific literature. Observed data supports this lack of consensus, as no trend was observed in annual peak flow on Black Earth Creek. The CHAT tool did not show a significant trend in projected annual maximum monthly streamflow, and while the VA tool showed Flood Magnification and Runoff Elasticity to be the main drivers of the vulnerability score for the Wisconsin River watershed (HUC 0707), flood risk reduction efforts in the Wisconsin basin are relatively less likely to be significantly impacted by climate change when compared to other basins in the region.

The agricultural best management practices BMPs studied for this project are likely to improve the basin's resilience to increased precipitation, particularly during winter and early spring when row crops have not been established. Both cover crops and prairie strips increase the amount of living cover on the landscape during these periods, decreasing runoff by improving infiltration and evapotranspiration. In

urban areas, green infrastructure improvements may decrease runoff from impervious surfaces, somewhat lessening impacts associated with increasing precipitation. Restored, or constructed, wetlands can provide additional flood storage across the landscape, which can help offset any increased stream discharge due to increased precipitation. As described in the main report, the restored wetland design methodology assumed in this study is off-channel wetlands with overflow structures that would begin to fill once the stream reaches a given discharge. Since the observed flow record on Black Earth Creek suggests extreme flood events are not increasing, it should not necessarily be assumed such wetland storage areas would be filled more often in the future. However, the increase in baseflow suggests any restored wetlands may be wet for longer periods before and after flood events. The observed increase in baseflow should also be considered when designing inlet and outlet structures of such projects.

The land management and green infrastructure alternatives studied for this project may also help offset some negative effects of climate change not related to flood risk management. All of the agricultural BMPs studied for this project reduce runoff to some degree, thereby reducing soil and nutrient loss, a problem that may worsen as precipitation increases. No-till may also play a role in reducing soil loss during winter months if snowpack decreases and the land surface is exposed to wind and water erosion for longer periods each year. A greener urban environment in general with less reflective, heat trapping impervious areas may also offer quality of life improvements in local communities as summer temperatures and the number of extreme heat days increase. In general, all of the alternatives studied for this project have some capacity to increase the resilience of the basin to a changing climate and are not expected to exacerbate any negative impacts associated with climate change. However, it is important the local sponsor continues to monitor change in the basin and reevaluates trends in hydroclimatic variables prior to constructing any project features to reduce flood risk.

8 References

1. Frankson, R., K. Kunkel, and S. Champion. 2017. “Wisconsin State Climate Summary.” NOAA Technical Report NESDIS 149-WI. https://statesummaries.ncics.org/chapter/wi/.
2. Frankson, R., K. Kunkel, S. Champion, and J. Runkle. 2017. “Iowa State Climate Summary.” NOAA Technical Report NESDIS 149-IA. https://statesummaries.ncics.org/chapter/ia/.
3. Gleckler, P.J., K.E. Taylor, and C. Doutriaux. 2008. “Performance Metrics for Climate Models.” JOURNAL OF GEOPHYSICAL 113 (D6). https://doi.org/10.1029/2007JD008972.
4. Graham, L. Phil, Johan Andreasson, and Bengt Carlsson. 2007. “Assessing Climate Change Impacts on Hydrology from an Ensemble of Regional Climate Models, Model Scales and Linking Methods – a Case Study on the Lule River Basin.” Climatic Change 81: 293–307. https://doi.org/10.1007/s10584-006-9215-2.
5. Hagemann, S., C. Chen, D.B. Clark, S. Folwell, S.N. Gosling, I. Haddeland, N. Hanasaki, et al. 2013. “Climate Change Impact on Available Water Resources Obtained Using Multiple Global Climate and Hydrology Models.” Earth System Dynamics 4 (May): 129–44. https://doi.org/10.5194/esd-4-129-2013, 201.
6. HEC. 2021. HEC-DSSVue (version 3.2.3). Davis, CA: Hydrologic Engineering Center (HEC).
7. Jha, M.K., and P.W. Gassman. 2014. “Changes in Hydrology and Streamflow as Predicted by a Modelling Experiment Forced with Climate Models.” Hydrological Processes 28 (5): 2772–81. https://doi.org/10.1002/hyp.9836.
8. Johnson, T.E., J.B. Butcher, A. Parker, and C.P. Weaver. 2012. “Investigating the Sensitivity of U.S. Streamflow and Water Quality to Climate Change: U.S. EPA Global Change Research Program’s 20 Watersheds Project.” Journal of Water Resources Planning and Management 138 (5): 453–64.
9. Juckem, Paul F., Randall J. Hunt, Mary P. Anderson, and Dale M. Roberston. 2008. “Effects of Climate and Land Management Change on Streamflow in the Driftless Area of Wisconsin.” Journal of Hydrology 355 (1–4): 20. https://doi.org/10.1016/j.jhydrol.2008.03.010.
10. Kunkel, Kenneth E., Xin-Zhong Liang, and Jinhong Zhu. 2010. “Regional Climate Model Projections and Uncertainties of U.S. Summer Heat Waves.” Journal of Climate 23 (16): 4447–58. https://doi.org/10.1175/2010JCLI3349.1.
11. Liu, Y., S.L. Goodrick, and J.A. Stanturf. 2013. “Future U.S. Wildfire Potential Trends Projected Using a Dynamically Downscaled Climate Change Scenario.” Forest Ecology and Management 294 (15): 120–35. https://doi.org/10.1016/j.foreco.2012.06.049.
12. Mauget, Steven A. 2004. “Low Frequency Streamflow Regimes over the Central United States: 1939–1998.” Climatic Change 63: 121–44. https://doi.org/10.1023/B:CLIM.0000018502.86522.57.
13. McRoberts, D.B., and J.W. Nielsen-Gammon. 2011. “A New Homogenized Climate Division Precipitation Dataset for Analysis of Climate Variability and Climate Change.” Journal of Applied Meteorology and Climatology 50: 1187–99. https://doi.org/10.1175/2010JAMC2626.1.
14. Ning, Liang, and Raymond S. Bradley. 2015. “Snow Occurrence Changes over the Central and Eastern United States under Future Warming Scenarios.” Scientific Reports 5 (17073). https://doi.org/10.1038/srep17073.
15. Notaro, Michael, David J. Lorenz, Christopher Hoving, and Michael Schummer. 2014. “Twenty-First-Century Projections of Snowfall and Winter Severity across Central-Eastern North America.” Journal of Climate 27 (17): 6526–50. https://doi.org/10.1175/JCLI-D-13-00520.1.

16. Notaro, Michael, David J. Lorenz, Daniel Vimot, Stephen Vavrus, Christopher Kucharik, and Kristie Franz. 2011. “21st Century Wisconsin Snow Projections Based on an Operational Snow Model Driven by Statistically Downscaled Climate Data.” International Journal of Climatology 31 (11): 1615–33. https://doi.org/10.1002/joc.2179.
17. Pryor, S.C., J.A. Howe, and K.E. Kunkel. 2009. “How Spatially Coherent and Statistically Robust Are Temporal Changes in Extreme Precipitation in the Contiguous USA?” International Journal of Climatology 29: 31–45.
18. Pryor, S.C., D. Scavia, M.G. Downer, L. Iverson, R. Nordstrom, J. Patz, and G.P. Robertson. 2014. “Ch. 18: Midwest. Climate Change Impacts in the United States.” The Third National Climate Assessment, 418–40. U.S. Global Change Research Program. http://nca2014.globalchange.gov/report/regions/midwest.
19. Scherer, Martin, and Noah S. Diffenbaugh. 2014. “Transient Twenty-First Century Changes in Daily-Scale Temperature Extremes in the United States.” Climate Dynamics 42: 1383–1404. https://doi.org/10.1007/s00382-013-1829-2.
20. Schwartz, M.D., T.R. Ault, and J.L. Betancourt. 2013. “Spring Onset Variations and Trends in the Continental United States: Past and Regional Assessment Using Temperature-Based Indices.” International Journal of Climatology 33: 2917–22. https://doi.org/10.1002/joc.3625.
21. Small, David, Shafiqul Islam, and Richard M. Vogel. 2006. “Trends in Precipitation and Streamflow in the Eastern U.S.: Paradox or Perception?” Geophysical Research Letters 33 (February). https://doi.org/10.1029/2005GL024995.
22. Steffens, Kayla K., and K.J. Franz. 2011. “Late 20th-century Trends in Iowa Watersheds: An Investigation of Observed and Modelled Hydrologic Storages and Fluxes in Heavily Managed Landscapes.” International Journal of Climatology 32 (9): 1373–91. https://doi.org/10.1002/joc.2361.
23. USACE. 2016. “Vulnerability Assessment (VA) Tool User Guide.” User Guide 1.1. Washington, DC: U.S. Army Corps of Engineers Climate Preparedness and Resilience Community of Practice.
24. ———. 2017. “Guidance for Detection of Nonstationarities in Annual Maximum Discharges.” Engineering Technical Letter 1100-2–3. U.S. Army Corps of Engineers. https://www.publications.usace.army.mil/Portals/76/Publications/EngineerTechnicalLetters/ETL_1100-2-3.pdf.
25. ———. 2020. “Guidance for Incorporating Climate Change Impacts to Inland Hydrology in Civil Works Studies, Designs, and Projects.” USACE Engineering Construction Bulletin (ECB) 2018-14. U.S. Army Corps of Engineers. https://www.wbdg.org/ffc/dod/engineering-and-construction-bulletins-ecb/usace-ecb-2018-14.
26. USGCRP. 2017. Climate Science Special Report: Fourth National Climate Assessment. Edited by D.J. Wuebbles, D.W. Fahey, K.A. Hibbard, D.J. Dokken, B.C. Stewart, and T.K. Maycock. Vol. 1. 2 vols. Washington, DC,: U.S. Global Change Research Program. https://science2017.globalchange.gov/.
27. ———. 2018. Impacts, Risks, and Adaptation in the United States: Fourth National Climate Assessment. Edited by D.R. Reidmiller, C.W. Avery, D.R. Easterling, K.E. Kunkel, K.L.M. Lewis, T.K. Maycock, and B.C. Stewart. Vol. 2. 2 vols. Washington, DC: U.S. Global Change Research Program. https://science2017.globalchange.gov/.
28. Vavrus, Stephen J., and Ruben J. Behnke. 2014. “A Comparison of Projected Future Precipitation in Wisconsin Using Global and Downscaled Climate Model Simulations: Implications for Public

Health." International Journal of Climatology 34 (10): 3106–24. https://doi.org/10.1002/joc.3897.
29. Veloz, Samuel, John W. Williams, David Lorenz, Michael Notaro, Steve Vavrus, and Daniel J. Vimot. 2012. "Identifying Climatic Analogs for Wisconsin under 21st-Century Climate-Change Scenarios." Climatic Change Volume 112: 1037–58. https://doi.org/10.1007/s10584-011-0261-z.
30. Westby, Rebeeca M., Yun-Young Lee, and Robert X. Black. 2013. "Anomalous Temperature Regimes during the Cool Season: Long-Term Trends, Low-Frequency Mode Modulation, and Representation in CMIP5 Simulations." Journal of Climate 26 (22): 9061–76. https://doi.org/10.1175/JCLI-D-13-00003.1.
31. Wolter, K., J.K. Eischeid, X.-W. Quan, N. Chase, M. Hoerling, R.M. Dole, G.J.V. Oldenborgh, and J.E. Walsh. 2015. "How Unusual Was the Cold Winter of 2013/14 in the Upper Midwest? In Explaining Extreme Events of 2014 from a Climate Perspective." Bulletin of the American Meteorological Society, 96 (12): S10–14. https://doi.org/10.1175/bams-d-15-00126.1.
32. Xu, Xianlu, Wen Liu, Rashad Rafique, and Kelin Wang. 2013. "Revisiting Continental U.S. Hydrologic Change in the Latter Half of the 20th Century." Water Resources Management 27: 4337–4348. https://doi.org/10.1007/s11269-013-0411-3.

US Army Corps of Engineers®
St. Paul District

Appendix E
Annual Peak Flow Frequency Analysis
Black Earth Creek at Black Earth, WI

Table of Contents

Table of Tables

Table of Figures

1 Introduction

To provide context to the calibration and validation events used in the Black Earth Creek hydrologic modeling study, the U.S. Army Corps of Engineers conducted an analytical flow frequency analysis of the Black Earth Creek at Black Earth, Wisconsin gage (USGS 05406500), shown in Figure 1. An updated flow frequency analysis was necessary, as the flood of record occurred in 2018, and the most recent flow frequency analysis had been conducted in the 1980s. The analysis discussed in this report utilized the methodology described in *Bulletin 17C: Guidelines for Determining Flood Flow Frequency* (USGS, 2018).

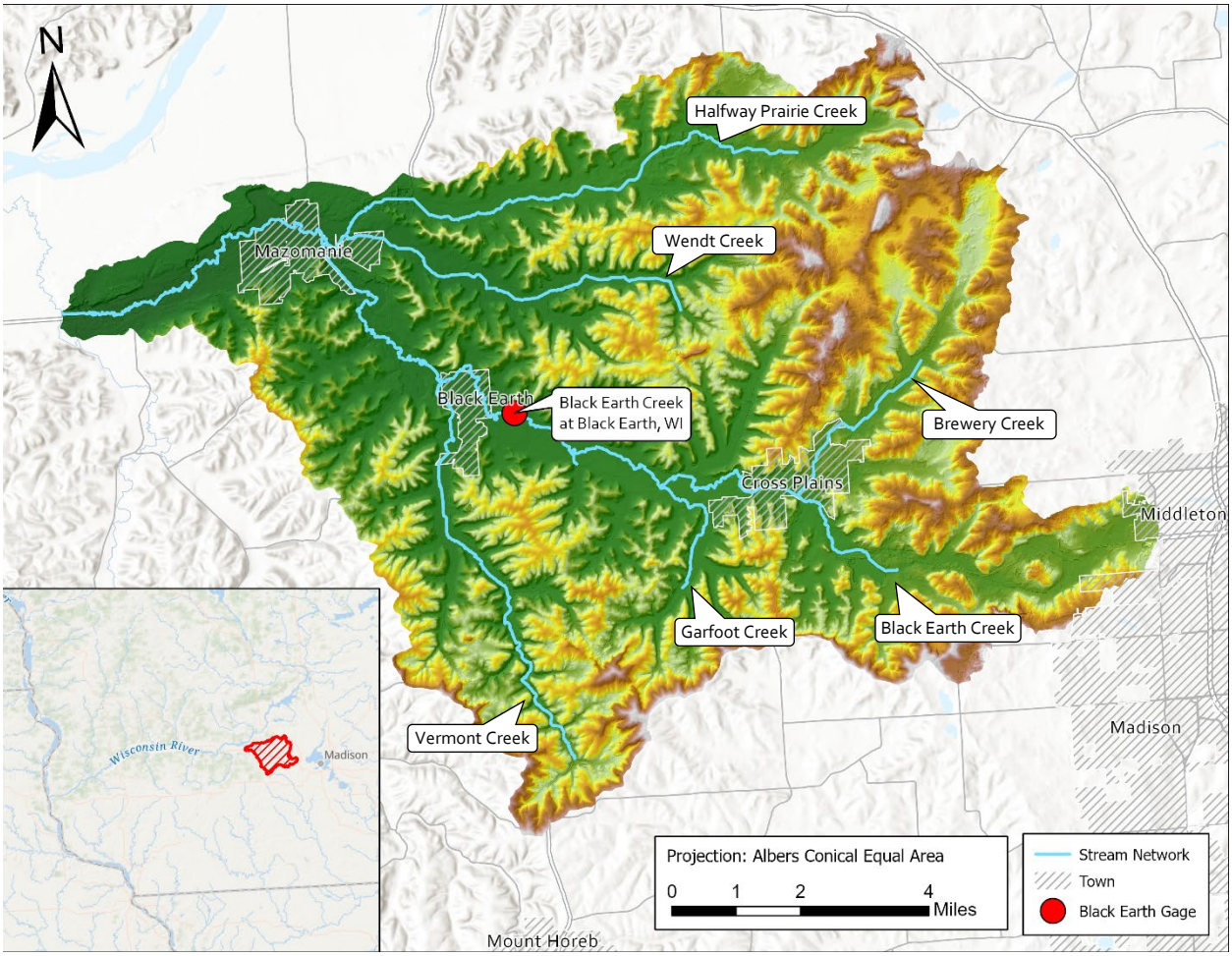

Figure 1. Map of the Black Earth Creek watershed

2 Previous Flow Frequency Analyses

According to the Dane County Flood Insurance Study (FIS) (FEMA, 2009), the most recent flow frequency analysis at the Black Earth, WI gage was conducted in 1988. This work was based on a Log Pearson Type III analysis of 32 years of data (1954-1985) and utilized weighted skew values of -0.2 and 0.14. According to the FIS, weighted skew values were determined based on the Wisconsin Administrative Code, NR116 (Wis. Admin. Code NR § 116.07); however, those skew values do not appear in NR116 in its current form. The computed flow frequency curve resulted in a 1% Annual Exceedance Probability (AEP) discharge of 1,800 cfs at Black Earth.

In addition to flow frequency analysis at the Black Earth USGS gage, the Dane County FIS also describes discharge frequency estimates on Brewery Creek; Vermont Creek; and Black Earth Creek at Mazomanie, Wisconsin (FEMA, 2009). For Brewery Creek and Vermont Creek, discharges for up to the 2% AEP (50-year return period) event were computed using the publication *Estimating Magnitude and Frequency of Floods in Wisconsin* (USGS, 1971). The computed frequency curves were then extrapolated to estimate the 1% AEP (100-year return period) and 0.2% AEP (500-year return period) discharges. For Black Earth Creek at Mazomanie, discharges were computed following the procedure published in *A Method of Estimating Flood-Frequency Parameters for Streams in Idaho* (USGS, 1981). This resulted in a 1% AEP (100-yr return period) discharge at Mazomanie of 3,000 cfs.

3 Historical Flooding on Black Earth Creek

The USGS gage at Black Earth, WI has a continuous record from 1954 to the present. The five largest flood events recorded during this period occurred in 2018, 1954, 2001, 1993, and 1959. The 2018 flood (2,930 cfs at Black Earth, WI) is the flood of record and is considered by many residents in the basin to be a catastrophic flood much larger than any that have occurred on the stream in the past.

According to a 1995 article posted on the Black Earth Historical Society's website, the village of Black Earth was first platted in 1850 and was first incorporated in 1857 (Schreiner, 1995). The Dane County FIS notes significant floods occurred along Black Earth Creek in 1875, 1882, 1893, and 1910 (FEMA, 2009). However, the recurrence interval and elevations associated with these floods are not known. For this study, it is assumed the floods of 1875, 1882, 1893, and 1910 did not exceed the peak discharge recorded during the 2018 flood event, as these flood events are not mentioned in any historical documents posted on the Black Earth Historical Society or Mazomanie Historical Society websites. The president of the Black Earth Historical Society, said he has never read or hear of any flood that was the magnitude of the 2018 event and agreed it was reasonable to assume a flood of that magnitude had never occurred in Black Earth before (W. Barsness, personal communication, June 6, 2021). Since the 2018 flood resulted in significant damages to infrastructure within the villages of Cross Plains, Black Earth, and Mazomanie, it is assumed any flood event of a similar magnitude would be documented in the local histories of the watershed.

Table 1 lists significant flood events that have occurred on Black Earth Creek.

Table 1. Significant observed flood events on Black Earth Creek

Rank (Largest to Smallest)	Date	Annual Peak Discharge (cfs)
1	August 21, 2018	2,930
2	July 3, 1954	1,750
3	August 2, 2001	1,720
4	July 6, 1993	1,320
5	April 1, 1959	1,120
6	October 2, 2019	1,060
7	June 11, 1957	1,030
8	March 14, 2019	1,030
9	July 3, 1960	1,020
10	June 8, 2008	1,020

4 Regulation on Black Earth Creek

Black Earth Creek is an unregulated stream. The only dam in the watershed listed in the National Inventory of Dams database is the Lake Marion Dam downstream of Black Earth near Mazomanie; however, the Lake Marion Dam was decommissioned in 2012 and is downstream of the Black Earth USGS gage. The period of record is assumed to be homogeneous. Therefore, an analytical discharge frequency curve is appropriate for this analysis.

5 Bulletin 17C Methodology

In 2005, the Hydrologic Frequency Analysis Work Group (HFAWG), under the Subcommittee on Hydrology, began development on *Bulletin 17C: Guidelines for Determining Flood Flow Frequency* (USGS, 2018). Bulletin 17C is a revision of *Bulletin 17B: Guidelines for Determining Flood Flow Frequency* (USGS, 1982). Bulletin 17B was published in 1982 and presents the previous standard of practice for performing analytical discharge frequency analysis. The final version of Bulletin 17C was published in March 2018. The HFAWG recommends using Bulletin 17C guidelines to estimate flood flow frequency curves. Version 2.2 of the Hydrologic Engineering Center Statistical Software Package (USACE Hydrologic Engineering Center, 2019) incorporates the methodology presented in Bulletin 17C. Bulletin 17C Guidelines improve on Bulletin 17B in the following ways:

1. **Low Outlier Detection**: Bulletin 17C applies the Multiple Grubbs-Beck test versus the simple Grubbs-Beck test recommended by Bulletin 17B. The low outlier detection tests are used to identify influential low flood observations which unduly influence the characterization of the exceedance probability associated with large flow magnitudes. The Multiple Grubbs-Beck Test (MGBT) facilitates the identification of multiple low outliers including zero flow values.
2. **Confidence Limits**: Large differences in confidence intervals may be observed between intervals computed with Bulletin 17B compared to intervals calculated with Bulletin 17C because the Bulletin 17B confidence intervals ignore uncertainty in estimating skew and has no provisions for recognizing the value of historical information. In Bulletin 17C the Expected Moments Algorithm (EMA) is applied to generate confidence limits and accounts for uncertainty in estimates of skew as well as historical flood information.
3. **Expected Moments Algorithm (EMA)**: Instead of applying the method of moments procedure to estimate parameters of the sample to fit a Log Pearson Type III distribution to the observed data as suggested by Bulletin 17B, Bulletin 17C facilitates the use of the EMA. The EMA is a generalized method of moments procedure to estimate the Pearson Type III distribution parameters. The EMA provides a direct fit of the Pearson Type III distribution using the entire dataset, simultaneously employing regional skew information and a wide range of historical flood and threshold-exceedance information, while adjusting for any potentially influential low floods, missing values from an incomplete record, or zero flood years (USGS, 2019).
4. **Record Extension:** To extend the period of record at a short-term gage using information from a nearby long-term gage, Bulletin 17C guidance recommends the Maintenance of Variance Extension Type 3 (MOVE.3) approach instead of relying on the two-station comparison.
5. **Plotting Positions**: Plotting positions are an empirical (non-parametric) method to judge the adequacy of the estimated flood frequency relationship for a particular set of data. In the previous Bulletin 17B guidelines, the adequacy of the Log Pearson Type III distribution applied to a series of annual peak flood flows was assessed using Median plotting positions. Bulletin 17C

guidelines utilize standard and non-standard flood data which are represented by perception thresholds and flow ranges; consequently, a multiple exceedance threshold plotting position formula is necessary to plot annual peak flood events. All flood events in the analytical frequency analysis cases are plotted with Hirsch-Stedinger plotting positions, except low outliers which are plotted using Median plotting positions.

5.1 Applicability of Bulletin 17C Guidelines

The guidelines in Bulletin 17C outline the process of defining flood potential at a specific location in terms of peak discharge and AEP. The Bulletin 17C guidelines are applicable for defining the frequency of flood events rarer than and including the 10% AEP event (10-yr return interval). Flood AEPs ranging from 10% (10-yr return interval) to 0.2% (500-yr return interval) are estimated using annual peak discharge time series data and the methods described in Bulletin 17C in this study.

If frequency estimates are desired for events which occur more frequently than the 10% AEP event, Bulletin 17C recommends a peaks over threshold analysis or partial duration series analysis using the generalized Pareto distribution (GPD) be performed to define that region of the frequency curve. A partial duration series analysis to define a broader range of the frequency curve was not included in this analysis, as an exploration of the daily discharge time series at Black Earth revealed a partial duration analysis using an applicable PDS threshold for this study (approximately 500 cfs) would be unlikely to yield significantly different results, as the number of events in the partial duration series would be approximately equal to the number of events in the annual maximum series.

5.2 Perception Thresholds

The Expected Moments Algorithm (EMA) uses interval data rather than discrete data points in computations. This allows for the use of non-standard flood information such as historical flood data or paleoflood information to be incorporated into the analysis, especially if the exact magnitude of the historical or paleoflood event is not known. Each flow value used in the analysis is represented as a flow range interval, with both a high and low value.

The EMA approach requires that each year in the systematic record be represented using perception thresholds and a flow range. Observed, systematic events are assumed to be known with a high degree of accuracy. Therefore, the perception thresholds for systematic events use a low perception threshold equal to zero and a high perception threshold equal to infinity. A perception threshold which spans zero to infinity assumes that all discharges that occurred during periods when measurements were taken would have been recorded, regardless of magnitude. Applying a perception threshold in this manner implies that the low flow range value is equal to the high flow range value. Both the low and high flow interval values are equivalent to the observed event magnitude.

Flow intervals for years with missing information are estimated using an exceedance bound perception threshold. The exceedance perception threshold is defined with a lower limit equal to a reference, observed flow magnitude and an upper limit of infinity. The corresponding flow interval for years with missing information is simply the complement of the perception threshold range. Years for which discrete flow measurements are unavailable, but relative flow magnitudes can be defined as described above are referred to as censored data points within HEC-SSP (USACE Hydrologic Engineering Center, 2019). If available, historical flood information recorded outside of the systematic record is applied to define the lower limit of the exceedance perception threshold. By adopting historical flood information

to define the lower limit, this implies that if a flood greater than the historical flood had occurred during the missing portion of the period of record, it would have been recorded.

6 Discharge Frequency Analysis

The Black Earth Creek at Black Earth, WI USGS gage (ID 05406500) is located just upstream of the Village of Black Earth, WI. The gage has a drainage area of 45.6 mi^2 and a continuous period of record of 1954-2020. A total of 67 annual peak discharge values are published for the gage. There are no nearby gages in hydrologically similar watersheds that could be used to extend the record at the Black Earth gage. For this analysis, historical information was used to extend the period of record to the year 1857, when the village was first incorporated and significant events in the village's history began to be recorded. As described in Section 3, it was assumed no flood event greater in magnitude than the 2018 flood occurred since 1857, as there is no documentation of any such flood in the region's recorded history.

To apply the Bulletin 17C methodology, a low perception threshold equal to the 2018 flood of record (2,930 cfs) and a high perception threshold equal to infinity was used to fill in the missing period of 1857-1953. This assumption indicates if an event larger than the 2018 event had occurred during the 1857-1953 period, it would have been documented. The perception thresholds used to compute the discharge frequency curve for Black Earth Creek at Black Earth are shown in Table 2.

Table 2. Perception thresholds used in Bulletin 17C analysis of Black Earth Creek at Black Earth, WI

Perception Thresholds				
Start Year	End Year	Low Threshold	High Threshold	Comments
1857	2020	0.0	inf	Total Record
1857	1953	2930.0	inf	Historical

The Expected Moments Algorithm was used to estimate the statistical parameters and fit the Log Pearson Type III distribution to the available systematic streamflow data as well as the information utilized for the historical period. Hirsch-Stedinger plotting positions were used to plot observed events. No low outliers were computed using the Multiple Grubbs-Beck test. A weighted skew value was calculated using the results from *Flood-Frequency Characteristics of Wisconsin Streams* (USGS, 2017). The adopted skew value of -0.109 was computed by weighting the station skew of -0.178 with a regional skew of 0.050 and a regional skew mean square error (MSE) of 0.309. Computation of the adopted flow frequency curve and its 5% and 95% confidence limits were performed with the HEC-SSP version 2.2 computer program (USACE Hydrologic Engineering Center, 2019). A summary of the adopted frequency curve is shown in Table 3. The final discharge frequency curve is shown in Figure 2. Peak flows used in the analysis are shown in Table 4.

Table 3. Discharge frequency estimates for Black Earth Creek at Black Earth, WI (USGS 05406500)

Annual Peak Discharge Frequency Analysis			
USGS Gage 05406500 Black Earth Creek at Black Earth, WI			
Methodology: Bulletin 17C/EMA - Log Pearson Type III Distribution			
Exceedance Probability	**Peak Estimate (cfs)**	**90% Confidence Limits (cfs)**	
		5%	**95%**
0.2%	3,150	4,840	2,260
0.5%	2,590	3,700	1,950
1%	2,200	2,990	1,710
2%	1,840	2,380	1,470
5%	1,400	1,720	1,160
10%	1,090	1,310	920
	Statistics		
Mean	2.644	**Systematic Record**	1954-2020
Standard Deviation	0.311	**Historical Period**	1857-1953 (164 years)
Station Skew	-0.178	**Systematic Years**	67
Regional Skew	0.050	**Missing Flows**	97
Regional Skew MSE	0.309	**Low Outlier Test**	Multiple Grubbs-Beck
Weighted Skew (Adopted)	-0.109	**Number of Low Outliers**	0

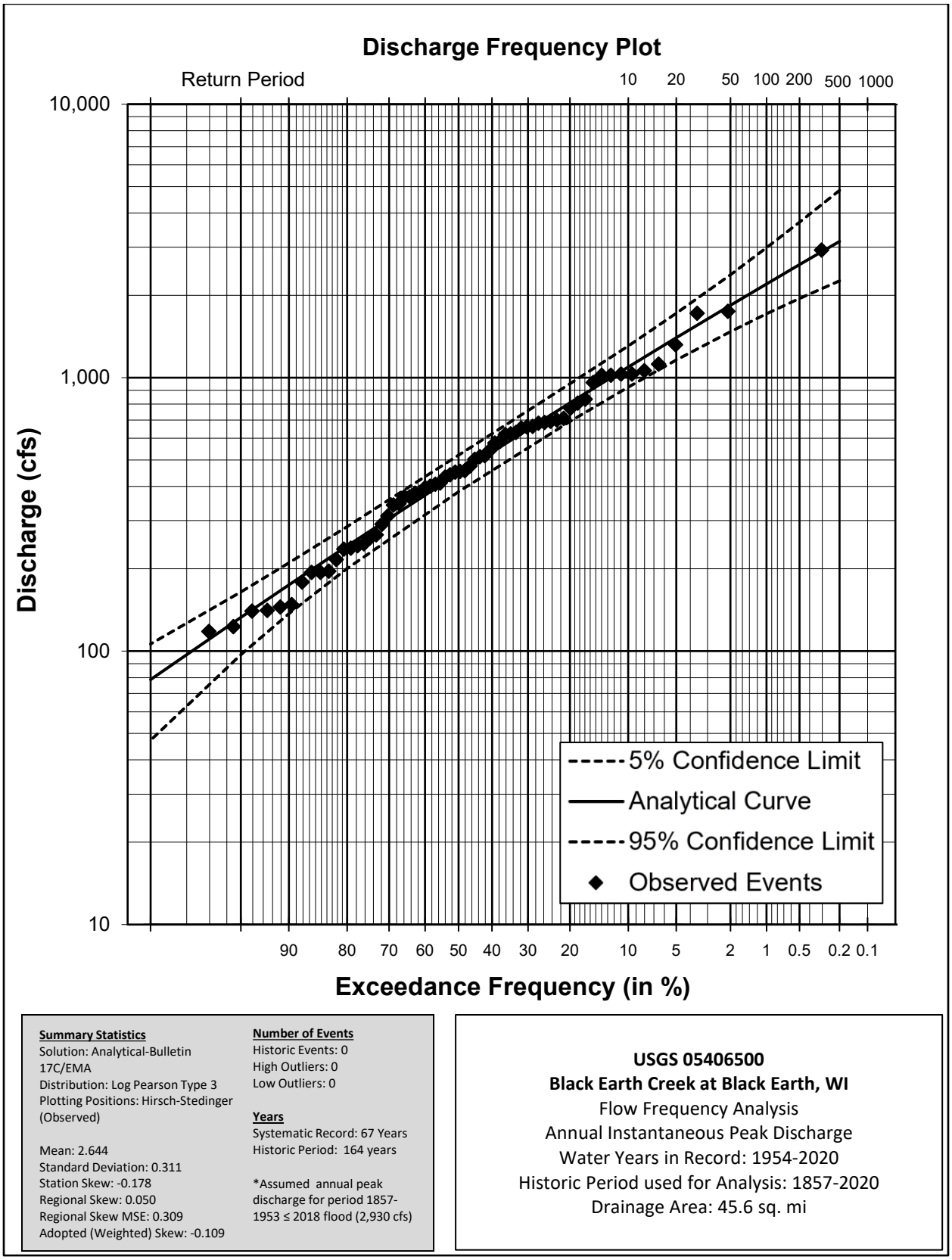

Figure 2. Annual Instantaneous Peak Discharge frequency curve - Black Earth Creek at Black Earth, WI

Table 4. Annual peak discharge timeseries - Black Earth Creek at Black Earth, WI

Date	Annual Peak Discharge (cfs)	Date	Annual Peak Discharge (cfs)
July 3, 1954	1,750	January 31, 1988	140
February 20, 1955	654	March 12, 1989	433
May 13, 1956	408	March 9, 1990	401
June 11, 1957	1,030	March 2, 1991	312
February 24, 1958	266	October 25, 1991	243
April 1, 1959	1,120	July 6, 1993	1,320
July 3, 1960	1,020	February 20, 1994	686
March 25, 1961	693	May 28, 1995	238
March 25, 1962	216	June 17, 1996	503
March 17, 1963	454	February 18, 1997	412
June 22, 1964	64	March 31, 1998	661
March 2, 1965	623	April 23, 1999	519
February 9, 1966	619	June 2, 2000	808
January 25, 1967	631	August 2, 2001	1,720
September 18, 1968	148	June 4, 2002	247
June 27, 1969	457	May 11, 2003	179
September 24, 1970	141	May 22, 2004	960
March 15, 1971	196	February 14, 2005	378
March 17, 1972	451	May 24, 2006	118
March 7, 1973	577	August 19, 2007	774
January 27, 1974	585	June 8, 2008	1,020
March 21, 1975	514	February 27, 2009	346
March 12, 1976	834	July 24, 2010	367
February 24, 1977	367	March 20, 2011	194
July 1, 1978	681	November 9, 2011	145
March 19, 1979	260	June 26, 2013	700
September 22, 1980	441	September 4, 2014	291
February 22, 1981	396	May 27, 2015	475
March 16, 1982	380	June 15, 2016	663
December 2, 1982	194	July 20, 2017	542
June 10, 1984	342	August 21, 2018	2,930
July 25, 1985	710	March 14, 2019	1,030
March 19, 1986	236	October 2, 2019	1,060
October 4, 1986	123		

7 Comparison with Previous Flow Frequency Analyses

The flow frequency curve developed for this study differs significantly from the curve developed for the Dane County FIS in 1988. In the FIS, the 1% AEP event corresponded to a discharge of 1,800 cfs. In the current study, the 1% AEP event corresponds to a discharge of 2,200 cfs, which is an increase of 22%. The 1% event magnitude increased because the 2018 flood of record was not included in the 1988 FIS analysis. The flow frequency curve developed in the current study is a better representation of reality

than the 1988 analysis, since the current study utilizes more observed data (67 years vs. 32 years) and accounts for historical flood data stretching back to 1857.

8 Opportunities for Further Study

The flow frequency analysis conducted in this study uses all available observed data at the Black Earth Creek at Black Earth, WI USGS gage and also accounts for all available historical flood data in the basin. The analysis adopted a weighted skew using station skew and a regional skew value from a 2017 USGS study. The USGS study adopted Bulletin 17B methods to define regional skew. Bulletin 17C recommends using a B-WLS/B-GLS method to define regional skew. If a regional skew study using EMA/B-WLS/B-GLS methodology becomes available in the future, the flow frequency curve for the Black Earth USGS gage should be updated.

9 References

1. Federal Emergency Management Agency (FEMA) (2009). *Flood Insurance Study: Dane County, Wisconsin and Incorporated Areas*. Volume 1 of 2. Washington, D.C.
2. Howarth, H., Moulton, H.Z. (1877). *Mazomanie*. From *Madison, Dane County and Surrounding Towns: Being a History and Guide to Places of Scenic Beauty and Historical Note…* 592-615. Madison, Wm. J. Park & Co. Accessed June 2, 2021 from https://mazomaniehistory.org/history/1877-history-of-mazomanie/.
3. Mt. Horeb Times (May 15, 1924). *Early History of Black Earth*. Accessed June 2, 2021 from https://www.wisconsinhistory.org/Records/Newspaper/BA5312.
4. Schreiner, T. (1995). *A Brief History of Black Earth*. Accessed June 2, 2021 from https://www.blackearthwihistory.org/black-earth-history.
5. U.S. Army Corps of Engineers (USACE) (1993). *EM 1110-2-1415: Hydrologic Frequency Analysis*. Washington, D.C.
6. U.S. Army Corps of Engineers (USACE) Hydrologic Engineering Center (2019). *HEC-SSP, Statistical Software Package, Version 2.2.* Davis, CA.
7. United States Geological Survey (USGS) (2018). *Bulletin 17C: Guidelines for Determining Flood Flow Frequency*. Reston, VA.
8. United States Geological Survey (USGS) (1971). *Estimating Magnitude and Frequency of Floods in Wisconsin*. Reston, VA. Accessed June 2, 2021 from https://pubs.er.usgs.gov/publication/ofr7176.
9. United States Geological Survey (USGS) (2017). *Flood-Frequency Characteristics of Wisconsin Streams*. Scientific Investigations Report 2016-5140, Version 2.1. Reston, VA.
10. United States Geological Survey (USGS) (1981). *Method of estimating flood-frequency parameters for streams in Idaho*. Reston, VA. Accessed June 2, 2021 from https://pubs.er.usgs.gov/publication/ofr81909.

US Army Corps of Engineers®
St. Paul District

Appendix F:
HEC-RAS Model Documentation

1 Table of Contents

Table of Tables

Table of Figures

1 Overview

A HEC-RAS model of Black Earth Creek was constructed to support the analysis of various green infrastructure and land use management alternatives evaluated in the Black Earth Creek Watershed Hydrologic Modeling Study and to help communicate the results of the alternative analysis to stakeholders in the basin. For this study, all alternative simulations are run using the HEC-HMS hydrologic model. Then, HEC-HMS model outputs are input into the HEC-RAS model to compute differences in inundated area for each alternative and develop inundation maps to communicate alternative results. The HEC-RAS model is a fully two-dimensional model that extends from the Black Earth Creek-Brewery Creek confluence in Cross Plains, WI to Black Earth Creek's confluence with Blue Mounds Creek downstream of Mazomanie, WI. The stream gage used to calibrate the model is the Black Earth Creek at Black Earth, WI USGS gage (05406500). A map of the model extents is shown in Figure 1.

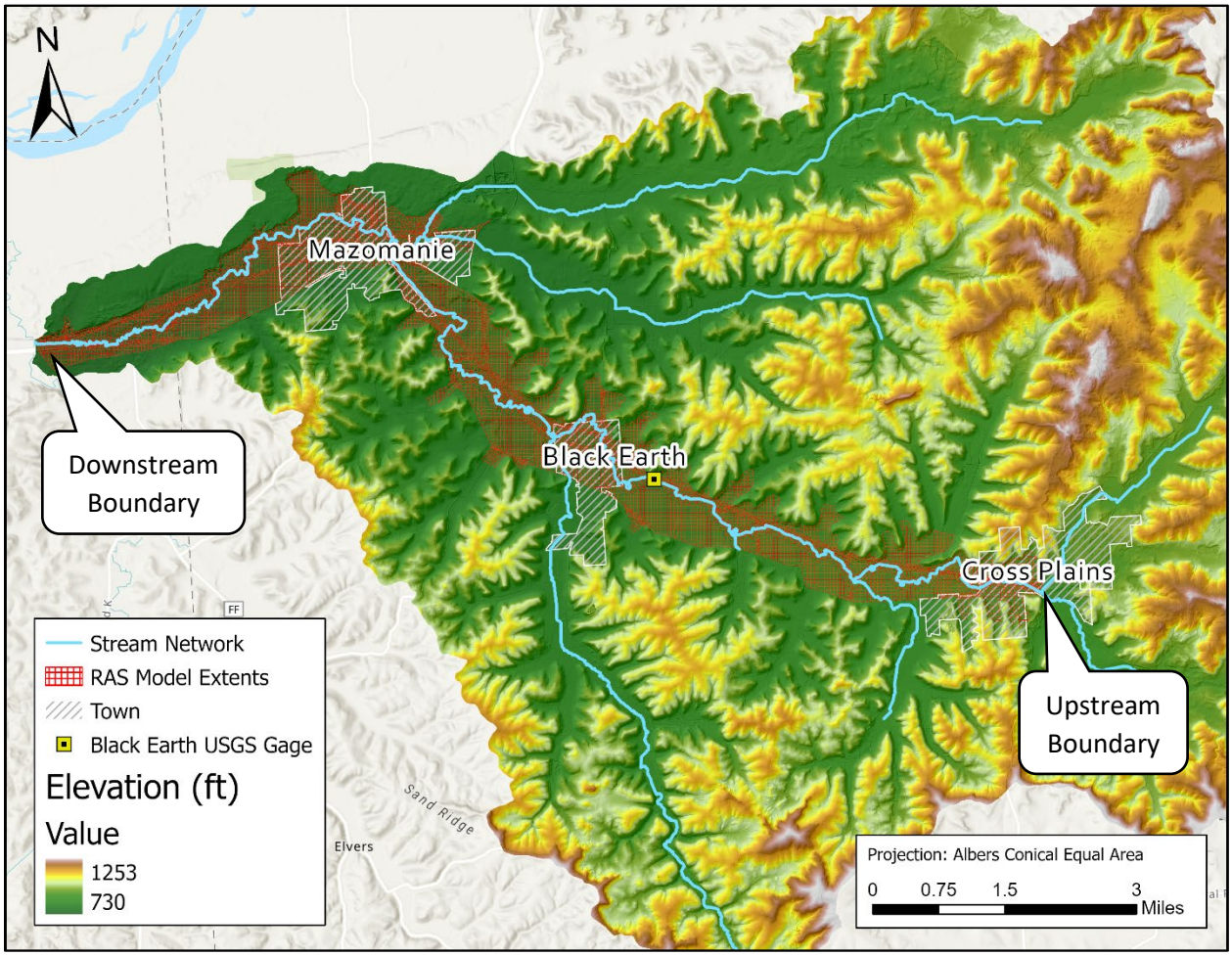

Figure 1. Extents of the Black Earth Creek HEC-RAS model

2 Vertical and Horizontal Control

All elevation data in this report references the North American Vertical Datum of 1988 (NAVD 88), unless otherwise stated. The horizontal projection of the HEC-RAS model is the USA Contiguous Albers Equal Area Conic USGS version projection. Horizontal and vertical units are feet.

3 Model Geometry

The Black Earth Creek HEC-RAS model is a fully 2D model developed in HEC-RAS version 6.1 using a digital elevation model (DEM) for the study area along with cross sections from an existing, one-dimensional HEC-RAS model of Black Earth Creek used for the Federal Emergency Management Agency (FEMA) 2016 Dane County Flood Insurance Study (FIS). A new, 2D model was developed for this study for a number of reasons. First, the existing, 1D FIS model was not georeferenced. This means the only model output available was water surface elevations at cross sections; the model could not be used to compute inundated areas or develop inundation maps. Second, a number of edits to cross section spacing, orientation, and extent would have to be made to the FIS model geometry to be able to accurately model the flood events used to evaluate alternatives in this study. Third, at least two 2D flow areas would have to be added to the FIS model geometry to accurately model overbank flow at Cross Plains and Mazomanie during the 2018 flood event. Due to the number of edits required to the existing FIS model, developing a new, fully 2D model was a more cost-effective means of achieving the goals of this study.

3.1 Terrain Development

The DEM has a cell size of 5 m x 5 m (16.4 ft x 16.4 ft) and was constructed from LiDAR data collected in 2010 and 2017. LiDAR data was obtained from each county directly. Channel bathymetry was added to the DEM by georeferencing cross sections from the existing, 1D FIS model, extrapolating the channel surface, and merging the channel surface with the DEM.

An important assumption during the development of the model terrain is the assumption that the original FIS model accurately captures the channel bathymetry. Due to a lack of documentation, it is not clear how the cross sections in the FIS model were developed and whether they incorporate channel survey data. Channel surveys are beyond the scope of this study, and since the primary purpose of the HEC-RAS model in this study is to compute differences in inundated area for various alternatives using large flood events, it is not absolutely necessary to have highly accurate channel bathymetry data. However, extra care should be taken if using this model to simulate small flood events or produce inundation maps that require a high degree of accuracy.

Regardless of whether the FIS model accurately captures the channel invert elevation, there is likely still some error associated with the channel bathymetry since the FIS model's stream centerline and cross section orientation did not precisely match physical space when first georeferenced in RAS Mapper. To properly georeferenced the FIS model, a new streamline was first drawn in RAS Mapper using the DEM and aerial imagery as a reference. Then, each cross section in the FIS model was moved and oriented by hand to match its approximate location in space. The original FIS model geometry, the location of its elements when first georeferenced in RAS Mapper, and the final georeferenced geometry are shown in Figure 2.

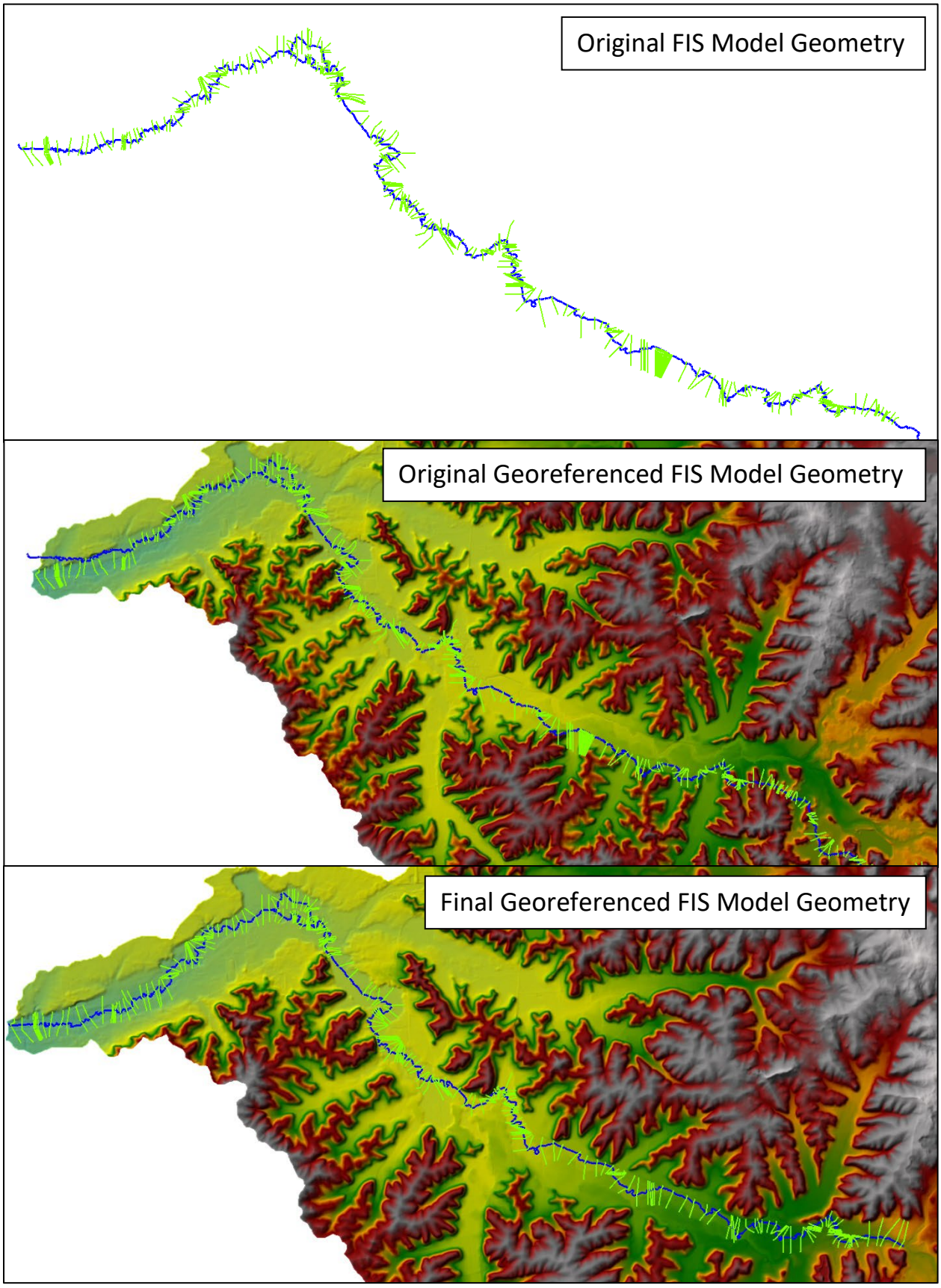

Figure 2. Georeferencing FIS model geometry

3.2 2D Flow Area

The 2D flow area covers the floodplain of Black Earth Creek from the Brewery Creek confluence in Cross Plains to the Blue Mound Creek confluence downstream of Mazomanie, WI. The typical cell size in overbank areas is 150 ft. Breaklines for roads and the banks of Black Earth Creek use a size cell of 100 ft, and bridges use a cell size of 80 ft. Cell sizes of the 2D mesh and its associated breaklines were originally selected based on the model terrain and engineering judgement. Then, cell sizes were refined to minimize run time, maintain model stability, and meet a target Courant number of less than or equal to 3. The final timestep selected for the model was 10 seconds. This computation interval resulted in a maximum Courant number during the 2018 flood event of approximately 1.24.

3.3 Calculation Options and Tolerances

The model uses the default calculation options and tolerances, which include a theta value of one and the Diffusion Wave equation set. The model was tested using the full momentum Shallow Water Equations (SWE); however, the difference in computed water surfaces when SWE was used was minimal and did not warrant the additional run time.

3.4 Manning's N

The 2016 National Land Cover Dataset was used to create a land use raster in RAS Mapper. Manning's N values were then assigned to each land use type using guidance from the USACE Modeling, Mapping, and Consequences Center's FY21 Technical Manual for Levees. The range of suggested Manning's N values for each land use type shown in the technical manual as well as the final, selected values used in the Black Earth Creek model are shown in Table 1.

Table 1. Manning's N values based on land cover

NLCD Land Cover ID	Land Cover Description	Suggested Range of Manning's N	Selected Manning's N
11	Open Water/Stream Channel	0.025-0.03	0.045
21	Developed, Open Space	0.03-0.04	0.04
22	Developed, Low Intensity	0.04-0.06	0.06
23	Developed, Medium Intensity	0.04-0.07	0.07
24	Developed, High Intensity	0.06-0.07	0.07
31	Barren Land	0.025-0.035	0.035
41	Deciduous Forest	0.15-0.2	0.2
42	Evergreen Forest	0.14-0.18	0.18
43	Mixed Forest	0.18-0.2	0.2
52	Shrub/Scrub	0.09-0.11	0.11
71	Grassland/Herbaceous	0.06-0.08	0.08
81	Pasture/Hay	0.05-0.07	0.07
82	Cultivated Crops	0.045-0.065	0.065
90	Woody Wetlands	0.07-0.09	0.09
95	Emergent Herbaceous Wetlands	0.06-0.08	0.08
-	Channel banks (dense vegetation)	-	0.085
-	Channel banks (limited vegetation)	-	0.065

To further refine Manning's N values in the channel and on the stream banks, two calibration regions were added to the model geometry, one that covers the main channel and one that covers the left and right banks. A Manning's N value of 0.045 was adopted for the entirety of the main channel. A value of 0.065 was selected for the left and right banks in reaches with limited vegetation surrounding the main channel, and a value of 0.085 was selected for the left and right banks in reaches with dense vegetation surrounding the channel. Areas of dense vegetation were identified using aerial imagery. An example of the calibration regions surrounding the main channel is shown in Figure 3. Each color corresponds to a different Manning's N value.

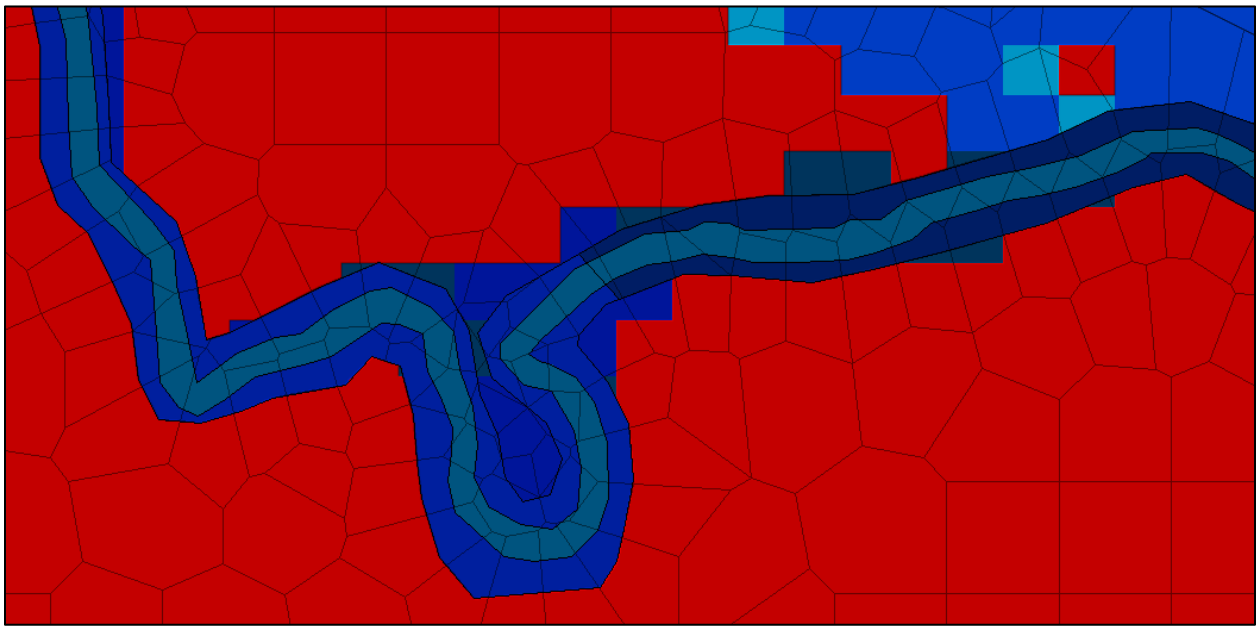

Figure 3. Example of calibration regions around the main channel of Black Earth Creek

3.5 Bridge Modeling

Bridges were added to the model as 2D connections. The geometry of each bridge and its corresponding weir coefficient were adopted from the FIS model. For low flow, the highest energy answer between the energy and Yarnell equations (if there are no piers, energy only) was used. If applicable, the pier shape K coefficient was adopted from the FIS model and ranged from 0.95 to 2.5. For high flow, the pressure and/or weir method was selected with the default submerged inlet + outlet coefficient of 0.8. The distance to the upstream and downstream cross sections ranged from 10 ft to 25 ft, and the Manning's N value for all upstream and downstream cross sections was set to 0.045. Ineffective flow areas were added to all bridges and correspond to the bridge opening and the top of the bridge abutments.

There are 31 bridges in the model, 10 of which are railroad bridges. In the 2018 flood event simulation, there were six bridges with a head loss of 0.5 feet or more: the two railroad and two Highway 14 bridges just downstream of Cross Plains, Main Street bridge in Black Earth, and the Olson Road bridge just west of Wisconsin Heights High School, approximately halfway between Black Earth and Mazomanie. Of these six, the railroad and Highway 14 bridges just downstream of Cross Plains were the only bridges whose backwater caused significant inundation in an urban area. The Highway 14 bridge just east of the Highway 14-Country Road KP intersection showed the greatest head loss of all bridges in the model (1.8

feet). The flow constriction caused by this bridge may cause flooding of the Plastic Ingenuity facility in Cross Plains during large events.

4 Boundary Conditions

The HEC-RAS model was designed to accept inputs from the HEC-HMS model developed for this study. Therefore, there are nine boundary condition lines that input a flow hydrograph at various points in the model. The downstream boundary condition is a normal depth of 0.00067, which is approximately equal to the slope of the channel throughout the modeled reach. Each of the nine flow hydrograph boundary conditions correspond to the discharge from a junction or subbasin in the HMS model and are located and named accordingly. Figure 4 shows a map of the boundary condition lines in the RAS model along with the subbasins in the HMS model. Note the boundary condition line adding flow from the subbasin between Cross Plains and Black Earth (S_BEC_ds_CP_to_BEC_us_BE) is not located at the outlet of the subbasin to allow flow to spread out across the floodplain prior to reaching the Black Earth USGS gage.

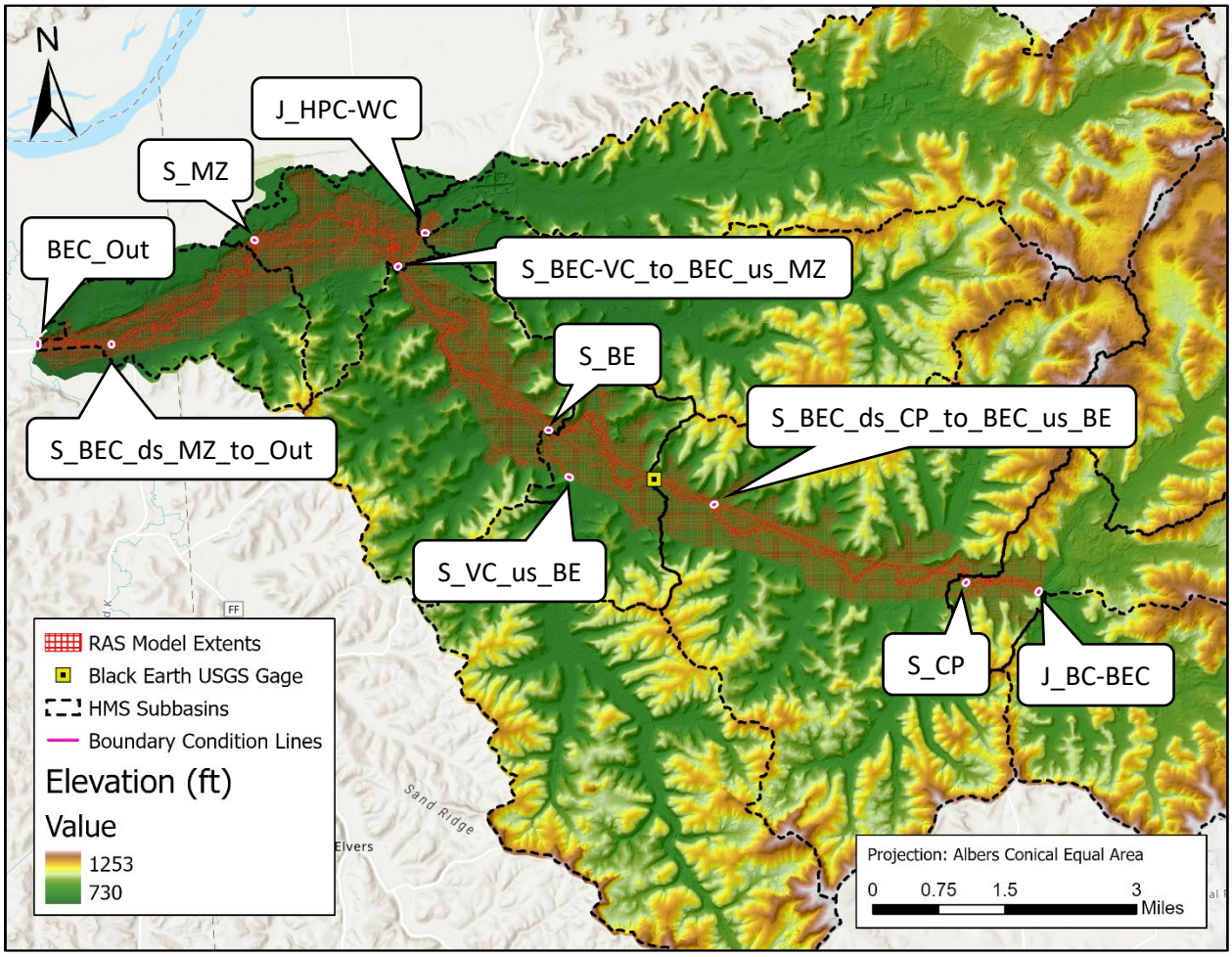

Figure 4. Boundary condition lines in the Black Earth Creek HEC-RAS model

5 Calibration

Calibration of the Black Earth Creek HEC-RAS model involved modifying channel, right and left bank, and overbank Manning's N values such that the model results matched the observed stage-discharge

relationship at the Black Earth USGS gage as well as observed stage and discharge hydrographs for the 2018 and 2019 flood events. These events, along with the 1993 events, are the flood events used in the study to evaluate alternatives. The 1993 event was not used to calibrate the RAS model due to the lack of observed stage data during the event. For each flood event, model outputs from the HMS model were used as inputs to the RAS model.

The 2018 flood event is the flood of record, with an annual chance exceedance (ACE) of approximately 0.3%. The 2019 and 1993 flood events have ACEs of approximately 13% and 6%, respectively. It is worthwhile to note the FIS was conducted prior to the 2018 flood event, and the 0.2% ACE event simulated for the FIS corresponded to a discharge at Black Earth of 2,146 cfs. According to the updated flow frequency curve shown in Appendix E, what was considered the 0.2% discharge in the FIS is now very close to the 1% discharge. What was considered the 1% discharge in the FIS (1,800 cfs) now corresponds to an ACE of approximately 3%.

5.1 2018 Flood Event

Figure 5 shows the flow hydrograph computed by the HMS model for each boundary condition in the RAS model for the 2018 flood event.

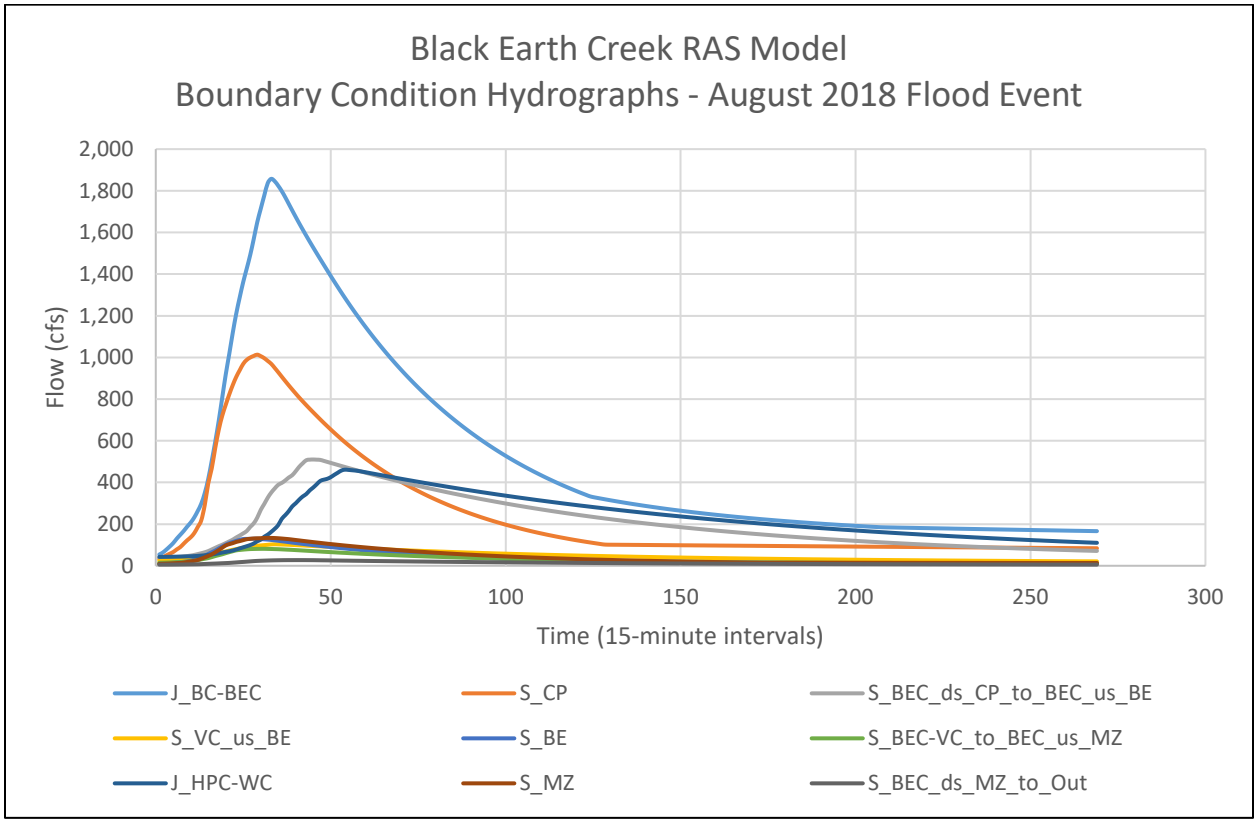

Figure 5. Boundary condition hydrographs - August 2018 flood event

Figure 6 shows the modeled rating curve at the Black Earth Creek gage along with the observed rating curve during the event. All USGS stage-discharge measurements are plotted for reference, as well as the simulated stage-discharge relationships at the cross section nearest the Black Earth gage in the FIS model. The modeled rating curve at the gage site was extracted from the model by drawing a profile line

across the floodplain in RAS Mapper and plotting the rating curve associated with the profile line. Figure 6 shows the model fits the observed rating curve well on the rising limb of the hydrograph when discharge exceeds approximately 500 cfs. On the falling limb, water pools across the floodplain adjacent to the gage site and recedes very slowly, leading to a much shallower rating curve slope. However, in the channel itself the slope of the rating curve is consistent on both the rising and falling limb. Below 500 cfs, flow is constrained within the channel, and the channel bottom elevation has a large impact on the computed water surface elevation. Since the computed water surface elevation is approximately one to two feet lower than measured water surface elevations at these flows, and the water surface elevation could not be raised by adjusting model parameters, it is assumed the channel invert elevation in the model is too low at the gage site. As discussed in Section 3.1, there is uncertainty regarding the channel invert elevations used in the model. However, since the purpose of this study is to evaluate differences in inundation for flood events with peak discharges greater than 500 cfs, the low channel invert is not expected to adversely impact the utility of the model.

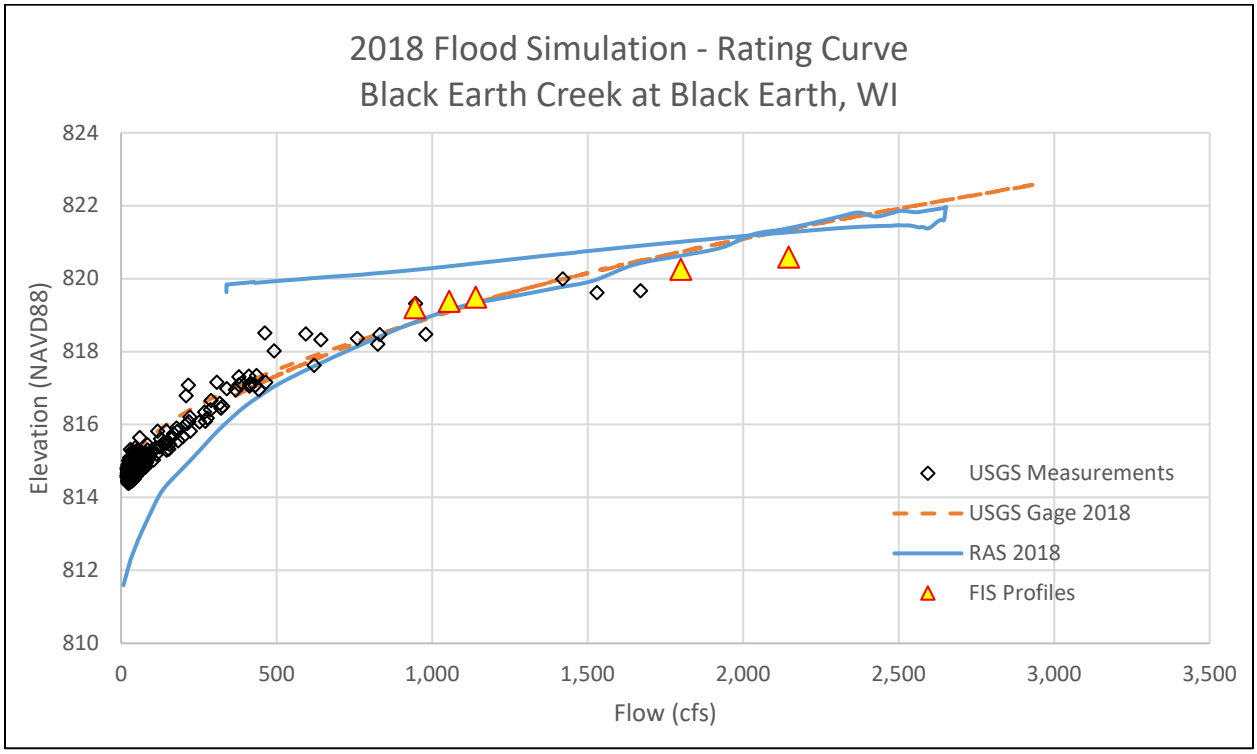

Figure 6. Observed vs. modeled rating curve, 2018 flood (Black Earth USGS gage)

Figure 7 and Figure 8 compare the modeled stage and discharge hydrographs to the observed stage and discharge hydrographs for the 2018 event at the Black Earth USGS gage. The model adequately matches the observed peak water surface elevation. The timing of the modeled flood peak is approximately three hours later than the observed flood peak; however, this timing is consistent with the timing in the HMS model.

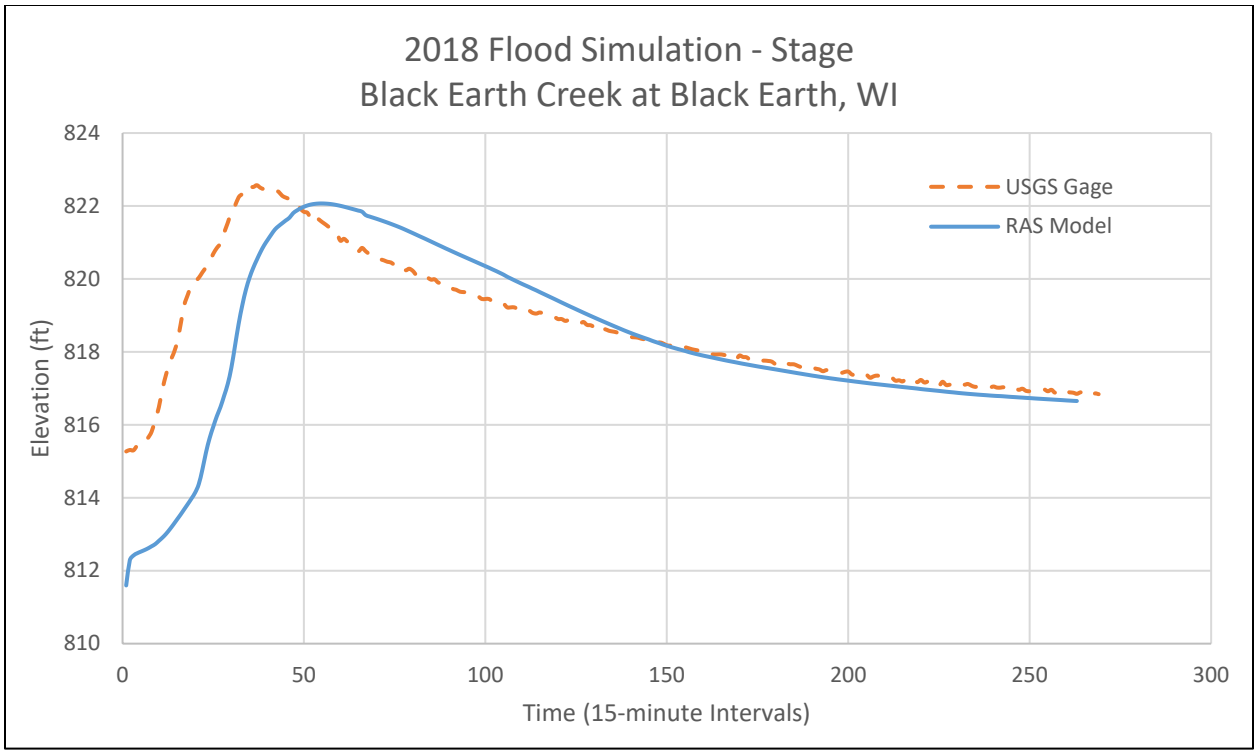

Figure 7. Observed vs. modeled stage hydrograph, 2018 flood (Black Earth USGS age)

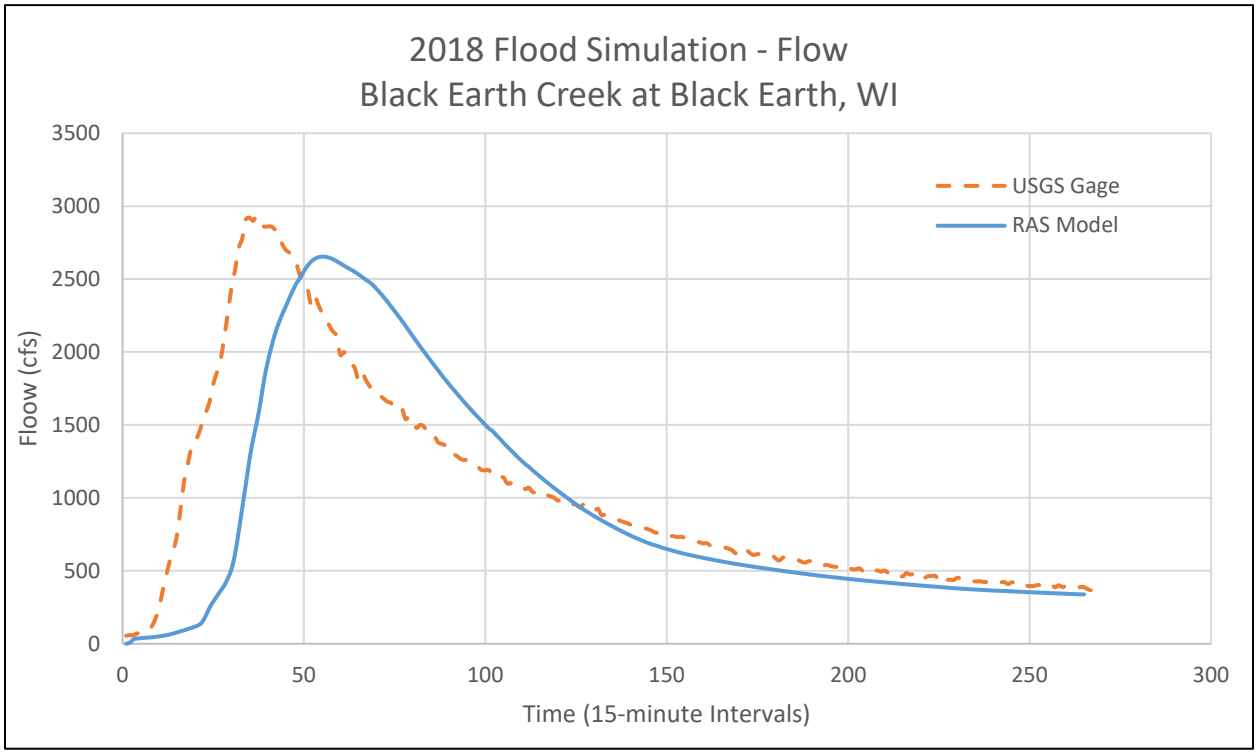

Figure 8. Observed vs. modeled discharge hydrograph, 2018 flood (Black Earth USGS gage)

5.2 2019 Flood Event

Figure 9 shows the flow hydrograph computed by the HMS model for each boundary condition in the RAS model for the 2019 flood event.

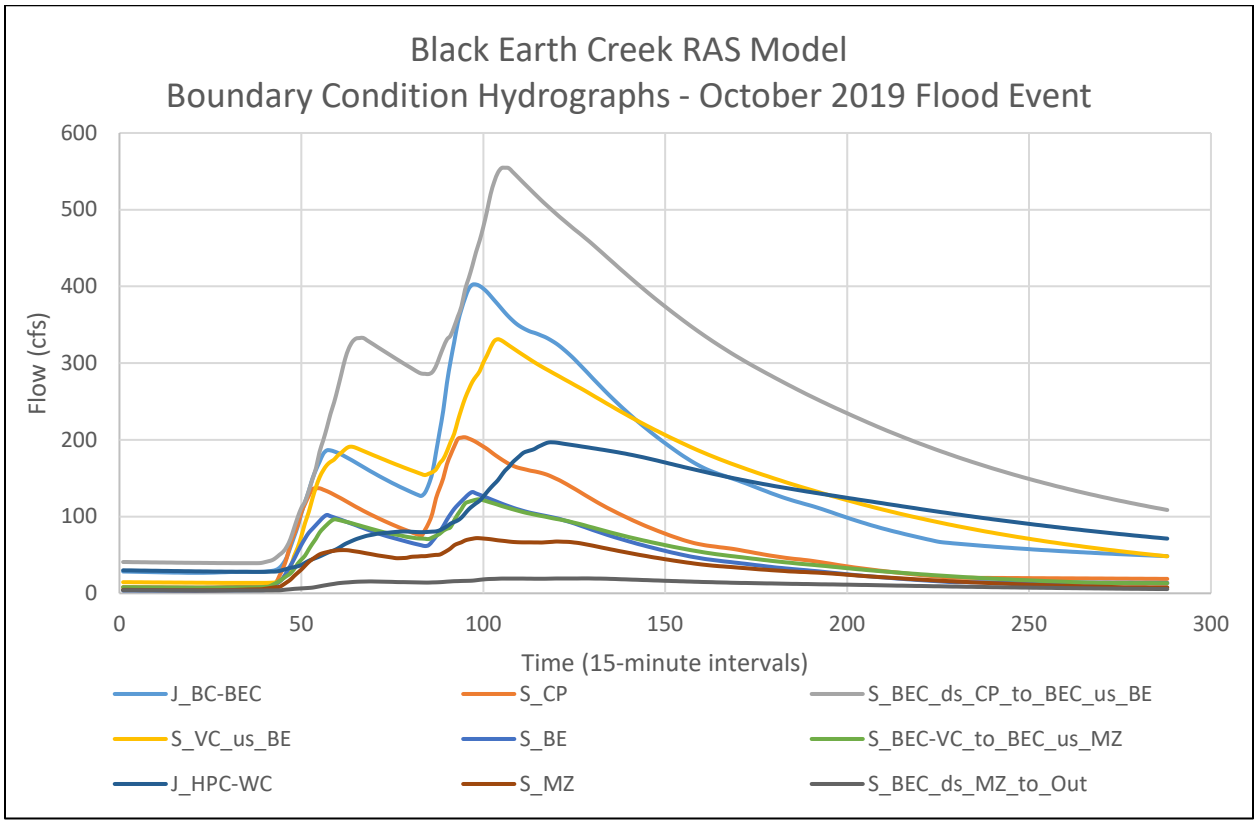

Figure 9. Boundary condition hydrographs - October 2019 flood event

Figure 10 shows the modeled rating curve at the Black Earth Creek gage along with the observed rating curve during the event. All USGS stage-discharge measurements are plotted for reference, as well as the simulated stage-discharge relationships at the cross section nearest the Black Earth gage in the FIS model. The model fits the observed rating curve fairly well on the rising limb of the hydrograph when discharge exceeds approximately 500 cfs, with the modeled rating curve falling within the bounds of the USGS measurement data. Similar to the 2018 simulation, slowly receding water on the floodplain causes a flatter slope on the receding limb of the hydrograph. However, in the channel itself the slope of the rating curve is consistent on both the rising and falling limb.

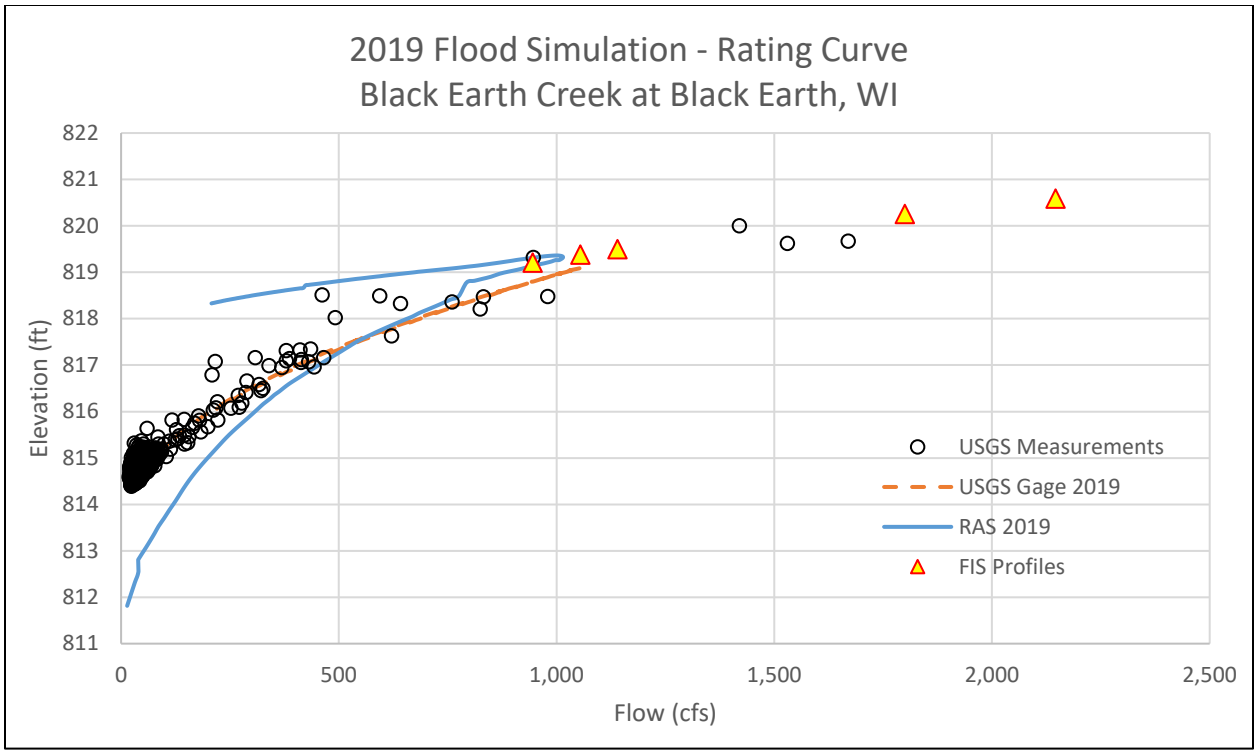

Figure 10. Observed vs. modeled rating curve, 2019 flood (Black Earth USGS gage)

Figure 11 and Figure 12 compare the modeled stage and discharge hydrographs to the observed stage and discharge hydrographs for the 2019 event at the Black Earth USGS gage. The model adequately matches the observed peak water surface elevation. The timing of the modeled flood peak is several hours earlier than the observed flood peak; however, this timing is consistent with the timing in the HMS model.

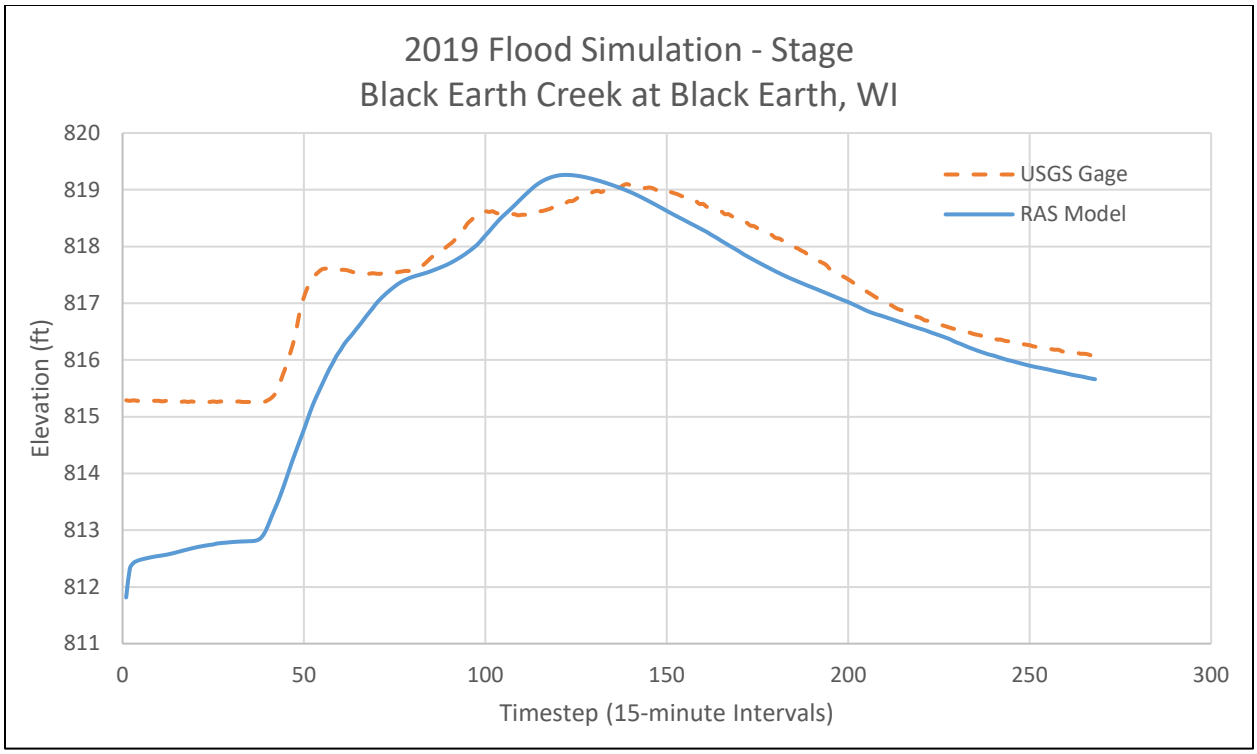

Figure 11. Observed vs. modeled stage hydrograph, 2019 flood (Black Earth USGS age)

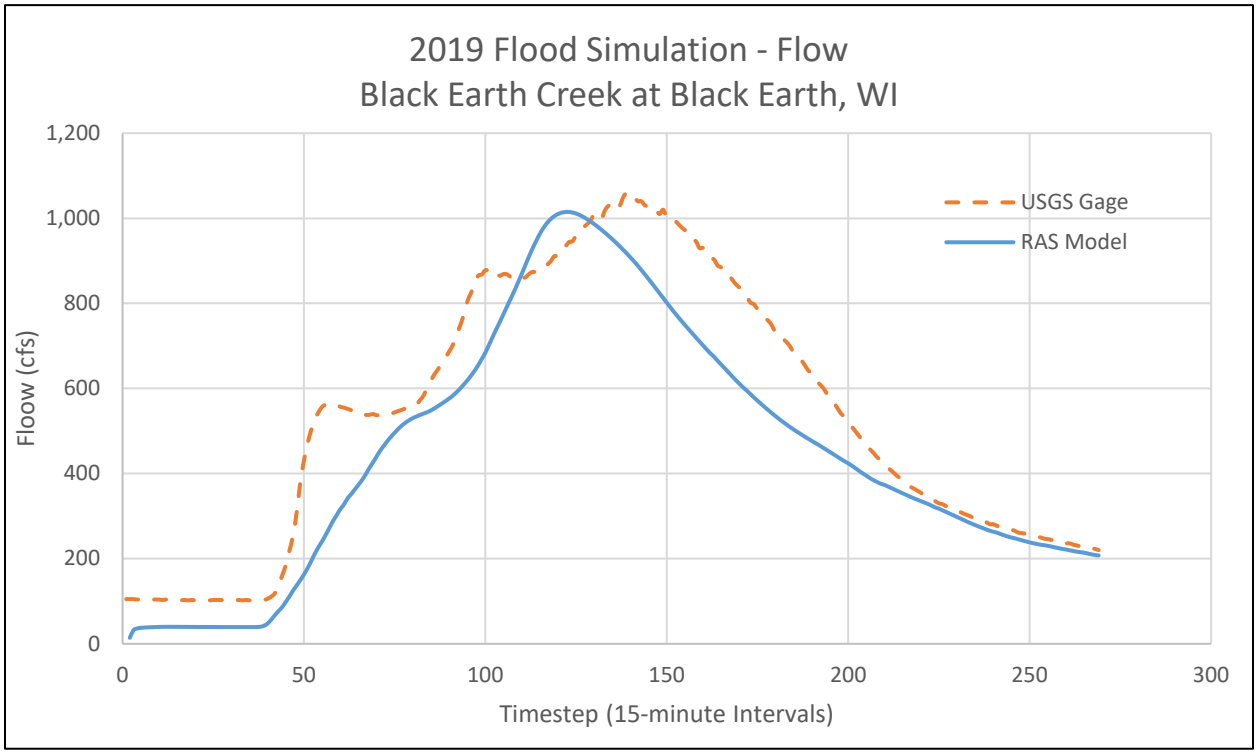

Figure 12. Observed vs. modeled discharge hydrograph, 2019 flood (Black Earth USGS age)

6 Recommendations

The HEC-RAS model developed for this project is a useful tool for comparing inundation extents of various HEC-HMS alternatives. It can be expected to reasonably estimate water surface elevations of flows greater than approximately 500 cfs at Black Earth, WI, and it has the capacity to capture breakout flows from the main river channel that would not be possible in a 1D model. However, due to the uncertainty surrounding the accuracy of the channel invert, this model should not be used to simulate small flood events where the majority of flow is contained within the streambanks. If that capability is required in a future study, additional bathymetric data should be collected to verify, and likely improve, the bathymetry in the current terrain dataset.

In addition to improving channel bathymetry, the terrain should be modified such that the channel aligns with the location of the channel in recent aerial imagery. Areas where the alignment of the channel can be improved are adjacent to Mill Creek Pkwy in the H.M. Zander Community Park area of Cross Plains and approximately 3,600 feet upstream of the Hwy 14 bridge in Mazomanie. While the channel alignment should be improved in these areas if the model will be used for detailed mapping of the floodplain during small flood events, for the purposes of this study the existing terrain is adequate.

One final item that may improve the model is a detailed culvert survey in the study area. There are many roads and railroads that intersect the floodplain, and culverts can be difficult to identify using aerial imagery alone. To more accurately capture the extent of inundation throughout the floodplain, all culverts through road and railroad embankments should be identified and incorporated in the model. While this additional accuracy is not necessary for the purpose of this study, it should be considered if using this model to produce detailed inundation maps.